UAB
Universitat Autònoma de Barcelona

Structural biology of α-synuclein toxic oligomers: Design of peptide ligands and architecture elucidation

Jaime Santos Suárez

ADVERTIMENT. L'accés als continguts d'aquesta tesi doctoral i la seva utilització ha de respectar els drets de la persona autora. Pot ser utilitzada per a consulta o estudi personal, així com en activitats o materials d'investigació i docència en els termes establerts a l'art. 32 del Text Refós de la Llei de Propietat Intel·lectual (RDL 1/1996). Per altres utilitzacions es requereix l'autorització prèvia i expressa de la persona autora. En qualsevol cas, en la utilització dels seus continguts caldrà indicar de forma clara el nom i cognoms de la persona autora i el títol de la tesi doctoral. No s'autoritza la seva reproducció o altres formes d'explotació efectuades amb finalitats de lucre ni la seva comunicació pública des d'un lloc aliè al servei TDX. Tampoc s'autoritza la presentació del seu contingut en una finestra o marc aliè a TDX (framing). Aquesta reserva de drets afecta tant als continguts de la tesi com als seus resums i índexs.

ADVERTENCIA. El acceso a los contenidos de esta tesis doctoral y su utilización debe respetar los derechos de la persona autora. Puede ser utilizada para consulta o estudio personal, así como en actividades o materiales de investigación y docencia en los términos establecidos en el art. 32 del Texto Refundido de la Ley de Propiedad Intelectual (RDL 1/1996). Para otros usos se requiere la autorización previa y expresa de la persona autora. En cualquier caso, en la utilización de sus contenidos se deberá indicar de forma clara el nombre y apellidos de la persona autora y el título de la tesis doctoral. No se autoriza su reproducción u otras formas de explotación efectuadas con fines lucrativos ni su comunicación pública desde un sitio ajeno al servicio TDR. Tampoco se autoriza la presentación de su contenido en una ventana o marco ajeno a TDR (framing). Esta reserva de derechos afecta tanto al contenido de la tesis como a sus resúmenes e índices.

WARNING. The access to the contents of this doctoral thesis and its use must respect the rights of the author. It can be used for reference or private study, as well as research and learning activities or materials in the terms established by the 32nd article of the Spanish Consolidated Copyright Act (RDL 1/1996). Express and previous authorization of the author is required for any other uses. In any case, when using its content, full name of the author and title of the thesis must be clearly indicated. Reproduction or other forms of for profit use or public communication from outside TDX service is not allowed. Presentation of its content in a window or frame external to TDX (framing) is not authorized either. These rights affect both the content of the thesis and its abstracts and indexes.

Structural biology of α-synuclein toxic oligomers: Design of peptide ligands and architecture elucidation

Universitat Autònoma de Barcelona
Departament de Bioquímica i Biologia Molecular
Institut de Biotecnologia i Biomedicina

Doctoral thesis presented by Jaime Santos Suárez for the degree of Ph. D. in Biochemistry, Molecular Biology and Biomedicine from the Autonomous University of Barcelona.

The work of the present thesis has been performed at the Department of Biochemistry and Molecular Biology and the Institute of Biotechnology and Biomedicine, supervised by Dr. Irantzu Pallarès Goitiz and Prof. Salvador Ventura Zamora.

Jaime Santos Suárez

Dr. Irantzu Pallarès Goitiz

Prof. Salvador Ventura Zamora

Bellaterra, February 2023

Table of contents

Table of contents **I**

Acknowledgements **III**

Summary **IX**

Resum en català **X**

Resumen en castellano **XI**

Articles included in the thesis **XIII**

Articles not included in the thesis **XIV**

Contribution statement **XVII**

List of abbreviations **XVIII**

Introduction **1**

1. Molecular basis of protein aggregation *3*
- 1.1. The proteins' journey: Protein folding vs aggregation 3
- 1.2. Sequence determinants of protein aggregation 6
- 1.3. Intrinsically disordered proteins and their aggregation landscape 7
- 1.4. Amyloid fibrils 9
- 1.5. Kinetics of amyloid formation 11
- 1.6. Oligomeric species 13
- 1.7. The aggregation mixture: coexistence of monomers, oligomers and fibrils across the aggregation reaction 15

2. α-Synuclein aggregation in neurodegenerative disorders *16*
- 2.1. α-Synuclein 16
- 2.2. α-Synuclein aggregates 19
  - 2.2.1. α-Synuclein oligomers 19
  - 2.2.2. Structural features of type B* kinetically trapped α-synuclein oligomers 21
  - 2.2.3. α-Synuclein fibrils 23
  - 2.2.4. Fuzzy coats: role of unstructured regions surrounding oligomers and fibrils 26
- 2.3. Parkinson's disease 28

2.4. Targeting α-synuclein aggregates for PD treatment and diagnosis; theoretical considerations based on our current biophysical knowledge 29

Objectives 31

Chapter 1: α-Helical peptidic scaffolds to target α-synuclein toxic species with nanomolar affinity 35

Chapter 2: Is a cure for Parkinson's disease hiding inside us? 53

Chapter 3: LL-37 and CsgC exemplify the crosstalk between anti-amyloid, antimicrobial, and anti-biofilm protein activities 61

Chapter 4: The structural architecture of an α -synuclein toxic oligomer 67

Concluding remarks 83

Discussion 87

1. Molecular basis of α-helical amphipathic peptides binding to α-synuclein oligomers 89

2. Kinetically trapped type-B oligomers as a model α-synuclein oligomers 90*

3. Oligomer structure and transition to fibril 90

4. G51D N-terminal polymorphism reshapes the disease landscape and impacts therapeutics 91

5. Where do oligomers come from? 92

6. Future perspectives and challenges ahead 93

References 95

Appendix 1 – Supplementary information of chapter 1 117

Appendix 2 – Supplementary information of chapter 2 139

Appendix 3 – Supplementary information of chapter 4 143

Acknowledgements

Aunque solo esté mi nombre en la portada, en esta tesis han participado un montón de personas que, en este pequeño rincón, merecen una mención especial. Por su ejemplo, su ayuda y su paciencia, científica y no científica. Ellos son los que han dado forma a esta tesis, y a mi. ¡Gracias a todos los nombrados y a los que me haya olvidado!

Primero quiero agradecer a mis directores de tesis Irantzu y Salva. ¡Hemos hecho un buen equipo! Sobretodo quiero agradeceros la confianza que habéis puesto en mi desde el primer día. Siempre me habéis hecho sentir muy respaldado y una parte fundamental del equipo. Creo que habéis sacado lo mejor de mi. Muchas gracias Salva por cultivar mi vocación y por inspirarnos a todos con tu pasión por la investigación. Esta tesis esta construida en lo que en su momento eran "ideas locas" y lo que me hace sentir más orgulloso de esta tesis es que hayamos tenido las ganas y la valentía de explorarlas. Para Irantzu no tengo suficientes palabras para agradecerle todo lo que ha hecho por mi y por los PRO's. Has sido mi compañera y un apoyo constante todos los días, los divertidos y los de nervios. Me has enseñado mucho y eres un ejemplo de líder. Por su puesto ha sido importantísima tu ayuda para mantenerme fit y no perder la línea ☺. Los tres nos lo hemos pasado muy bien juntos.

También he tenido la suerte de poder pasármelo muy bien en el laboratorio; en el departamento, en el IBB y en PRO's. Gracias a Jordi, Valen, Samu y Francisca que me acogieron y me enseñaron el *abc* del lab. A Jordi entre otras muchas cosas quiero agradecerle el ejemplo y la inspiración. Eres la persona que más ha influido en mi forma de entender la ciencia y el trabajo en un laboratorio. Esos momentos de excitación son lo mejor del trabajo. ¡A Valen lo bien que nos lo hemos pasado! Siempre atesoraré la primera frase que me dijiste en el laboratorio. Hemos currado juntos como bestias, midiendo a escuadra y cartabón y siempre con buen humor. Samu y Francisca que han compartido estos años conmigo, de principio a fin, les agradezco su compañía en los días buenos y en los malos (aunque a veces se cojan de la mano). ¡Muchas placas hemos medido! A Samu tengo que des-agradecerle el viaje a Bruselas, que se portó fatal jajajaja. A Sebas, un ejemplo de trabajo y dedicación, cuando parece que las cosas no van bien me acuerdo de su: "Resiliencia, Jaime resiliencia, si no sale hoy, vuelvo mañana por la mañana y lo hago otra vez.". De la gente que ha pasado por el lab me acuerdo especialmente de Júlia, de su fiesta de navidad y del reencuentro que tuvimos en Leuven. De las nuevas incorporaciones; Marc que ya lleva un tiempo con nosotros, y aunque ahora viva en el IBB es un

Pro de nacimiento ¡Tenemos un par de meses entretenidos por delante! Y por último gracias a Zoe por ser la mejor y regalarnos cada día una sonrisa y una dosis de alegría. Entre los dos os quedáis con las líneas de investigación en las que he trabajado los últimos años: espero que os den tantas alegrías como me han dado a mi.

Al resto de miembros del grupo, que, aunque habitasen en otro edificio, han compartido estos años conmigo. Cristina, Marta, Manu, Anita, Weiqiang, Molood, Andrea, Carla, Chari, Javi y Marcos. Por su ayuda y su buen rollo. Un trocito de mi tesis también es de Susanna, que se ha encargado de que tuviera todo lo necesario para mis experimentos, y eso que doy bastante guerra. Gracias también por las birras que nos hemos tomado juntos. A Carlos y Oriol, porque una de las mayores recompensas de mi trabajo es ver como vosotros habéis desarrollado líneas de investigación que arrancamos Valen y yo hace ya años. Me hace mucha ilusión. A big big shout out to Mihal and his parties! What a supernice incorporation to the lab.

También quiero agradecer al resto de compañeros del departamento. Empezando como no por el titán del departamento, Alejandro Ramos. Has estado presente en casi todo mi recorrido en la torre, y cuando no has estado, te he echado mucho de menos. Gracias por estar siempre dispuesto a un café, pero sobretodo a una cerveza. En las pistas de padel todavía se habla del equipo TITANLUX. También al otro cabeza de la revolución (la “perla de la segunda”), el Guillem que, además de amigo, es un científico de los pies a la cabeza. Mucho me has ayudado y Ribos siempre es el mejor sitio a donde ir a buscar una opinión crítica. A Gabri, el paradigma de la felicidad *postdoctorado* y todo un atleta que hace mates al baloncesto. A Helena, que compartió conmigo el máster y ha seguido estando presente en cada celebración y fiesta. De Pilar me guardo la pasión que compartimos por Mothman (o mojatman), eso si que es cine. También agradecer a la vieja guardia, Jofre, Gisela y Laia, por el buen rollito que había el departamento y por seguir viniendo a vernos. A Nuria, Li, Lu, Roberto, Dani, Marta, Jofre, Raquel, Rafa y demás compañeros de la unidad. A Mohammed por ser tan divertido y cercano.

También quiero agradeceros a la gente del IBB de otros grupos, EP, Llevats, Enzimo, Molekos y Nano. A todos los del Volei, aunque siempre lleguéis tarde. A Eloi el capo del vóley y nakama. A Sergi Torres, al otro Sergi, a David, a Eric, Hector (el puma), Eddi, Jovi, Jan. Gracias Marina por permitirme ser un as en el tiro con arco, por el tutorial de las croquetas y por las veces que nos has acogido en tu casa. A Olivia por llevarnos a subir pinganetas, aunque Santo no estará de acuerdo en agradecertelo. A Nathalia, que es una gran compañera de cervezas y gin tonics.

A Magda y Santi por su ayuda con las prácticas y por mantener la torre funcionando. A los miembros del servei de microscopía, Alex, Martí, Cristina, Helena y Núria. A mi comisión de seguimiento por supervisarme y por sus buenas palabras.

Otros dos trocitos de la tesis se los reparten Helena y Salva. Helena, que más allá de ser una pieza fundamental de nuestro laboratorio, es un sol y siempre me ha dado mucho cariño. A Salva le tengo que agradecer el soporte constante, a nivel de equipos, de diseño experimental, pero sobretodo por todo el cariño y lo bien que me has tratado. Gracias por la paciencia a los dos.

During this thesis I also had the chance to collaborate with fantastic scientists. Gracias a Nunilo y Pablo por creer en el proyecto en sus orígenes y acogerme en vuestro laboratorio. Mis estancias express en Zaragoza siempre han sido superexcitantes científicamente. To Antoine Loquet that hosted me in his lab during 3 months in which I had the chance to learn a bit about ssNMR, lipids and enjoy the beautiful city of Bordeaux. I also want to thank Axelle Grélard for her help and dedication, and Erick Dufourc for insightful discussion. Of course, to the other members of the lab and specially to the two *amigos* Alons and Bilal, for their contribution in the lab and their friendship outside. También agradecer a Jose María Valpuesta por participar en este proyecto cuando apenas estábamos seguros de lo que esperábamos ver y por invitarme a su laboratorio. A Jorge Cuellar le tengo que agradecer enormemente su contribución al proyecto y las ganas e iniciativa que le ha echado a todo lo que ha hecho. Pero sobretodo por todo lo que me ha enseñado sobre el crio y los crosslinkings, siempre estando dispuesto a contestar mis dudas. Finally, to Daniel Otzen, Jan Skov Pedersen, Sheena E Radford, Arturo Muga and their labs and coworkers. It has been an honor to collaborate with you these last years and thank you for your contribution and kind words.

A toda la gente que me ha apoyado desde casa. Sobretodo el Club de fans del ciclismo de Pontevedra. Gracias por vuestra amistad y hacer que siempre quiera volver a casa y nunca quiera marcharme. A Matías por ser ejemplo de transparencia, el eterno ganador de los Matías Awards y querer hacer de Pontevedra una ciudad mejor (PTV 2030). En serio, gracias por todos estos años, por escucharme siempre y por conseguir arrancarnos a todos una sonrisa. ¡Si hasta me acogiste en tu casa para hacer experimentos! A Óscar le quiero agradecer su apoyo constante desde 2010 ;) y que me regalase su vaso del Starbucks. Milagroso que esta persona me siga hablando después de haber estado gafándolo durante años. Gracias también a Zuko, majísimo, siempre moviendo zu-kolita. Gracias Alvaro, la mujer florero del año y a su sugardaddy, además de a Crespo por todos los sábados, vermuts, peregrinas y peñas; y los que quedan. Gracias a

Paola que tenía tantas ganas de venir a ver mi tesis que vino el año pasado. Espero que después de esto tu madre me respete un poco más. Gracias por ser un poco canalla y maestra de la petaca :3. También gracias a ti y a Mikel Landa por ser el ejemplo de que no todo es ganar. Gracias a Nacho por darme tantos premios y ser un ejemplo de dedicación a su trabajo y a Nuria, sobretodo por invitarme a su fiesta, pero también por ser un autentico sol. Al tormentoso Iago que ha fomentado mi *sandersonismo* el muy famélico.

Esta aventura empezó cuando me mudé a Barcelona y los biotecs han sido una parte muy importante de ella. Ainoa, Cris, Eric, Kath, Juls, Lluis, Javi, Jorge, Ruben, Pauli, Lluc, Sales, Lillo, Rocío, Ivan, Pere, Cris, Carmen, Ramón, Cris Séneca. Una lista especial para los doctores; el Dr. Granero Moya y el Dr. Lillo Jove. Gracias por los años de la carrera, por los siguientes y por los reencuentros en Huesca.

Un abrazo a la mejor compañera de escalada que hay, “Helena”, que además es un tema superdivertido y la segunda EPera a la que más quiero. Ya sabes que puedes venir a casa a hacer puzles cuando quieras.

A los maños et al., por hacernos sentir a mi y a Lucía que Sabadell era casa. Me habéis regalado una cantidad de resacas escandalosa. Entre todos hemos conseguido pagar la universidad de los hijos y nietos de los de la vermutería. A Diego por ser un ávido descriptor de la realidad (Maria Jesus, primero de la ESO) y a Patri por querernos, aunque muchas veces tenga que comerse las chapas científico-faltonas. A Santo no le puedo perdonar su increíble guapitud, pero habrá que agradecerle todo lo bien que se ha portado conmigo y que me haya enseñado la preciosa ciudad de Sabiñánigo. A Marcel que tiene el humor tan fino, siempre listo para tirar una pullita, le quiero agradecer su participación fundamental en los juegos de mesa. Sobretodo por su gestión en el pandemic y su clarividencia jugando al código secreto. A Raquel, que está de enviada en Ciudad Real para explicarnos cuanto vale un trofeo, por traernos quesos y platos típicos. También por enseñarnos la maravillosa saga de Halloween. A nuestros flamantes nuevos vecinos Jarita y Carlos. Jara ya sabes que yo siempre testificaré a tu favor, eres la primera exEP que más quiero (ver referencia en el párrafo anterior). A Carlos por enseñarme -en colaboración con Valen- que la edad solo es un número y se puede seguir jugando al padel y al volley aún con achaques. Gracias por tener tan buen perder. A Bad Bunny. A Mireia por tener siempre unas buenas palabras, bueno, bastantes palabras jajaja. A Pablito por ser un ser de luz y alojarme en Zaragoza

A Miguel, Noemi, Lucía y Amaya, muchas gracias por acogerme en vuestra familia. Gracias por vuestras visitas. También a Josele, Lucía y Pilar.

A mi familia, porque al final, vengo de donde vengo y soy como soy gracias a ellos. El valor del conocimiento y el espíritu de superación son algo que me han inculcado siempre. Los 4 primos compartimos esto, así que de algún lado tendrá que salir. A mis padres, por su ayuda y por su paciencia, sobretodo en mis peores momentos. A mi hermano con quien además de compartir aficiones (las hormigas por ejemplo), compartimos el orgullo en uno mismo, necesario para que todo vaya bien. Sorprendentemente también le tengo que agradecer su colaboración activa científicamente, con ¡3 papers! que hemos publicado juntos. Aunque llores mucho cuando pierdes, los vicios juntos son lo mejor de estar en casa. A Apolo que siempre me espera despierto para comerse un bocadillo antes de ir a dormir. A Fernando, Susana y Joni, porque es un gusto tener una familia cohesionada y poder vernos los domingos. También porlos gin tonics. A Jorge por ser el mayor e ir siempre abriendo paso, el otro doctor de la familia. Also, to him and Liam for the time we spent together in Bordeaux; most of it searching for a good bar. A Pedro, que durante muchos años me empujó a mejorar cada semana. Los “a por Pilín” nos enseñaban a trabajar en equipo, la traición (a veces), pillar skill y el sabor de la dulce victoria.

Por último (en posición de corresponding), está la persona que ha compartido conmigo esta aventura. Gracias por hacerme feliz, antes durante y después de la tesis. ¡Gracias Lucía!

Viaje antes que destino

Summary

α-Synuclein (αS) aggregation is the main neurological hallmark of a group of debilitating neurodegenerative disorders, collectively referred to as synucleinopathies, of which Parkinson's disease is the most prevalent. Oligomers populated during the early events of αS aggregation are considered key pathogenic drivers of disease onset and progression, standing as privileged targets for therapeutic intervention and diagnosis. However, the structure of αS oligomers and the mechanistic basis of oligomer to fibril conversion are yet unknown, precluding the rational design of oligomer-targeting strategies. In this thesis dissertation, we exploited the main shared physicochemical properties of αS oligomers and fibrils to identify a family of α-helical peptides that bind αS pathogenic species with high affinity and conformational selectivity. These peptides have the potential to inhibit protein aggregation and abrogate oligomer associated cellular damage, with non-detectable monomer binding. These properties make them promising tools for disease diagnosis and treatment. Noteworthy, LL-37, one of such peptides, is constitutively expressed in disease-relevant tissues in humans, suggesting that this or similar endogenous peptides may have a physiological role in control protein aggregation.

We then exploited this peptide binding to interrogate oligomer's structural features. Peptide binding to oligomers reduces their fuzziness and conformational heterogenicity, allowing a more detailed structural characterization. We determined for the first time the symmetry and architecture of an αS oligomer and dissected the conformational properties of individual chains. We also identified a short N-terminal region fundamental for oligomer to fibril conversion. The familial G51D mutation associated with early onset Parkinson's disease affects the conformational of this region, causing an accumulation of oligomers resistant to the Hsp70 disaggregation machinery.

Overall, our results build a new structural and biophysical framework for oligomer targeting in therapeutics and diagnosis while unveiling new structural and mechanistic features of αS oligomers.

Resum en català

L'agregació de l'alfa-sinucleïna (αS) és la principal característica neurològica d'un grup de trastorns neurodegeneratius debilitants, coneguts col·lectivament com sinucleinopaties, dels quals la malaltia de Parkinson és la més freqüent. Els oligòmers poblats durant els primers esdeveniments de l'agregació d'αS son elements patogènics clau tant per l'inici com la progressió de la malaltia, i per tant son considerats dianes privilegiades per a la intervenció terapèutica i el diagnòstic d'aquestes malalties. Malauradament, l'estructura dels oligòmers de αS i les bases moleculars que dirigeixen la seva conversió a fibres son encara desconegudes, impedint el disseny racional d'estratègies que tinguin els oligòmers com diana. En aquesta tesi, hem aprofitat les principals propietats fisicoquímiques compartides entre els oligòmers i les fibres d'αS per identificar una família de pèptids helicoïdals que s'uneixen amb alta afinitat i selectivitat conformacional a aquestes espècies patogèniques d'αS. Aquests pèptids tenen el potencial d'inhibir l'agregació d'aquesta proteïna i eliminar el dany cel·lular associat als oligòmers, sense interaccionar amb els monòmers funcionals d'αS. Aquestes propietats, els converteixen en eines prometedores per al diagnòstic i tractament d'aquestes malalties. Cal destacar que un d'aquests pèptids, LL-37, s'expressa de manera constitutiva en humans en teixits rellevants per la malaltia, suggerint que aquest o altres pèptids endògens similars poden tenir un paper rellevant en el control de la l'agregació d'αS a nivell fisiològic.

A més, hem fet valdre la interacció d'aquestes pèptids per poder desxifrar les característiques estructurals dels oligòmers. La unió de pèptids als oligòmers en redueix la seva flexibilitat i heterogeneïtat conformacional, permetent assolir una caracterització estructural més detallada. Aquesta aproximació ens ha permès determinar per primera vegada la simetria i l'arquitectura d'un oligòmer d'αS arribant a poder disseccionar les propietats conformacionals de les seves cadenes individuals. També hem identificat una regió curta al N-terminal de l' αS fonamental per a la conversió dels oligòmers a fibres. La mutació familiar G51D, associada al desenvolupament primerenc de la malaltia de Parkinson, afecta la conformació d'aquesta regió, provocant una acumulació d'oligòmers resistents a la maquinària de desagregació de Hsp70.

Globalment, els nostres resultats revelen noves característiques estructurals i mecanístiques dels oligòmers d'αS i construeixen un nou marc estructural i biofísic per al desenvolupament de noves estratègies terapèutiques i de diagnòstic per a la malaltia de Parkinson i altres sinucleinopaties.

Resumen en castellano

La agregación de la alfa-sinucleína (αS) es la principal característica neurológica de un grupo de trastornos neurodegenerativos debilitantes, conocidos como sinucleinopatías, de los cuales la enfermedad de Parkinson es la más frecuente. Los oligómeros poblados durante los primeros eventos de la agregación de αS son elementos patogénicos clave en el inicio y la progresión de la enfermedad, y por tanto son considerados dianas privilegiadas para la intervención terapéutica y el diagnóstico de estas enfermedades. Desgraciadamente, la estructura de los oligómeros de αS y las bases moleculares que dirigen su conversión a fibras son todavía desconocidas, impidiendo el diseño racional de estrategias que los tengan como diana. En esta tesis, hemos aprovechado las principales propiedades fisicoquímicas compartidas entre los oligómeros y las fibras de αS para identificar una familia de péptidos helicoidales que se unen con alta afinidad y selectividad conformacional a estas especies patogénicas. Estos péptidos tienen el potencial de inhibir la agregación de esta proteína y eliminar el daño celular asociado a los oligómeros, sin interaccionar con los monómeros funcionales. Estas propiedades los convierten en herramientas privilegiadas para el diagnóstico y tratamiento de estas enfermedades. LL-37, uno de estos péptidos, se expresa de forma constitutiva en humanos en tejidos relevantes para la enfermedad, sugiriendo que este u otros péptidos endógenos similares pueden tener un papel relevante en el control de la agregación de αS a nivel fisiológico.

Además, hemos aprovechado estos péptidos para poder descifrar características estructurales de los oligómeros. La unión de estos péptidos a los oligómeros reduce su flexibilidad y heterogeneidad conformacional, permitiendo una caracterización estructural más detallada. Esta aproximación nos ha permitido determinar por primera vez la simetría y la arquitectura de un oligómero de αS, llegando a diseccionar las propiedades conformacionales de sus cadenas individuales. También hemos identificado una región corta en el N-terminal fundamental para la conversión de los oligómeros a fibras. La mutación familiar G51D, asociada al desarrollo temprano de la enfermedad de Parkinson, afecta a la conformación de esta región, provocando una acumulación de oligómeros resistentes a la maquinaria de desagregación de Hsp70.

Globalmente, nuestros resultados revelan nuevas características estructurales y mecanísticas de los oligómeros de αS y construyen un nuevo marco estructural y biofísico para el desarrollo de nuevas estrategias terapéuticas y de diagnóstico para la enfermedad de Parkinson y otras sinucleinopatías.

Articles included in the thesis

This thesis dissertation is in the format of a compendium of the following publications:

1. **J. Santos**, P. Gracia, S. Navarro, S. Peña-Díaz, J. Pujols, N. Cremades, I. Pallarès, S. Ventura, *α-Helical peptidic scaffolds to target α-synuclein toxic species with nanomolar affinity*. Nat Commun. 12, 3752 (2021).
2. **J. Santos**, I. Pallarès, S. Ventura, *Is a cure for Parkinson's disease hiding inside us?* Trends Biochem Sci. 47, 641–644 (2022).
3. **J. Santos**, S. Ventura, I. Pallarès, *LL-37 and CsgC exemplify the crosstalk between anti-amyloid, antimicrobial, and anti-biofilm protein activities*. Neural Regen Res. 18, 1027–1028 (2023).

Additionally, chapter 4 contains a preprint version of an article deposited in BioRxiv:

4. **J. Santos**, J. Cuellar, I. Pallarès, E. J. Byrd, A. Lends, F. Moro, M. B. Abdul-Shukkoor, J.Pujols, L. Velasco-Cameros, F. Sobott, D. E Otzen, A. Calabrese, A. Muga, J. S. Pedersen, A. Loquet, J. M. Valpuesta, S. E. Radford and S. Ventura, *The structural architecture of an α-synuclein toxic oligomer.* bioRxiv 2023.02.10.527650
   doi: 10.1101/2023.02.10.527650

Articles not included in the thesis

1. **J. Santos**, V. Iglesias, J. Santos-Suárez, M. Mangiagalli, S. Brocca, I. Pallarès, S. Ventura, *pH-Dependent Aggregation in Intrinsically Disordered Proteins Is Determined by Charge and Lipophilicity*. Cells. 9, 145 (2020).
2. **J. Santos**, J. Pujols, I. Pallarès, V. Iglesias, S. Ventura, *Computational prediction of protein aggregation: Advances in proteomics, conformation-specific algorithms and biotechnological applications*. Comput Struct Biotechnol J. 18, 1403–1413 (2020).
3. **J. Santos**, I. Pallarès, V. Iglesias, S. Ventura, *Cryptic amyloidogenic regions in intrinsically disordered proteins: Function and disease association*. Comput Struct Biotechnol J. 19, 4192–4206 (2021).
4. **J. Santos**, V. Iglesias, C. Pintado, J. Santos-Suárez, S. Ventura, *DispHred: A Server to Predict pH-Dependent Order-Disorder Transitions in Intrinsically Disordered Proteins*. Int J Mol Sci. 21, 5814 (2020).
5. **J. Santos**, S. Ventura, *Functional Amyloids Germinate in Plants*. Trends Plant Sci. 26, 7–10 (2021).
6. **J. Santos**, V. Iglesias, S. Ventura, *Computational prediction and redesign of aberrant protein oligomerization*. Prog Mol Biol Transl Sci. 169, 43–83 (2020).
7. C. Pintado, **J. Santos**, V. Iglesias, S. Ventura, *SolupHred: a server to predict the pH-dependent aggregation of intrinsically disordered proteins*. Bioinformatics. 37, 1602–1603 (2021).
8. F. Pinheiro, **J. Santos**, S. Ventura, *AlphaFold and the amyloid landscape*. J Mol Biol. 433, 167059 (2021).
9. V. Iglesias, **J. Santos**, J. Santos-Suárez, C. Pintado-Grima, S. Ventura, *SGnn: A Web Server for the Prediction of Prion-Like Domains Recruitment to Stress Granules Upon Heat Stress*. Front Mol Biosci. 8, 718301 (2021).
10. J. Pujols, **J. Santos**, I. Pallarès, S. Ventura, *The Disordered C-Terminus of Yeast Hsf1 Contains a Cryptic Low-Complexity Amyloidogenic Region*. Int J Mol Sci. 19, 1384 (2018).
11. E. Medina-Carmona, I. Betancor-Fernández, **J. Santos**, N. Mesa-Torres, S. Grottelli, C. Batlle, A. N. Naganathan, E. Oppici, B. Cellini, S. Ventura, E. Salido, A. L. Pey, *Insight into the specificity and severity of pathogenic mechanisms associated with missense mutations through experimental and structural perturbation analyses*. Hum Mol Genet. 28, 1–15 (2019).

12. S. Peña-Díaz, J. Pujols, M. Conde-Giménez, A. Čarija, E. Dalfo, J. García, S. Navarro, F. Pinheiro, **J. Santos**, X. Salvatella, J. Sancho, S. Ventura, *ZPD-2, a Small Compound That Inhibits α-Synuclein Amyloid Aggregation and Its Seeded Polymerization*. Front Mol Neurosci. 12, 306 (2019).
13. F. Pinheiro, N. Varejão, S. Esperante, **J. Santos**, A. Velázquez-Campoy, D. Reverter, I. Pallarès, S. Ventura, *Tolcapone, a potent aggregation inhibitor for the treatment of familial leptomeningeal amyloidosis*. FEBS J. 288, 310–324 (2021).
14. S. Peña-Díaz, J. Pujols, F. Pinheiro, **J. Santos**, I. Pallarés, S. Navarro, M. Conde-Gimenez, J. García, X. Salvatella, E. Dalfó, J. Sancho, S. Ventura, *Inhibition of α-Synuclein Aggregation and Mature Fibril Disassembling With a Minimalistic Compound*, ZPDm. Front Bioeng Biotechnol. 8, 588947 (2020).
15. C. Pintado-Grima, V. Iglesias, **J. Santos**, V. N. Uversky, S. Ventura, *DispHScan: A Multi-Sequence Web Tool for Predicting Protein Disorder as a Function of pH*. Biomolecules. 11, 1596 (2021).
16. S. Peña-Díaz, J. Pujols, E. Vasili, F. Pinheiro, **J. Santos**, Z. Manglano-Artuñedo, T. F. Outeiro, S. Ventura, *The small aromatic compound SynuClean-D inhibits the aggregation and seeded polymerization of multiple α-synuclein strains*. J Biol Chem. 298, 101902 (2022).
17. C. Pintado-Grima, O. Bárcenas, Z. Manglano-Artuñedo, R. Vilaça, S. Macedo-Ribeiro, I. Pallarès, **J. Santos**, S. Ventura, *CARs-DB: A Database of Cryptic Amyloidogenic Regions in Intrinsically Disordered Proteins*. Front Mol Biosci. 9, 882160 (2022).
18. M. R. Fernández, I. Pallarès, V. Iglesias, **J. Santos**, S. Ventura, *Formation of Cross-Beta Supersecondary Structure by Soft-Amyloid Cores: Strategies for Their Prediction and Characterization*. Methods Mol Biol. 1958, 237–261 (2019).
19. F. Quaglia, B. Mészáros, E. Salladini, A. Hatos, R. Pancsa, L. B. Chemes, M. Pajkos, T. Lazar, S. Peña-Díaz, **J. Santos**, V. Ács, N. Farahi, E. Fichó, M. C. Aspromonte, C. Bassot, A. Chasapi, N. E. Davey, R. Davidović, L. Dobson, A. Elofsson, G. Erdős, P. Gaudet, M. Giglio, J. Glavina, J. Iserte, V. Iglesias, Z. Kálmán, M. Lambrughi, E. Leonardi, S. Longhi, S. Macedo-Ribeiro, E. Maiani, J. Marchetti, C. Marino-Buslje, A. Mészáros, A. M. Monzon, G. Minervini, S. Nadendla, J. F. Nilsson, M. Novotný, C. A. Ouzounis, N. Palopoli, E. Papaleo, P. J. B. Pereira, G. Pozzati, V. J. Promponas, J. Pujols, A. C. S. Rocha, M. Salas, L. R. Sawicki, E. Schad, A. Shenoy, T. Szaniszló, K. D. Tsirigos, N. Veljkovic, G. Parisi, S. Ventura, Z. Dosztányi, P. Tompa, S. C. E. Tosatto, D. Piovesan, *DisProt in 2022: improved quality and accessibility of protein intrinsic disorder annotation*. Nucleic Acids Res. 50, D480–D487 (2022).

20. V. Iglesias, C. Pintado-Grima, **J. Santos**, M. Fornt, S. Ventura, *Prediction of the Effect of pH on the Aggregation and Conditional Folding of Intrinsically Disordered Proteins with SolupHred and DispHred*. Methods Mol Biol. 2449, 197–211 (2022).
21. J. Pujols, V. Iglesias, **J. Santos**, A. Kuriata, S. Kmiecik, S. Ventura, *A3D 2.0 Update for the Prediction and Optimization of Protein Solubility*. Methods Mol Biol. 2406, 65–84 (2022).
22. C. Pintado-Grima, **J. Santos**, V. Iglesias, Z. Manglano-Artuñedo, I. Pallarès, S. Ventura, *Exploring cryptic amyloidogenic regions in prion-like proteins from plants*. Front. Plant Sci. 13, 1060410 (2023).

Contribution statement

This thesis dissertation is composed by four research works carried out under the supervision of Prof. Salvador Ventura Zamora and Dr. Irantzu Pallarès Goitiz. I am the first author of these works, but it would not have been possible without the contribution of the fantastic collaborators I had the opportunity to work with.

In chapter 1, the time-resolved fluorescence spectroscopy experiments were performed at the Institute for Biocomputation and Physics of Complex Systems (BIFI-Zaragoza) in collaboration with Pablo Gracia and Nunilo Cremades. I participated in data acquisition and analysis during two short stays (≈1 month) in their laboratory.

Chapter 4 includes several collaborations with international research groups. Solid-state nuclear magnetic resonance measurements were performed in the laboratory of Antoine Loquet during an international 3-month stay in Bordeaux. The cryoelectron microscopy and crosslinking mass spectrometry analysis was carried out by Jose María Valpuesta and Jorge Cuellar. This collaboration implicated a 2-week stay in their laboratory. Jan Skov Pedersen and Daniel Otzen acquired and analyzed the small-angle X-ray scattering data at the iNANO (Aarhus). Emily J Byrd, Antonio Calabrese, Frank Sobott and Sheena E Radford performed proton-deuterium exchange mass spectrometry in the Astbury Centre for Structural Molecular Biology (Leeds). Finally, chaperone disaggregation experiments were carried out by Fernando Moro, Lorea Velasco-Carneros and Arturo Muga at the Instituto Biofisika (UPV/EHU, CSIC).

I would like to thank them for their contribution to this thesis and for their insights and advices. Another big “thank you” to those who welcomed me in their laboratories.

List of abbreviations

αS	α-Synuclein
Aβ	Amyloid-β peptide (Aβ)
APR	Aggregation-prone region
cryoEM	Cryoelectron microscopy
DARR	Dipolar-assisted rotational resonance
dcFCCS	Dual-color fluorescence crosscorrelation spectroscopy
DLB	Dementia with Lewy's bodies
EGCG	(-)-EpiGalloCatechin-3-Gallate
fPD	Familial Parkinson's disease
FRET	Forster resonance energy transfer
FTIR	Fourier transform infrared spectroscopy
IAPP	Islet amyloid polypeptide
IDP	Intrinsically disordered protein
INEPT	Insensitive nuclei enhanced by polarization transfer
JOS	Juvenile onset synucleinopathy
MAS	Magic angle spinning
MSA	Multiple systemic atrophy
NAC	Non amyloid-β component
P1	α-Synuclein region (36-42)
P2	α-Synuclein region (45-57)
PBS	Phosphate-buffered saline
PD	Parkinson's disease
PDD	Parkinson's disease dementia
SAXS	Small-angle X-ray scattering
smFRET	Single-molecule fluorescence crosscorrelation spectroscopy
ssNMR	Solid-state nuclear magnetic resonance
Th-T	Thioflavin-T
WT	Wild-type

Introduction

1. Molecular basis of protein aggregation

1.1.The proteins’ journey: Protein folding vs aggregation

Proteins are the ultimate and essential cellular effectors in living organisms, coordinating a myriad of functions through the establishment of molecular networks in the crowded cellular milieu (Huttlin et al. 2017; Pastore and Temussi 2022). To perform the intended biological functions, proteins have to adopt their native three-dimensional structure through a process known as protein folding (Anfinsen 1973; Dill and MacCallum 2012). However, proteins are not static molecular machines trapped in one single rock-solid native state, but they sample a wide range of conformational states through their life cycle (Wright and Dyson 2009; Grant, Gorfe, and McCammon 2010; Fuxreiter 2018). This dynamism confers proteins a certain plasticity and promiscuity essential for their activities and indispensable for the emergence of new protein functions (Tokuriki and Tawfik 2009; Dishman et al. 2021). Unfortunately, proteins do not only populate functional conformations, but they may transit through non-native states and stablish aberrant interactions that result in cellular dysfunction and disease (Chiti and Dobson 2017).

Proteins are synthetized as linear polypeptides in the ribosome and need to attain their native conformation and localize in their designated cellular compartments to become functional. This journey begins as soon as protein synthesis starts, since proteins might co-translationally fold as they emerge from the ribosome, even forming native complexes before ribosome release (Waudby, Dobson, and Christodoulou 2019; Kramer, Shiber, and Bukau 2019; Bertolini et al. 2021). To fold, polypeptides need to sample their energy landscape and transit from their initial disordered state to their thermodynamically favored native conformations (Anfinsen 1973; Nassar et al. 2021) (**Figure 1**). In this process, proteins overcome kinetic barriers and populate partially folded intermediate states while advancing through their folding funnel (Englander and Mayne 2014; 2017). This energy search can be spontaneous, require the assistance of molecular chaperones or only occur upon translocation to certain cellular compartments (Nassar et al. 2021; Chatzi, Manganas, and Tokatlidis 2016). The energy landscape of a protein is usually funneled towards protein native states to favor folding and optimal stability (In green in **Figure 1**). This folding funnel is carved by evolution and intrinsically imprinted in protein sequences (Schafer et al. 2014).

Protein folding is a complex process (Levinthal 1969; 1968) and, on its success or failure, depends biological health or disease (Luheshi, Crowther, and Dobson 2008). During folding or even after it, proteins can misfold and populate non-native states. Protein misfolding inherently implies a loss-of-function, but it can also lead to a gain-of-toxicity through the establishment of non-native contacts with other functional cellular components (Luheshi, Crowther, and Dobson 2008; Chiti and Dobson 2017). Misfolded polypeptides may undergo aberrant oligomerization and aggregation into proteinaceous deposits (Ke et al. 2020; Dobson, Knowles, and Vendruscolo 2020). Protein aggregates range from amorphous assemblies lacking a defined internal order to well-organized thread-like structures called amyloid fibrils.

The risk of aggregation is ubiquitous to any polypeptide chain, and almost every protein in a proteome is predicted to contain at least one aggregation-prone region (APR) sufficient to drive the aggregation of the full protein (Ventura et al. 2004; Santos, Pujols, et al. 2020). During protein translation in the ribosome, nascent unfolded polypeptides are elongated, exposing their APRs to the solvent, which may trigger intermolecular aggregation even before folding

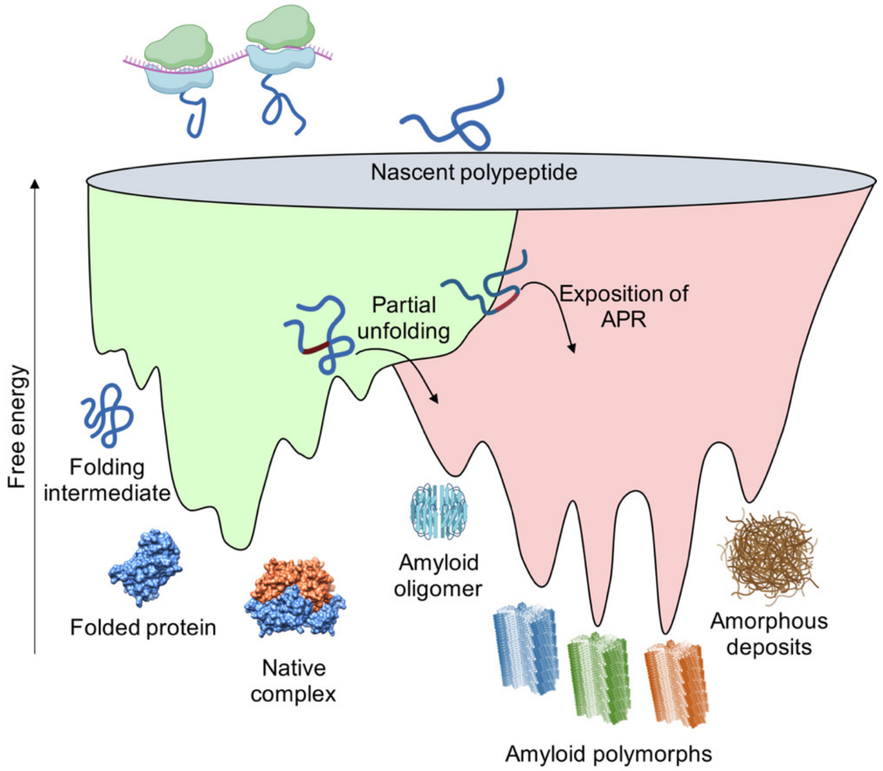

Figure 1: Schematic representation of the free energy landscape of protein folding and aggregation. The green surface represents the folding funnel leading to the thermodynamically favored native state of the protein. The red-colored area represents the multi-funneled energy landscape characteristic of protein aggregation. Red segments in proteins indicate aggregation-prone regions (APRs).

(Jahn and Radford 2008). This scenario draws a kinetic competition between folding and aggregation. Departing from an initially disordered state, the establishment of native contacts competes with non-native interactions. As the folding reaction advances, APRs are steeply shielded by native contacts and buried inside the hydrophobic core of the protein, thus reducing the risk of aggregation and contributing to create a high energy barrier that separates the native and the aggregated states in the energy landscape (Baldwin et al. 2011) (In red in **Figure 1**). However, proteins are dynamic entities and can transiently populate folding intermediates or non-native conformations that expose their APRs and trigger aggregation (Jahn et al. 2006; Neudecker et al. 2012). Thus, proteins are susceptible to aggregation at any stage of their life cycle.

Contrary to protein folding, aggregation has not been the subject of a selective pressure to shape the reaction pathway. Whereas the same type of interactions and physicochemical determinants are involved -hydrophobic effect, hydrogen bonding, and backbone-to-backbone interactions- the aggregation reaction is not funneled towards one single and functional state (Strodel 2021; Mendoza-Espinosa et al. 2009) (**Figure 1**). This concept explains the polymorphism frequently observed in protein aggregation reactions (Gallardo, Ranson, and Radford 2020). The same polypeptide sequence can aggregate into amorphous aggregates or structurally divergent amyloid fibrils, known as polymorphs, with the protein microenvironment being a major regulator of the process. This multi-funneled aggregation landscape also includes small intermediate oligomeric species formed by the association of a limited number of polypeptide chains that can be on- or off-pathway to the amyloid state. The interconversion between these metastable states and their evolution toward the final aggregation product are currently an area of intense research.

Cells have evolved a complex system to cope with the risks of aggregation either by favoring spontaneous folding, chaperone driven refolding, or aggregate disaggregation and degradation (Monsellier and Chiti 2007; Balchin, Hayer-Hartl, and Hartl 2016; Reinle, Mogk, and Bukau 2022). Indeed, cells spend a significant fraction their of cellular energy in funneling proteins toward functional states (Sherman and Goldberg 2001). In healthy cells, these protective systems are sufficient to maintain proteostasis, but changes in the environment -such as aging or oxidative stress- or in the protein -point mutations or truncations- might compromise their functioning.

Overall, the protein energy landscape is the result of a tug-of-war between folding and aggregation.

1.2.Sequence determinants of protein aggregation

The information needed for a protein to fold into its three-dimensional structure is imprinted on its primary sequence. Likewise, the propensity of a protein to aggregate is dictated by the physicochemical properties of its residues side chains. As aforementioned, the molecular determinants favoring both processes are inherently similar (Chiti and Dobson 2006; 2017).

Hydrophobicity plays a fundamental role in driving protein folding or protein-protein interactions and is also considered a major determinant of protein aggregation (Jahn and Radford 2008; Durell and Ben-Naim 2017; Castillo and Ventura 2009; Linding et al. 2004). The exposition of hydrophobic patches due to partial unfolding or conformational fluctuations facilitates non-native contacts and aggregation (Münch and Bertolotti 2010). Similarly, substitutions of polar by non-polar residues usually results in increased aggregation propensity, whereas changes in the opposite direction promote solubility (Jahn and Radford 2008). It is thus not surprising to observe that the consecutive occurrence of three or more hydrophobic residues in protein sequences is constrained by evolution (Schwartz and King 2006).

Protein aggregation does not always imply the adoption of a β-sheet conformation, but this conformational transition is often associated with protein deposition (Ventura 2005; Chiti et al. 2002). β-sheet elements are virtually accessible to any polypeptide sequence and allow the formation of extensive hydrogen-bonding networks that stabilize protein aggregates. β-sheets also provide a platform for linear propagation by stacking multiple polypeptide chains (Pallarès et al. 2004; Roterman, Banach, and Konieczny 2017). Thus, the β-sheet propensity of a sequence or the presence of pre-existing β-sheet has been reported to condition the aggregation propensity of a protein (Ventura 2005; Chiti et al. 2002). Complementarily, the propensity to form an α-helical structure introduces a significant kinetic barrier for aggregation, since it needs to be unwound for β-sheet conversion (Nerelius et al. 2009; Castillo, Chiti, and Ventura 2013).

The linear combination of these physicochemical properties in certain short sequence stretches leads to the formation of hotspots of aggregation, or APRs. APR are both sufficient and necessary to nucleate protein aggregation, implying that the solvent exposition of a short stretch of few residues can trigger the complete protein deposition (Ventura et al. 2004; Santos, Iglesias, and Ventura 2020). APRs are characterized by an enrichment in aromatic and aliphatic residues together with a certain β-sheet propensity. The properties of an APR can also be recapitulated by residues not continuous in sequence but in close proximity in the folded state, giving rise to the formation of structural APRs (Ganesan et al. 2016).

On the other side of the spectra, gatekeeper residues act as negative regulators of protein aggregation (Beerten, Schymkowitz, and Rousseau 2012). Charged residues (Beerten, Schymkowitz, and Rousseau 2012; Houben et al. 2020; Gil-Garcia et al. 2018) and β-sheet disruptors (Parrini et al. 2005; Abedini, Meng, and Raleigh 2007; Abedini and Raleigh 2006) oppose to the properties mentioned above and thus buffer protein aggregation. APRs are frequently flanked by gatekeepers that mitigate the risk of aggregation and facilitate chaperone recognition (Reumers et al. 2009; Rousseau, Serrano, and Schymkowitz 2006; Beerten et al. 2012). This concomitant evolution of gatekeepers and APRs evidences a selective pressure controlling the impact of these sticky stretches.

1.3. Intrinsically disordered proteins and their aggregation landscape

The aforementioned dichotomy between folding and aggregation has yet another layer of complexity when we consider protein disorder. Intrinsically disordered proteins (IDPs) lack a defined three-dimensional structure; therefore, the competition between folding and aggregation becomes blurry in these polypeptides.

IDPs are proteins that do not require a defined globular structure to perform their functions but populate a dynamic ensemble of unfolded or partially folded conformations (H. Jane Dyson and Wright 2005; H. J. Dyson and Wright 1998). The concept of disorder is not restricted to fully disorder IDPs but encompasses a whole continuum of structural manifestations; folded proteins that contain only local disorder in short loops or tails, modular proteins linked by disorder regions, molten globules with certain secondary structure and disordered domains in multidomain proteins (R. van der Lee et al. 2014). The disordered nature of IDPs stems from their lack of hydrophobic cores and their particular compositional bias, being enriched in polar and charged residues and depleted in aliphatic amino acids (Radivojac et al. 2007). Thus, they usually have a high net-charge and low hydrophobicity, populating a defined space in the charge-hydropathy plot (**Figure 2A**) (Uversky, Gillespie, and Fink 2000; Santos, Iglesias, et al. 2020).

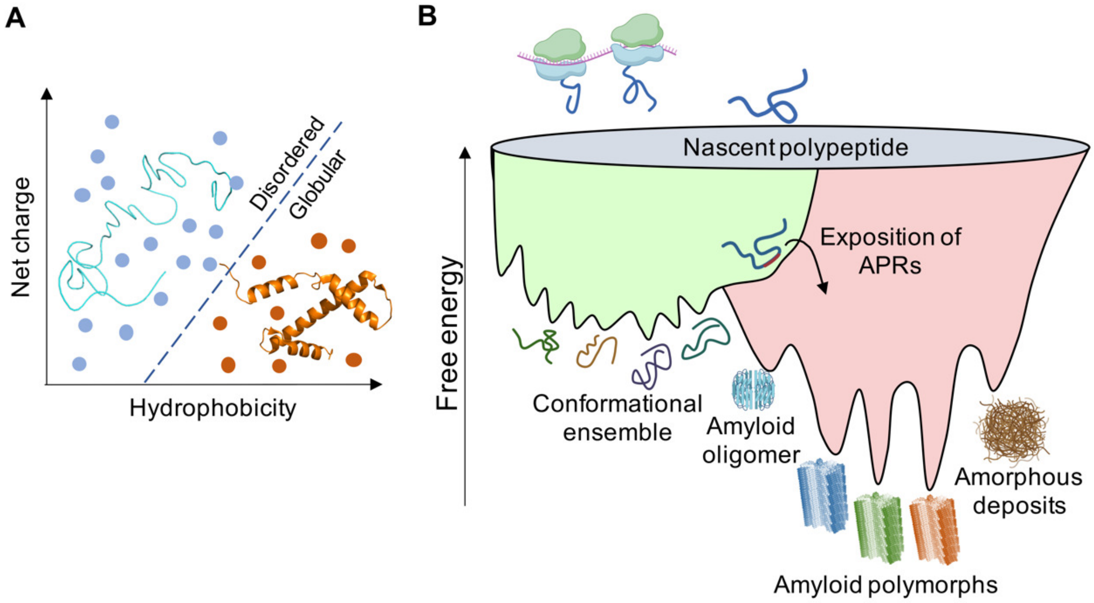

Figure 2: Charge-hydropathy plot and free energy landscape of intrinsically disordered proteins. (**A**) Net charge-hydropathy plot illustrating the sequence space covered by intrinsically disordered (blue) and globular (orange) proteins. (**B**) Schematic representation of the energy landscape of protein folding and aggregation adapted to intrinsically disordered proteins. The color code is equivalent to **Figure 1**.

The conformational plasticity and dynamism of IDPs allow them to adapt to structurally diverse targets and perform a plethora of functions (Tompa, Szász, and Buday 2005; Van Roey et al. 2014). IDPs are often involved in mediating protein-protein interactions, acting as molecular switches and signal integrators that coordinate complex networks in biologically relevant processes. Noteworthy, recognition and binding of their physiological ligands often involve disorder-to-order transitions (a process known as folding-upon-binding) and the formation of complexes that retain a diverse grade of disorder (Robustelli, Piana, and Shaw 2020; Tompa and Fuxreiter 2008; Bonetti et al. 2018).

From the aggregation perspective, IDPs have been traditionally considered depleted in APRs since their compositional bias -high content of gatekeepers and β-breaker residues- should protect them against aggregation (Langenberg et al. 2020; Linding et al. 2004). However, the aggregation of several IDPs is associated with human disorders, including some of the most studied amyloidogenic proteins such as α-synuclein (αS), the amyloid-β peptide (Aβ), the islet amyloid polypeptide, or huntinting 1 (Dobson, Knowles, and Vendruscolo 2020). This apparent contradiction can be explained by three factors. (i) The free energy landscape of IDPs does not funnel into a single or few low energy states but is composed of multiple shallow energy minima that represent the conformations sampled by the IDP (Strodel 2021) (**Figure 2B**). This implies that thermodynamically the native conformation of IDPs is less protective than in globular proteins, being easier to switch to the aggregation side of the energy landscape conformed by deeper energy minima. (ii) Albeit the global compositional bias of IDPs, the interaction with other proteins or macromolecules entails regions that display a higher local hydrophobicity and hydrogen-bonding capacities. In a recent computational analysis, we demonstrated that these functional regions retain a cryptic amyloidogenic potential (Santos et al. 2021) (iii) The extended nature of IDPs increases the solvent-exposition of these regions, having a higher risk of switching to the aggregation side of the energy landscape (**Figure 2B**). Together, these three factors help to explain the enrichment of IDPs in amyloid-related diseases and expand the aggregation-folding dichotomy beyond globular proteins.

1.4. Amyloid fibrils

The aggregation of proteins into amyloid fibrils has been related to the onset of more than 40 human diseases, including Alzheimer's disease, Parkinson's disease (PD), and type II diabetes. Recently, the amyloid fold has been connected with the development of different biological functions, acting as an evolutionary conserved quaternary structure. Accordingly, the amyloid fold is of great significance for biology and medicine.

Amyloid fibrils are long, unbranched thread-like structures with few nanometers in diameter and microns in length (**Figure 3A**). Fibrils can comprise one or more protofilaments laterally associated and often twisting around each other (Paravastu et al. 2008; Close et al. 2018). The core of the protofilament is formed by β-strands stacked perpendicular to the fibril, forming extended networks of intermolecular β-sheets with a characteristic arrangement known as cross-β (**Figure 3B**) (D. Eisenberg and Jucker 2012; D. S. Eisenberg and Sawaya 2017). This structural architecture results in a distinctive X-ray diffraction pattern (**Figure 3C**) (Sunde and Blake 1997; Iłowska et al. 2022). This extensive array of hydrogen bonded β-sheets confers high mechanic and thermodynamic stability to amyloid fibrils (Knowles et al. 2007). Indeed, the amyloid state generally has higher thermodynamic stability than native states (Baldwin et al. 2011; Gazit 2002). Amyloid fibrils bind to generic amyloid dyes such as Congo Red and Thioflavin-T (Th-T) that are universally employed to monitor fibril formation (Chiti and Dobson 2017). These generic properties are common to amyloids formed by structural and sequentially diverse protein precursors.

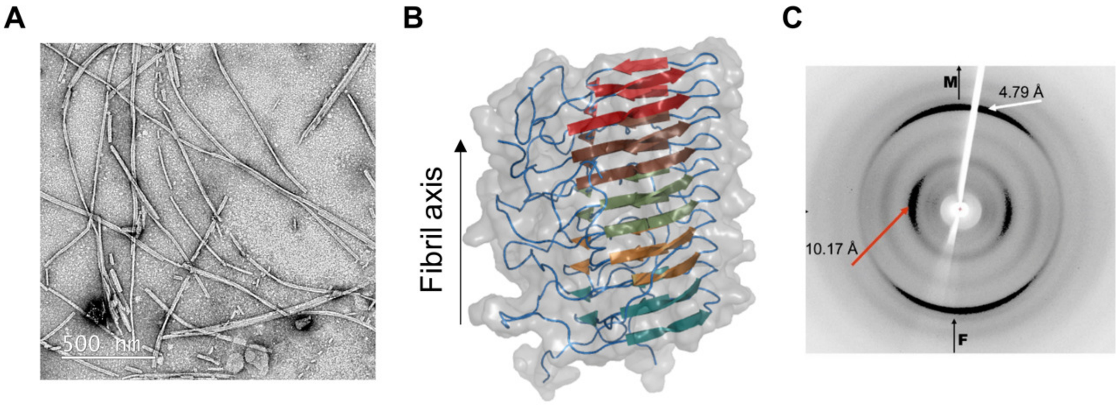

Figure 3: Structural features of amyloid fibrils. (**A**) Electron microscopy micrograph showing the morphology of amyloid fibrils. (**B**) Atomic structure of the HETs amyloid fibril (PDB: 2RMN). Colors indicate different chains. (**C**) Characteristic X-ray diffraction pattern of an amyloid fibril. Extracted from reference (Iłowska et al. 2022).

From a low-resolution perspective and considering the common properties of amyloid fibrils, amyloids may be seen as a uniform structural arrangement that only permits a limited set of conformations at their tightly packed core. However, the recent advances in fibril structure determination by cryoelectron microscopy (cryoEM) and solid-state nuclear magnetic resonance (ssNMR) proved that the same polypeptide sequence can adopt a surprising variety of dispositions in the amyloid state (Close et al. 2018; Shi et al. 2021; Guerrero-Ferreira et al. 2019). This phenomenon, known as polymorphism, has several layers of complexity; the same polypeptide sequence can adopt multiple folds in the fibril, the amyloid core can be formed by different residue stretches or fibrils can differ in protofilament number and packing. *In vitro* amyloid polymorphism is known to be modulated by the aggregation conditions, mutations or posttranslational modifications and the presence of binding partners (Bousset et al. 2013; Sun et al. 2021; Frieg et al. 2022; Watson and Lee 2019). *In vivo*, amyloid polymorphs of the same proteins are associated with different pathologies. For instance, in tauopathies such as Alzheimer's disease, Pick's disease, Chronic Traumatic Encephalopathy, or Progressive Supranuclear Palsy, disease-specific structural polymorphs have been reported (Falcon, Zhang, Murzin, et al. 2018; Falcon, Zhang, Schweighauser, et al. 2018; Shi et al. 2021). It is though that the cellular type and environment, the molecular mechanism triggering aggregation and the specific aggregation pathway play fundamental roles in this phenomenon.

Finally, amyloid fibrils have the potential to recruit functional monomers and catalyze their conversion to fibrils, self-perpetuating the amyloid state (D. S. Eisenberg and Sawaya 2017; Meisl et al. 2022). In several neurodegenerative disorders, such "prion-like" activity propagates the disease through the brain, with amyloid fibrils acting as "seeds" that induce the aggregation of the native protein in healthy cells (Luk et al. 2012; Aguzzi and Rajendran 2009). This seeding process tends to replicate the structure of parental seeds (Riek and Eisenberg 2016), perpetuating the specific polymorph that started the infectious cascade and thus explaining the dominance of particular polymorphs in specific diseases.

1.5. Kinetics of amyloid formation

The process of amyloid fibril formation involves the transition of proteins from their soluble monomeric conformation to the macromolecular amyloid state. This complex process is highly dependent on the intrinsic sequence features and strongly modulated by environmental conditions. External factors such as pH, salt concentration, or the presence of lipid membranes strongly reshape the kinetic profile of amyloid formation (Morel et al. 2010; Nielsen et al. 2001; Kurochka et al. 2021).

Macroscopically, in most cases, the kinetics of amyloid formation can be described as a nucleation-dependent polymerization with three well-defined phases (Jarrett and Lansbury 1993) (**Figure 4A**): (i) A first *nucleation phase* (also known as lag phase) defined as the slow and thermodynamically unfavorable association of monomers to form the first aggregation nucleus able to self-propagate. Accordingly, the addition of preformed fibrils skips this nucleation phase. (ii) The *elongation phase* in which these first nuclei elongate by monomer addition in a fast and thermodynamically favorable process that leads to exponential amyloid fibril formation. (iii) The *plateau phase* when fibril growth stops due to monomer exhaustion. These three phases result in the characteristic sigmoidal profile observed in time-dependent fibril formation experiments.

However, microscopically, this process is far more complex (Michaels et al. 2018; Dobson, Knowles, and Vendruscolo 2020) (**Figure 4B**). The formation of the first nucleus involves the association of few precursors to form oligomeric species that can dissociate back to monomers or interconvert to other oligomers (that can be on- or off-pathway to the amyloid fibril) before the formation of the first elongation-competent nucleus (Dear et al. 2020; Kjaergaard et al. 2018; Nunilo Cremades et al. 2012) (Yellow background in **Figure 4B**). Then, the elongation phase not only includes monomer addition to the tips of the fibrils (Blue background in **Figure 4B**) but also secondary nucleation mechanisms such as fragmentation or surface catalyzed secondary nucleation that led to the formation of new nucleus (Törnquist et al. 2018; Arosio, Knowles, and Linse 2015) (Red background in **Figure 4B**). Fibrils can also dissociate back into monomers or release oligomers (Nunilo Cremades et al. 2012; Cascella et al. 2021) (Green background in **Figure 4B**).

Although the mechanistic bases of these processes are still a subject of intense research, recent mathematic and analytical efforts thrived to describe this intricate phenomenology of associative, dissociative and structural transitions in terms of chemical kinetics and microscopic rate laws (Meisl et al. 2016; Dear et al. 2020; Meisl, Knowles, and Klenerman 2022). This understanding is instrumental to shed light into the aggregation process and discover new ways to fight it (Linse et al. 2020; Cohen et al. 2013; Meisl et al. 2014; Chia et al. 2018). Unfortunately, this kinetic description is still waiting for structural and mechanistic information of these microscopic conversions, being this a large unmet need in the field.

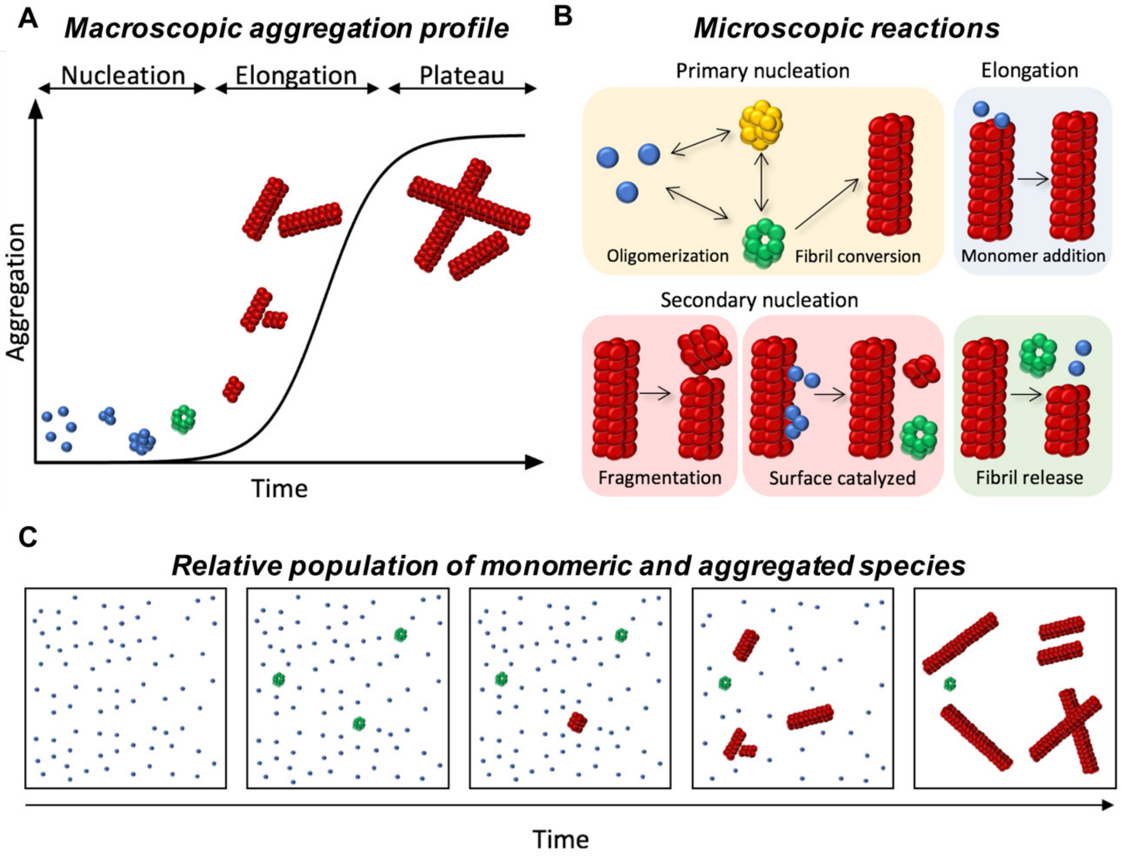
A
Macroscopic aggregation profile
Nucleation
Elongation
Plateau
Aggregation
Time
B
Microscopic reactions
Primary nucleation
Elongation
Oligomerization
Fibril conversion
Monomer addition
Secondary nucleation
Fragmentation
Surface catalyzed
Fibril release
C
Relative population of monomeric and aggregated species
Time

Figure 4: Kinetics of amyloid formation. (**A**) Illustration of the sigmoidal aggregation profile representing the three macroscopic phases of amyloid formation. Monomers (blue) initially present in the aggregation reaction self-associate into oligomers (green) that later convert into amyloid fibrils (red). (**B**) Microscopic reactions occurring in amyloid formation. (**C**) Schematic representation of the different species coexisting in an aggregation reaction.

1.6. Oligomeric species

In the amyloid field, the term “oligomer” is commonly used to englobe a myriad of relatively low molecular weight prefibrillar aggregates populated during the nucleation phase. The specific aggregation determinants of each particular amyloidogenic protein, together with the multiplicity of pathways that can lead to amyloid formation, result in an extremely high level of structural diversity in the oligomer universe. This heterogenicity is reflected in terms of size (i.e. dimers, tetramers, high order multimers), β-sheet content (from fully disorder to amyloid-like contents), degree of solvent exposed hydrophobicity, amyloid dye binding, relative life-time in the aggregation reaction (transient or more persistent) and elongation capacities (Dear et al. 2020; Glabe 2008; Nguyen et al. 2021). On a practical level, it implies that it is intrinsically difficult to define common structural and physicochemical traits shared by all oligomeric species, which contrast the well-defined features of the amyloid state.

Despite their diversity, there are two key features of oligomers that help to explain the increasing association of oligomers with cellular disfunction. (i) Compared to fibrils composed of thousands of monomer copies, oligomers have a much lower molecular weight and therefore a higher diffusion coefficient. Their higher diffusivity implies a higher chance to stablish aberrant interactions with cellular components, easier cell-to-cell transmission and cellular uptake (Morten et al. 2022). (ii) Fibrils are at a thermodynamic global minimum in the free energy landscape, being very stable and difficult to disaggregate (Baldwin et al. 2011; Gazit 2002). This also implies that they are less prone to interact with other cellular components compared to metastable oligomers that display higher dynamism and might expose hydrophobic regions to the solvent.

From a kinetic perspective, amyloid oligomers have been shown to be critical intermediates in the formation of amyloid fibrils (Dear et al. 2020). In various amyloidogenic proteins, the relative concentrations of monomers, oligomers and fibrils can be fitted to a model of oligomer-mediated fibril formation that proves their kinetic importance in the reaction (Dear et al. 2020). These analyses also demonstrate that oligomers are nonfibrillar species that need a structural transition to maturate into amyloid fibrils before being able to rapidly grow by monomer addition. This is not a unidirectional process, and the majority of oligomers do not evolve into fibrils; they dissociate back to monomers or persist in the oligomeric state due to a relatively high kinetic stability. Even though in the literature, the term “oligomer” is also assigned to any small fibrillar and prefibrillar aggregates (Glabe 2008), this kinetic analysis provides a stricter definition of amyloid oligomers as nonfibrillar and non-capable of elongation metastable intermediates, that better reflects the type of oligomers studied in this thesis.

This scenario also indicates that the oligomer to fibril transition is a rate-limiting step that supposes a major barrier to fibril formation and therefore, it constitutes a privileged target for therapeutic intervention in amyloid-linked diseases. By targeting a small population of oligomers and blocking this step, the kinetic productivity of amyloid formation will be severely reduced.

Unfortunately, we currently have very limited structural information on amyloid oligomers. The cylindrin β-barrel constitutes the first high resolution evidence of a globular oligomer but only corresponds to a 11-residue protein fragment, having thus limited biological relevance (Laganowsky et al. 2012). Aβ42 tetramers and octamers formed in the presence of a detergent (Dodecylphosphorylcholine) have also been determined by NMR but it is not clear if they represent a relevant conformation or have a kinetic role in the aggregation (Ciudad et al. 2020). Thus, to date, there is no atomic structure of a natural full-length oligomer in solution. The dynamic and transient nature of oligomers generally precludes a high-resolution characterization, even if certain structural traits have been extracted from ssNMR, Fourier transform infrared spectroscopy (FTIR), small-angle X-ray scattering (SAXS), CryoEM and atomic force microscopy analysis (Chen et al. 2015; Fusco et al. 2017; Lorenzen et al. 2014). For instance, it is worth noting that a significant number of amyloidogenic proteins have been reported to form oligomers with a doughnut-like shape, including Aβ, αS, IAPP and serum amyloid A (Kayed et al. 2003; Lashuel, Hartley, et al. 2002; Quist et al. 2005).

Regarding their implication in disease, oligomers are thought to be important pathogenic species in the onset and progression of amyloid related disorders. Generally, oligomers are associated with gain-of-toxicity activities such as membrane disruption (Flagmeier et al. 2020), induction of oxidative stress (Deas et al. 2016), proteasome impairment (Thibaudeau, Anderson, and Smith 2018) and mitochondrial disfunction (Lasagna-Reeves et al. 2011). Accordingly, oligomeric forms of different amyloidogenic proteins have been identified in the tissue of patients suffering from neurodegenerative disorders and in correlation with cellular dysfunction (Pountney et al. 2004; De et al. 2019; Emin et al. 2022; Choi et al. 2022; Kolarova et al. 2017; Sanderson et al. 2020). Yet, it is not clear if oligomers can propagate the disease in a prion-like manner as amyloid fibrils do (Froula et al. 2019). Considering this, it is now hypothesized that oligomers are the primary cytotoxic agents, whereas amyloid fibrils are responsible for disease spreading; a framework in which oligomer formation occurs via fibril surface catalysis or amyloid disaggregation is attracting increasing attention (Michaels et al. 2020; Cascella et al. 2021).

1.7. The aggregation mixture: coexistence of monomers, oligomers and fibrils across the aggregation reaction

Studying the species populated along an aggregation reaction is challenging. Whereas it is possible to study isolated preparations of monomeric proteins or mature amyloid fibrils at the end of aggregation reactions, intermediate species are usually low populated, transient and coexist with a mixture of diverse monomeric and aggregated forms (Dear et al. 2020; Nunilo Cremades et al. 2012). When describing an aggregation reaction, it is common to think in sequential steps where we have monomers, then oligomers, small fibrils and finally the amyloid fibrils. One should, however, keep in mind that these species are populated simultaneously and at different concentrations, creating a mixture here referred to as “aggregation soup” (**Figure 4C**).

Once the aggregation reaction begins, oligomeric species -a heterogenous mixture of structurally diverse oligomers- start forming and accumulating up to 10% of the total protein (Dear et al. 2020). During this period, oligomers coexist with >90% of monomeric protein. After the formation of the first fibrillar nucleus and the beginning of the elongation phase, monomers, oligomers, and fibrils coexist at different concentrations until monomer exhaustion in the steady phase. Therefore, for most of the aggregation reaction, several species are simultaneously populated. On top of that, oligomers are often in equilibrium with monomers which implies that monomer exhaustion causes oligomer dissociation (Dear et al. 2020).

It is then highly challenging to identify, quantify, characterize or isolate intermediate species. They are difficult to purify due to the excess of other species and in the process a significant part of the population dissociates back into monomers or progresses to fibrillar aggregates. Likewise, the contribution of low populated oligomers is usually not reflected in ensemble averaged experimental techniques, hidden by the monomer signal.

In this scenario, many of the advances we have witnessed in the last decade relied on two pillars; the use of single-molecule approaches to quantify and characterize low-populated species, and the development of protocols that allow the preparation of isolated oligomeric samples for structural characterization. For instance, the kinetic analyses discussed in the previous sections stem from oligomer quantification using single-molecule approaches.

Overall, the aggregation soup concept illustrates the challenges and constrains of studying amyloid oligomers.

2. α-Synuclein aggregation in neurodegenerative disorders

αS is a small IDP whose aggregation has been extensively studied due to its association with the onset of a series of debilitating neurodegenerative disorders known as synucleinopathies. αS oligomers and fibrils have been identified in patients' brains and are implicated in the development and progression of such disorders. In this thesis, we focus on the structural characterization and targeting of αS toxic assemblies with the aim of increasing our current understanding of their structural biology and developing therapeutic and diagnosis alternatives with translational potential. In this section, I will introduce some key features of αS, its aggregation process and its relevance to disease in order to contextualize the research performed here.

2.1. α-Synuclein

αS is a 140 residue IDP abundantly expressed in neurons in the mammalian nervous system (Uéda et al. 1993). αS localizes in the presynaptic terminals, both in the cytosol or synaptic membranes (Maroteaux, Campanelli, and Scheller 1988). Within the cytosolic context, αS behaves as an IDP and adopts short-lived compact conformations with continuous structural fluctuations (Theillet et al. 2016; Dedmon et al. 2005). Up to a third part of the αS pool is found interacting with lipid moieties, folding upon lipid binding in an amphipathic α-helix that anchors the protein to membranes (Trexler and Rhoades 2009; Fusco, Sanz-Hernandez, and De Simone 2018) . This ability to fluctuate between both states is postulated to be directly related to αS biological function (Fusco et al. 2016). Although still not fully understood, αS seems to be implicated in synaptic vesicle trafficking and neurotransmitter release and known to interact with several synaptic proteins.

The accumulation of αS aggregates in neurons, nerve fibers, or glial cells is the main histopathological signature of synucleinopathies (Spillantini et al. 1997; McCann et al. 2014;

Spillantini and Goedert 2000). Parkinson's disease (PD) is the most prevalent disorder of this group of syndromes, which also includes dementia with Lewy bodies (DLB), Parkinson's disease dementia (PDD), multiple system atrophy (MSA) and juvenile onset synucleinopathy (JOS) (Y. Yang, Garringer, et al. 2022). Additionally, αS deposits have been found in a number of patients suffering from Alzheimer's disease (Arai et al. 2001; Hamilton 2000).

αS primary sequence is typically divided in three domains according to their differential physicochemical properties and activities (**Figure 5A**). The N-terminal domain (1-60) is an amphipathic and lysine-rich region that participates in membrane interactions adopting a helical conformation (Ulmer et al. 2005) (**Figure 5B**). The NAC (Non amyloid-β component) region (61-95) has a marked hydrophobic character and can also be incorporated into the helical structure in the membrane bound state (Ulmer et al. 2005). Finally, a very flexible C-terminal domain that is highly anionic and remains disordered both in solution and in the membrane bound state (Ulmer et al. 2005; McClendon, Rospigliosi, and Eliezer 2009). αS contains seven imperfect repeats (KTKEGV) covering the N-terminal and part of the NAC region, responsible for the hydrophobicity patterning driving membrane binding (Bussell and Eliezer 2003). Charge distribution is uneven across the sequence with +4 in the N-terminal, -1 in the NAC and -12 in the C-terminal.

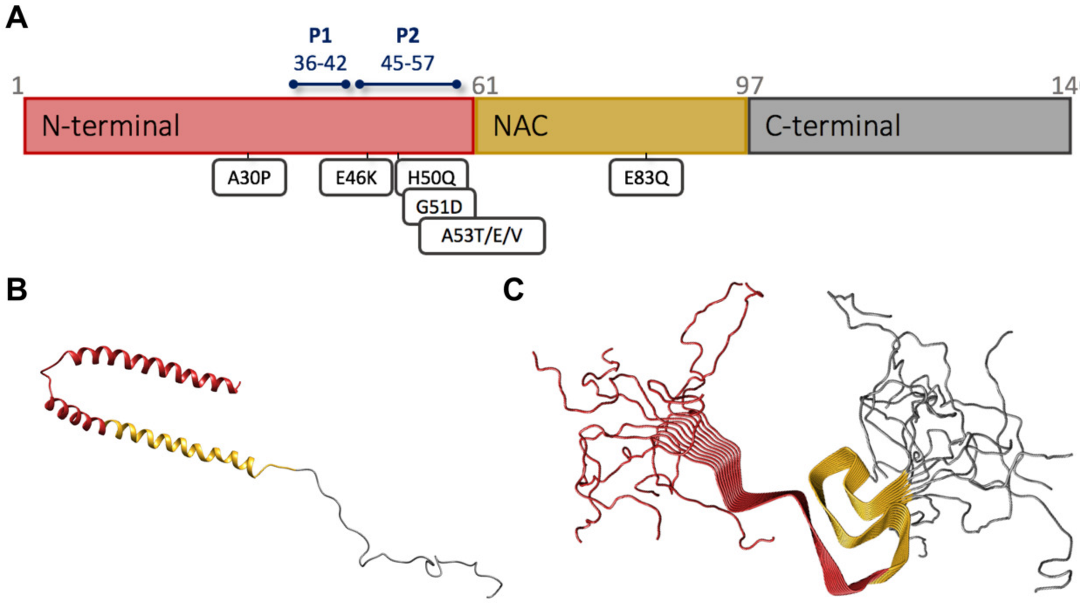

Figure 5: α-Synuclein sequence and structure. (**A**) Schematic domain organization of α-synuclein. fPD mutations and P1 and P2 regions are indicated. (**B**) Structure of a micelle-bound α-synuclein monomer (PDB: 1XQ8). (**C**) Structure of an α-synuclein fibril determined by solid-state nuclear magnetic resonance (PDB: 2N0A). The three domains are color-coded according to (A).

This asymmetric organization of the αS biochemical properties is also related to its aggregation. The NAC domain is considered the principal element driving αS aggregation (**Figure 5C**), being essential and sufficient for amyloid fibril formation (Giasson et al. 2001). This region also forms the core of αS fibrils (Tuttle et al. 2016; B. Li et al. 2018). However, full-length αS aggregation requires the contribution of other regions. The N-terminal domain is gathering increasing attention due to recent reports identifying regions modulating amyloid formation. The extreme N-terminal residues (1-11), are fundamental for monomer recruitment to oligomers and fibrils, actively participating in surface-catalyzed secondary nucleation (X. Yang et al. 2021; Kumari et al. 2021). Accordingly, extreme N-terminal truncations delay amyloid formation. It was recently reported that two N-terminal segments, named P1 (36-42) and P2 (45-57), act as master regulators of amyloid formation; P1 deletion or single alanine substitutions at positions Y39 and S42 inhibit amyloid formation (Doherty et al. 2020; Ulamec et al. 2022). The effect of P2 deletion is milder but acts synergistically with P1. This renewed interest in the modulatory N-terminal domain also stems from the fact that most single point mutations associated with familial PD (fPD) map into this region (Positions 30, 46, 50, 51, 53), while only the recently identified mutation at position 83 is in the NAC domain (Kumar et al. 2022) (**Figure 5A**). In contrast, the C-terminal tail acts as a solubilizing element due to its extremely anionic character (Z. A. Sorrentino and Giasson 2020; Farzadfard et al. 2022). C-terminal truncations or charge compensation by pH or ionic strength increase the aggregation propensity (Buell et al. 2014; Z. A. Sorrentino et al. 2018).

In solution, monomeric αS populates an ensemble of compact states with a smaller radius of gyration than expected if it was an extended random coil (Dedmon et al. 2005; Theillet et al. 2016). This compaction is driven by long range interactions involving distinct domains, with identified contacts between the N- and C-terminal domain and both of them with the NAC (Zhang et al. 2021; Theillet et al. 2016; Bertoncini et al. 2005). These tertiary contacts are thought to be fundamental to maintain αS solubility in the cell by shielding the hydrophobic residues of the amyloidogenic NAC region. This protective mechanism -similar to burying the hydrophobic core in globular proteins- explains why αS can accommodate such a high amyloidogenic load and justifies the chaperoning activity of the C-terminal domain.

2.2. α-Synuclein aggregates

In this section, I will review the properties of αS oligomers and fibrils with a special focus on oligomers formed during aggregation kinetics and their kinetically trapped analogs.

2.2.1. α-Synuclein oligomers

The observation of small spherical and/or annular oligomers in αS aggregation reactions in both WT and fPD-associated variants more than 20 years ago prompted the hypothesis that these species may have an important role in cellular dysfunction in PD (Lashuel, Hartley, et al. 2002; Lashuel, Petre, et al. 2002) (**Figure 6A**). The annular shape of these oligomers suggested that they may behave as pore-forming bacterial toxins and cause membrane permeabilization. These annular oligomers have also been observed in post-mortem biopsies from patients with MSA (Pountney et al. 2004). Yet, their study and characterization using conventional techniques has been hampered by their low-population and transient nature. Many approximations were developed to trap oligomers of diverse morphologies through the use of chemical compounds, covalent crosslinking or modification of the solvent conditions (detailed review in (N. Cremades, Chen, and Dobson 2017)), but it was unclear to which extent those trapped oligomers recapitulate the properties of those populating standard aggregation reactions.

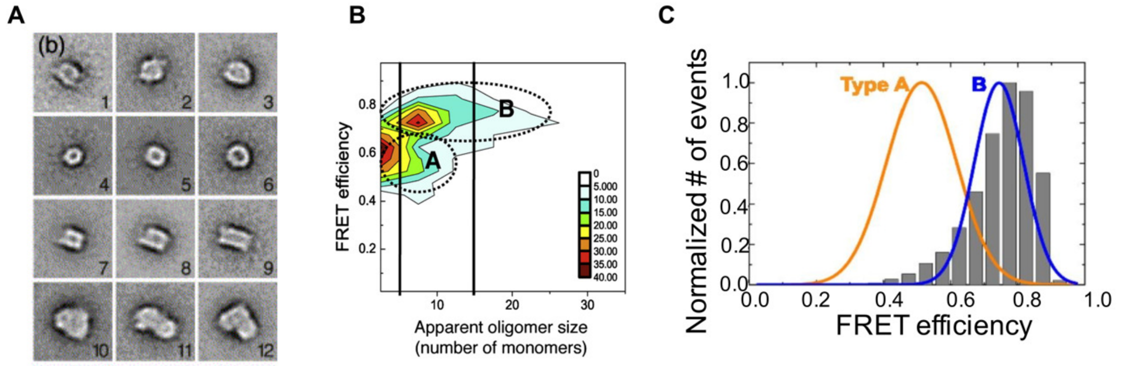

Figure 6: α-Synuclein oligomers. (**A**) Microelectron micrographs of α-synuclein oligomers. Reproduced with permission from (Lashuel, Petre, et al. 2002). (**B**) 2D plot of the number distribution of oligomers after 60 hours of incubation showing their FRET efficiency distributions (vertical lines corresponding to apparent oligomer sizes of 5- and 15-mer). Two oligomer populations (named A and B) can be identified. Reproduced from (Nunilo Cremades et al. 2012). (**C**) Single-molecule FRET efficiency distribution of type-B* oligomers (shown in gray bars) and the two main oligomeric species (type-A and type-B) found during αS fibril formation. Reproduced with permission from (Chen et al. 2015).

Single molecules techniques boosted the field by allowing quantitative and qualitative analysis of the populations of oligomers formed during aggregation reactions. Under standard aggregation conditions (Neutral pH, 37 °C and under agitation), two populations of oligomers (named type-A and type-B) are sequentially populated during αS lag phase, showing distinct structural arrangements, as evidenced by their different single-molecule Förster resonance energy transfer (smFRET) signature (Nunilo Cremades et al. 2012) (**Figure 6B**). smFRET efficiency is inversely related to the sixth power of the distance between the fluorescence labels, being a sensitive method to distinguish different oligomer's conformations. The initially formed type-A oligomers have a low-FRET-efficiency, are protease sensitive and devoid of cellular toxicity. Type-A oligomers later convert into protease resistant, high-FRET-efficiency type-B oligomers that elicit high cellular toxicity. Recently, Choi and coworkers exploited smFRET to observe the formation of type-A oligomers and their conversion to type-B oligomers inside neurons, which confirmed the biological relevance of these oligomers (Choi et al. 2022). Type-B oligomers are then considered disease relevant oligomers that can be assembled by αS under physiological conditions.

Oligomers with similar smFRET signatures than type-B can also be released from amyloid fibrils (Nunilo Cremades et al. 2012). Notably, such oligomer release has been shown to account for fibril toxicity indicating, that fibrils can act as reservoirs of these toxic assemblies (Cascella et al. 2021).

Leveraging smFRET information, Chen et al. developed a new strategy to obtain stable and kinetically trapped oligomers structurally analogous to type B (named type B* to reflect their kinetically trapped nature) (Chen et al. 2015). Type B* oligomers show the same smFRET signature as type B, indicating an equivalent molecular architecture, and have the same annular morphology (**Figure 6C**). Type B* oligomer preparations only require a lyophilization step of monomeric αS followed by resuspension in phosphate-buffered saline (PBS), incubation for 20 hours at 37 °C and centrifuge-based separation. Purified type B* oligomer preparations are stable for days, contain around a 90% of the sample in the oligomeric state, the rest is monomeric and can be produced at yields sufficient for structural characterization (1% of total initial protein). Importantly, type B* oligomers reproduce the cellular toxicity observed in type B oligomers, being commonly used as the model αS oligomers in cellular and animal-related experiments (Chen et al. 2015; Froula et al. 2019; Perni et al. 2018; Cascella et al. 2022).

Additionally, the inhibitory molecule (-)-EpiGalloCatechin-3-Gallate (EGCG) has been used to produce kinetically trapped type-A* oligomers with a smFRET signal equivalent to type-A, being used as non-toxic counterparts of type-B* oligomers (Fusco et al. 2017). Unfortunately, EGCG mechanism of action is unclear, restraining the relevance of the structural and biophysical information that can be obtained.

Type-B* oligomers are then the gold standard for structural (further discussed in the next section) and functional characterization of αS oligomers. In spite of this, there is a certain controversy in the field since it is not clear why these oligomers are kinetically trapped, and which are the specific differences between them and type B. Demonstrating the potential of type-B* oligomers to provide insights on αS disease-relevant oligomerization is then of critical importance to understand the role played by these species in synucleinopathies.

2.2.2. Structural features of type B* kinetically trapped α-synuclein oligomers

The analysis of type-B* oligomers revealed critical structural features of these toxic assemblies. Reconstruction of type-B* oligomers by cryoEM rendered a cylindrical shape architecture with a central hollow core (Chen et al. 2015) (**Figure 7A**). Two populations of different sizes were identified in agreement with analytical sedimentation experiments. These oligomers had an average of 19 or 29 αS monomers respectively and dimensions ranging from 120-140 Å in length and 90-100 Å in diameter. The central cavity had approximately 25 Å. The rigid core of the oligomer is formed by residues 70 to 89 as probed by magic-angle spinning (MAS) (ssNMR) ^{13}C–^{13}C dipolar-assisted rotational resonance (DARR) (Fusco et al. 2017) (**Figure 7B**). Highly mobile regions corresponding to residues 1 to 38 and 95 to 140 were assigned using insensitive nuclei enhanced by polarization transfer (INEPT) (**Figure 7B**). Based on this analysis, only 15% of the αS sequence is sufficiently rigid for ssNMR characterization, illustrating the structural heterogenicity and fuzziness of αS oligomers.

Since disordered segments are averaged out in cryoEM reconstructions, SAXS measurements of type-B* oligomers were essential to characterize the outer shell of disordered tails that surrounds the denser core of the oligomer (Farzadfard et al. 2022) (**Figure 7C**). The anionic C-terminal tail of αS, known to be intrinsically disordered in the oligomer, gives a negative character to this unfolded fuzzy coat. This outer unstructured corona is not visible by EM but contributes to a significant part of the oligomer volume and protects them from lateral

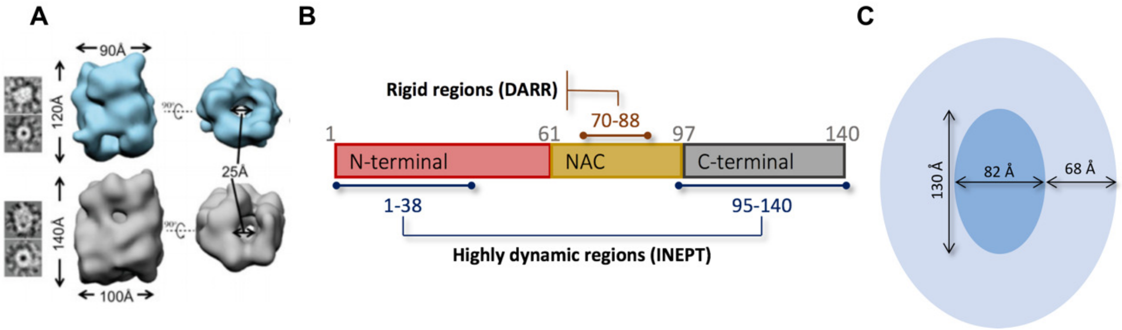

Figure 7: Structural features of α-synuclein oligomers. (**A**) CryoEM 3D reconstruction of type-B* oligomers. Two size populations are represented in blue and gray. Reproduced with permission from (Chen et al. 2015). (**B**) Schematic representation of ssNMR assignments in type-B* oligomers as reported in (Fusco et al. 2017) (**C**) SAXS reconstruction of type-B* oligomers. Adapted from reference (Farzadfard et al. 2022).

associations (Franco, Cuéllar, et al. 2021). Such repulsion between oligomers' anionic fuzzy coats probably explains why these oligomers can be manipulated at the high concentrations required for cryoEM or ssNMR without undesired associations.

Analysis of αS type-B*oligomers using FTIR spectroscopy revealed ≈ 35 % of β-sheet content with a predominantly antiparallel geometry that contrast the parallel β-sheet observed in all αS polymorphs (Chen et al. 2015). This orientation was recurrently observed in other oligomers formed by αS and several other amyloidogenic proteins, including the cylindrin β-barrel (Laganowsky et al. 2012). This apparent structural contradiction is, however, in line with the here discussed nonfibrillar nature of oligomers (section 1.6) (Dear et al. 2020); the parallel β-sheet signature in αS amyloids arises from the contacts between different fibril layers and such contacts are not expected in a nonfibrillar oligomer. Consistently, αS type-B*oligomer preparations show marginal Th-T binding (Chen et al. 2015). Together, the kinetic and thermodynamic metastability of αS oligomers can be explained by the energy barrier imposed by the structural divergence between the contacts sustaining the oligomer and fibril structure.

The solvent-exposed hydrophobicity of αS type-B* oligomers exceeds that of the fibrils and monomers and has been proposed to account for oligomer promiscuous interactions and subsequent cellular toxicity (J.-E. Lee et al. 2018; Chen et al. 2015). Type-B* oligomer toxicity has also been associated with membrane binding, known to be mediated by the N-terminal domain and impaired by extreme N-terminal deletion and the genetic A30P mutation associated with fPD. Additionally, type-B* oligomers induced cellular toxicity has been associated with lipid binding, metal interactions and Ca^{2+} dysregulation (Fusco et al. 2017; Deas et al. 2016; Angelova et al. 2016).

Finally, genetic mutations associated with fPD (A30P, E46K, H50Q, G51D and A53T) have been reported to affect oligomers structure, generating oligomer polymorphism (Xu et al. 2022). Whereas the overall structural features of these mutants in terms of size and antiparallel β-sheet content are relatively similar, with only slightly different population distributions or relative β-sheet content, the most remarkable difference observed in this work was captured by circular dichroism spectroscopy. G51D oligomers presented a batch-dependent α-helical contribution that contrasted with the β-sheet rich conformation observed in the WT. Such structural variation was associated with decreased solvent exposition of hydrophobic regions. In A30P and E46K oligomers a certain deviation towards helical structures can also be intuited. This conformational heterogenicity evidences certain plasticity in αS oligomers while preserving an antiparallel β-sheet core. Noteworthy, G51D oligomers displayed higher cellular toxicity on SH-SY5Y cells, decoupling the previously stablished association between hydrophobicity and toxicity. Together with the previous observation that G51D mutation reduces oligomer's membrane disruption properties (Stefanovic et al. 2015), it can be proposed that oligomer toxicity is not unequivocally associated with membrane disruption.

2.2.3. α-Synuclein fibrils

The recent advances in cryoEM and ssNMR in the last decade crystallized in the resolution of more than 100 amyloid structures. Since the first determination of an αS fibril structure at atomic resolution in 2016, more than 20 polymorphs have been determined at atomic resolution including fibrils generated *in vitro*, extracted from patients' tissues, with point mutations or truncations and in presence of lipids (Tuttle et al. 2016; McGlinchey et al. 2021; Zhao et al. 2020; Schweighauser et al. 2020; Sun et al. 2021; Y. Yang, Shi, et al. 2022; Frieg et al. 2022). This plethora of distinct structures have been instrumental to understand the amyloid polymorphism phenomenon.

The β-sheets in αS amyloid fibrils are in-register and parallel, with the core of αS amyloid fibrils centered in the NAC domain; in agreement with its high amyloidogenic load; this region is considered the principal stabilizing element of the fibril (van der Kant et al. 2022). The flanking regions of the NAC are also incorporated in the fibrils' rigid and proteolysis resistant core of the

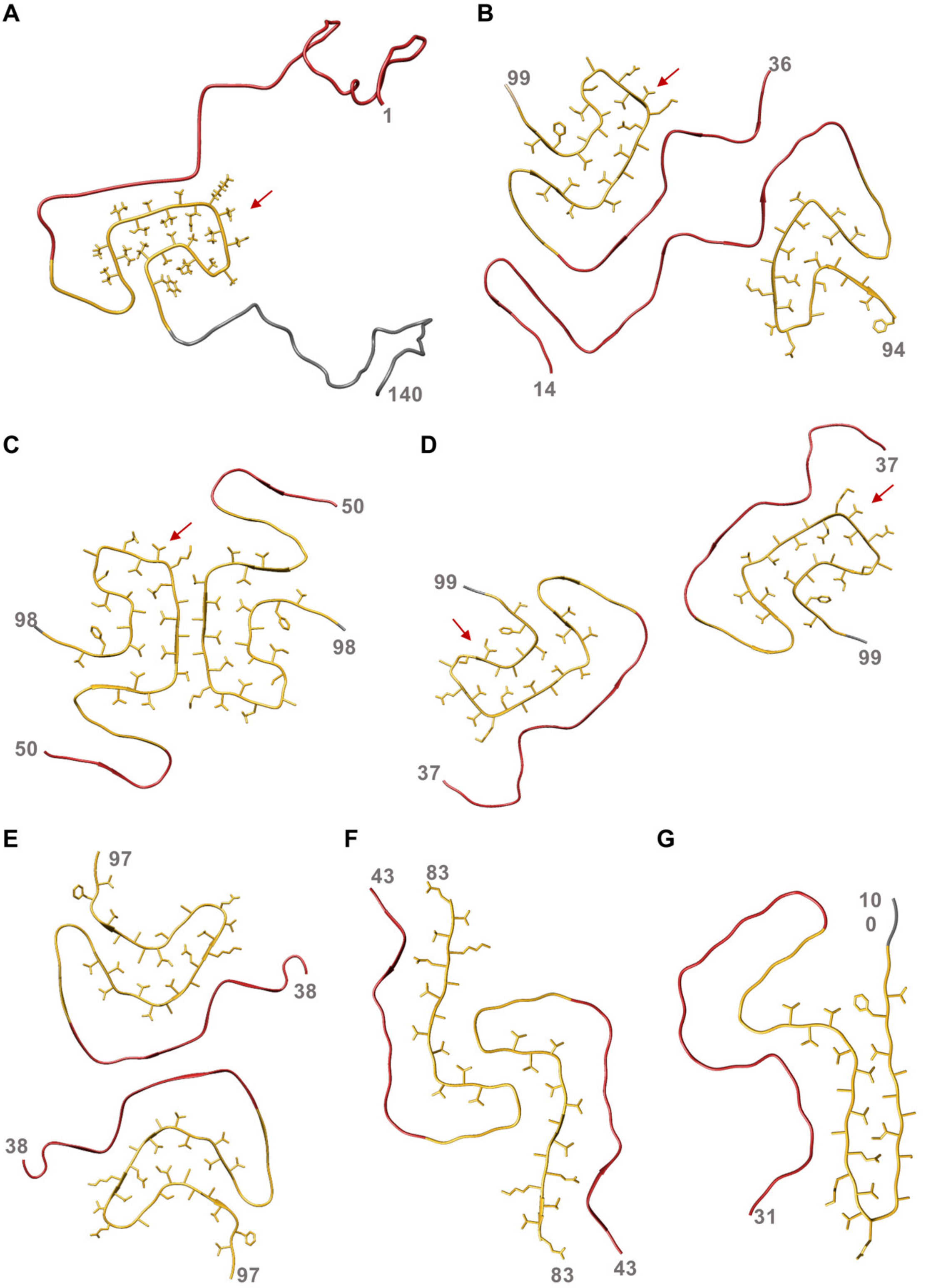

Figure 8: α-Synuclein polymorphism. Structural diversity of α-synuclein fibrils illustrated by seven polymorphs. N-terminal, NAC and C-terminal domains are colored in red, yellow and gray respectively. Side chains are showed for residues 70 to 95. Greek-key folds are indicated with an arrow. (**A**) α-synuclein structure solved by ssNMR (PDB: 2N0A). (**B**) Filament extracted from a brain with MSA (PDB: 6XYQ). (**C**) α-synuclein structure with G51D mutation (PDB: 7E0F). (**D**) α-synuclein structure with A53T mutation (PDB: 6LRQ). (**E-F**) Two *in vitro* α-synuclein polymorphs form the same study (PDB: 6CU7 and 6CU8). (**G**) Fibril extracted from a brain with Lewy pathology (PDB: 8A9L).

fibrils, which often extends from residues 35 to 100 (Vilar et al. 2008; Gracia et al. 2020) (**Figure 8**). The C-terminal domain (from residue 100) is not incorporated in the fibrils due to its disordered and anionic nature. The N-terminal is also considered a flanking region, with residues 1-35 being usually invisible, even if some residues are ordered in specific structures (**Figure 8B**). Noteworthy, in many polymorphs the P1-P2 region is involved in protofilament contacts highlighting a role in mature fibril stabilization, which is of significant relevance due to the clustering of familial mutations in these regions (Y. Li et al. 2018; Sun et al. 2021; Schweighauser et al. 2020) (**Figure 8B and E**).

In general, the specific fold, β-strand location and residue to residue contacts vary between polymorphs (**Figure 8**). The diversity observed in protofilament packing also increases the degree of divergence; similar protofilament folds can stablish different inter-filament interactions modifying the global fibril architecture (Guerrero-Ferreira et al. 2019). Overall, certain structures have several commonalities and only show subtle differences, whereas others are radically different.

The most common motif observed in αS amyloid structures is a Greek-key or Greek-key like motif involving residues 60-100 (Gracia et al. 2020). Originally identified in the first full-length αS fibril, this Greek-key fold has been repeatedly observed to different extents in different polymorphs, including *ex vivo* fibrils extracted from the brain of MSA suffering patients (Tuttle et al. 2016; Schweighauser et al. 2020; Sun et al. 2020; Zhao et al. 2020; Sun et al. 2021; Boyer et al. 2019; Y. Yang, Garringer, et al. 2022) (present in **Figure 8A-D**). The specific position of αS residues in the Greek-key and, thus, their neighbor interactors shows a certain heterogenicity. Yet, the Greek-key is still evident, indicating that it admits a certain plasticity. This common NAC fold on the otherwise diverse amyloid structures is intriguing and hints that certain contacts involving fibril core formation may be common and could involve somehow defined pathways of assembly.

Importantly, amyloid polymorphism is not only a phenomenological observation but has been demonstrated to play a neuropathological role in synucleinopathies. The amyloid fold observed in fibrils extracted from MSA and PD patients show distinct structures and even differ in the number of protofilaments (Schweighauser et al. 2020; Y. Yang, Shi, et al. 2022; Y. Yang, Garringer, et al. 2022) (**Figure 8B and G**). Of particular importance, exogenous administration of αS aggregates has been reported to induce the seeded assembly of endogenous αS and aggregate propagation, demonstrating the prion-like nature of synucleinopathies (Mougenot et al. 2012; Luk et al. 2012; Masuda-Suzukake et al. 2013; Osterberg et al. 2015). Since each polymorph has distinct seeding capacity (Peelaerts et al. 2015), disease progression in terms of time and the tissues affected is strongly associated with the specific amyloid polymorph.

Regarding *ex vivo* structures, one additional note should be considered; most of the amyloid fibrils (≈75 %) extracted from PD, PDD and DLB patients' brains do not show a helical twist, impeding their structure determination by helical reconstruction. Thus, a significant part of the αS fibril space remains yet uncharted.

2.2.4. Fuzzy coats: role of unstructured regions surrounding oligomers and fibrils

The outstanding burst in high-resolution structures of amyloid fibrils has provided unprecedented molecular details to understand the amyloid phenomenon. Yet, it is increasingly clear that what we are seeing is only a partial picture that does not fully explain the aggregates properties. In αS fibrils, only ≈50 % of the total protein sequence is visible by cryoEM whereas in type-B* oligomers just ≈15 % has been assigned as rigid by ssNMR (Guerrero-Ferreira et al. 2020; Fusco et al. 2017). Thus, a significant portion of the αS sequence populates a continuum of disordered and partially folded states that surround the core of oligomers and fibrils. This flexible outer shell, also known as "fuzzy coat", has a higher solvent exposition than the core, being more accessible to interactions and greatly contributing to the aggregate physicochemical properties.

In the fibril, the N- and C-terminal tails are of paramount importance for fibril amplification, cellular toxicity, and cell-to-cell spreading. Monomer recruitment to fibrils is mediated by monomer N-terminals contacts with the C-terminal of the fibril, being fundamental for monomer capturing in surface catalyzed secondary nucleation and elongation (Ulamec, Brockwell, and Radford 2020; X. Yang et al. 2021; Kumari et al. 2021) . The N-terminal tail in the fibrils also participates in membrane binding, being involved both in membrane disruption and cell-to-cell spreading via membrane vesicles (Grey et al. 2011; Pieri et al. 2012; Emmanouilidou et al. 2010).

Complementarily, the C-terminal tail mediates pathological cellular uptake by cellular receptors (Zhang et al. 2021). These receptors preferentially bind to fibrils rather than monomers, since in the monomer this C-terminal tail is compacted and shielded by long-range tertiary contacts. αS fibrils also interact with tau through their C-terminal tails, resulting in microtubule destabilization (Lu et al. 2020; Ulamec, Brockwell, and Radford 2020).

Less information is available for oligomers even if the similitude of the αS regions (N- and C-terminal) participating in their outer shell suggest equivalent interactions. Indeed, as in the fibril, the N-terminal domain also participates in membrane binding (Fusco et al. 2017; X. Yang et al. 2021; Musteikytė et al. 2021).

From a functional perspective, the fuzzy coat is a target of the protein quality control system. αB-crystallin and Hsp27 bind to fibrils surfaces disrupting secondary nucleation by targeting non-core regions (Cox et al. 2018; Waudby et al. 2010). αS fibrils depolymerization by the Hsp70, DNAJB1 and Apg2 disaggregation machinery also relies on interactions with the N- and C-termini (Wentink et al. 2020; Franco, Gracia, et al. 2021). DNAJB1 binds to the C-terminal tails, whereas Hsp70 has two binding sites in the N-terminal. Consistently, the binding sites of six divergent human molecular chaperones were found to map in the first N-terminal residues and around position 39 (Burmann et al. 2020).

Mimicking these natural strategies, fuzzy coat targeting molecules have shown promising therapeutic potential *in vitro* and *in vivo*. β-wrapins binding to the 37-54 region inhibit both primary nucleation and surface catalyzed secondary nucleation by binding the monomer and fibrils, respectively (Agerschou et al. 2019; Mirecka et al. 2014). Antibodies targeting αS flanking regions also demonstrated efficacy in binding aggregated species (Hmila et al. 2022; Vaikath et al. 2019; Brundin et al. 2022). For instance, cinpanemab targets residues 1-10 and prasinezumab the C-terminus and both have a higher affinity for aggregated over monomeric αS (Weihofen et al. 2019; Games et al. 2014; Lang et al. 2022; Pagano et al. 2022).

In the first chapter of this thesis, we also exploit fuzzy coat targeting to develop our own strategy for oligomer and fibril binding.

2.3. Parkinson’s disease

PD is the most common synucleinopathy and the second most prevalent neurodegenerative disorder affecting more than 6.1 million people worldwide (Bloem, Okun, and Klein 2021). Aging is the principal risk factor for PD and thus its incidence is steeply increasing in our aging societies (Clarke 2007; Bloem, Okun, and Klein 2021). Indeed, PD is now considered one of the fastest growing neurological disorders worldwide. This alarming reality has made PD the most studied synucleinopathy and great efforts are being devoted to its understanding and clinical intervention.

Neurodegeneration in PD is primarily associated with accelerated neuronal death of dopaminergic neurons in the *substantia nigra pars compacta* (Sveinbjornsdottir 2016). The loss of dopaminergic neurons leads to the characteristic movement disorder classically associated with PD. As PD progresses, disease spreads through the brain and manifests as multiple symptoms such as emotional and cognitive impairment (Sveinbjornsdottir 2016). This results in a heterogeneous spectrum of clinical presentations -including both motor and non-motor symptoms- such as motor disfunction, impaired posture and balance, gastrointestinal symptoms, and memory and cognitive impairment (Bloem, Okun, and Klein 2021; Kalia and Lang 2015).

PD etiology is considered multifactorial and involves an intricate balance between genetic, epigenetic and environmental factors affecting disease onset and progression. For sporadic PD, aging is the principal risk factor; in contrast in fPD the presence of genetic mutations causes early onset PD and accelerated disease progression (Bloem, Okun, and Klein 2021). fPD is estimated to affect a 5% of PD-suffering patients. Despite being multifactorial, the main neuropathological hallmark of PD is the accumulation of intracellular deposits of aggregated proteins in neurons, known as Lewy’s bodies (LB) and Lewy’s neurites (Goedert et al. 2013; Spillantini et al. 1997). αS is the principal component of LB and its aggregation elicits toxicity and subsequent cellular death (Dickson 2012; Spillantini et al. 1998). αS is also genetically linked to PD since hereditary single point αS mutations and gene duplications lead to autosomal dominant fPD (Polymeropoulos et al. 1997; Krüger et al. 1998; Zarranz et al. 2004; Appel-Cresswell et al. 2013; Pasanen et al. 2014; Yoshino et al. 2017; Liu et al. 2021; Kumar et al. 2022; Konno et al. 2016). Polymorphisms in the locus coding αS were also defined as risk factors in genome-wide analysis (Maraganore et al. 2006). Consistently, injection of αS fibrils in mouse brains is reported to induce the formation of αS inclusions and a PD-like phenotype (Froula et al. 2019; Luk et al. 2012).

αS aggregation is a keystone process in PD. Targeting αS aggregation is then considered a promising strategy for therapeutic and diagnostic interventions in PD and other synucleinopathies.

2.4. Targeting α-synuclein aggregates for PD treatment and diagnosis; theoretical considerations based on our current biophysical knowledge

By the time of PD diagnosis, around 60% of dopaminergic neurons within *substantia nigra pars compacta* are lost (Sveinbjornsdottir 2016). Such neuronal damage is irreversible, significantly reducing life-quality and the potential positive impact of PD treatments. Current treatments focus on symptom amelioration, but we lack disease-modifying therapies. This tragic reality highlights the urgent need for early diagnosis strategies and their coupling to disease-modifying therapies that halt or delay the molecular events that cause PD.

Targeting αS aggregates stands as an appealing alternative for both diagnosis and therapeutics. αS oligomers are increasingly identified as the primary effector of cellular dysfunction (Choi et al. 2022; Emin et al. 2022), whereas fibrils can self-propagate and act as a vehicle for the prion-like spreading of the disease (Luk et al. 2012; Froula et al. 2019). In this scenario, a multitargeted strategy against both oligomers and fibrils would be desirable. Considering our current structural knowledge, this is a challenging task. Little information is available about fibrils' non-structured regions, and the structural data about oligomers is scarce. Nevertheless, we could hypothesize that the fuzzy coats of flexible tails that surround αS oligomers and fibrils share similar physicochemical properties, being a potential solvent-accessible target. Both are formed by αS C-terminal domains plus some segments of the N-terminal, and their polymeric nature distinguishes them from the properties of equivalent regions in a single monomer. Besides, in αS monomers the presence of intramolecular contacts that shield the C-terminal tail reduces its ability to stablish interactions with other proteins (Zhang et al. 2021). In our opinion, targeting this outer corona of flexible tails displayed to the solvent offers a promising avenue to develop novel aggregate binders that do not interfere with the functional monomeric protein.

Targeting preferentially aggregates and not the monomers provides significant advantages compared with panreactive molecules. Interactions with the functional monomer will perturb αS natural functions potentially causing side effects. More importantly, the huge excess of monomer in the central nervous system will dilute the intended therapeutic effect. The same paradigm is true for diagnosis, monomer excess compromises an accurate determination of the aggregate concentration. Some molecules have been reported to target specifically oligomers and fibrils, but they generally exhibit certain crossreactivity with the monomer. This is the case for many antibodies since they usually target protein primary sequences (Kumar et al. 2020).

Overall, we believe that targeting structural and physicochemical features only present in αS aggregates provides an avenue for developing molecules selective for αS pathogenic species. We expect that such molecules would benefit both diagnosis and therapeutic endeavors. This is the conceptual starting point of this thesis and its initial objective.

Objectives

This Ph.D. dissertation revolves around the use and molecular characterization of αS oligomers as promising targets to fight synucleinopathies. To pursue this aim, in chapter 1, we identify and characterize a family of α-helical peptides that bind oligomers with nanomolar affinity in a conformation specific manner. In chapter 2 and 3 we explore and discuss the possible physiological implications of this type of peptides in protein homeostasis and how to exploit it for therapeutic applications. Finally, in chapter 4, we use these peptides to gain novel insights into the structural architecture of αS and elucidate the mechanism of oligomer to fibril transition.

- **Objective 1**: To rationally design high affinity and conformational specific binders of αS pathogenic species. With that aim, we used α-helical peptides as scaffolds and exploited the main share physicochemical properties of αS oligomers and fibrils.

- **Objective 2**: To characterize the effect of the α-helical binders identified in objective 1 on αS aggregation and toxicity.

- **Objective 3**: To dissect the molecular basis of the interaction between α-helical binders and αS pathogenic species.

- **Objective 4**: To explore if the identified family of peptides could have therapeutic and diagnosis applications or a physiological role in regulating αS proteostasis.

- **Objective 5**: To use these peptides to interrogate oligomers' structural properties.

Chapter 1: α-Helical peptidic scaffolds to target α-synuclein toxic species with nanomolar affinity

This chapter contains the article published in Nature Communications "*α-Helical peptidic scaffolds to target α-synuclein toxic species with nanomolar affinity, J. Santos, P. Gracia, S. Navarro, S. Peña-Díaz, J. Pujols, N. Cremades, I. Pallarès, S. Ventura, Nature Communications. 12, 3752 (2021)*."

DOI: 10.1038/s41467-021-24039-2

The supplementary data associated with this work is available in Section "Appendix 1" of this thesis.

nature COMMUNICATIONS

ARTICLE

https://doi.org/10.1038/s41467-021-24039-2 OPEN

Check for updates

α-Helical peptidic scaffolds to target α-synuclein toxic species with nanomolar affinity

Jaime Santos[1], Pablo Gracia[2], Susanna Navarro[1], Samuel Peña-Díaz[1], Jordi Pujols[1], Nunilo Cremades[2]✉, Irantzu Pallarès[1]✉ & Salvador Ventura[1]✉

α-Synuclein aggregation is a key driver of neurodegeneration in Parkinson's disease and related syndromes. Accordingly, obtaining a molecule that targets α-synuclein toxic assemblies with high affinity is a long-pursued objective. Here, we exploit the biophysical properties of toxic oligomers and amyloid fibrils to identify a family of α-helical peptides that bind to these α-synuclein species with low nanomolar affinity, without interfering with the monomeric functional protein. This activity is translated into a high anti-aggregation potency and the ability to abrogate oligomer-induced cell damage. Using a structure-guided search we identify a human peptide expressed in the brain and the gastrointestinal tract with analogous binding, anti-aggregation, and detoxifying properties. The chemical entities we describe here may represent a therapeutic avenue for the synucleinopathies and are promising tools to assist diagnosis by discriminating between native and toxic α-synuclein species.

---

[1] Institut de Biotecnologia i Biomedicina and Departament de Bioquímica i Biologia Molecular, Universitat Autònoma de Barcelona, Bellaterra, Barcelona, Spain. [2] Institute for Biocomputation and Physics of Complex Systems (BIFI)-Joint Unit BIFI-IQFR (CSIC), University of Zaragoza, Zaragoza, Spain.
✉email: ncc@unizar.es; irantzu.pallares@uab.cat; salvador.ventura@uab.es

α-Synuclein (αS) is a 140 amino acid protein whose aggregation into amyloid fibrils in a subset of neuronal and glial cells lies behind the onset of a group of progressive and, ultimately, fatal neurodegenerative disorders, including Parkinson's disease (PD)[1–4], that are collectively referred to as synucleinopathies. A causative link between αS and disease is supported by the discoveries that multiplications and missense mutations in SNCA, the αS gene, cause dominantly-inherited familial forms of PD[5].

Interfering with αS amyloid formation and abrogating the associated toxicity is considered a promising therapeutic strategy for synucleinopathies[6–8]. However, the design of molecular entities that target specific αS toxic assemblies is challenging because of the heterogeneous, dynamic, and transient nature of these species. High-throughput screening initiatives have rendered promising αS aggregation inhibitors[9–11]. However, these selection procedures are blind to the ligand mechanism of action. In the absence of a structure-activity relationship, it is difficult to evolve the affinity and specificity of the identified hits to generate drugs that can reach the clinics. The lack of specific and sensitive molecules to detect the pathogenic forms of αS also constrains the early diagnosis of these diseases.

The in vitro aggregation of αS displays a sigmoidal growth profile, suggesting that it follows a nucleation-polymerization mechanism[12], where soluble αS undergoes a nucleation process that produces oligomers able to grow through further monomer addition to form insoluble amyloid fibrils. Oligomeric forms of αS have been detected in the brains and other tissues of patients suffering from PD, and growing evidence suggests that they constitute the primary cytotoxic agents accounting for the gain-of-toxicity associated with αS aggregation, whereas both oligomers and fibrils would be responsible for pathology dissemination in the brain[2,13–15]. We have recently identified the sequential occurrence of two conformationally distinct types of oligomers during αS in vitro fibrillation. The initial non-toxic disordered oligomers, named as type A oligomers, undergo a structural reorganization to form more stable and compact β sheet-enriched, and proteinase K-resistant species that exhibit intrinsic cytotoxicity, named as type B oligomers[16]. Stable, trapped analogues of these two well-defined types of transient oligomers (referred to as type A* and type B* oligomers, where the star refers to the kinetically trapped nature of these isolated oligomeric forms) have been isolated and characterized in detail[13,16] and, therefore, constitute important tools for the development of specific therapeutic and diagnostic strategies.

In this work, we exploit our recent advances in the understanding of the structural determinants of toxicity of αS oligomers to rationally identify peptide molecules able to target αS toxic species. By using a time-resolved single-particle fluorescence approach, we demonstrate that short, amphipathic, and cationic α-helical peptides do not interact with the functional monomeric αS, but they bind toxic oligomers and fibrils with nanomolar affinity, resulting in the substoichiometric inhibition of αS aggregation and abrogation of oligomer-induced damage in neuronal cell models. We then use a protein engineering approach to dissect the molecular determinants accounting for this interaction, which allow us to identify a human peptide, constitutively expressed in the brain and gastrointestinal tract, that binds with low nanomolar affinity to αS toxic assemblies, thus suppressing the aggregation cascade and its associated neurotoxicity. Thus, we describe here the rational identification and characterization of a family of highly potent peptidic ligands able to bind to αS toxic species and abrogate their detrimental effects in neuronal cells. This discovery may open previously unexplored avenues for the diagnosis and/or therapeutics of PD and related disorders.

Results

Identification of an αS species-specific peptide ligand. We rationalized that the particular properties of the four main αS conformers identified during αS amyloid aggregation, namely monomers, non-toxic (type A/A*) oligomers, toxic (type B/B*) oligomers and fibrils, could be exploited to identify a selective ligand for the main species responsible for induction and propagation of toxicity, which are currently believed to be type B-like oligomers and amyloid fibrils, respectively[17]. In Fig. 1a, we illustrate the dissection of the differential traits of αS species (for a more detailed morphological, size and structural characterization of the different αS species in isolated preparations see Supplementary Fig. 1). Type B-like oligomers and amyloid fibrils share two features: (i) they expose relatively large lipophilic clusters to the solvent (Supplementary Fig. 1e). These hydrophobic surfaces induce cellular toxicity and drive subsequent fibrillation[16,18–20]. (ii) They possess a high anionic character at neutral pH, as a result of the stacking of αS monomers (net charge −9). In αS, the negative charge is concentrated at the C-terminal region (residues 95–140), which clusters 15 E/D amino acids. This αS segment remains disordered, and solvent exposed in both oligomers and fibrils[13,21–23], being thus accessible to putative ligands.

While the solvent exposure of hydrophobic surfaces seems to be a general feature of toxic pre-fibrillar oligomers[13,24], the combination of highly exposed hydrophobicity and negative charge is likely unique to these two toxic αS assemblies. Thus, we hypothesized that hydrophobic patches embedded in an anionic environment might delineate a diffuse, but physicochemically-defined, binding surface in these two types of αS aggregates for a complementary molecule; ideally an amphipathic and cationic entity. A short α-helical peptide might provide a structurally stable scaffold to merge both features.

We identified a naturally occurring peptide bearing a short, stable, amphipathic, and cationic helical fold. PSMα3 is a 22-residue bacterial extracellular peptide that has been shown to remain in an α-helical conformation for weeks[25]. It has a net charge of +2, a mean hydrophobicity (H) of 0.54, an α-helical hydrophobic moment (μ_H) of 0.56, and the helical wheel plot evidences its amphipathic character (Fig. 1b, c). The far-UV circular dichroism (CD) spectrum of PSMα3 confirms that it folds into an α-helix under our assay conditions (Fig. 1d). Thus, according to our hypothesis, this peptide fulfills all the requirements to bind specifically to type B-like αS oligomers and amyloid fibrils.

We engineered PSMα3 to obtain a negative control peptide in which the formation of an α-helix is strongly disfavored. This will disrupt the peptide amphipathic character and, theoretically, abolish binding to αS type B* oligomers and amyloid fibrils. After a computational proline scanning of PSMα3 using the AGADIR algorithm[26] (Supplementary Fig. 2a), we selected the K9P and F11P mutations, as they have a significant impact in helical propensity and map to opposite faces of the α-helix (Supplementary Fig. 2b, c). The characterization of the secondary structure of the K9P-F11P PSMα3 peptide (further referred to as disrupted PSMα3 or dPSMα3) in solution by CD confirmed the disruption of the α-helix fold (Supplementary Fig. 2d). Thus, dPSMα3 constitutes a suitable negative control for further studies, as it keeps a sequence identity of 91% with PSMα3, but lacks its amphipathic character, a feature that we propose is key for the species-specific binding to the αS toxic assemblies.

Selective interaction of PSMα3 with αS toxic species. We then addressed the interaction of PSMα3 and dPSMα3 with the above described four αS species. As multiple peptides are expected to bind multiple αS molecules in the aggregated states, the binding

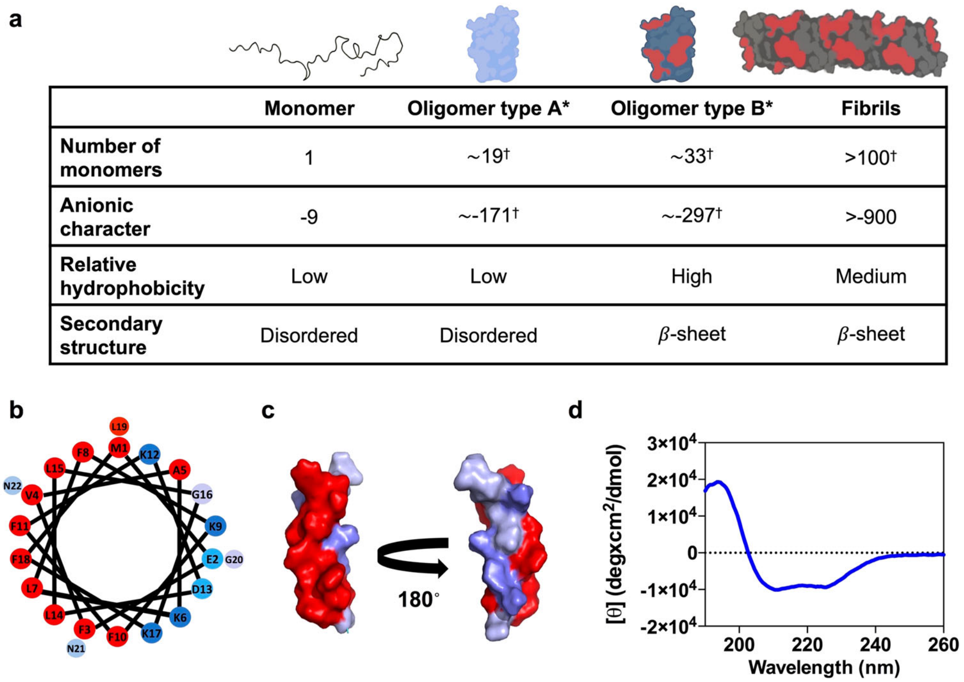

	Monomer	Oligomer type A*	Oligomer type B*	Fibrils
Number of monomers	1	~19†	~33†	>100†
Anionic character	-9	~-171†	~-297†	>-900
Relative hydrophobicity	Low	Low	High	Medium
Secondary structure	Disordered	Disordered	β-sheet	β-sheet

Fig. 1 Rational identification of a peptide ligand for αS toxic species. a Main molecular features of the four isolated α-synuclein (αS) species. Values with a dagger (†) represent extrapolations based on the average number of monomers in each species. In the upper schemes of αS oligomeric and fibrillar species, the acidic C-terminal region is not depicted since it has been described to be in a disordered and conformationally flexible state[21–23]. **b** Helical wheel projection of PSMα3 sequence (red, hydrophobic residues; blue pallet, hydrophilic residues depending on their character). **c** Surface representation of the three-dimensional structure of PSMα3 with hydrophobic residues in red and hydrophilic residues in blue. **d** Far-UV circular dichroism spectra of PSMα3.

process can only be well described if both the stoichiometry of the complex and the affinity of the peptide for the αS molecules in a particular conformer is known. In order to obtain good estimates of both parameters, we exploited the power of dual-color fluorescence cross-correlation spectroscopy (dcFCCS), a time-resolved fluorescence fluctuation technique that allows the direct observation of co-diffusing fluorescent species arising from interactions between differently labeled molecules or assemblies in solution[27,28]. To this end, αS species were cysteine-labeled with maleimide-AlexaFluor488 (AF488), with each αS molecule of the different species containing one fluorophore at position 122, and the peptides were cysteine-labeled with maleimide-Atto647N at the N-terminus (see “Methods” for details). Simultaneously, we assessed complex formation by single-particle fluorescence spectroscopy (SPF) analysis, including Förster Resonance Energy Transfer (FRET) and donor/acceptor stoichiometry (S), in order to validate and complement the dcFCCS approach. These approaches allow us to monitor distinct individual species simultaneously by avoiding measurements of ensemble averages (Supplementary Fig. 3) and have been previously used for the characterization of αS aggregation pathways and the study of αS interactors[29–31].

We first assessed the binding of PSMα3 to monomeric αS and found by dcFCCS analysis that these molecules were unable to interact when mixed in an equimolar ratio (even at concentrations as high as 15 nM of each molecule) (Fig. 2a), as reflected by a flat cross-correlation curve comparable to that of the negative control of cross-correlation (Supplementary Fig. 4). We then analyzed the interaction of PSMα3 with the different αS aggregated species by means of dcFCCS at approximately equimolar ratios of peptide and αS molecules. Due to the different stabilities of the various aggregated species upon single-molecule dilution and their differential adsorption to the surface of the coverslips, the total αS concentration of each aggregate sample was adjusted between 1 and 5 nM (in mass concentration) so that the frequency of events in the measurements was very similar between the various aggregated samples. It is important to note that, for αS aggregated species, consisting of several tens of monomers, the species concentrations are in the picomolar range and, as further explained in the “Methods”, single-particle conditions are ensured throughout the experiments. Under these conditions, a marginal cross-correlation amplitude was observed for the type A* oligomers (Fig. 2b), whereas a clear cross-correlation was obtained for the interaction of the peptide with both type B* oligomers and fibrils (Fig. 2c and d, respectively), already indicating a stark difference in the binding ability of the peptide to the different aggregates. Consistently, single-particle burst-wise analysis revealed a high number of FRET events, thus validating the direct interaction of the peptide with these two αS species (Supplementary Fig. 5a, b). In contrast, the same analysis yielded either a statistically insignificant number of FRET events or none at all for the interaction between PSMα3 and αS type A* oligomers and monomers, respectively (Supplementary Fig. 5c). These results offer a single-particle understanding of a complex binding scenario and further reinforce the observations derived from dcFCCS experiments.

We next performed a titration experiment for analyzing the binding of the peptide to the three αS aggregated species. For this, we developed a model-independent saturation binding curve, based on the theoretical framework previously developed by Kruger and coworkers[32]. This analysis allowed us to quantify the number of peptide molecules bound to each αS species (N_P) as a function of the concentration of unbound peptide ($C_{\mathrm{p,free}}$) (Fig. 2e). Using a simplistic Langmuir isotherm model, we estimated the single-state dissociation constant (K_D) of the interactions and the average maximum number of peptide

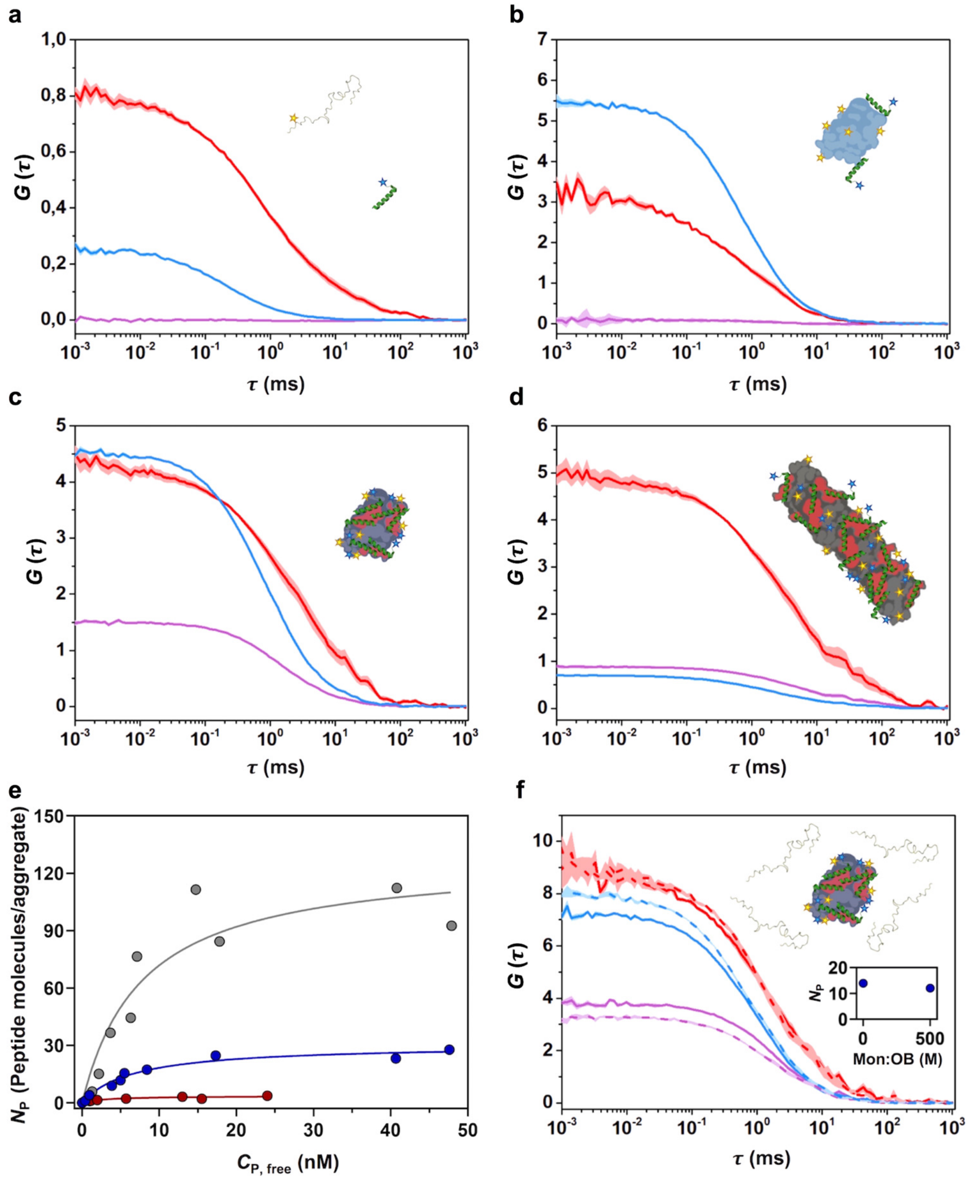

Fig. 2 Interaction of PSMα3 with different αS species by dcFCCS. a–d Representative auto-correlation curves for α-synuclein (αS) (blue line) and PSMα3 (red line) and cross-correlation curves for interacting molecules (purple line). The amplitude (G) error is shown as faint colored area for the corresponding correlation curves. Samples contained (**a**) ~15 nM αS monomer and ~15 nM PSMα3, (**b**) 1 nM type A* and ~5 nM PSMα3, (**c**) 1 nM type B* oligomers and ~5 nM PSMα3 or (**d**) ~5 nM sonicated fibrils and ~5 nM PSMα3. **e** Titration binding curves for the interaction of PSMα3 with type A* oligomers (red circles), type B* oligomers (blue circles) or sonicated fibrils (gray circles) obtained by dcFCCS, showing their corresponding analysis assuming a model of *n* identical and independent binding sites (referred in equation 7 as N_{max}) per αS aggregated species (solid lines). N_P represents the number of bound peptides per aggregate. **f** Auto-correlation curves (αS in blue, PSMα3 peptide in red) and cross-correlation curve for the interacting molecules (in purple) obtained in samples containing ~1 nM αS type B* oligomers and ~2 nM PSMα3 in the absence (solid lines) or presence (dashed lines) of a 500-molar excess of unlabeled monomer with respect to the particle concentration of oligomers. The inset shows the number of bound peptides (N_P) per aggregate in both conditions. For αS aggregated species, each consisting of several tens of monomers, the species concentrations are in the picomolar range and, as further explained above, single-particle conditions are ensured throughout the experiments.

binding sites (N_{max}) in each type of αS species. Interestingly, while the K_D values for the peptide-αS interaction obtained for type A* oligomers, type B* oligomers and fibrils are very similar, in all cases in the very low nM range (3.07 nM, 6.67 nM, and 7.8 nM, respectively), the average maximum number of peptides per aggregate (N_P) varies remarkably, being 3, 30, and 120, respectively. This indicates that the main difference between the three aggregated species in terms of PSMα3 interaction is the number of binding sites per aggregate rather than the affinity of the peptide for them. Of note, the average maximum number of binding sites obtained for the type B* oligomers and fibrils nearly matches the average number of αS molecules per aggregate species (19, 33, and 107 for type A*, type B* oligomers, and fibrils, respectively, estimated by comparing the molecular brightness of the aggregated species to that of the αS monomer), while for the type A* oligomers represents only one sixth of the average αS molecules in this type of aggregate. This data is in agreement with the single-particle fluorescence analysis obtained for the different complexes, where decreasing fluorescence stoichiometry values are found for the interacting pairs with increasing PSMα3 concentrations (Supplementary Fig. 6) yielding a binding curve remarkably similar to that obtained by dcFCCS

(Supplementary Fig. 7). In addition, only very few FRET events were observed for the binding of PSMα3 to type A* oligomers, in contrast to the numerous FRET events with a defined FRET efficiency (E) distribution observed for the binding to type B* oligomers and fibrils (Supplementary Fig. 5). Together, the dcFCCS and single-particle fluorescence spectroscopy data demonstrate that PSMα3 is a high affinity ligand of αS toxic species, with affinities in the low nanomolar range, and with a high avidity for the toxic αS species, namely the type B-like oligomers and fibrils. Note that a 500-fold molar excess (in monomer equivalents) of unlabeled monomeric αS does not interfere with the binding of PSMα3 to type B* oligomers (Fig. 2f), which indicates a high specificity towards toxic aggregated species and negligible monomer binding, a feature difficult to find in previously reported αS ligands.

It might be important to indicate that PSMα3 could present a certain degree of oligomerization that results in a slower diffusion than expected for a peptide monomer ($14.6 \pm 3.6\ \mu m^2\ s^{-1}$, Fig. 2). Despite this, our dcFCCS-derived binding curves indicate that the monomeric form of the peptide can effectively bind the αS aggregated species with N_P values as low as 1 (further information is provided in the "Methods").

Interestingly, when we analyzed the binding of the PSMα3 analogous, but disordered peptide, dPSMα3, we could not detect any interaction with any of the four αS species (Supplementary Fig. 8), indicating that an amphipathic distribution of the peptide residues, achieved through an α-helical conformation, is a requirement for the interaction.

Overall, our dcFCCS and single-particle fluorescence spectroscopy-derived binding analysis indicates that PSMα3 binds with low nanomolar affinity to αS aggregated species. The degree of binding is limited by the number of available interaction sites, which is likely associated with the extent of solvent-exposed hydrophobic surface per aggregate, which depends on both the size and the lipophilicity of the aggregate, in agreement with our initial reasoning.

PSMα3 inhibits αS amyloid aggregation. We hypothesized that the high affinity and number of binding sites of type B* oligomers for PSMα3 might result in the partial or full coverage of the surface of these assemblies, as well as their structurally homologous type B oligomers, thus preventing their progression to fibrils during the αS amyloid aggregation process. To assess if this was the case, we set up in vitro αS aggregation reactions in the absence and presence of an equimolar concentration of PSMα3 (70 µM) and followed its progression by monitoring the increase in thioflavin-T (Th-T) fluorescence. After 32 h of incubation, a ~90% decrease in Th-T fluorescence emission, relative to the untreated sample, was observed in the presence of PSMα3, suggesting that the peptide acts as a potent inhibitor of αS amyloid aggregation (Fig. 3a). Inhibition was orthogonally confirmed by quantifying the fraction of αS that remains soluble at the endpoint of the reaction spectroscopically and by SDS-PAGE (Supplementary Fig. 9a, b). The inhibitory activity of PSMα3 was concentration-dependent and significant inhibition was observed even at a substoichiometric 20:1 ratio (αS:PSMα3) (Fig. 3b). Transmission electron microscopy (TEM) images confirmed that samples incubated with PSMα3 contained very few fibrils per field, in comparison to untreated samples (Fig. 3c). The observation that dPSMα3 exhibited a negligible anti-aggregative activity (Supplementary Fig. 10) reinforces the connection between the binding of the amphipathic (hydrophobic/cationic) helical peptide to αS oligomers and its potent amyloid inhibition activity.

PSMα3 is a better inhibitor of αS amyloid aggregation than SynuClean-D (Fig. 3a), a small molecule with high neuroprotective activity in *Caenorhabditis elegans* models of PD that we have recently discovered[9].

To gain further information on the inhibitory mechanism and pinpoint the αS species targeted along the complex pathway of aggregation, we isolated the low molecular weight species generated at the early stages of aggregation (see "Methods"). Electron microscopy analysis revealed that in control aggregation reactions, after 12 h of incubation, αS mainly populates small fibrillar species and round prefibrillar aggregates (average diameter between 20 and 40 nm) (Fig. 3d and Supplementary Fig. 11a–b). In contrast, at the same time point, samples incubated with PSMα3 contained a large fraction of small oligomers of annular shape with diameters between 9 and 14 nm, morphologically similar to type B* oligomers (Fig. 3d and Supplementary Fig. 11c) and other annular oligomers previously described in the literature[24,33,34]. Together with the time-resolved fluorescence spectroscopy data, this evidence strongly suggests that PSMα3 could be preventing or retarding the conversion of type B-like oligomers into fibrillar species. Notably, this result endorses the use of the kinetically stabilized type B* oligomers as mimicries of the toxic oligomers that populate αS aggregation reactions.

PSMα3 protects cells from αS oligomer-induced cell damage. As it occurs with toxic oligomers from other amyloidogenic systems, the toxicity of type B* oligomers relies on their ability to interact and disrupt cellular membranes[13]. In αS this activity is encoded in two of their characteristic structural elements[13]: (i) an exposed N-terminal region that acts as the initial anchor to the membrane surface, similarly as with the monomeric functional form of the protein, and (ii) a β-sheet core, composed primarily by the central region of the protein, with significant hydrophobic surface exposed to the solvent that then inserts into the lipid bilayer causing major perturbations. The highly negatively charged C-terminal region of the protein remains disordered without significant interactions with the membrane.

We hypothesized that the binding of PSMα3 to type B* oligomers, mediated in part by the solvent-exposed hydrophobic regions of the β-sheet core, would block their exposed lipophilic elements, thus decreasing its ability to insert into and perturb the membrane bilayer and induce cellular toxicity. We treated human SH-SY5Y neuroblastoma cells with 10 µM of oligomers and observed that, as previously reported[35], they possess a high affinity for cellular membranes (Fig. 4a–b). When the oligomers were preincubated with an equimolar concentration of PSMα3, we observed a ~60% reduction in the amount of αS bound to cells relative to untreated oligomers, indicating that PSMα3 binding to type B* oligomers directly affects the binding of the oligomers to cellular membranes. As expected, pretreatment of the oligomers with dPSMα3 did not interfere with their interaction with cells.

One of the earliest effects of type B* oligomer-mediated membrane perturbation is the substantial increase in the levels of intracellular reactive oxygen species (ROS)[24], which in turn elicits mitochondrial dysfunction[36]. We assessed if the blockage of the oligomer regions involved in membrane perturbation by PSMα3 binding could protect membrane integrity and therefore prevent its associated increase in intracellular ROS levels. Treatment of neuroblastoma cells with 10 µM of oligomers induced a drastic increase in ROS levels (Fig. 4c–d). However, when these oligomers were preincubated with equimolar (1:1) and substoichiometric (1:0.2) concentrations of PSMα3, the ROS levels of treated cells approached those of healthy, untreated, cells, indicating that PSMα3 protects against oligomers-induced damage. This detoxifying activity seems to be associated with the particular structural and physicochemical properties of this

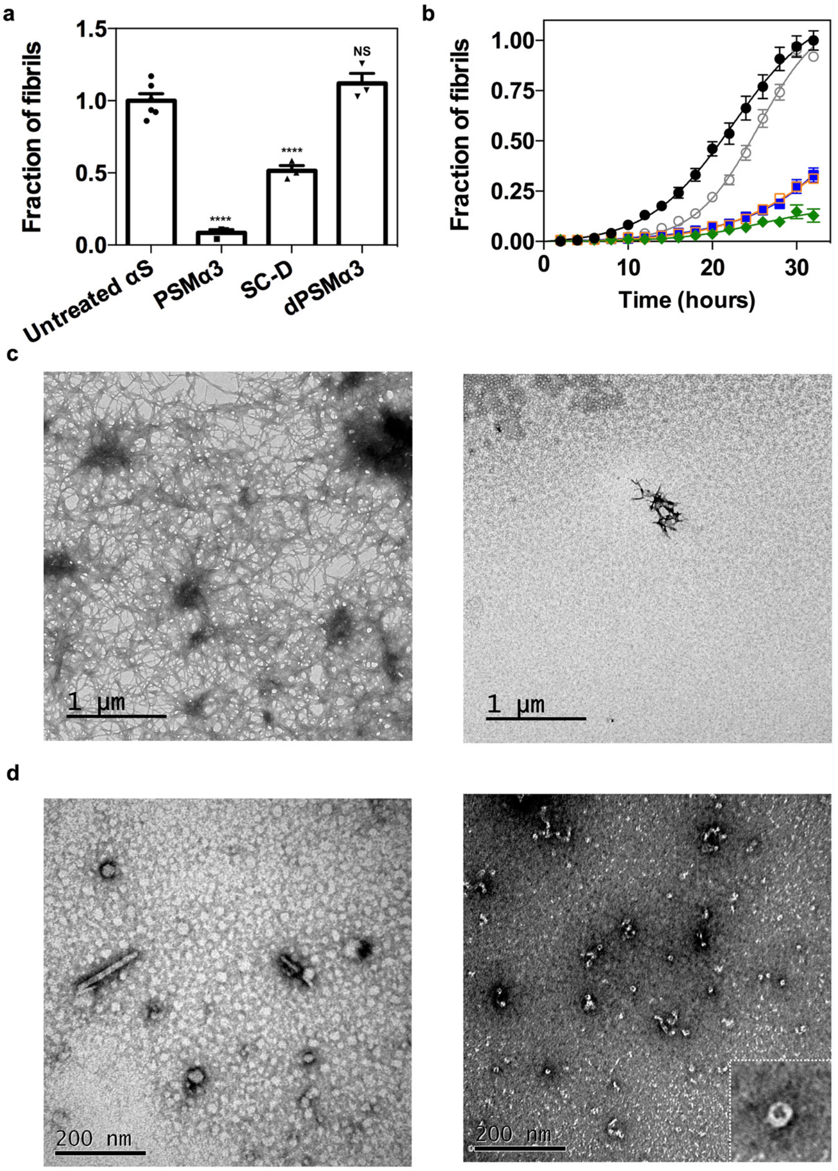

Fig. 3 Effect of PSMα3 on in vitro αS amyloid fibrillation. a Inhibition of α-synuclein (αS) amyloid aggregation as measured by Th-T fluorescence after 32 h incubation in the presence of equimolar concentrations of PSMα3, SynuClean-D (SC-D), and dPSMα3. **** $p < 0.0001$ relative to untreated αS (unpaired two-tailed *t* tests (Welch-corrected)). Data were expressed as mean ± s.e.m ($n = 6$ and 3 independent experiments for untreated and treated conditions respectively). *NS* no significant, $p = 0.23$. **b** Aggregation kinetics of 70 μM αS and titration of the inhibitory activity of PSMα3 at different concentrations: 35 μM (green), 14 μM (orange), 7 μM (blue), 3.5 μM (gray) and in the absence of PSMα3 (black). Data were expressed as mean ± s.e.m ($n = 9$ independent experiments). **c** Representative TEM micrographs of αS aggregated for 32 h in the absence (left) and presence of an equimolar concentration of PSMα3 (right) that came from two independent replicates. **d** Representative TEM micrographs illustrating the morphological differences between low-molecular weight aggregates of αS after 12 h of incubation in absence (left) and presence of PSMα3 (right). Results are consistent in two independent replicates. Inset shows an annular oligomer at high magnification.

peptide since treatment with equimolar concentrations of dPSMα3 failed to exert any protective effect.

Dissection of PSMα3 aggregation-inhibitory determinants. To this point, we have assigned the αS binding, anti-aggregation and cytoprotective properties of PSMα3 to its helical, amphipathic and cationic character. To confirm that this is the case, we reverse-engineered PSMα3 into a non-natural peptide scaffold with low sequence complexity that keeps its critical properties. We employed a set of bioinformatics tools to predict the helical propensity, helical hydrophobic moment, and thermodynamic stability of our successive designs using AGADIR[26], HELIQUEST[37], and FOLDX[38], respectively. Data regarding those predictions are displayed in Supplementary Table 1. Then, we evaluated the anti-aggregative properties of these molecules, under the assumption that the inhibitory capacity is connected with the oligomer-peptide interaction affinity.

A first requirement for binding is a continuous hydrophobic face to interact with the surface of oligomers or fibrils. In our view, the specific sequence of this helical side would be irrelevant, as long as it keeps its lipophilic character. To demonstrate that this assumption is correct, we mutated all the residues in the hydrophobic face of the PSMα3 α-helix to leucine (All_Leu), generating an amphipathic peptide devoid of any sequence diversity in this side. Simultaneously, we designed a variant of All-Leu devoid of the last three C-terminal residues (All_Leu19) since they are not part of the α-helix,

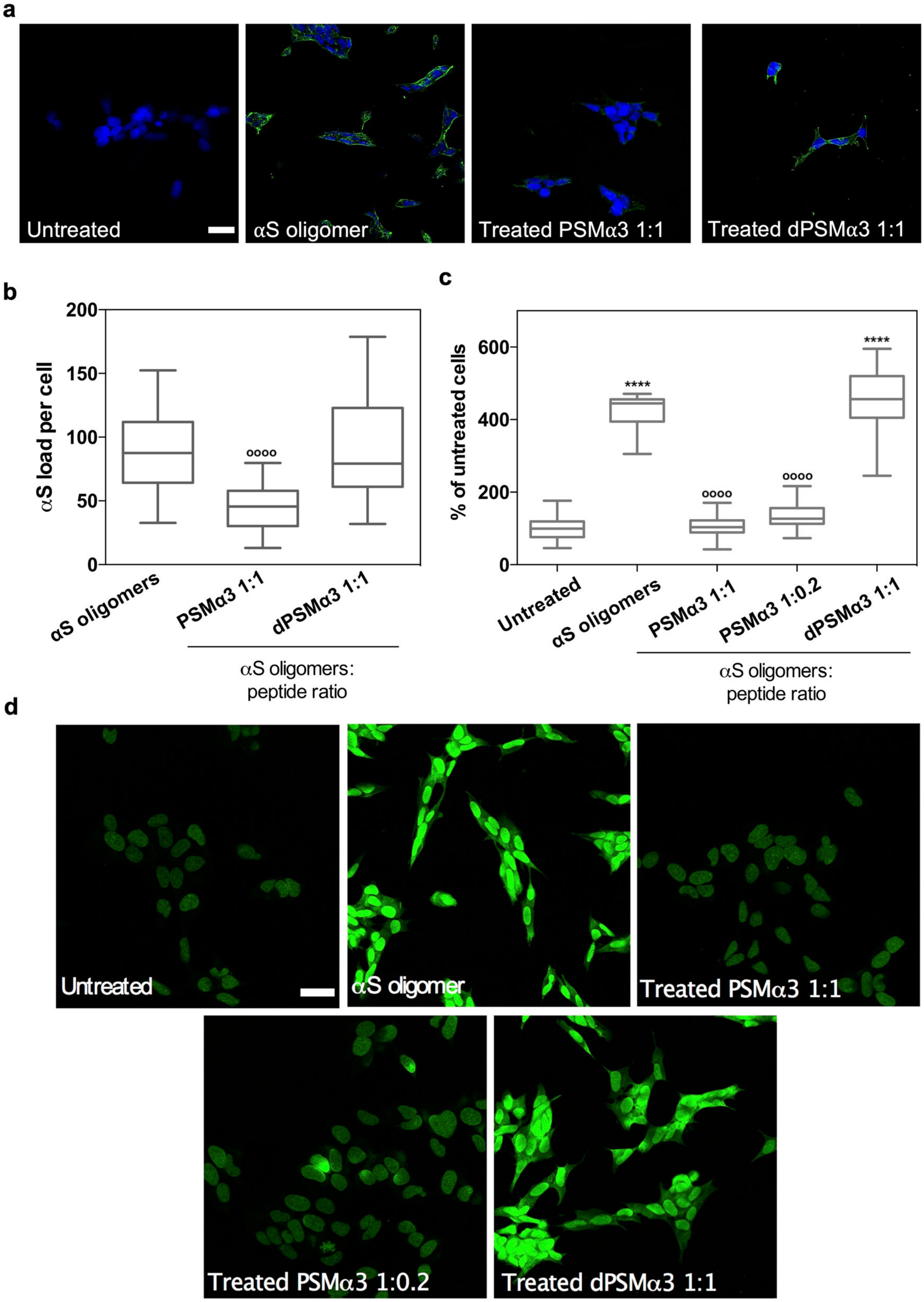

and thus they are not expected to contribute significantly to the binding. Both redesigned peptides folded into α-helices and retained the inhibitory activity, with a potency that approaches that of PSMα3 (Fig. 5a–b). Thus, we concluded that it is the generic hydrophobic character of the helical face and not its sequence or composition that is relevant for the binding.

Next, to further reduce the peptide sequence complexity, we redesigned the hydrophilic face in such a way that it only contained ionizable residues. We designed a new variant (Scaffold_19) with only four different amino acids (Leu, Asp, Glu, and Lys) by introducing two point-mutations (A5E_G16K) in the All_Leu19 peptide. We decided to maintain the peptide net charge by introducing residues with opposed charges. Thus, Scaffold_19 only has Leu in the hydrophobic face and charged residues in the hydrophilic one. This variant folded into an α-helix and showed the same anti-aggregation activity than the parental variant (Fig. 5c).

Fig. 4 Suppression of the αS oligomers-induced damage in neuroblastoma cells. a Representative confocal images showing the α-synuclein (αS) load per cell after the treatment with 10 μM of type B* oligomers pretreated with an equimolar concentration of PSMα3 or dPSMα3. Scale bar represents 30 μm. **b** Quantification of the αS load per cell. ****$p < 0.0001$ relative to untreated cells. °°°°$p < 0.0001$ relative to cells treated with αS type B* oligomers. Unpaired two-tailed *t* tests (Welch-corrected). 76, 72, and 67 cells, (respectively, for αS oligomers, PSMα3 1:1, PSMα3 1:02 and dPSMα3) were analyzed from two independent experiments. **c** Quantification of the levels of intracellular ROS of SH-SY5Y cells incubated with 10 μM of type B* oligomers preincubated with different concentrations of PSMα3 or dPSMα3. °°°°$p < 0.0001$ relative to cells treated with αS type B* oligomers. (Unpaired two-tailed *t* tests (Welch-corrected)). 233, 230, 240, 212, and 100 cells, (respectively, for untreated, αS oligomers, PSMα3 1:1, PSMα3 1:02 and dPSMα3) were analyzed from two independent experiments **d** Representative confocal images of the analysis of panel (**c**). Scale bar represents 30 μM. In (**b**) and (**c**) data are represented as box and whiskers plots where the middle line is the median, the lower and upper hinges correspond to the first and third quartiles, the upper whisker extends from the hinge to the largest value no further than 1.5 × IQR from the hinge (where IQR is the inter-quartile range) and the lower whisker extends from the hinge to the smallest value at most 1.5 × IQR of the hinge.

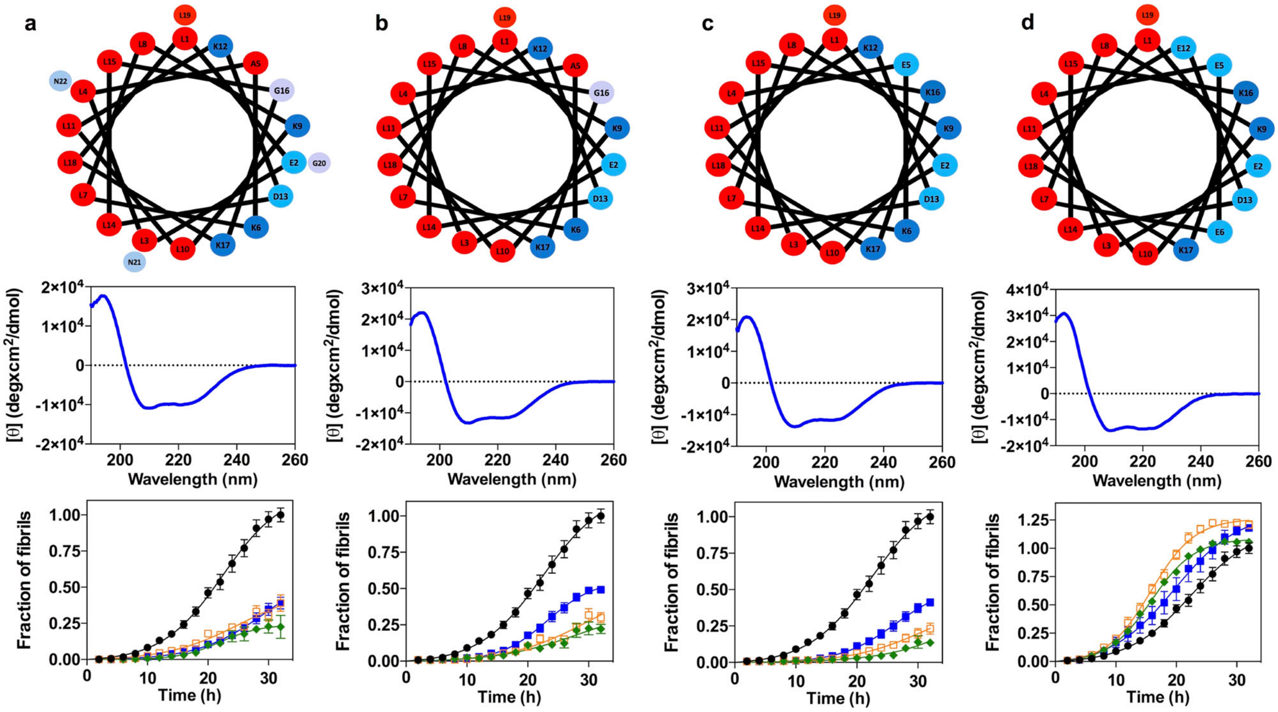

Fig. 5 Redesign of PSMα3 variants to dissect the molecular determinants of the anti-aggregative activity. a–d Helical wheel (red, hydrophobic residues; blue pallet, hydrophilic residues) (up), circular dichroism spectra (mid) and titration of the inhibitory activity of PSMα3 variants at different concentrations (down): 35 μM (green), 14 μM (orange), 7 μM (blue) and in the absence of PSMα3 variants (black). Variants: All_Leu (**a**), All_Leu19 (**b**), Scaffold_19 (**c**), and Anionic_scaffold (**d**). Data were expressed as mean ± s.e.m (*n* = 9 independent experiments).

The simplicity of Scaffold_19 allowed us to redesign the net charge of the peptide, to validate the other physicochemical property theoretically contributing to binding: a net positive charge. We generated a peptide with a net charge of −2 by introducing two charge-reversing mutations (K6E_K12E). This anionic peptide (Anionic_scaffold) folds into an α-helix and has a helical hydrophobic moment (μ_H) of 0.65, indicative of an amphipathic nature, but does not inhibit αS amyloid aggregation, confirming that a cationic character in the hydrophilic face is a requirement for binding (Fig. 5d).

Overall, we succeeded in dissecting the peptide features responsible for aggregation inhibition. In the process, we generated, Scaffold_19, a short peptide with low sequence complexity whose inhibitory activity does not stem from the primary sequence, but instead from a defined spatial distribution of two physicochemical traits.

LL-37 inhibits αS aggregation and oligomers-induced cell damage. Once we elucidated the determinants of this mechanism of αS amyloid inhibition, we wondered if this activity could also be encoded in natural human peptides. First, we screened the EROP-Moscow oligopeptide database[39] for human cationic peptides longer than 10 residues (≥3 helical turns), obtaining 287 hits. Next, we run AGADIR on them to exclude peptides with a low helical propensity, which resulted in 25 peptides, from which only 9 peptides were predicted to have at least a partial amphipathic character, according to their helical hydrophobic moment (μ_H) (Supplementary Table 2). Then we screened the literature for candidates whose tissue distribution overlapped with that of αS and selected LL-37, the only human member of the cathelicidin family of antimicrobial peptides, for its further characterization. LL-37 is a 37-residue peptide resulting from a post-translational cleavage at the C-terminus of cathelicidin hCAP18[40]. This peptide is constitutively expressed in the brain and the gastrointestinal tract; its presence in both tissues is engaging, as the brain-gut axis connection is gaining momentum in PD[41–43].

First, we confirmed that LL-37 adopts an α-helical conformation under our assay conditions (Fig. 6a, b). With α-helical hydrophobic moment (μ_H) of 0.52, the helical-wheel projection and the available 3D-structures[37] indicate that this α-helix would be both cationic and amphipathic (Fig. 6a, b). Then, we titrated

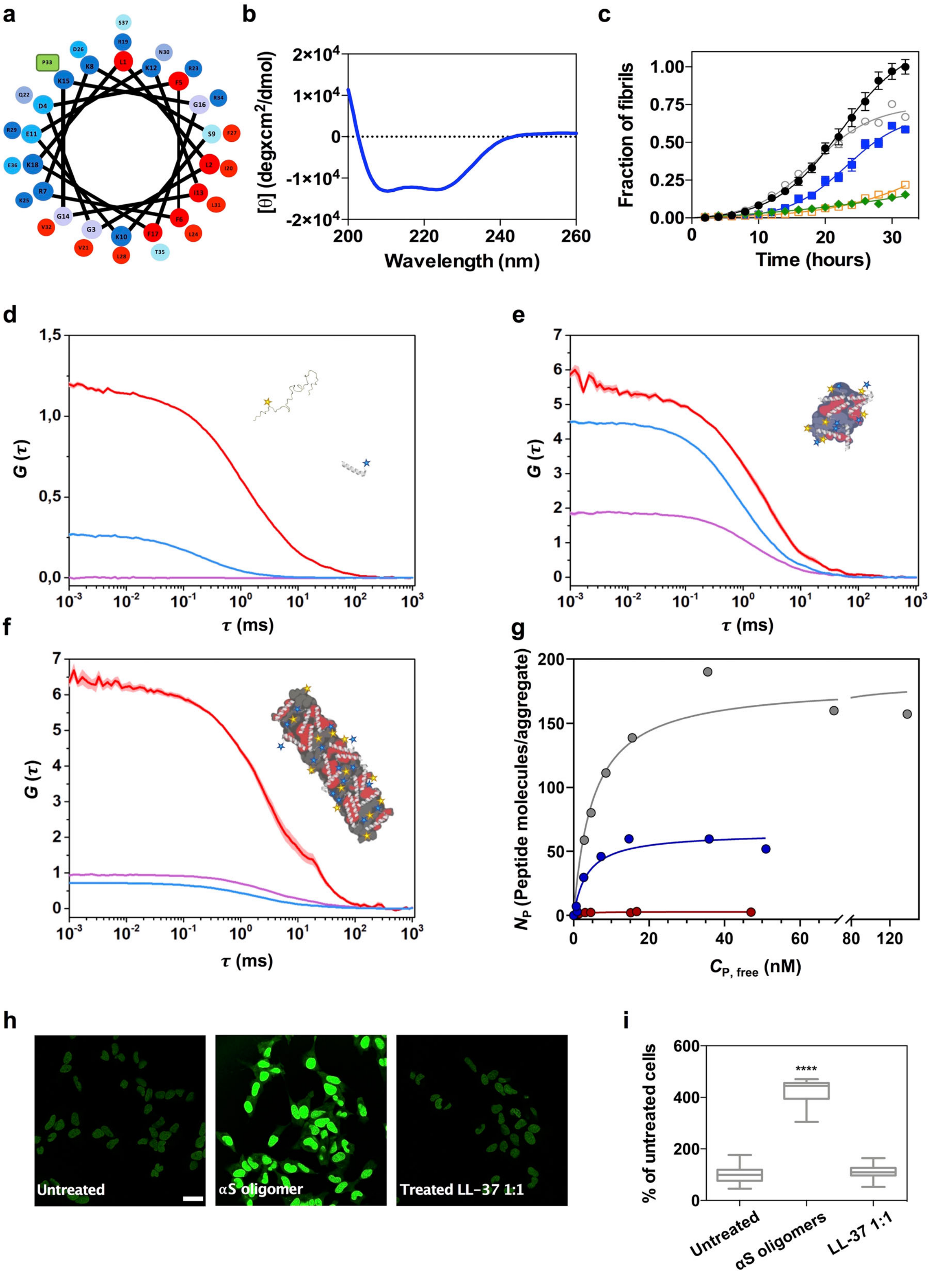

the anti-aggregative activity of LL-37, confirming that it suppresses αS amyloid formation at substoichiometric concentrations (Fig. 6c). Sedimentation analysis provides orthogonal support for the αS aggregation inhibitory activity of LL-37 (Supplementary Fig. 9). Next, we labeled LL-37 with maleimide-Atto647N at a single engineered cysteine at the N-terminus, and we performed time-resolved dual-color fluorescence spectroscopy experiments as described previously for PSMα3. Both dcFCCS and spFRET (Fig. 6d, f and Supplementary Fig. 12) reported a strong binding to type B* oligomers and fibrils, a weak interaction with type A* oligomers and the absence of any interaction with the αS monomer, indicating that LL-37 and PSMα3 share a very similar binding mechanism (Fig. 6g). In this case, LL-37 displays slightly higher affinities than PSMα3 (K_D = 3.62 nM for type B* oligomers, K_D = 5.14 nM for sonicated fibrils and K_D = 1.92 nM for type A* oligomers), and a significantly

Fig. 6 Characterization of the interaction of LL-37 with the αS toxic species. a Helical wheel projection of LL-37 sequence (red, hydrophobic residues; blue pallet, hydrophilic residues; green, proline). **b** Far-UV circular dichroism spectra of LL-37 in PBS pH 7.4. **c** Aggregation kinetics of 70 μM α-synuclein (αS) and titration of the inhibitory activity of LL-37 at different concentrations: 35 μM (green), 14 μM (orange), 7 μM (blue), 3.5 μM (gray) and in the absence of peptide (black). Data were expressed as mean ± s.e.m ($n = 9$ independent experiments). Representative auto-correlation curves for αS and LL-37 peptide and cross-correlation curves for interacting molecules are shown in blue, red and purple lines, respectively. The amplitude (G) error is shown as faint colored area for the corresponding correlation curves. Samples contained (**d**) ~15 nM αS monomers and ~15 nM LL-37, (**e**) 1 nM type B* oligomers and ~5 nM LL-37 or (**f**) ~5 nM sonicated fibrils and ~5 nM PSMα3. **g** Titration binding curves for the interaction of LL-37 with type A* oligomers (red circles), type B* oligomers (blue circles) or sonicated fibrils (gray circles) obtained by dcFCCS, showing their corresponding analysis assuming a model of n independent binding sites per αS aggregated species (solid lines). N_P represents the number of bound peptides per aggregate. **h** Representative confocal images of SH-SY5Y cells treated with 10 μM of type B* oligomers in the presence of an equimolar concentration of LL-37. Scale bar represents 30 μm. **i** Quantification of the intracellular ROS of the experiment displayed in panel (**h**). ****$p < 0.0001$ relative to untreated cells. $^{oooo}p < 0.0001$ relative to cells treated with αS type B* oligomers. Unpaired two-tailed t tests (Welch-corrected). A total of 233, 230, and 199 cells, (respectively, for untreated αS oligomer and LL-37 1:1) were analyzed from two independent experiments. For αS aggregated species, consisting of several tens of monomers, the species concentrations in (**d**–**g**) are in the picomolar range and, as further explained above, single-particle conditions are ensured throughout the experiments. In (**i**) data are represented as box and whiskers plots where the middle line is the median, the lower and upper hinges correspond to the first and third quartiles, the upper whisker extends from the hinge to the largest value no further than 1.5 × IQR from the hinge (where IQR is the inter-quartile range) and the lower whisker extends from the hinge to the smallest value at most 1.5 × IQR of the hinge.

higher number of binding sites in type B* oligomers ($N_{\max} = 64$) and sonicated fibrils ($N_{\max} = 181$), while remain the same as PSMα3 for the number of binding sites in the type A* oligomers, which was in any case marginal ($N_{\max} = 3$). Consistent with the LL-37 ability to bind type B* oligomers with high affinity, the preincubation of these toxic species with the human peptide at an equimolar concentration completely abolished the production of ROS in neuroblastoma cells (Fig. 6h, i). LL-37 is not related in sequence to PSMα3 or Scaffold_19, but the three peptides share the same structural and physicochemical traits. This confirms that a linear combination of these properties suffices to identify, and potentially design, potent inhibitors of αS aggregation.

Whether LL-37 is actually involved or not in the pathogenesis of PD remains unexplored. However, it is tempting to speculate that small peptides able to interact actively with αS aggregated species might cohabitate with this protein in tissues relevant to the disease. These human peptides may open an unexplored avenue for PD treatment, i.e., by stimulating their endogenous expression.

Discussion

Because of its involvement in PD and other synucleinopathies, αS aggregation remains a promising target for therapeutic intervention. Herein, we propose a strategy for targeting the αS species behind the onset of these neurodegenerative diseases selectively. By binding to αS toxic oligomers and fibrils, the described collection of peptides inhibits the progression of αS aggregation, while suppressing oligomer mediated cell damage. Importantly, because the binding determinants are structurally encoded, these peptidic molecules do not recognize monomeric αS. Furthermore, the avidity of these peptides for early non-toxic oligomers is more than one order of magnitude lower than the one for type-B* oligomers and fibrils, indicating that they are very selective for these toxic species.

We describe here, non antibody-related biomolecules targeting αS aggregated species, which have been rationally predicted, identified, and engineered. PSMα3 is a first-in-class hit molecule that sets the ground for the future advancement of a generation of leads for disease modification in PD and other synucleinopathies. The requisites for a high peptide binding affinity and αS toxic species selectivity are relatively simple: hydrophobic and positively charged surfaces with opposed orientations in space. This is best exemplified by Scaffold_19, a short and low complexity peptide that fulfills those conditions. This defined binding mode should help in the development and diversification of ligands with increased activities.

Many small bioactive peptides are derived from larger precursors and generated after proteolytic cleavage[44]. In some cases, these peptides are encrypted inside globular proteins, and their processing results in the manifestation of a new biological function. LL-37 is a cathelicidin-derived peptide constitutively expressed in the human brain[45]. Here, we show that LL-37 is a tight binder of αS toxic assemblies, with anti-aggregation and cytoprotective properties. LL-37 has been reported to inhibit the amyloid aggregation of two other disease-linked peptides, Aβ-42[46] and IAPP[47]. However, the mechanism behind this activity is different from the one we describe here since it relies on a certain degree of sequence homology between short linear stretches in these molecules, with LL-37 binding to both the monomers and the aggregated species[46,47]. The K_{D}s for the binding of LL-37 to freshly resuspended and 24-days-incubated Aβ-42 peptide are 13.30 μM and 20.30 μM, respectively[46]; thus, several orders of magnitude weaker than the ones we report here for αS. Irrespective of the affinity and species selectivity, it is tempting to suggest that endogenous peptides, similar to those described here, could compose a regulatory system where they act as silent guardians of the proteome by targeting aggregation-prone proteins.

Apart from potential future therapeutic implications, the ability of the amphipathic cationic helical peptides to bind to αS toxic species with high affinity might find a direct application in diagnosis. The presence of αS aggregates in biofluids is considered a biomarker for PD and other synucleopathies[48,49]. However, current detection methods are not specific and sensitive enough for their clinical implementation. For instance, ELISA approaches based on the so-called conformation-specific antibodies, perform better when the detection is normalized relative to the total levels of αS or when the same epitope-blocking antibody is used for both capture and detection[50]. This indicates that a major limitation of these methods is the unwanted cross-reaction of the antibodies with the large excess of αS monomer in the fluid. The peptides we describe here do not interact with monomeric αS, and the presence of up to 500-fold molar excess of monomeric αS does not interfere with the detection of nanomolar amounts of toxic oligomers. This property, together with their close-to-antibody affinities, may turn useful for diagnostic purposes. We envision that a strategy which combines sequence-specific αS ligands (i.e., available antibodies) with our species-specific peptides might succeed in the selective and sensitive detection of toxic αS species in biological fluids.

Overall, the molecular entities we describe in this work may help to develop therapeutic and diagnostic strategies for the synucleinopathies.

Methods

αS expression and purification. *Escherichia coli* BL21 (DE3) cells containing a pET21a plasmid encoding the αS gene were grown in LB medium supplemented with 100 μM/mL ampicillin. Protein expression was induced at an optical density of 0.8 (600 nm) with 1 mM isopropyl β-D-thiogalactopyranoside (IPTG) for 4 h. Cells were harvested by centrifugation and washed up by resuspension and centrifugation in PBS pH 7.4. Next, pellets were resuspended in 50 mL per culture liter in lysis buffer (50 mM Tris pH 8, 150 mM NaCl, 1 μg/mL pepstatin, 20 μg/mL aprotinin, 1 mM benzamidine, 1 mM PMSF, 1 mM EDTA, and 0.25 mg/mL lysozyme) and sonicated using a LabSonic® U sonicator (B. Braun Biotech International, Melsungen, Germany). Samples were boiled during 10 min at 95 °C and centrifugated at 20,000 g at 4 °C for 40 min. The soluble fraction was treated with 136 μL/mL of 10% w/v streptomycin sulfate and 228 μL/mL of pure acetic acid. Upon centrifugation, soluble extracts were fractionated by adding 1:1 of saturated ammonium sulfate and resuspending the insoluble fraction with 50% ammonium sulfate. The pellet was resuspended in 100 mM pH 8 ammonium acetate (5 mL per culture liter) and pure EtOH 1:1 (v/v) and harvested by centrifugation. The insoluble fraction was resuspended in Tris 20 mM pH 8, filtered with a 0.22 μm filter and loaded into an anion exchange column HiTrap Q HP (GE Healthcare, Chicago, USA) coupled to an ÄKTA purifier high performance liquid chromatography system (GE Healthcare, Chicago, USA). Tris 20 mM pH 8 and Tris 20 mM pH 8, NaCl 1 M were used as buffer A and buffer B. αS was eluted using a using a step gradient: Step 1: 0%–20% buffer B, 5 cv; Step 2: 20%–45% buffer B, 11 cv; Step 3: 100% buffer B, 5 cv. Purified αS was dialyzed against 5 L ammonium acetate 50 mM in two steps; 4 h and overnight. Finally, protein purity was addressed using 15% SDS-PAGE. The purest fractions were lyophilized and stored at −80 °C. For the experiments, αS lyophilized aliquots were resuspended to a final concentration of 210 μM using PBS pH 7.4 and filtered using 0.22 μm filters. αS concentration was determined measuring the absorbance at 280 nm and using the extinction coefficient 5960 M^{-1} cm^{-1}.

Peptide preparation. PSMα3, dPSMα3, All_Leu, All_Leu_19, Scaffold_19, Anionic Scaffold and LL-37 were purchased from Synpeptide (Shanghai, China) with a purity >95%. Single cysteine containing variants were purchased from Genscript (Piscataway, USA) with a purity >95%. LL-37 was diluted in Milli-Q sterilized water, divided into aliquots and lyophilized. Cysteine containing peptides were resuspended in PBS pH 7.4, 5 mM TCEP and subsequently labeled with the corresponding fluorophore. PSMα3, dPSMα3, All_Leu, All_Leu_19, Scaffold_19 and Anionic Scaffold were dissolved in a 1:1 mixture of trifluoroacetic acid and hexafluoroisopropanol and sonicated for 10 min. Stock solutions were divided into aliquots and vacuum dried with a SpeedVac (Thermo Fisher Scientific, Waltham, USA) and stored at −80 °C until assayed. Peptide aliquots were resuspended in pure Milli-Q water prior their use.

αS and peptide labeling. Site-specific labeling of αS was performed in an αS variant with a single engineered cysteine at position 122 (αS N122C). This variant was expressed and purified as described above but including 5 mM DTT in all purification steps. The protein was labeled with maleimide-modified Alexa Fluor 488 (AF488) (Invitrogen, Carlsbad, USA) for 15–20 h at 4 °C in the dark. After quenching the reaction with 10 mM DTT, free unreacted dye in the protein solution was subsequently separated using a P10 desalting column (GE Healthcare, Waukesha, USA), and the labeled protein solution was flash frozen with liquid nitrogen and stored at −80 °C. The different peptides, PSMα3, dPSMα3, and LL-37, were labeled at a single engineered cysteine at the N-terminus with maleimide-modified Atto647N (ATTO-TEC, Siegen, Germany). The same labeling and purification strategy were followed as for αS, although in this case the unreacted free dye was removed from the protein solution using a polyacrylamide desalting column (Thermo Fisher Scientific, Waltham, USA). Two cleaning steps were required to remove completely the free dye from the labeled peptide solution.

Preparation of the different isolated αS aggregates samples. For the isolation of type B* oligomers purified αS was dialyzed against Milli-Q water and lyophilized for 48 h in aliquots of 6 mg. The aliquots were resuspended in 500 μL of PBS pH 7.4 to a final concentration of ca. 800 μM, filtered through 0.22 μm filters and incubated at 37 °C without agitation for 20–24 h. The sample was then ultracentrifuged at 288,000 *g* in a SW55Ti Beckman rotor, in order to remove any possible fibrillar species formed during the incubation, and later filtered by four consecutive cycles of filtration through 100 kDa centrifuge filters (Merck, Darmstadt, Germany) in order to remove the great excess of monomeric protein from the oligomeric solution. Type A* oligomers were generated by incubating 210 μM of αS in PBS pH 7.4 with ten molar equivalents of (-)-epigallocatechin-3- gallate (EGCG) (Merck, Darmstadt, Germany) for 48 h at 37 °C. The excess of compound and unreacted monomeric protein were then removed by six consecutive cycles of filtration through 100 kDa centrifuge filters (Merck, Darmstadt, Germany). The concentration of the final oligomeric solutions was determined measuring the absorbance at 280 nm and using an extinction coefficient of 5960 M^{-1} cm^{-1} or absorbance at 495 nm and an extinction coefficient of 72,000 M^{-1} cm^{-1} for AF488-labeled oligomers. In all cases, the oligomers were kept at room temperature and were used within 3 days after their production. The fibrillar samples were produced as explained in the aggregation kinetics methodology section. The non-reacted protein and small non-fibrillar species that could be formed during the aggregation reaction were removed from the sample by 3 consecutive steps of centrifugation and resuspension of the precipitated fraction in PBS buffer at pH 7.4. Fibrils were then sonicated 1 min, 50% cycles, 80% amplitude in a Vibra-Cell VC130 Ultrasonic Processor (Sonics, Newton, USA) to generate fibrillar samples with a relatively homogeneous size distribution of small fibrils. The concentration of the AF488-labeled fibrillar samples was determined by subtracting the absorbance of the monomer after centrifugation at 495 nm using an extinction coefficient of 72,000 M^{-1} cm^{-1}, with respect to the total soluble protein at time 0. For type A* oligomers, the concentration was adjusted in situ for each experiment so that a suitable and consistent burst-rate was reached. Thus, an interference of EGCG in quantifying the sample was avoided.

Far circular dichroism analysis. Far-UV CD spectra of the different peptide solutions were recorded on a Jasco J-815 CD spectrometer (Halifax, Canada) Software- Jasco spectra manager v2 at 25 °C using samples of 15 μM peptide final concentration in Milli-Q water. CD signal was measured from 260 nm to 190 nm at 0.2 nm intervals, 1 nm bandwidth, 1 sec of response time and a scan speed of 100 nm/min on a 0.1 cm quartz cell. Ten accumulations were recorded and averaged for each measurement. For LL-37 peptide samples, CD spectra were recorded in PBS pH 7.4, because of structural differences of this peptide in water and saline solvents.

Time-resolved fluorescence spectroscopy. Dual-Color Time-Resolved Fluorescence Spectroscopy experiments were performed on a commercial MT200 (PicoQuant, Berlin, Germany) time-resolved fluorescence confocal microscope with a Time-Correlated Single Photon Counting (TCSPC) unit. Laser diode heads were used in Pulsed Interleaved Excitation (PIE), and the beams were coupled through a single-mode waveguide and adjusted to laser powers of 6 μW (481 nm) and 5 μW (637 nm) measured after the dichroic mirror for optimal count rates while avoiding photobleaching and saturation. The coverslip was placed directly on the immersion water on top of a Super Apochromat 60x NA 1.2 objective with a correction collar (Olympus Life Sciences, Waltham, USA). A dichroic mirror of 488/640 nm (Semrock, Lake Forest, IL, USA) was used as the main beam splitter. Out-of-focus emission light was blocked by a 50 μm pinhole and the in-focus emission light was then split by a 50/50 beamsplitter into two detection paths. Bandpass emission filters (Semrock, Lake Forest, IL, USA) of 520/35 for the green dye (AF488) and 690/70 for the red dye (Atto647N) were used before the detectors. Single Photon Avalanche Diodes (SPADs) (Micro Photon Devices, Bolzano, Italy) served as detectors. Each measurement had an acquisition time of 1–3 min.

For FCS experiments, the effective focal volume of the green channel and its structural parameters in our system were determined using a 1 nM solution of Atto488 (ATTO-TEC GmbH, Siegen, Germany) yielding $V_{\mathrm{eff,\,g}} = 0.51$ fL and $\kappa_g = 3.97$. Positive and negative cross-correlation controls were performed with a dual-labeled dsDNA (10 nM) and an equimolar mixture (15 nM each) of AF488- and Atto647N-labeled monomeric αS (Supplementary Fig. 4). The positive control was also used for the determination of the red and dual-color effective focal volume and their structural parameter, yielding $V_{\mathrm{eff,r}} = 0.1$ fL, $V_{\mathrm{eff,gr}} = 0.091$ fL, $\kappa_r = 2.78$, and $\kappa_{gr} = 2.67$, respectively.

AF488-labeled aggregated αS samples were diluted in PBS pH 7.4 to a final protein concentration of ~1-5 nM in a 50 μL droplet which was spotted directly onto a cover glass (Corning, Corning, USA) previously coated with a 1 mg/mL BSA solution. Atto 647N-labeled peptides were titrated into the droplet and the peptide concentration was measured individually for each experiment by autocorrelation analysis of the red dye. No significant changes in correlation amplitudes were observed over time after equilibrating the samples for 2 min. Experiments were performed at 20 °C and samples were covered to avoid evaporation. It is important to note that, for αS aggregated species, consisting of several tens of monomers, the species concentrations are in the picomolar range and, as further explained below, single-particle conditions are ensured throughout the experiments. The aggregated species coexist with a certain amount of monomeric αS due to the stark sample dilution employed in the experiments and, therefore, the donor auto-correlation curves in Figs. 2, 6 and Supplementary Figs. 8, 12, 13, show both the diffusion component of the monomer and the aggregate. A similar behavior is observed for peptides PSMα3 and LL-37, which can exist as oligomerized species. For obtaining the diffusion coefficients of the different aggregates the diffusion component of the monomeric species in the samples was filtered out by intensity-filtered dcFCCS analysis as explained below. The diffusion coefficient (D_g or D_r) fitted to data for αS species are 103 ± 16 $\mu m^2\,s^{-1}$, 4 ± 0.9 $\mu m^2\,s^{-1}$, 3.46 ± 1.2 $\mu m^2\,s^{-1}$ and 0.81 ± 0.12 $\mu m^2\,s^{-1}$ for the monomer, type A*oligomers, type B* oligomers and fibrils, respectively, in very good agreement with the diffusion coefficients expected according to their corresponding sizes as determined by AFM and DLS (see Supplementary Fig. 1) and as reported before[13,19]. In addition, such intensity thresholding yields a confocal volume mean occupancy (N) well below 1 for all fluorescent species involved, with $N = 0.019$, $N = 0.043$, and $N = 0.053$ for type A*oligomers, type B* oligomers, and fibrils, respectively. Therefore, in terms of burst selection for the PIE-FRET and fluorescence stoichiometry analysis, where the same intensity threshold is applied, the experiments were conducted under single-particle conditions. This becomes even more evident when looking at the raw data in the form of intensity time traces of, for instance, the PSMα3 - type B* oligomer interaction experiments (Supplementary Fig. 14).

D_r values of 14.6 ± 3.6, 19.2 ± 4.2 $\mu m^2 s^{-1}$ and 108 ± 18 $\mu m^2 s^{-1}$ were calculated for PSMα3, LL-37, and dPSMα3, respectively, with $N = 0.053$ and $N = 0.11$, for PSMα3 and LL-37, respectively. These data indicate that PSMα3 and LL-37 exhibit a certain degree of oligomerization, despite no aggregates were detected in TEM images of peptides alone (not shown), and the data indicates that they bind to their targets in the monomeric form (Figs. 2, 6 and Supplementary Fig. 7).

Both data acquisition and analysis were performed on the commercially available software SymphoTime64 version 2.3 (PicoQuant, Berlin, Germany). For the oligomeric and fibrillar samples, a lower intensity threshold of 27 photons in the green dye autocorrelation analysis was applied to filter out the low intensity signal arising from the monomeric αS events generated upon dilution-induced disaggregation of the aggregated samples. This threshold was calculated as three times the mean intensity of monomeric αS obtained from the analysis of a sample of pure αS monomers. In addition, an upper intensity threshold was applied to auto-correlation and cross-correlation analysis to filter out any possible artifacts such as dust particles or aggregate clusters (even though these events were very scarce): 500 photons for monomer, type A* and type B* oligomers and 1500 photons for sonicated fibrils. Data on the red channel corresponding to the peptide fluorescence signal was intensity-filtered with a lower intensity threshold in analogy to the green channel owing to the fact that the peptide can also exist as self-assembled species. The reference signal was that of the monomer-only dPSMα3 sample. The PIE excitation scheme together with the TSCPC acquisition enabled the application of a lifetime-weighted filter, which aided removal of background and spectral cross-talk.

The corrected auto-correlations of the green and the red channel (G_i) were given by

$$G_{\mathrm{i}}(\tau) = \frac{\langle F_{\mathrm{i}}(t) \cdot F_{\mathrm{i}}(t+\tau) \rangle}{F_{\mathrm{i}}{}^{2}} - 1 \tag{1}$$

where F_i (t) denotes the fluorescence intensity either the green or the red channel, τ is the correlation time and the angled brackets indicate a time average over the acquisition time. The cross-correlation (G_x) between the green and the red channel was given by

$$G_{\mathrm{x}}(\tau) = \frac{\langle F_{\mathrm{g}}(t) \cdot F_{\mathrm{r}}(t+\tau) \rangle}{\langle F_{\mathrm{g}} \rangle \langle F_{\mathrm{r}} \rangle} - 1 \tag{2}$$

Auto-correlation curves for both the green and red channel were fitted with a 2 diffusion-component model accounting for residual monomeric αS and bound and unbound peptide, respectively, using the following equation:

$$G_{\mathrm{i}}(\tau) = G_{\mathrm{i}}^{0} \frac{f_{\mathrm{i},1}}{\left(1+\frac{\tau}{\tau_{D_{\mathrm{i},1}}}\right)\sqrt{1+\frac{\tau}{\kappa^{2} \mathrm{x} \tau_{D_{\mathrm{i},1}}}}} + \frac{f_{\mathrm{i},2}}{\left(1+\frac{\tau}{\tau_{D_{\mathrm{i},2}}}\right)\sqrt{1+\frac{\tau}{\kappa^{2} \mathrm{x} \tau_{D_{\mathrm{i},2}}}}}, \tag{3}$$

whereG_i^0 is the correlation amplitude at correlation time 0, $f_{i,1}$ and $f_{i,2}$ denote the fractional amplitudes of the monomeric and aggregated αS for the green channel (where i = g) and the bound and unbound peptide for the red channel (where i = r) and κ^2 is the structure parameter of the focal volume. The same applies for the diffusion terms $\tau_{D_{i,1}}$ and $\tau_{D_{i,2}}$. No correlated blinking is expected when multiple dyes are present on one particle as it is our case and therefore a blinking term was not included.

Cross-correlation amplitudes were fitted with a 1-component simple diffusion model since only one diffusion coefficient is expected for the interacting species (Supplementary Fig. 13) using the following equation:

$$G_{\mathrm{x}}(\tau) = G_{\mathrm{x}}^{0} \frac{1}{\left(1+\frac{\tau}{\tau_{D,\mathrm{x}}}\right)\sqrt{1+\frac{\tau}{\kappa^{2} \mathrm{x} \tau_{D,\mathrm{x}}}}}. \tag{4}$$

With the corrected green dye autocorrelation function and the mean intensity of monomeric αS, the average aggregate particle number (N_{Ag}) for each αS aggregated sample was estimated as

$N_{\mathrm{Ag}} = \frac{1}{G_{\mathrm{g}}^{0}}$. The average particle number for the peptide was calculated in analogy to that of αS. The peptide concentration was calculated as

$C_{\mathrm{P}} = \frac{N_{\mathrm{r}}}{V_{\mathrm{eff,r}} \mathrm{x} \mathrm{N}_{\mathrm{A}}}$,where N_r is the average number of particles in the red confocal volume, $V_{eff,r}$ is the red focal volume and N_A is the Avogadro number. The cross-correlation amplitudes, dual-laser focal volume, $V_{eff,\ x}$, and peptide concentrations, C_P, were used for calculating the number of peptides bound to each αS species (N_P) and the free peptide concentration ($C_{P,\ Free}$) as described by Kruger and coworkers[32].

For single-burst FRET and stoichiometry analysis, an acceptor (red dye) direct excitation lower threshold based on the mean intensity of the time trace ($I_{A,mean} + 2 \times \sigma$) was used to filter out those events without an active acceptor molecule. To further select those events arising from αS aggregates, a burst selection intensity threshold of 100 photons was used. In the FRET analysis, experimentally determined correction factors were applied: spectral cross-talk α was 0.004, direct excitation β was 0.0305 and detection efficiency γ was 0.517. Burst-wise FRET efficiency and stoichiometry were calculated as given by

$$E = \frac{F_{\mathrm{A,IE}}}{F_{\mathrm{D}} + F_{\mathrm{A,SE}}} \tag{5}$$

$$S = \frac{F_{\mathrm{D}} + F_{\mathrm{A,IE}}}{F_{\mathrm{D}} + F_{\mathrm{A,IE}} + F_{\mathrm{A,DE}}} \tag{6}$$

where F_D is the fluorescence intensity in the donor (green) channel, $F_{A,IE}$ is the fluorescence intensity in the acceptor (red) channel through indirect excitation and $F_{A,DE}$ is the fluorescence intensity in the acceptor (red) channel after direct excitation by PIE pulse.

Stoichiometry values were corrected for the difference in mean intensity between the monomeric αS and peptide bursts, obtained from monomeric αS-only and peptide-only measurements; the obtained mean intensity ratio $I_{mean,\alpha S}$: $I_{mean,peptide}$ was found to be 0.77. Stoichiometry distributions were fitted to a log-normal distribution to obtain the mean stoichiometry value for each measurement. The number of bound peptides per aggregate (N_P) was then estimated by multiplying the mean stoichiometry value previously obtained by the mean number of αS monomers present on each aggregate as calculated empirically from the molecular brightness in FCCS experiments. The free peptide concentration ($C_{P,\ Free}$) and N_P obtained by either FCCS or single-burst stoichiometry analysis were used for calculating the binding curves as described by Kruger and coworkers[32]. To obtain the dissociation constant K_D and the maximum specific binding sites N_{max}, the resulting binding curves were fitted to the following specific binding model with n identical and independent binding sites:

$$Y = \frac{N_{\max} \cdot X}{(K_{\mathrm{D}} + \mathrm{X})} \tag{7}$$

The binding curves and binding parameters obtained from either FCCS or single-burst stoichiometry analysis were compared (Supplementary Fig. 7) and found to be remarkably similar, which validates the analysis. OriginPro9.1 software was used for graphical data representation and statistical analysis.

Aggregation kinetics. αS amyloid aggregation was monitored in a 96 wells plate (non-treated) (Sarstedt, Germany) containing Teflon polyballs (1/8″ diameter) (Polysciences Europe GmbH, Eppelheim, Germany) as described by Pujols and coworkers[9]. Each well contained 150 µL solutions of 70 µM αS in PBS buffer with 40 µM thioflavin-T and the corresponding concentration of peptide. Plates were incubated at 37 °C, 100 rpm in an orbital culture shaker Max-Q 4000 (Thermo Fisher Scientific, Waltham, USA). Aggregation was analyzed every 2 h using a Victor3.0 Multilabel Reader Software-PerkinElmer 2030. (PerkinElmer, Waltham, USA). End-point measurements were performed after 32 h of incubation. Fluorescence intensity was measured in triplicate by exciting with a 430–450 nm filter and collecting the emission with a 480–510 nm filter. The resulting kinetics were normalized to the maximum fluorescence of the αS control (untreated).

Atomic force microscopy. αS samples were diluted to a protein concentration of 0.1–0.5 µM and deposited on cleaved Muscovite Mica V-5 (Electron Microscopy Sciences; Hatfield, Pensilvania, USA). Slides were washed with double distilled water and allowed to dry before imaging acquisition on a Bruker Multimode 8 (Bruker; Billerica, USA) using a FMG01 gold probe (NT-MDT Spectrum Instruments Ltd., Russia) in intermittent-contact mode in air. Images were processed using Gwyddion (version 2.48) and the width measurements were corrected for the tip shape and size (10 nm).

Polyacrylamide gel electrophoresis. For monomeric and fibrillar αS species, 5 µg protein in denaturing loading buffer were loaded onto a 15% acrylamide SDS-PAGE. For type A* and type B*, 2 µg protein in non-denaturing buffer were loaded onto a 15% native-PAGE. The only difference between the denaturing and non-denaturing gel electrophoresis was the absence of SDS in the sample, gel and buffer of the native PAGE. No boiling step was included in either case. Unprocessed scans of the gels are presented in the Source Data file.

Dynamic light scattering. Estimations of the hydrodynamic radius of αS species were made on a DynaPro NanoStar (Wyatt, USA) equipped with a Peltier temperature control. Protein samples were prepared at a 25 µM concentration in filtered PBS (0.22 µm cellulose acetate syringe filters). DLS measurements were performed at 25 °C at a fixed angle of 90 °. Twenty acquisitions per measurement were collected using a 2 s acquisition time. An average of 10 measurements were performed for the statistical size analysis. Data was analyzed using the Dynamics software (version 6.12.03).

Fourier-Transform infrared (FT-IR) spectroscopy. αS aggregates species were transferred to deuterated buffer, by either centrifugation/resuspension or filtering cycles, to a final protein concentration of ca. 4 mg/ml. Samples were then deposited between two CaF2 polished windows separated by a PTFE Spacer (Harrick Scientific Products Inc., USA). Spectra were collected in transmission mode at room temperature using a VERTEX 70 FTIR Spectrometer (Bruker, USA) equipped with a cryogenic MCT detector cooled in liquid nitrogen. IR spectra were processed and analyzed using standard routines in OPUS version 6.5 (Bruker, USA), RAMOPN (NRC, National Research Council of Canada) and Spectra-Calc-Arithmetic© version A2.21 (Galactic Inc., USA).

ANS fluorescence spectroscopy. 10 µM of each αS sample was incubated with 500 µM 8-anilo-1-naphtalene-sulfonic acid (ANS) in PBS for 45 min before recording the spectra. The extinction coefficient of ANS at 350 nm was assumed to be 5000 cm^{-1} M^{-1}. In order to monitor ANS binding to the each αS species, samples were excited at 350 nm and their emission spectra were recorded from 400 to 650 nm in 1-nm steps. Spectra were collected at room temperature in a Cary Eclipse Fluorescence Spectrophotometer (Varian, Palo Alto, California, United States) with slit-widths of 5/5 nm. An averaging time of 100 ms was used.

Transmission electron microscopy. For electron microscopy analyses, end-point aggregated samples were sonicated for 5 min at minimum intensity in an ultrasonic bath (VWR ultrasonic cleaner) and placed onto carbon-coated copper grids and allowed to adsorb for 5 min. The grids were then washed with distilled water and negative stained with 2% (w/v) uranyl acetate for 1 min. Finally, the excess of uranyl acetate was absorbed using ashless filter paper and the grids were left to air-dry for 15 min. A TEM JEM-1400 Software-Gatan Digital Micrograph 1.8 (JEOL, Peabody, USA) microscope was used operating at an accelerating voltage of 120 kV. The more representative images of each grid were selected. Images were processed and analyzed with Image J (version 1.52p)

Sedimentation assay. αS aggregation was performed as previously described. End-point samples were subjected to ultracentrifugation at 100,000 g for 30 min at 20 °C in a SW55Ti Beckman rotor in order to fractionate soluble and fibrillar species. αS concentration in the soluble fraction was determined by measuring the absorbance at 280 nm ($\varepsilon = 5960\ M^{-1}\ cm^{-1}$). Soluble fractions in denaturing loading buffer were boiled for 5 min and loaded onto a 15% acrylamide SDS-PAGE. Proteins were revealed with BlueSafe (NZYTech, Portugal). Unprocessed scans of the gels are presented in the Source Data file.

Isolation of low molecular weight aggregates generated during αS in vitro aggregation. αS aggregation was performed as previously described in absence and presence of PSMα3. Aliquots at the analyzed time point were taken and flash frozen in liquid nitrogen and stored at −80 °C until assayed. To fractionate our sample into insoluble species, low-molecular weight aggregates and monomers, we adapted the centrifugation-based protocol developed by Kumar and coworkers[51]. αS preparations were subjected to ultracentrifugation at 100,000 g for 30 min at 20 °C in a SW55Ti Beckman rotor in order to isolate larger fibrillar species. The soluble fraction (100 µl) containing low molecular weight aggregates and monomeric αS was then filtrated through 100 kDa centrifuge filters (Merck, Darmstadt, Germany) in order to fractionate these two species. The filtrated samples contain monomeric or -theoretically- dimeric αS. The excess of monomeric species retained in the filter were then washed by filtrating 400 µl of PBS. Finally, aggregated species retained in the filter were recovered by adding 100 µl of PBS to the membrane and carefully pipetting. This fraction containing low molecular weight aggregates was subsequently analyzed by transmission electron microscopy as previously described above.

Neuroblastoma culture. Human SH-SY5Y neuroblastoma cells (ATCC) were cultured in DMEM/F12 medium supplemented with 15% FBS and 1xNEAA. Cells were grown at 37 °C in a 5% CO_2 humidified atmosphere until an 80% confluence for a maximum of 20 passages.

Analysis of intracellular ROS. SH-SY5Y cells were seeded onto glass coverslips (Ibidi, Gräfelfing, Germany) at 0.5×10^6 cells/mL and treated for 15 min with 10 µM of type B* oligomers or type B* pretreated for 15 min with the tested peptide (PSMα3, dPSMα3, and LL-37). Then, CellROX® Green (Invitrogen, Carlsbad, USA) at a final concentration of 5 µM was added and incubated for 30 min at 37 °C. Cells were washed with PBS and fixed with 3.7% paraformaldehyde (PFA) for 15 min. The intracellular fluorescence of the SH-SY5Y cells was analyzed on a Leica TCS SP5 Software-Gatan Digital Micrograph 1.8 (Leica Microsystems, Wetzlar, Germany) with a HCX PL APO 63 × 1.4 oil immersion objective, under UV light by using a 488 nm excitation laser for CellROX and collecting the emission with a 515–560 nm filter range. Images were processed and analyzed with Image J (version 1.52p)

Oligomer binding to cells. SH-SY5Y cells were seeded onto glass coverslips (Ibidi, Gräfelfing, Germany) and treated for 45 min with 10 µM of type B* oligomers or type B* pretreated for 15 min with an equimolar concentration of PSMα3 or dPSMα3. Cells were then washed with PBS and fixed with 3.7% PFA for 15 min. Then cells were washed with PBS containing 0.1% Triton X-100 for 10 min. Cells were blocked with 5% BSA-PBS and incubated with 1/200 dilution rabbit polyclonal anti-αS antibody (Abcam, Cambridge, UK) overnight at 4 °C, and with 1:1000 anti-rabbit secondary antibodies conjugated with AF488. Cell nuclei was stained using Hoescht 33342 at a concentration of 0.5 µg/mL for 5 min. Images of intracellular αS were obtained under UV light using double excitation at 488 nm and 350 nm lasers, for AF488 and Hoescht, and the emission was collected at 515–560 nm and 405 nm, respectively. Images were processed and analyzed with Image J (version 1.52p)

A dot blot assay was performed as a control to discard epitope-masking artifacts caused by the potential primary or secondary antibodies binding to the peptide. 2 µL of type B* oligomers untreated and treated for 15 min with an equimolar concentration of PSMα3 were spotted onto a nitrocellulose membrane and allowed to dry. Antibody incubations were performed as described for the cellular assay. No significant differences in the signals of oligomers assayed in the presence or the absence of PSMα3 were detected (data not shown).

Redesign of PSMα3 variants. To guide and assist the design of PSMα3 peptide variants some computational tools were employed. Briefly, AGADIR was used to predict the helical propensity of the peptide variants based on the helix/coil transition theory[26]. FoldX allows a rapid evaluation of the effect of mutations on the stability, folding and dynamics of proteins[38]. We exploited it to evaluate if the designed mutations may compromise the stability of the α-helix specially regarding extensive redesign or those involving electrostatic repulsions. The peptides mean hydrophobicity (H), and their helical hydrophobic moment (μ_H), a measure of the amphiphilicity of a helix, were calculated according to Eisenberg and coworkers[52].

Reporting summary. Further information on research design is available in the Nature Research Reporting Summary linked to this article.

Data availability

All the data presented in this study are available in the paper or in the Supplementary Information. Further raw data (i.e., Time traces of the time-resolved fluorescence spectroscopy) supporting the findings of this study are available from the corresponding author upon reasonable request. The screened database of human peptides was obtained from the EROP-Moscow oligopeptide database (http://erop.inbi.ras.ru/)[39]. Source data are provided with this paper.

Received: 5 June 2020; Accepted: 27 May 2021;
Published online: 18 June 2021

References

1. Spillantini, M. G., Schmidt, M. L., Lee, V. M., Trojanowski, J. Q., Jakes, R. & Goedert, M. Alpha-synuclein in Lewy bodies. *Nature* **388**, 839–840 (1997).
2. Winner, B. et al. In vivo demonstration that alpha-synuclein oligomers are toxic. *Proc. Natl Acad. Sci. U.S.A.* **108**, 4194–4199 (2011).
3. Spillantini, M. G. & Goedert, M. The alpha-synucleinopathies: Parkinson's disease, dementia with Lewy bodies, and multiple system atrophy. *Ann. N. Y Acad. Sci.* **920**, 16–27 (2000).
4. McCann, H., Stevens, C. H., Cartwright, H. & Halliday, G. M. Alpha-Synucleinopathy phenotypes. *Parkinsonism Relat. Disord.* **20**, S62–S67 (2014).
5. Goedert, M., Jakes, R. & Spillantini, M. G. The synucleinopathies: twenty years on. *J. Parkinsons Dis.* **7**, S51–S69 (2017).
6. Kalia, L. V. & Lang, A. E. Parkinson's disease. *Lancet* **386**, 896–912 (2015).
7. Wong, Y. C. & Krainc, D. Alpha-synuclein toxicity in neurodegeneration: mechanism and therapeutic strategies. *Nat. Med.* **23**, 1–13 (2017).
8. Dehay, B. et al. Targeting alpha-synuclein for treatment of Parkinson's disease: mechanistic and therapeutic considerations. *Lancet Neurol.* **14**, 855–866 (2015).
9. Pujols, J. et al. Small molecule inhibits alpha-synuclein aggregation, disrupts amyloid fibrils, and prevents degeneration of dopaminergic neurons. *Proc. Natl Acad. Sci. U.S.A.* **115**, 10481–10486 (2018).
10. Wagner, J. et al. Anle138b: a novel oligomer modulator for disease-modifying therapy of neurodegenerative diseases such as prion and Parkinson's disease. *Acta Neuropathol.* **125**, 795–813 (2013).
11. Kurnik, M. et al. Potent alpha-synuclein aggregation inhibitors, identified by high-throughput screening, mainly target the monomeric state. *Cell Chem. Biol.* **25**, 1389–1402 e1389 (2018).
12. Jarrett, J. T. & Lansbury, P. T. Jr. Amyloid fibril formation requires a chemically discriminating nucleation event: studies of an amyloidogenic sequence from the bacterial protein OsmB. *Biochemistry* **31**, 12345–12352 (1992).
13. Fusco, G. et al. Structural basis of membrane disruption and cellular toxicity by alpha-synuclein oligomers. *Science* **358**, 1440–1443 (2017).
14. Grey, M., Linse, S., Nilsson, H., Brundin, P. & Sparr, E. Membrane interaction of alpha-synuclein in different aggregation states. *J. Parkinsons Dis.* **1**, 359–371 (2011).
15. Froula, J. M. et al. Defining alpha-synuclein species responsible for Parkinson's disease phenotypes in mice. *J. Biol. Chem.* **294**, 10392–10406 (2019).

16. Cremades, N. et al. Direct observation of the interconversion of normal and toxic forms of alpha-synuclein. *Cell* **149**, 1048–1059 (2012).
17. Cremades, N. & Dobson, C. M. The contribution of biophysical and structural studies of protein self-assembly to the design of therapeutic strategies for amyloid diseases. *Neurobiol. Dis.* **109**, 178–190 (2018).
18. Lee, J. E. et al. Mapping surface hydrophobicity of alpha-synuclein oligomers at the nanoscale. *Nano Lett.* **18**, 7494–7501 (2018).
19. Chen, S. W. et al. Structural characterization of toxic oligomers that are kinetically trapped during alpha-synuclein fibril formation. *Proc. Natl Acad. Sci. U.S.A.* **112**, E1994–2003 (2015).
20. Chen, S. W. & Cremades, N. Preparation of alpha-synuclein amyloid assemblies for toxicity experiments. *Methods Mol. Biol.* **1779**, 45–60 (2018).
21. Tuttle, M. D. et al. Solid-state NMR structure of a pathogenic fibril of full-length human alpha-synuclein. *Nat. Struct. Mol. Biol.* **23**, 409–415 (2016).
22. Li, B. et al. Cryo-EM of full-length alpha-synuclein reveals fibril polymorphs with a common structural kernel. *Nat. Commun.* **9**, 3609 (2018).
23. Guerrero-Ferreira R, et al. Cryo-EM structure of alpha-synuclein fibrils. *Elife* 7, e36402 (2018).
24. Cremades, N., Chen, S. W. & Dobson, C. M. Structural characteristics of alpha-synuclein oligomers. *Int Rev. Cell Mol. Biol.* **329**, 79–143 (2017).
25. Marinelli, P., Pallares, I., Navarro, S. & Ventura, S. Dissecting the contribution of Staphylococcus aureus alpha-phenol-soluble modulins to biofilm amyloid structure. *Sci. Rep.* **6**, 34552 (2016).
26. Munoz, V. & Serrano, L. Elucidating the folding problem of helical peptides using empirical parameters. *Nat. Struct. Biol.* **1**, 399–409 (1994).
27. Bacia, K. & Schwille, P. Practical guidelines for dual-color fluorescence cross-correlation spectroscopy. *Nat. Protoc.* **2**, 2842–2856 (2007).
28. Schwille, P., Meyer-Almes, F. J. & Rigler, R. Dual-color fluorescence cross-correlation spectroscopy for multicomponent diffusional analysis in solution. *Biophys. J.* **72**, 1878–1886 (1997).
29. Tosatto, L. et al. Single-molecule FRET studies on alpha-synuclein oligomerization of Parkinson's disease genetically related mutants. *Sci. Rep.* **5**, 16696 (2015).
30. Nath, S., Meuvis, J., Hendrix, J., Carl, S. A. & Engelborghs, Y. Early aggregation steps in alpha-synuclein as measured by FCS and FRET: evidence for a contagious conformational change. *Biophys. J.* **98**, 1302–1311 (2010).
31. Whiten, D. R. et al. Single-molecule characterization of the interactions between extracellular chaperones and toxic alpha-synuclein oligomers. *Cell Rep.* **23**, 3492–3500 (2018).
32. Kruger, D., Ebenhan, J., Werner, S. & Bacia, K. Measuring protein binding to lipid vesicles by fluorescence cross-correlation spectroscopy. *Biophys. J.* **113**, 1311–1320 (2017).
33. Lashuel, H. A., Hartley, D., Petre, B. M., Walz, T. & Lansbury, P. T. Jr. Neurodegenerative disease: amyloid pores from pathogenic mutations. *Nature* **418**, 291 (2002).
34. Lashuel, H. A. et al. Alpha-synuclein, especially the Parkinson's disease-associated mutants, forms pore-like annular and tubular protofibrils. *J. Mol. Biol.* **322**, 1089–1102 (2002).
35. Perni, M. et al. Multistep inhibition of alpha-synuclein aggregation and toxicity in vitro and in vivo by trodusquemine. *ACS Chem. Biol.* **13**, 2308–2319 (2018).
36. Ludtmann, M. H. R. et al. alpha-synuclein oligomers interact with ATP synthase and open the permeability transition pore in Parkinson's disease. *Nat. Commun.* **9**, 2293 (2018).
37. Stothard, P. The sequence manipulation suite: JavaScript programs for analyzing and formatting protein and DNA sequences. *Biotechniques* **28**, 1102–1104 (2000).
38. Schymkowitz, J. et al. The FoldX web server: an online force field. *Nucleic Acids Res* **33**, W382–W388 (2005).
39. Zamyatnin, A. A., Borchikov, A. S., Vladimirov, M. G. & Voronina, O. L. The EROP-Moscow oligopeptide database. *Nucleic Acids Res.* **34**, D261–D266 (2006).
40. Durr, U. H., Sudheendra, U. S. & Ramamoorthy, A. L. L.-37 the only human member of the cathelicidin family of antimicrobial peptides. *Biochim Biophys. Acta* **1758**, 1408–1425 (2006).
41. Brundin, P. & Melki, R. Prying into the prion hypothesis for Parkinson's disease. *J. Neurosci.* **37**, 9808–9818 (2017).
42. Braak, H., Rub, U., Gai, W. P., Del & Tredici, K. Idiopathic Parkinson's disease: possible routes by which vulnerable neuronal types may be subject to neuroinvasion by an unknown pathogen. *J. Neural Transm. (Vienna)* **110**, 517–536 (2003).
43. Lionnet, A. et al. Does Parkinson's disease start in the gut? *Acta Neuropathol.* **135**, 1–12 (2018).
44. Kastin AJ. *Handbook of biologically active peptides*. (Elsevier, 2013).
45. Burton, M. F. & Steel, P. G. The chemistry and biology of LL-37. *Nat. Prod. Rep.* **26**, 1572–1584 (2009).
46. De Lorenzi, E. et al. Evidence that the human innate immune peptide LL-37 may be a binding partner of amyloid-beta and inhibitor of fibril assembly. *J. Alzheimers Dis.* **59**, 1213–1226 (2017).
47. Armiento, V. et al. The human cathelicidin LL-37 is a nanomolar inhibitor of amyloid self-assembly of islet amyloid polypeptide (IAPP). *Angew. Chem. Int Ed. Engl.* **59**, 128337–12841 (2020).
48. Tokuda, T. et al. Detection of elevated levels of alpha-synuclein oligomers in CSF from patients with Parkinson disease. *Neurology* **75**, 1766–1772 (2010).
49. Zhao, H. et al. AlphaLISA detection of alpha-synuclein in the cerebrospinal fluid and its potential application in Parkinson's disease diagnosis. *Protein Cell* **8**, 696–700 (2017).
50. Bengoa-Vergniory, N., Roberts, R. F., Wade-Martins, R. & Alegre-Abarrategui, J. Alpha-synuclein oligomers: a new hope. *Acta Neuropathol.* **134**, 819–838 (2017).
51. Kumar, S. T., Donzelli, S., Chiki, A., Syed, M. M. K. & Lashuel, H. A. A simple, versatile and robust centrifugation-based filtration protocol for the isolation and quantification of alpha-synuclein monomers, oligomers and fibrils: towards improving experimental reproducibility in alpha-synuclein research. *J. Neurochem.* **153**, 103–119 (2020).
52. Kyte, J. & Doolittle, R. F. A simple method for displaying the hydropathic character of a protein. *J. Mol. Biol.* **157**, 105–132 (1982).

Acknowledgements

This work was funded by the Spanish Ministry of Economy and Competitiveness (MINECO) BIO2016-78310-R and BIO2017-91475-EXP to S.V, by the Ministry of Science and Innovation (MICINN) PID2019-105017RB-I00 to S.V, by ICREA, ICREA-Academia 2015 to S.V. N.C. was supported by MINECO RYC-2012-12068, MINECO/FEDER, EU BFU2015-64119-P and MICIU/FEDER, EU PGC2018-096335-B-100. J.S. was supported by MICINN via a doctoral grant (FPU17/01157). We thank the members of the Microscopy Services of the UAB for their assistance, Dr. Salvador Bartolomé from the Laboratori de Luminiscència i Espectroscòpia de Biomolècules, UAB, and Dr. Evangelos Sisamakis, PicoQuant, for insightful discussions.

Author contributions

S.V. conceived the project. J.S., I.P., and S.V. designed all the peptide sequences. J.S., S.P-D., and J.P. performed in vitro experiments. J.S. and S.N. designed, conducted and analyzed cellular experiments. P.G. and N.C. performed and analyzed time-resolved fluorescence spectroscopy experiments. J.S., I.P., and S.V. analyzed the data. J.S., P.G., N. C., I.P., and S.V. prepared the paper with contributions from all the authors.

Competing interests

Authors have submitted a patent application on the bases of the here presented research. It is protected the use of LL-37 for therapy and PSMα3 for therapy and diagnosis. Inventors: S.V., I.P., J.S., N.C., P.J.G. Title: inhibitors of alpha synuclein aggregation and uses thereof. Property: Universidad Autónoma de Barcelona. Universidad de Zaragoza. Request number: EP20382658. Priority date and Country: 22-07-2020, EU. All other authors declare no competing interests.

Additional information

Supplementary information The online version contains supplementary material available at https://doi.org/10.1038/s41467-021-24039-2.

Correspondence and requests for materials should be addressed to N.C., I.P. or S.V.

Peer review information *nature communications* thanks Hilal Lashuel and other, anonymous, reviewers for their contributions to the peer review of this work. Peer review reports are available.

Reprints and permission information is available at http://www.nature.com/reprints

Publisher's note Springer Nature remains neutral with regard to jurisdictional claims in published maps and institutional affiliations.

Open Access This article is licensed under a Creative Commons Attribution 4.0 International License, which permits use, sharing, adaptation, distribution and reproduction in any medium or format, as long as you give appropriate credit to the original author(s) and the source, provide a link to the Creative Commons license, and indicate if changes were made. The images or other third party material in this article are included in the article's Creative Commons license, unless indicated otherwise in a credit line to the material. If material is not included in the article's Creative Commons license and your intended use is not permitted by statutory regulation or exceeds the permitted use, you will need to obtain permission directly from the copyright holder. To view a copy of this license, visit http://creativecommons.org/licenses/by/4.0/.

© The Author(s) 2021

Chapter 2: Is a cure for Parkinson’s disease hiding inside us?

This chapter contains the article published in Trends in Biochemical Sciences “*Is a cure for Parkinson’s disease hiding inside us?, J. Santos, I. Pallarès, S. Ventura, Trends Biochemical Sciences. 47, 641–644 (2022)*”. This article is reused in this thesis dissertation with permission from Elsevier.

DOI: 10.1016/j.tibs.2022.02.001

In Section “Appendix 2” of this thesis we show the experimental validation of two human endogenous peptides that inhibit αS aggregation that we were asked to perform during the peer-review process but are not contained in the body of the manuscript.

Trends in
Biochemical Sciences

CellPress

Forum

Is a cure for Parkinson's disease hiding inside us?

Jaime Santos, [1,@]
Irantzu Pallarès, [1,*,@] and
Salvador Ventura [1,*]

α-Synuclein (a-syn) oligomers and fibrils are behind neurodegeneration in Parkinson's disease (PD), but therapeutically targeting them is challenging. Amphipathic and cationic helical peptides inhibit amyloid formation and suppress neurotoxicity by selectively binding the solvent-accessible regions in these toxic species. Can endogenous peptides, like LL-37, constitute a new therapeutic paradigm in PD?

PD is the second most common neurodegenerative disorder and remains incurable. Current treatments help to alleviate early motor symptoms, but they become ineffective as the pathology progresses. Therefore, there is an urgent need for disease-modifying agents that can halt or slow down the progression of the disease. Growing evidence suggest that a-syn oligomers and fibrils are the culprits of neural damage in PD [1]. Their neurotoxicity has been associated with membrane disruption and prion-like neuron-to-neuron spreading of the disease [2,3]. Thus, targeting a-syn oligomers and fibrils as a therapeutic strategy for PD is gaining momentum.

Common structural traits behind toxic a-syn forms

In the past decade, advanced crystallography, cryoelectron microscopy (cryo-EM), and NMR techniques have provided unprecedented molecular details on the architecture and interactions driving the formation of toxic a-syn species. Both a-syn toxic oligomers and fibrils consist of a rigid β-sheet core with solvent-exposed hydrophobic clusters and a disordered outer corona formed by the flexible N- and C-terminal regions of a-syn (Figure 1A) [3,4]. The core includes the highly amyloidogenic NAC domain, which is both necessary and sufficient for a-syn aggregation. Despite its importance for fibril formation and stability, this hydrophobic region remains significantly buried in the aggregates and contributes only partially to their surface physicochemical properties. Indeed, between 50% and 70% of the 140 a-syn residues remain unstructured in the assembly, forming a dynamic and solvent-accessible 'fuzzy coat' around the core [3,4]. Because their flexible shells involve similar regions and both expose a certain degree of hydrophobicity to the solvent, the external features of a-syn oligomers and fibrils overlap significantly.

At present, we have atomic information on the molecular contacts that sustain the amyloid core of various a-syn polymorphs [4]. However, little is known about the properties of the disordered flanking regions once aggregates form, although recent data indicate that they actively modulate a-syn aggregation, toxicity, and cell-to-cell propagation [3,5–9]. Therapeutic intervention requires understanding the complete structural properties of a-syn aggregates, both regarding their rigid and flexible regions.

Outside the core: role of a-syn C termini

Recent structural and functional analyses of a-syn aggregates concur in the active role of the C-terminal tails in pathogenesis. This a-syn region promotes monomer recruitment to oligomers and fibrils via electrostatic N–C terminal interactions, being involved in fibril elongation [6,7], and participates in oligomer membrane-associated toxicity by mediating the interaction with the head groups of the lipids [3]. Moreover, a-syn fibrils impair microtubule stability by sequestering tau through their C-terminal tails [5].

Notably, the lymphocyte activation gene 3 (LAG3) and amyloid precursor-like protein 1 (APLP1) cell surface receptors bind the C-terminal tails of a-syn fibrils using a complementary cationic surface [8]. This receptor-mediated electrostatic recognition is fundamental for fibril internalization, seeding, and pathological cell-to-cell transmission. Furthermore, these receptors bind preferentially to a-syn fibrils rather than monomers (K_D 200-fold higher), even if the C terminus is present in both species, because intramolecular interactions shield this domain in the monomer, whereas it remains accessible in the fibrils. In a similar mechanism, exposure of these tails in a-syn fibrils accounts for binding to the proteasome and blockage of its proteolytic activity [9].

This new body of evidence converges to indicate that blocking the disordered C terminus in a-syn fibrils and oligomers might hold therapeutic potential due to their role in oligomer/fibril growth, neurotoxicity, and cellular transmission, together with its high accessibility and its differential conformation in functional and aberrant a-syn species. Furthermore, the LAG3 and APLP1 selective binding to aggregates constitutes a natural proof-of-concept demonstrating that the C-terminal domain can be targeted with conformational specificity. This opens a therapeutic opportunity for molecules displaying analogous structural selectivity.

LL-37: a human peptide that binds selectively to exposed surfaces in a-syn toxic species

LL-37 is a human antimicrobial peptide with immunomodulatory properties [10], expressed in the gut and the brain, that binds a-syn toxic species with low nanomolar affinity without interfering with the functional form of the protein [11]. LL-37 binding exploits the complementarity between

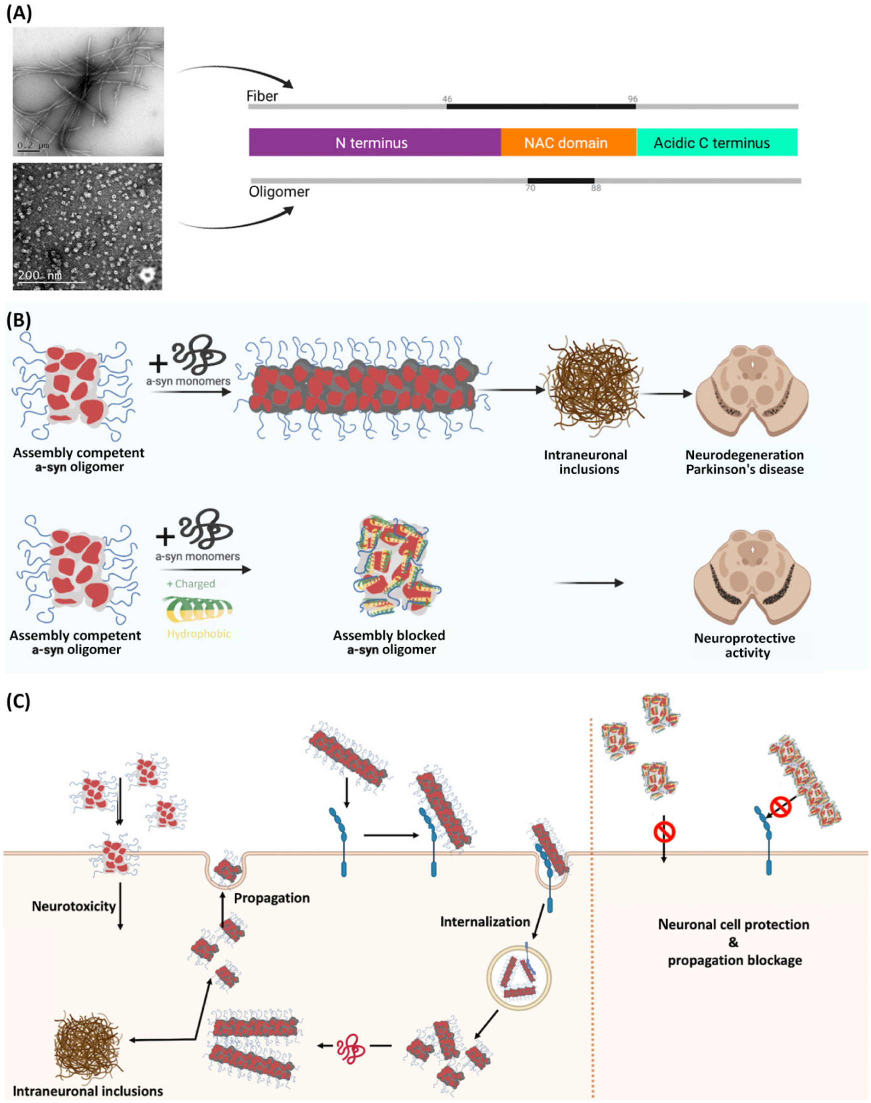
(A)
0.2 μm
200 nm
Fiber
46
96
N terminus
NAC domain
Acidic C terminus
Oligomer
70
88
(B)
+
a-syn monomers
Assembly competent a-syn oligomer
Intraneuronal inclusions
Neurodegeneration Parkinson's disease
+
a-syn monomers
+ Charged
Hydrophobic
Assembly competent a-syn oligomer
Assembly blocked a-syn oligomer
Neuroprotective activity
(C)
Neurotoxicity
Propagation
Internalization
Neuronal cell protection
&
propagation blockage
Intraneuronal inclusions

Trends in Biochemical Sciences

Figure 1. Selective interaction of LL-37 with α-synuclein (a-syn) toxic species stalls aggregation and suppresses cell damage. (A) The left panels show electron microscopy images of a-syn fibrils (top) and a-syn oligomers (bottom); these images correspond to the rigid core of both assemblies (scale 200 nm). The right panel shows a schematic view of the a-syn primary sequence, divided into three domains. Long segments flanking the a-syn central rigid region (unbroken black line) have been described as disordered and conformationally flexible state (unbroken gray line) [3,4]. (B) Schematic model that illustrates the interaction between amphipathic and cationic helical peptides, such as LL-37, and a-syn toxic species, stalling aggregation and potentially preventing substantia nigra pars compact neuronal loss. (C) Mechanisms of a-syn aggregate-induced neurotoxicity and pathological spreading. a-syn oligomers bind to the cell surface, disrupting the membrane and causing cellular toxicity. a-syn fibrils can enter neurons via internalization after binding to cell surface receptors [e.g., lymphocyte activation gene 3 (LAG3) and amyloid precursor-like protein 1(APLP1)] [8]. Internalized fibrils lead to neurotoxic events and cell-to-cell a-syn spreading. LL-37 binding to these species may abrogate their toxicity and propagation in the brain. This figure was generated using BioRender (https://biorender.com/).

amphipathic and cationic helical peptides with spatially opposed hydrophobic and positively charged surfaces- and the solvent-exposed features of a-syn toxic assemblies: hydrophobic patches and a ‘fuzzy coat’ of acidic C-terminal regions.

In a way, the mechanism of action of LL-37 resembles that of LAG3 and APLP1, exploiting the C-terminal tails of oligomers and fibrils to attain aggregate-specific binding with nanomolar affinity. LL-37 binding has been shown to inhibit a-syn aggregation and suppress oligomer toxicity [11] (Figure 1B). This activity likely results from LL-37 being evolved to inhibit the formation of bacterial biofilm amyloids like curli [12], which share the acidic character of the a-syn C-terminal tail. In any case, this peptide illustrates how molecules targeting the hydrophobic and charged surfaces of a-syn assemblies simultaneously hold potential to interfere with many of the molecular processes responsible for aggregates associated toxicity and propagation (Figure 1C).

LL-37 expression in humans is upregulated by a variety of natural substances, such as vitamin D or butyrate [13]. These same molecules ameliorate PD symptoms in humans and animal models (Table 1) [14]. Although a causative link between these two activities has yet to be established, it is tempting to propose that this connection responds to a modulatory role of LL-37 in the progression of PD. If this is confirmed, the immediate corollary is that restoring or increasing endogenous peptide expression with these natural molecules would contribute to neutralizing a-syn aggregates toxicity and their propagation in the brain. This might provide a nontoxic and noninvasive strategy to fight PD that, in our opinion, is worth investigating. A related LL-37 upregulating approach exploiting its antimicrobial activity demonstrated clinical efficacy against tuberculosis [13].

An endogenous repertory of peptides for therapeutic intervention of PD?

Recent studies suggest that in PD, a-syn aggregation may begin in the gastrointestinal tract decades before the pathology manifests in the brain [2]. The

Table 1. Natural source inducers of LL-37 expression in humans and their association with PD[a]

Name	Molecular structure	Origin	Deficiency/insufficiency in PD	Supplementation promotes PD amelioration	
				Human	Animal model
Vitamin D	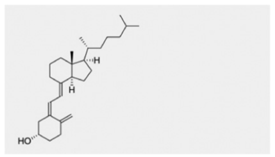	Endogen	Yes	Yes	Rodents
Docosahexaenoic acid	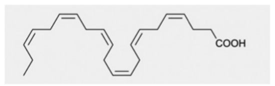	Endogen	Yes	Yes	Rodents
Retinoic acid	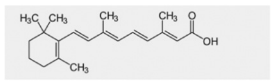	Endogen	Yes	NA	Rodents
Butyrate	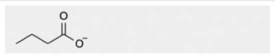	Endogen (intestinal microbiota)	Yes	Yes	Rodents
Sulforaphane	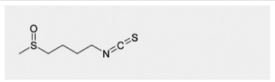	Diet (cruciferous vegetables)	NA	NA	Mice
Curcumin	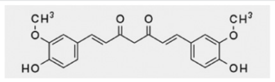	Diet (rhizomes of *Curcuma longa*)	NA	Yes	Rodents
Resveratrol	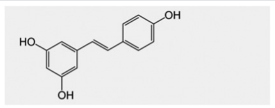	Diet (i.e., grapes, mulberries and peanuts)	NA	NA	Rodents

[a] Abbreviation: NA, not available/not applicable.

constitutive expression of LL-37 in these organs leads to the thought-provoking hypothesis that this small peptide might constitutively protect against a-syn aggregation.

The control of protein aggregation is primarily exerted by chaperone proteins, but natural small peptides with chaperone-like activity exist [15]. The binding to a-syn toxic species by helical peptides like LL-37 does not rely on their specific sequence [11], and our cells produce myriads of endogenous peptides either as bioactive molecules or byproducts of protein processing and degradation. It should come as no surprise that a pool of them would share LL-37 physicochemical properties and chaperoning activity. If this endogenous peptide repository exists, it may constitute a privileged target for disease-modifying approaches in the synucleinopathies. Is it possible that a cure for PD is hidden within us?

Acknowledgments

This work was funded by the Spanish Ministry of Economy and Competitiveness (BIO2017-91475-EXP to S.V.), by the Ministry of Science and Innovation (PID2019-105017RB-I00 to S.V.), and by ICREA, (ICREA-Academia 2020 to S.V.). J.S. was supported by the Spanish Ministry of Science and Innovation via a doctoral grant (FPU17/01157). The authors sincerely apologize to colleagues whose work could not be included due to space limitations.

Declaration of interests

No interests are declared.

[1]Institut de Biotecnologia i Biomedicina and Departament de Bioquímica i Biologia Molecular, Universitat Autònoma de Barcelona, Bellaterra, Barcelona, Spain

*Correspondence:
irantzu.pallares@uab.cat (I. Pallarès) and
salvador.ventura@uab.es (S. Ventura).
@Twitter: @JaimeSantos_S (J. Santos), @IrantzuPallares (I. Pallarès), and @PPMC_UAB

https://doi.org/10.1016/j.tibs.2022.02.001

© 2022 Elsevier Ltd. All rights reserved.

References

1. Kingwell, K. (2017) Zeroing in on neurodegenerative α-synuclein. *Nat. Rev. Drug Discov.* 16, 371–373
2. Brás, I.C. and Outeiro, T.F. (2021) Alpha-synuclein: mechanisms of release and pathology progression in synucleinopathies. *Cells* 10, 375

3. Fusco, G. *et al.* (2017) Structural basis of membrane disruption and cellular toxicity by α-synuclein oligomers. *Science* 358, 1440–1443
4. Guerrero-Ferreira, R. *et al.* (2020) New insights on the structure of alpha-synuclein fibrils using cryo-electron microscopy. *Curr. Opin. Neurobiol.* 61, 89–95
5. Ulamec, S.M. *et al.* (2020) Looking beyond the core: the role of flanking regions in the aggregation of amyloidogenic peptides and proteins. *Front. Neurosci.* 14, 611285
6. Yang, X. *et al.* (2021) NMR unveils an N-terminal interaction interface on acetylated-α-synuclein monomers for recruitment to fibrils. *Proc. Natl. Acad. Sci. U. S. A.* 118, e2017452118
7. Kumari, P. *et al.* (2021) Structural insights into α-synuclein monomer-fibril interactions. *Proc. Natl. Acad. Sci. U. S. A.* 118, e2012171118
8. Zhang, S. *et al.* (2021) Mechanistic basis for receptor-mediated pathological α-synuclein fibril cell-to-cell transmission in Parkinson's disease. *Proc. Natl. Acad. Sci. U. S. A.* 118, e2011196118
9. Suzuki, G. *et al.* (2020) α-synuclein strains that cause distinct pathologies differentially inhibit proteasome. *eLife* 9, e56825
10. Yang, B. *et al.* (2020) Significance of LL-37 on immunomodulation and disease outcome. *Biomed. Res. Int.* 2020, 8349712
11. Santos, J. *et al.* (2021) α-Helical peptidic scaffolds to target α-synuclein toxic species with nanomolar affinity. *Nat. Commun.* 12, 3752
12. Kai-Larsen, Y. *et al.* (2010) Uropathogenic *Escherichia coli* modulates immune responses and its curli fimbriae interact with the antimicrobial peptide LL-37. *PLoS Pathog.* 6, e1001010
13. Mily, A. *et al.* (2013) Oral intake of phenylbutyrate with or without vitamin D3 upregulates the cathelicidin LL-37 in human macrophages: a dose finding study for treatment of tuberculosis. *BMC Pulm. Med.* 13, 23
14. Fullard, M.E. and Duda, J.E. (2020) A review of the relationship between Vitamin D and Parkinson disease symptoms. *Front. Neurol.* 11, 454
15. Sponne, I. *et al.* (2004) Humanin rescues cortical neurons from prion-peptide-induced apoptosis. *Mol. Cell. Neurosci.* 25, 95–102

Chapter 3: LL-37 and CsgC exemplify the crosstalk between anti-amyloid, antimicrobial, and anti-biofilm protein activities

This chapter contains the article published in Neuronal Regeneration Research “*LL-37 and CsgC exemplify the crosstalk between anti-amyloid, antimicrobial, and anti-biofilm protein activities, J. Santos, S. Ventura, I. Pallarès. Neural Regeneration Research. 18, 1027–1028 (2023)*”.
DOI: 10.4103/1673-5374.355757

NEURAL REGENERATION RESEARCH
www.nrronline.org

LL-37 and CsgC exemplify the crosstalk between anti-amyloid, antimicrobial, and anti-biofilm protein activities

Jaime Santos, Salvador Ventura*, Irantzu Pallarès*

Protein misfolding and aggregation into amyloid fibrils is the main pathological hallmark of neurodegenerative diseases, including Alzheimer's, Parkinson's, Huntington's, and prion diseases (Chiti and Dobson, 2017). These insoluble fibrillar deposits possess a common structure characterized by a cross-β-sheet conformation in which β-strands run transversely to the fiber axis and form an intermolecular network of hydrogen bonds. However, amyloid formation is not only found in disease; the unique properties of this protein fold are also exploited by nature to perform a growing list of relevant and highly conserved cellular functions (Otzen and Riek, 2019). Pathogenic and functional amyloid formation needs to be regulated to sustain organism fitness, and a wide range of strategies have evolved to prevent uncontrolled aggregation. Importantly, we are not only exposed to our endogen amyloidogenic proteins, but we also face the threat of food and bacterial amyloids. For instance, many bacterial species in the gut microbiome can form an amyloid scaffolded biofilm, which facilitates bacterial proliferation, promotes the synergy between the host and the microbiome, and may eventually play a role in the pathogenesis of different diseases. It is then plausible to speculate that our own systemic defense against endogenous amyloids can work to fight this exogenic risk. Indeed, given the common structural properties shared by unrelated amyloids, it could be expected that the same cellular agents would mediate the response to human amyloids and those from other sources. In this perspective, we provide context for this idea by exploring the overlap between anti-microbial, anti-biofilm, and anti-amyloid activities, defining a framework for developing novel therapies for neurodegenerative diseases.

LL-37, an antimicrobial peptide with anti-amyloid and anti-biofilm activities: Found in all kingdoms of life, antimicrobial peptides are short, cationic, and amphipathic sequences that act as the primary innate immune response against a broad spectrum of pathogens. In a recent study, we demonstrated that the prototypical α-helical cathelicidin, LL-37; the active C-terminal component of the human cationic antimicrobial protein hCAP18, can bind to α-synuclein oligomers and fibrils, the molecular culprits of neurodegeneration in Parkinson's disease, with nanomolar affinity and without interfering with the functional form of the protein (Santos et al., 2021). This high-affinity interaction stalls aggregation and abrogates α-synuclein oligomers' toxicity. Notably, this is not the first evidence of LL-37 working as an anti-amyloid molecule. Previous reports indicate that it inhibits amyloid β peptide and islet amyloid polypeptide self-assembly, which have been shown to be associated with the loss of cortical neurons, a critical step towards Alzheimer's disease pathogenesis, and pancreatic β-cell degeneration in type 2 diabetes, respectively; even if, in these cases, LL-37 also interacts with the monomeric form of the peptides, acting in a less specific way (Armiento et al., 2020).

Strikingly, LL-37 is a potent antibiofilm agent, interfering with bacterial amyloid polymerization (Kai-Larsen et al., 2010). In many enteric bacteria like *Escherichia coli* and Salmonella, the curli system promotes the formation of extracellular amyloid fibers that entangle into a biofilm matrix. CsgA, the precursor of curli fibers, is transported to the cell surface as an unfolded polypeptide; there, the interaction with CsgB triggers amyloid formation. LL-37 has been shown to inhibit curli fibrillogenesis and biofilm formation by precluding CsgA polymerization at substoichiometric concentrations (Kai-Larsen et al., 2010).

Thus, LL-37 is an outstanding example of a molecule that intertwines different anti-amyloid activities. One could speculate that the original function of LL-37 as an antimicrobial peptide was interfering with bacterial amyloid polymerization. Eventually, the molecular determinants for this original anti-amyloid function, also encode for a side activity as an α-synuclein chaperone. Noteworthy, LL-37 coexists with α-synuclein in disease-relevant tissues, like the brain or the gut, suggesting that LL-37-mediated α-synuclein protection occurs naturally.

Supporting this hypothesis, CsgA and α-synuclein inhibition by LL-37 share some common mechanistic traits. In α-synuclein, the interaction occurs between the opposed hydrophobic and positively charged surfaces at the antimicrobial peptide amphipathic helix and the complementary hydrophobic exposed regions adjacent to the negatively-charged and disordered C-terminal tails in the aggregates. The surface complementary rather than specific intermolecular residue-to-residue contacts drive selective binding, as demonstrated (Santos et al., 2021). Notably, Brauner and co-workers concluded that the mechanism underpinning the CsgA inhibitory activity of LL-37 is similar to that we proposed for α-synuclein (Kai-Larsen et al., 2010), with electrostatic encounters between the two molecules occurring independently of the primary sequence, and playing a crucial role in both the specificity of CsgA recognition and the blockage of amyloidogenic regions. The observed inhibitory potency at substoichiometric concentrations suggests that LL-37 binds to soluble oligomeric species of CsgA, preventing their conversion to a fibrillar structure, as it does for α-synuclein.

CsgC, the other side of the coin: The above-described LL-37 activities match those of CsgC, a protein component of the curli system. The biogenesis of extracellular amyloids requires exquisite control to prevent premature amyloidogenesis within the cell. CsgC is a member of the curli system that acts as a periplasmatic chaperone that inhibits intracellular CsgA aggregation at substoichiometric concentrations (Evans et al., 2015). CsgC is a monomeric protein of 110 residues arranged in an immunoglobulin-like β fold, with seven strands forming two sheets. A dramatic loss of the inhibitory potency was observed when basic side chain residues located in a CsgC exposed and positively charged patch were mutated. In contrast, CsgC mutations that do not involve charge changes have little effect. Interestingly, the CsgC chaperone anti-amyloid mechanism of action exploits the same biophysical traits in its protein target as LL-37 and, not surprisingly, the positive charge pattern on the CsgC beta-sheet surface is highly conserved among homologues (Taylor et al., 2016). Indeed, CsgC structural homologues displaying low sequence identity but holding the electrostatic surface retain the inhibitory potential, while those with a high sequence similarity but a less pronounced basic patch are ineffective in blocking CsgA aggregation.

Closing the circle, the data reported by Evans et al. (2015) evidence that CsgC also inhibits α-synuclein amyloid formation. CsgA and α-synuclein sequence alignment detects relevant sequence similarity between the CsgA imperfect repeat R3 and the α-synuclein C-terminal domain, thus explaining how molecules targeting these charged recognition motives with electrostatic complementary could bind transiently to the soluble prefibrillar oligomers and stall the transition into fibrillar species of two proteins that could not be less related evolutionarily.

More than a casual encounter: LL-37 and CsgC activities define a two-way road, a human molecule that inhibits human and bacterial amyloids and a bacterial protein that blocks human and bacterial fibrillation. They are likely two of many molecules that exhibit moonlighting anti-amyloid functions. In support of this idea, our results suggest that the ability of LL-37 to inhibit α-synuclein aggregation may be common to other antimicrobial peptides that share the same physicochemical properties, such as the phenol-soluble modulin α3 (Santos et al., 2021) or the LL-III peptide (Oliva et al., 2021).

The anti-microbial anti-amyloid conundrum has been described in other structural folds, such as two antimicrobial α-defensins that exhibit multi-target inhibitory activities against amyloid formation (Zhang et al., 2021). A final intriguing case is transthyretin, one of the proteins responsible for the transport and delivery of the thyroid hormone thyroxine and retinol to cells in humans, which combines amyloidogenic and antimicrobial properties with inhibitory and anti-biofilm activities (Jain et al., 2017).

Taken together, the above-discussed examples are in support of the emerging perspective that anti-amyloid, antimicrobial, and anti-biofilm crosstalk can be molecularly encoded in unrelated protein structures (**Figure 1A**). If true, there might be a repertoire of therapeutically relevant molecules awaiting discovery at the intersection of these worlds.

The microbiome, ally or foe? To add a new layer of complexity to this scenario, recent studies support that amyloid formation can be enhanced through heterologous seeding between human and nonhuman amyloidogenic proteins, bypassing the species barrier. This is relevant because the human organism is more than 99% microbial, in terms of genes. Indeed, the gut microbiome alone encodes many more amyloidogenic proteins than those observed so far in human tissues. With a growing body of evidence suggesting that initial amyloid formation of neuronal proteins may originate in the gut and then be transmitted to the brain through the enteric nervous system (Kim et al., 2019), understanding interspecies amyloid cross-reactivity is becoming increasingly necessary. In a recent study, Wang et al. (2021) identified 38 genes in the bacterial genome as host neurodegeneration promoting agents, including those related to curli formation. It was subsequently demonstrated that bacteria-derived CsgA cross-seeds and colocalizes with α-synuclein in human neuroblastoma cells and a *Caenorhabditis elegans* (*C. elegans*) Parkinson's disease model. This process is bidirectional and seems widespread, since CsgA has also been observed to promote fibrillation of Aβ, SOD1, and polyQ-expanded huntingtin in *C. elegans* models of Alzheimer's disease, amyotrophic lateral sclerosis, and Huntington's disease, respectively (Wang et al., 2021).

In addition to its role in unwanted cross-seeding, functional microbial amyloids are recognized by the host's innate immune system as displaying a pathogen-associated molecular signature recognized by toll-like receptor 2 and the inflammasome, eliciting a proinflammatory response. This constitutes an evolutionary selected strategy to fight exogenous amyloids. However, in turn, it compromises homeostasis, inducing the production of proinflammatory chemokines in microglia, which ultimately can lead to pathogenic protein aggregation of neuronal proteins in the brain.

In this framework, one last reckless question remains. May microbiota also plays a protective role? As well as microbiota amyloids may trigger disease, to which extent anti-amyloid bacterial proteins, like CsgC, might counterbalance them? May they already play a role in preventing the endogenous aggregation of human proteins in the enteric nervous system?

All in all, it is now clear that amyloid formation and amyloid inhibition are connected phenomena that transcend individual species. Exploring this crosstalk appears as a promising strategy for understanding the etiology of human amyloid diseases, but also to fight them. Bacterial amyloids are suspicious of being pathogenesis triggers, especially at the brain-gut axis, and targeting this initial propagation needs to be explored as a therapeutic alternative (**Figure 1B**). In turn, bacteria and hosts possess a repertoire of structurally diverse molecules with the ability to control endogenous and exogenous amyloidogenesis. These molecules may hold biomedical value themselves or set the bases for discovering structurally related therapeutic entities.

Jaime Santos, Salvador Ventura[*], Irantzu Pallarès[*]
Institut de Biotecnologia i Biomedicina, Departament de Bioquímica i Biologia Molecular, Universitat Autònoma de Barcelona, Bellaterra, Barcelona, Spain
***Correspondence to:** Salvador Ventura, PhD, salvador.ventura@uab.es; Irantzu Pallarès, PhD, irantzu.pallares@uab.cat.
https://orcid.org/0000-0002-9652-6351 (Salvador Ventura)
https://orcid.org/0000-0002-8205-2060 (Irantzu Pallarès)

Date of submission: June 12, 2022
Date of decision: July 30, 2022
Date of acceptance: August 17, 2022
Date of web publication: October 10, 2022

https://doi.org/10.4103/1673-5374.355757

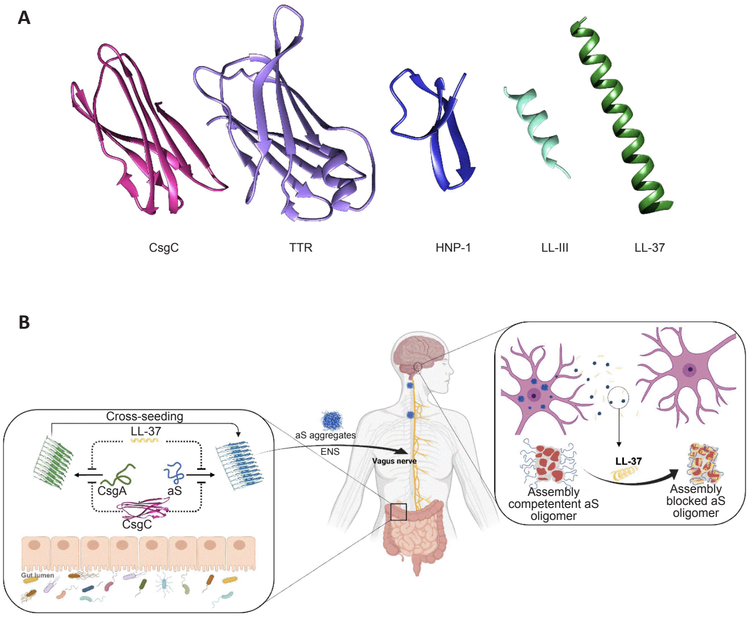

Figure 1 | Structures of selected peptides with anti-amyloid, antimicrobial and anti-biofilm activities and visual overview of the gut-brain axis.
(A) Left to right CsgC (2xsk), monomeric transthyretin (TTR) (4D7B), α-defensin HNP-1 (3HJD); LL-III peptide (structure generated using AlphaFold) and human cathelicidin LL-37 peptide (2K6O). The structures were visualized in Chimera (UCSF). (B) Overview of the proposed LL-37 and CsgC anti-amyloid, antimicrobial, and anti-biofilm crosstalk in the microbiome-gut-brain axis in Parkinson's disease. aS: α-Synuclein; ENS: enteric nervous system; HNP: human neutrophil peptides 1. Created with BioRender.com.

How to cite this article: *Santos J, Ventura S, Pallarès I (2023) LL-37 and CsgC exemplify the crosstalk between anti-amyloid, antimicrobial, and anti-biofilm protein activities. Neural Regen Res 18(5):1027-1028.*
Availability of data and materials: *All data generated or analyzed during this study are included in this published article and its supplementary information files.*
Open access statement: *This is an open access journal, and articles are distributed under the terms of the Creative Commons AttributionNonCommercial-ShareAlike 4.0 License, which allows others to remix, tweak, and build upon the work non-commercially, as long as appropriate credit is given and the new creations are licensed under the identical terms.*
Open peer reviewers: *Maya Maor-Nof, Stanford University School of Medicine, USA.*
Additional file: *Open peer review report 1.*

References

Armiento V, Hille K, Naltsas D, Lin JS, Barron AE, Kapurniotu A (2020) The human host-defense peptide cathelicidin LL-37 is a nanomolar inhibitor of amyloid self-assembly of islet amyloid polypeptide (IAPP). Angew Chem Int Ed Engl 59:12837-12841.
Chiti F, Dobson CM (2017) Protein misfolding, amyloid formation, and human disease: a summary of progress over the last decade. Annu Rev Biochem 86:27-68.
Evans ML, Chorell E, Taylor JD, Aden J, Gotheson A, Li F, Koch M, Sefer L, Matthews SJ, Wittung-Stafshede P, Almqvist F, Chapman MR (2015) The bacterial curli system possesses a potent and selective inhibitor of amyloid formation. Mol Cell 57:445-455.
Jain N, Aden J, Nagamatsu K, Evans ML, Li X, McMichael B, Ivanova MI, Almqvist F, Buxbaum JN, Chapman MR (2017) Inhibition of curli assembly and Escherichia coli biofilm formation by the human systemic amyloid precursor transthyretin. Proc Natl Acad Sci U S A 114:12184-12189.
Kai-Larsen Y, Luthje P, Chromek M, Peters V, Wang X, Holm A, Kadas L, Hedlund KO, Johansson J, Chapman MR, Jacobson SH, Romling U, Agerberth B, Brauner A (2010) Uropathogenic Escherichia coli modulates immune responses and its curli fimbriae interact with the antimicrobial peptide LL-37. PLoS Pathog 6:e1001010.
Kim S, Kwon SH, Kam TI, Panicker N, Karuppagounder SS, Lee S, Lee JH, Kim WR, Kook M, Foss CA, Shen C, Lee H, Kulkarni S, Pasricha PJ, Lee G, Pomper MG, Dawson VL, Dawson TM, Ko HS (2019) Transneuronal propagation of pathologic alpha-synuclein from the gut to the brain models Parkinson's disease. Neuron 103:627-641.
Oliva R, Mukherjee SK, Ostermeier L, Pazurek LA, Kriegler S, Bader V, Prumbaum D, Raunser S, Winklhofer KF, Tatzelt J, Winter R (2021) Remodeling of the fibrillation pathway of alpha-synuclein by interaction with antimicrobial peptide LL-III. Chemistry 27:11845-11851.
Otzen D, Riek R (2019) Functional amyloids. Cold Spring Harb Perspect Biol 11:a033860.
Santos J, Gracia P, Navarro S, Pena-Diaz S, Pujols J, Cremades N, Pallares I, Ventura S (2021) Alpha-Helical peptidic scaffolds to target alpha-synuclein toxic species with nanomolar affinity. Nat Commun 12:3752.
Taylor JD, Hawthorne WJ, Lo J, Dear A, Jain N, Meisl G, Andreasen M, Fletcher C, Koch M, Darvill N, Scull N, Escalera-Maurer A, Sefer L, Wenman R, Lambert S, Jean J, Xu Y, Turner B, Kazarian SG, Chapman MR, et al. (2016) Electrostatically-guided inhibition of Curli amyloid nucleation by the CsgC-like family of chaperones. Sci Rep 6:24656.
Wang C, Lau CY, Ma F, Zheng C (2021) Genome-wide screen identifies curli amyloid fibril as a bacterial component promoting host neurodegeneration. Proc Natl Acad Sci U S A 118:e2106504118.
Zhang Y, Liu Y, Tang Y, Zhang D, He H, Wu J, Zheng J (2021) Antimicrobial alpha-defensins as multi-target inhibitors against amyloid formation and microbial infection. Chem Sci 12:9124-9139.

P-Reviewers: Maor-Nof M, Sun T; C-Editors: Zhao M, Liu WJ, Wang Lu; T-Editor: Jia Y

Chapter 4: The structural architecture of an α -synuclein toxic oligomer

This chapter contains a preprint version of the article deposited in BioRxiv "*The structural architecture of an α -synuclein toxic oligomer, J. Santos, J. Cuellar, I. Pallarès, E. J. Byrd, A. Lends, F. Moro, M. B. Abdul-Shukkoor, J. Pujols, L. Velasco-Carneros, F. Sobott, D. E. Otzen, A. N. Calabrese, A. Muga, J. S. Pedersen, A. Loquet, J. M. Valpuesta, S. E. Radford, S. Ventura. bioRxiv 2023.02.10.527650 (2023)*".

DOI: 10.1101/2023.02.10.527650

The materials and methods and supplementary data associated with this work is available in Section "Appendix 3" of this thesis. Supplementary data 1 and 2 containing crosslinking raw data are available online.

bioRxiv preprint doi: https://doi.org/10.1101/2023.02.10.527650; this version posted February 10, 2023. The copyright holder for this preprint (which was not certified by peer review) is the author/funder. All rights reserved. No reuse allowed without permission.

Title: The structural architecture of an α-synuclein toxic oligomer.

Authors: Jaime Santos[1], Jorge Cuellar[2]†, Irantzu Pallarès[1]†, Emily J Byrd[3], Alons Lends[4], Fernando Moro[5], Muhammed Bilal Abdul-Shukkoor[4], Jordi Pujols[1], Lorea Velasco-Carneros[5], Frank Sobott[3], Daniel E Otzen[6], Antonio N Calabrese[3], Arturo Muga[5], Jan Skov Pedersen[7], Antoine Loquet[4], Jose María Valpuesta[2], Sheena E Radford[3] and Salvador Ventura[1]*.

Affiliations:

[1]Institut de Biotecnologia i Biomedicina and Departament de Bioquímica i Biologia Molecular, Universitat Autònoma de Barcelona; Bellaterra, Barcelona, Spain.

[2]Department of Macromolecular Structures, Centro Nacional de Biotecnología (CNB-CSIC); Madrid, Spain.

[3]Astbury Centre for Structural Molecular Biology, School of Molecular and Cellular Biology, Faculty of Biological Sciences, University of Leeds; Leeds, LS2 9JT, UK.

[4]Univ. Bordeaux, CNRS, Bordeaux INP, CBMN, UMR 5248, IECB; Pessac, France.

[5]Instituto Biofisika (UPV/EHU, CSIC) y Dpto. de Bioquímica y Biología Molecular, Facultad de Ciencia y Tecnología, Universidad del País Vasco; Barrio Sarriena S/N, 48940 Leioa, Spain.

[6]Interdisciplinary Nanoscience Center (iNANO) and Department of Molecular Biology and Genetics, Aarhus University; Gustav Wieds Vej 14, 8000 Aarhus C, Denmark.

[7]Interdisciplinary Nanoscience Center (iNANO) and Department of Chemistry, Aarhus University; Gustav Wieds Vej 14, 8000 Aarhus C, Denmark.

*Corresponding author: salvador.ventura@uab.es

†Authors contributed equally

Abstract: Oligomeric species populated during α-synuclein aggregation are considered key drivers of neurodegeneration in Parkinson's disease. However, their structure and the molecular determinants driving their conversion to fibrils remain elusive. In this work, we determined the symmetry and architecture of α-synuclein oligomers, dissecting the conformational properties of individual chains within these toxic assemblies. We demonstrate that the NAC domain is insufficient to promote oligomer to fibril conversion; instead, this transition is controlled by a short α-synuclein N-terminal motif. A missense mutation causing early-onset Parkinson's disease remodels this N-terminal region conformation, which results in a population of long-lived oligomers less susceptible to disaggregation by the human Hsp70 machinery. Our results provide a structural understanding of oligomer to amyloid conversion and identify targets for therapeutic intervention.

One sentence summary:

α-Synuclein oligomers are symmetric and well-organized particles with a short N-terminal region controlling fibril conversion.

bioRxiv preprint doi: https://doi.org/10.1101/2023.02.10.527650; this version posted February 10, 2023. The copyright holder for this preprint (which was not certified by peer review) is the author/funder. All rights reserved. No reuse allowed without permission.

Main text:

α-Synuclein (αS) is a 140 residue intrinsically disordered protein whose aggregation into amyloid fibrils is implicated in the onset of Parkinson's disease and other synucleinopathies (*1*–*3*). The aggregation landscape of αS is characterized by the early formation of transient oligomeric species that later convert into amyloid fibrils, whose accumulation is a defining hallmark of brain pathology (*4*–*8*). Oligomers are considered responsible for the gain-of-toxic function associated with αS aggregation (*9*, *10*) and, therefore, offer promising targets for therapeutics and diagnosis (*11*). However, knowledge of αS oligomer structure is limited, and the underlying mechanism for oligomer to fibril conversion is yet to be elucidated. Significant efforts have been devoted to gathering structural information on kinetically trapped αS oligomers (*8*, *12*–*14*), but their highly dynamic nature (*13*) makes this a challenging task.

Tight molecular binders, such as antibodies, can stabilize and reduce the conformational heterogeneity of target proteins, facilitating 3D structure determination of otherwise intractable proteins and their complexes. Here we mimicked this approach and used the amphipathic 22-residue peptide phenol-soluble modulin α3 (PSMα3), a nanomolar binder of αS oligomers (K_D = 6.67 nM; 1:1 PSMα3 per αS molecule at saturation) (*15*), as a tool to investigate their structural nature.

Architecture of αS oligomers

Isolated oligomer preparations were generated by incubating 800 μM of ^{13}C, ^{15}N labeled monomeric αS for 20 hours at 37 °C quiescently, followed by centrifugation-based fractionation as previously described (*12*). Oligomer-PSMα3 complexes were prepared by incubating oligomers with a 3-fold molar excess of PSMα3 and subsequent removal of the unbound peptide. Magic-angle spinning (MAS) solid-state nuclear magnetic resonance (ssNMR) cross-polarization (CP) and insensitive nuclei enhanced by polarization transfer (INEPT) were used to measure ^{13}C signals in rigid (CP) and mobile (INEPT) molecular segments of αS oligomers in the absence or presence of PSMα3. Peptide binding to oligomers increased the CP signal and CP/INEPT ratio, indicating oligomer rigidification upon interaction (**Fig. 1A; and Fig. S1A and B**). Nevertheless, the chemical shifts in the CP- and INEPT-based 2D spectra remained largely unchanged (**Fig. 1B and Fig. S1C**), ruling out major structural alterations upon PSMα3 binding. The unique set of resonances in the 2D CP-based spectrum of oligomers revealed a

bioRxiv preprint doi: https://doi.org/10.1101/2023.02.10.527650; this version posted February 10, 2023. The copyright holder for this preprint (which was not certified by peer review) is the author/funder. All rights reserved. No reuse allowed without permission.

monomorphic rigid core that we assigned as residues 70 to 89 based on previous studies (*16*) of αS fibrils (**Fig. S1D**). The assignments agree with those reported for a previously characterized toxic αS oligomer (*13*). Hence, 60% of residues seem to share a similar secondary structural context in oligomers and fibrils, with chemical shift differences < 1 ppm in both alpha (Cα) and beta (Cβ) carbons (**Fig. S1D and Table S1**).

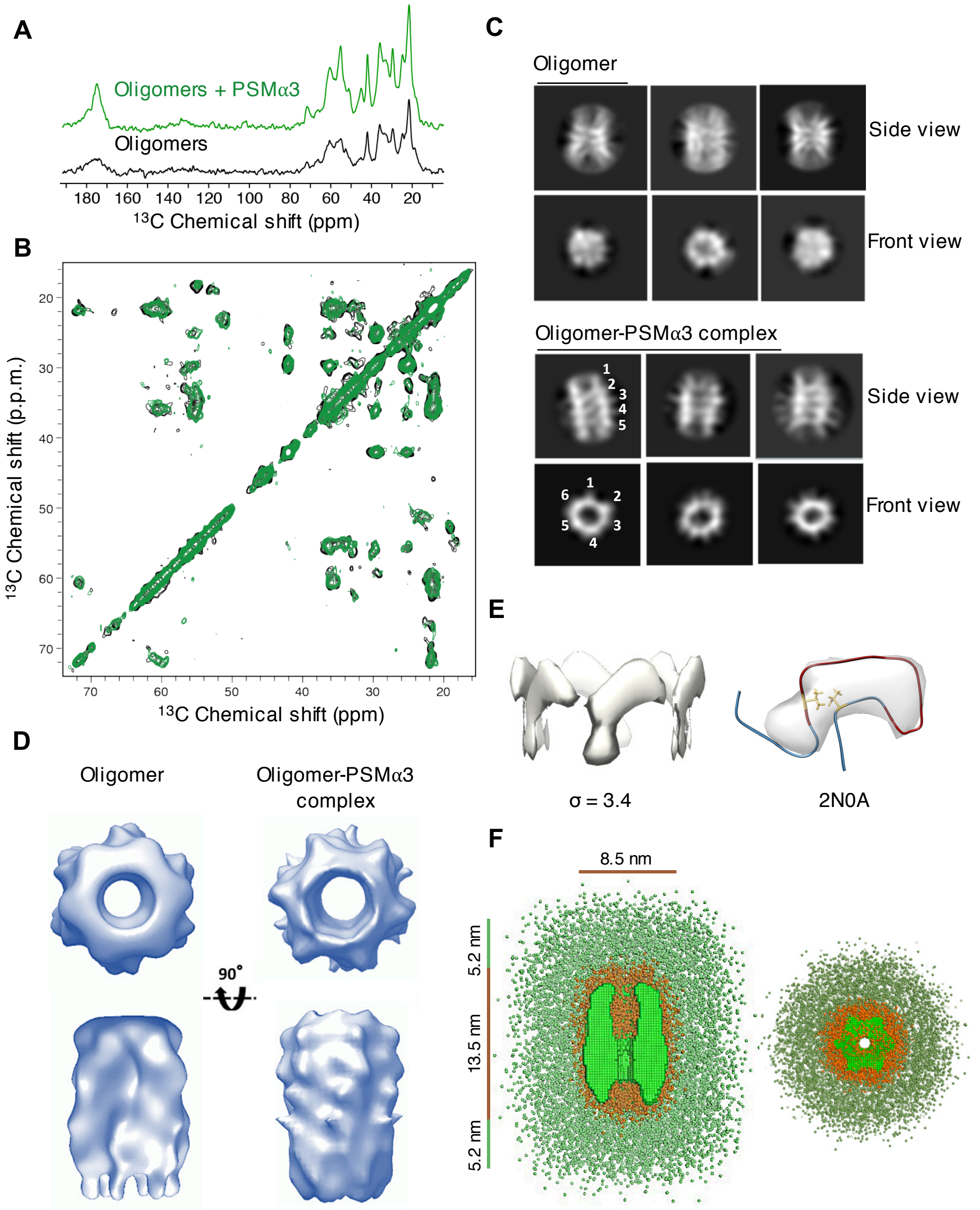

Fig. 1. Structural characterization of αS oligomers. (**A**) 1D ^{13}C spectra of oligomers and oligomers in complex with PSMα3 detected using cross-polarization (CP) ssNMR. (**B**) 2D ^{13}C-^{13}C PDSD correlation spectra (mixing time of 50 ms) of oligomers (black) and oligomers + PSMα3 (green). (**C**) 2D cryoEM classes of oligomers and oligomers in complex with PSMα3. The observed symmetry and architecture are labeled with numbers. (**D**) 3D reconstruction, six-fold symmetry

bioRxiv preprint doi: https://doi.org/10.1101/2023.02.10.527650; this version posted February 10, 2023. The copyright holder for this preprint (which was not certified by peer review) is the author/funder. All rights reserved. No reuse allowed without permission.

imposed, in the absence and presence of PSMα3 with resolutions of 16 Å and 16.7 Å, respectively. (**E**) The left panel shows the visualization of an αS oligomer CryoEM density at a high visualization threshold (σ = 3.4). The right panel shows the overlay of the same density with the NAC domain from resolved αS fibrils (PDB: 2N0A). Residues assigned as the rigid core of αS oligomers by ssNMR are shown in red (70-89). Valine 71 and threonine 92 in yellow. (**F**) Two views of the SAXS-based 3D reconstruction of αS oligomers. The compact core (orange) is surrounded by an outer disordered shell (green). The cryoEM density map is shown inside the oligomer core (bright green).

Consistent with the ssNMR data, PSMα3 binding reduced the conformational heterogeneity of αS oligomers as judged by negative stain transmission electron microscopy (nsEM) images (**Fig. S2A and B**). We exploited this increase in structural order for cryo-electron microscopy (cryoEM) 3D density reconstruction. In the presence of PSMα3, two structural features were evident in the 2D classes generated during 3D reconstruction: i) end-on views showed a 6-fold symmetry, also visible in the nsEM, ii) side views revealed an arrangement of five layers (**Fig. 1C**). These two traits were also apparent in the PSMα3-free oligomers. A 3D reconstruction of the two sets of particles was performed and, in both cases, the obtained structure displayed a cylindrical architecture with a central hollow core (**Fig. S2C, D and E**). Despite their limited resolution, both 3D reconstructions evidenced a 6-fold symmetry (**Fig. 1C and Fig. S2B, D and E**). This symmetry was applied to improve the quality of the two 3D reconstructions to a final resolution of 16 Å and 16.7 Å (**Fig. 1D**).

A 6-fold symmetry and 5-layer organization provide the structural context to accommodate the 30 αS monomers known to form these oligomers (*8*, *12*, *15*). The stacking of five hexameric rings best explains the EM data, while the single set of resonances evidenced by ssNMR suggests that all αS subunits have equivalent conformations and chemical environments. Our data thus demonstrate unequivocally that these αS oligomers have a well-defined and symmetric internal architecture.

Increasing the sigma (σ) value of the 3D reconstruction reveals the region of highest density (**Fig. S3**). At high sigma values (σ = 3.4), we observed a relatively well-defined region of cryoEM density, with a shape similar to a hammerhead (**Fig. 1E**), which we hypothesized should correspond to the residues identified as the rigid core by ssNMR. Given the similarities in the chemical shifts of αS oligomers and fibrils (PDB entry 2N0A (*16*)), we overlaid the structure of αS subunits in 22 different fibril structures with the cryoEM density of αS oligomers (**Fig. S4**). The 2N0A Greek key motif fitted the oligomer density (**Fig. 1E**), and was observed in several independent protofilament subunits, including fibrils extracted from multiple system atrophy

bioRxiv preprint doi: https://doi.org/10.1101/2023.02.10.527650; this version posted February 10, 2023. The copyright holder for this preprint (which was not certified by peer review) is the author/funder. All rights reserved. No reuse allowed without permission.

(MSA) patients (**Fig. S4**). In the Greek key motif of eight of the analyzed fibril structures, residues 71 and 92 face each other at < 10 Å distance (Cα to Cα) (**Fig. S4**). We tested whether this pattern is consistent with the oligomer structure by engineering a disulfide bond (design described in Methods) to covalently link these residues (**Fig. S5A**). Oxidized V71C-T92C monomers assembled into oligomers identical in size, morphology, and secondary structure content to those of wild-type (WT) αS (**Fig. S5**), demonstrating that a structural constraint < 7 Å between Val71 and Thr92 Cα is compatible with the proposed oligomer structure. These data suggest that the Greek key arrangement is already imprinted in the oligomer and maintained upon oligomer-to-fibril conversion.

By leveraging the cryoEM map, we used small-angle X-ray scattering (SAXS) to build a structural model that includes the dynamic and disordered αS regions averaged out in cryoEM reconstructions (**Fig. 1F; Fig. S6A and Table S2**). The oligomer core visible in the cryoEM maps is surrounded by an outer shell of disordered tails, resulting in an oligomer radius of gyration of 76.1 ± 0.3 Å, a dimension consistent with previous reports (*8*, *17*). Additionally, we confirmed that αS oligomers have an aggregation number close to 30 (**Table S2**). Surprisingly, our experimental data fitted better to a model with a single random coil chain per monomer, including 48% of αS residues, rather than two (**Fig. S6B**), as would be expected if both the N- and C-terminal domains remained fully disordered. Consistent with this, hydrogen-deuterium exchange-mass spectrometry (HDX-MS) analysis confirmed that the N-terminal domain became protected against deuterium uptake in the oligomer compared with the monomer. In contrast, the HDX protection in the C-terminal region remained unchanged (**Fig. 2A and Fig. S7**). The enhanced protection in the N-terminal domain is endowed by contacts between different residues in this domain, as well as by interdomain interactions of the N-terminal and NAC regions, as identified by crosslinking mass spectrometry (XL-MS) (**Fig. S8A and Supplementary Data 1**).

The N-terminal P1 and P2 regions control oligomer-to-fibril conversion

XL-MS of the oligomer-PSMα3 complex revealed that peptide binding is mediated by four regions in the N-terminal domain; residues 1-6, 24-32 and the previously identified P1 and P2 regions (residues 36-42 and 45-57, respectively) (*18*) (**Fig. 2B and Supplementary Data 2**). Additionally, HDX-MS indicated that the P1 and P2 regions (40-61) become protected from deuterium uptake upon PSMα3 binding (**Fig. 2B, Fig. S7 and S8B**). This suggests that, despite

bioRxiv preprint doi: https://doi.org/10.1101/2023.02.10.527650; this version posted February 10, 2023. The copyright holder for this preprint (which was not certified by peer review) is the author/funder. All rights reserved. No reuse allowed without permission.

being protected from HDX in the oligomer, the N-terminal region is still accessible and available for interactions.

We recently described that the P1 and P2 regions (**Fig. 2B**) act as 'master controllers' of αS amyloid formation *in vitro* and in *C. elegans* (*18*, *19*). The deletion of P1 (ΔP1) inhibits αS amyloid formation, in agreement with our previous results, with the deletion of P2 (ΔP2) also retarding amyloid formation under the conditions used here (*18*, *19*) (**Fig. 2C and Fig. S9**). The fact that PSMα3 stalls amyloid formation by blocking oligomer-to-fibril conversion (*15*) and the evidence that PSMα3 targets these αS motifs, suggest that the P1 and P2 regions are involved in this pivotal stage of amyloid formation. As expected, few low molecular weight species (isolation of this fraction is described in materials and methods) were visible at the endpoint of the amyloid assembly assay of WT αS (**Fig. 2D**). By contrast, oligomers identical in shape and size to WT oligomers were the primary components for ΔP1 and ΔP2 (**Fig. 2D and Fig. S2**). Similar results were obtained with a double deletion of P1 and P2 in tandem (ΔΔ) (**Fig. S10A**). The modulation of amyloid formation by the P1 region has been shown to be dependent on specific residues (*19*). Hence we characterized two αS variants, Y39A and S42A, which we found previously to mimic the ΔP1 phenotype (*19*). Consistent with our prior results, the Y39A and S42A amino acid substitutions inhibited αS amyloid formation to different extents (**Fig. S10B and C**). In both cases, oligomers with a WT-like architecture were the predominant species at the time points of maximal inhibition, indicating an impact in the oligomer to fibril transition (**Fig. S10B and C**). The WT αS and S42A proteins differ only in a single hydroxymethyl group, evidencing the precise control that small sequence changes exert in oligomer to fibril conversion.

To discard oligomer presence being intrinsic to any αS inhibited reaction, we characterized an N-terminal truncated variant (ΔN11) whose reduced amyloid assembly is due to decreased secondary nucleation (*7*, *20*). Importantly, deletion of the N-terminal eleven residues inhibited amyloid formation, but oligomers were marginal in the low-molecular weight fraction (**Fig. S10D**).

Our data argue that P1 and P2 are not necessary for αS oligomerization, but instead serve as 'master controllers' of oligomer-to-fibril conversion. The sequence dependence of this transition and the HDX protected, but PSMα3-accessible, nature of P1 and P2 in the oligomer suggest that this αS motif samples structured or partially structured conformations critical for amyloid formation, emphasizing the essential role these core-flanking regions play in generating the amyloid fold.

bioRxiv preprint doi: https://doi.org/10.1101/2023.02.10.527650; this version posted February 10, 2023. The copyright holder for this preprint (which was not certified by peer review) is the author/funder. All rights reserved. No reuse allowed without permission.

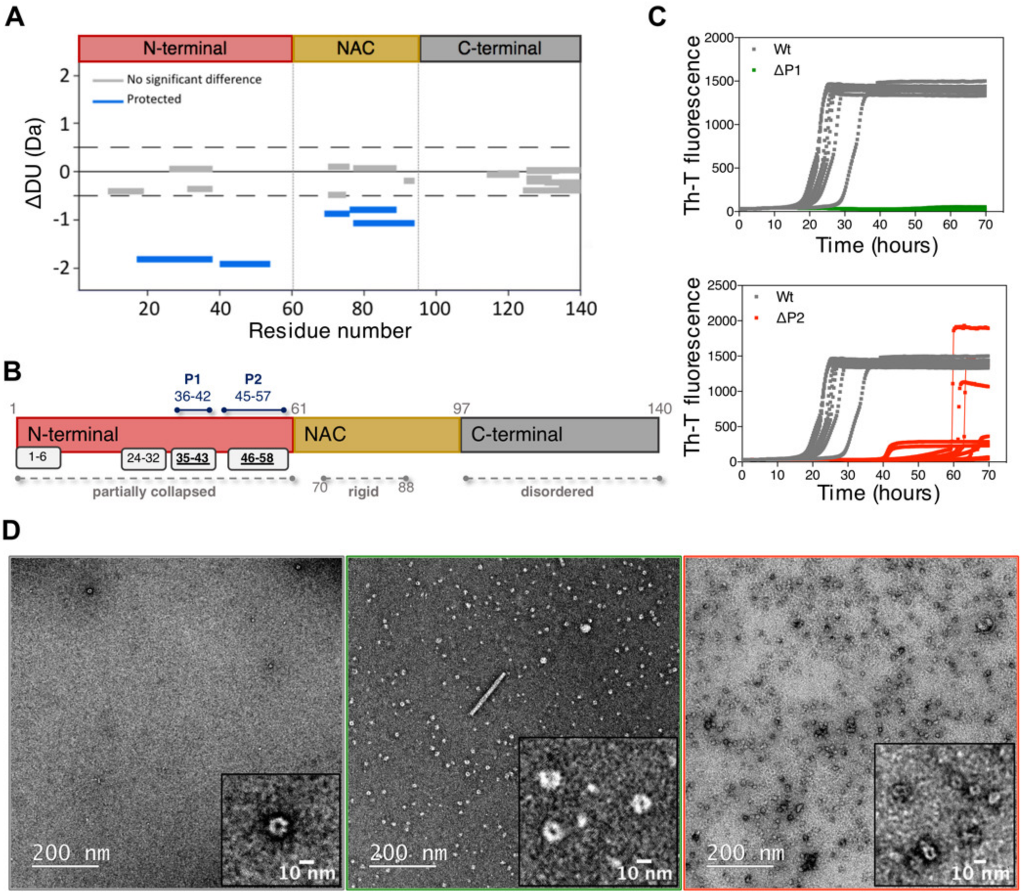

Fig. 2. Dynamics of the N-terminal domain and contribution to amyloid formation. (**A**) Wood's plots showing the difference in deuterium uptake (ΔDU) between αS monomers and oligomers by HDX-MS at the 60 seconds exposure timepoint to deuterium. Peptides colored in blue are protected from exchange in αS oligomers, suggesting they are less solvent-exposed. (**B**) Schematic representation of the conformational state of each αS domain. White boxes represent PSMα3 binding sites in the N-terminal domain identified by XL-MS; bold underlined numbers indicate PSMα3 binding sites that overlay between XL-MS and HDX-MS. P1 and P2 regions (*18*) are labeled in blue. (**C**) Kinetics of amyloid formation of the WT, ΔP1 and ΔP2 variants monitored using Th-T fluorescence. (**D**) Representative nsEM images of the oligomeric fraction of the WT, ΔP1 and ΔP2 variants (left, center and right, respectively) isolated at the endpoint of the assembly reaction

The hereditary mutation G51D impairs N-terminal mediated oligomer-to-fibril conversion and chaperone-assisted disaggregation.

The oligomer architecture we describe here also provides a structural context to rationalize the clustering of mutations associated with familial PD around P2 sequence (positions 46, 50, 51, and 53). According to this model, changes in the side chains of these residues can influence N-terminal domain conformational dynamics, oligomer's physicochemical properties and its ability to convert into amyloid fibrils. The familial G51D mutation best exemplifies this effect, since it results in structurally diverse oligomers characterized by a distinctive α-helical component, as

bioRxiv preprint doi: https://doi.org/10.1101/2023.02.10.527650; this version posted February 10, 2023. The copyright holder for this preprint (which was not certified by peer review) is the author/funder. All rights reserved. No reuse allowed without permission.

previously reported (*21*) and shown here (**Fig. 3A**). HDX-MS reveals that this point-mutation causes significant deprotection from deuterium uptake specifically in the N-terminal region of the oligomers (**Fig. S7 and Fig. S11**). We observed that the delayed aggregation of G51D αS is associated with the presence of WT-like oligomers at the timepoint of maximal difference (t = 28 hours) with the WT kinetics (**Fig. 3B and C**). The G51D variant exemplifies how a disease-associated mutation in P2 elicits a structural rearrangement of the N-terminal domain of the oligomer, including P1, which further impacts oligomer-to-fibril conversion.

The N-terminal domain of monomeric αS encompasses two binding sites (residues 1-10 and 37-43) for Hsp70 (*22*, *23*). WT and G51D oligomers display conformational differences in this region, which might impact how these αS assemblies interact with, and are processed by the Hsp70-based human disaggregation system (*24*). Accordingly, while WT αS oligomers are efficiently disaggregated into monomers by the synergistic action of Hsc70, DNAJB1 and Apg2 chaperones, the G51D oligomers show a significantly greater degree of resistance to Hsc70-mediated disaggregation (**Fig. 3D and Fig. S12**). Hsc70-mediated processing of αS oligomers is therefore critically dependent on the conformational organization of the N-terminal domain in the oligomer. Thus, under normal physiological conditions, αS oligomerization can be effectively counteracted by the chaperone machinery. However, familial mutations, like G51D, impacting the dynamics of the N-terminal regions involved in oligomer-to-fibril transition and Hsc70 interaction would lead to the accumulation of long-lived, toxic (*21*), oligomers that are not efficiently processed by the human disaggregase machinery. This might be why these mutations cause PD onset at ages at which protein homeostasis is still preserved.

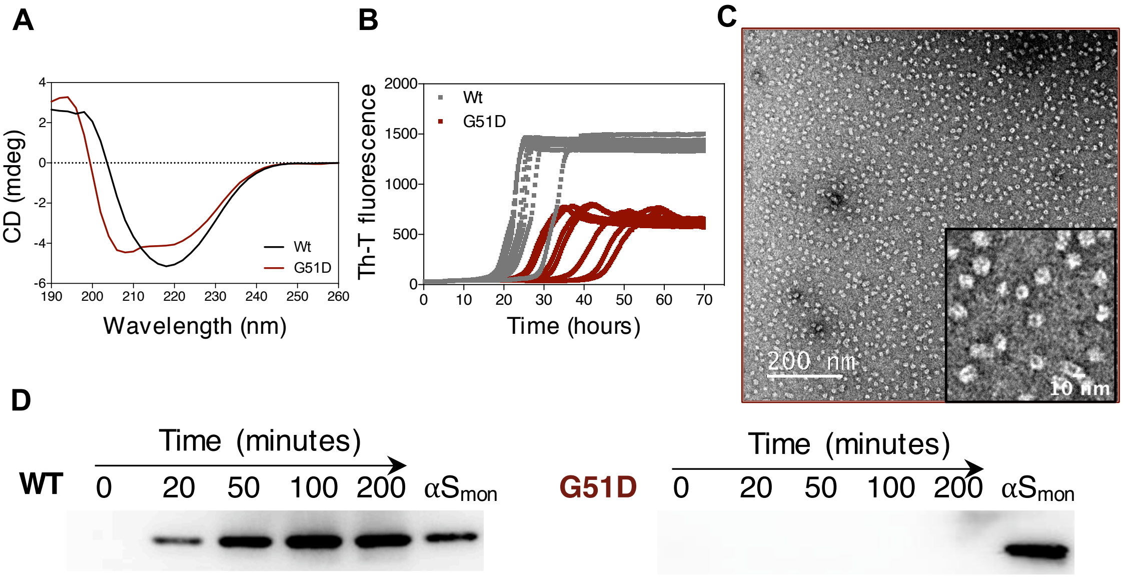

bioRxiv preprint doi: https://doi.org/10.1101/2023.02.10.527650; this version posted February 10, 2023. The copyright holder for this preprint (which was not certified by peer review) is the author/funder. All rights reserved. No reuse allowed without permission.

Fig. 3. The effect of the familial G51D mutation on αS amyloid and oligomer formation and disaggregation by molecular chaperones. (**A**) Circular dichroism spectra of kinetically trapped oligomers of G51D (dark red) and WT αS (black). (**B**) Assembly kinetics of G51D into amyloid fibrils monitored using ThT fluorescence. (**C**) Representative nsEM micrographs of the G51D oligomeric fraction after 28 hours of assembly. (**D**) Disaggregation of WT (left) and G51D (right) oligomers by the human Hsp70 chaperone disaggregation machinery at different time points analyzed by native-PAGE and western blot. 2 μM of monomeric αS (αS_{mon}) was added as a control.

Discussion

Overall, we show that the here studied αS oligomers have a symmetric and well-defined core molecular architecture, mainly sustained by the rigid NAC domain in a conformation structurally akin to that observed in many αS amyloid fibrils. Nevertheless, the NAC region is not sufficient to drive the oligomer to fibril conversion, likely because of its rigidity and burial in the assembly. Instead, the N-terminal flanking region, and especially the P1 and P2 sequences therein, modulate oligomer-to-fibril conversion, with the dynamic but partially collapsed P1-P2 region becoming engaged in sequence-specific contacts responsible for this structural transition (**Fig. 4**). This motif is solvent accessible and targetable in the oligomeric state, offering the opportunity to develop molecular binders for therapeutic and diagnostic use, as exemplified here using the PSMα3 peptide. The G51D oligomer polymorphism and its decreased susceptibility to chaperone-mediated disaggregation suggest a molecular basis for understanding why this and possibly other point mutations clustering at P2 are associated with familial PD.

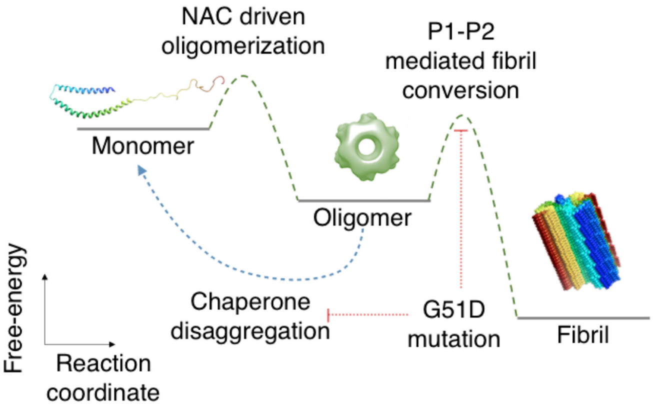

Fig. 4. Schematic representation of the αS aggregation landscape.

bioRxiv preprint doi: https://doi.org/10.1101/2023.02.10.527650; this version posted February 10, 2023. The copyright holder for this preprint (which was not certified by peer review) is the author/funder. All rights reserved. No reuse allowed without permission.

References:

1. M. G. Spillantini, M. L. Schmidt, V. M. Lee, J. Q. Trojanowski, R. Jakes, M. Goedert, Alpha-synuclein in Lewy bodies. *Nature*. **388**, 839–840 (1997).
2. M. H. Polymeropoulos, C. Lavedan, E. Leroy, S. E. Ide, A. Dehejia, A. Dutra, B. Pike, H. Root, J. Rubenstein, R. Boyer, E. S. Stenroos, S. Chandrasekharappa, A. Athanassiadou, T. Papapetropoulos, W. G. Johnson, A. M. Lazzarini, R. C. Duvoisin, G. Di Iorio, L. I. Golbe, R. L. Nussbaum, Mutation in the alpha-synuclein gene identified in families with Parkinson's disease. *Science*. **276**, 2045–2047 (1997).
3. M. Goedert, R. Jakes, M. G. Spillantini, The Synucleinopathies: Twenty Years On. *J Parkinsons Dis*. **7**, S51–S69 (2017).
4. N. Cremades, S. I. A. Cohen, E. Deas, A. Y. Abramov, A. Y. Chen, A. Orte, M. Sandal, R. W. Clarke, P. Dunne, F. A. Aprile, C. W. Bertoncini, N. W. Wood, T. P. J. Knowles, C. M. Dobson, D. Klenerman, Direct observation of the interconversion of normal and toxic forms of α-synuclein. *Cell*. **149**, 1048–1059 (2012).
5. E. Zurlo, P. Kumar, G. Meisl, A. J. Dear, D. Mondal, M. M. A. E. Claessens, T. P. J. Knowles, M. Huber, In situ kinetic measurements of α-synuclein aggregation reveal large population of short-lived oligomers. *PLoS One*. **16**, e0245548 (2021).
6. A. J. Dear, T. C. T. Michaels, G. Meisl, D. Klenerman, S. Wu, S. Perrett, S. Linse, C. M. Dobson, T. P. J. Knowles, Kinetic diversity of amyloid oligomers. *Proc Natl Acad Sci U S A*. **117**, 12087–12094 (2020).
7. X. Yang, B. Wang, C. L. Hoop, J. K. Williams, J. Baum, NMR unveils an N-terminal interaction interface on acetylated-α-synuclein monomers for recruitment to fibrils. *Proc Natl Acad Sci U S A*. **118**, e2017452118 (2021).
8. N. Lorenzen, S. B. Nielsen, A. K. Buell, J. D. Kaspersen, P. Arosio, B. S. Vad, W. Paslawski, G. Christiansen, Z. Valnickova-Hansen, M. Andreasen, J. J. Enghild, J. S. Pedersen, C. M. Dobson, T. P. J. Knowles, D. E. Otzen, The role of stable α-synuclein oligomers in the molecular events underlying amyloid formation. *J Am Chem Soc*. **136**, 3859–3868 (2014).
9. B. Winner, R. Jappelli, S. K. Maji, P. A. Desplats, L. Boyer, S. Aigner, C. Hetzer, T. Loher, M. Vilar, S. Campioni, C. Tzitzilonis, A. Soragni, S. Jessberger, H. Mira, A. Consiglio, E. Pham, E. Masliah, F. H. Gage, R. Riek, In vivo demonstration that alpha-synuclein oligomers are toxic. *Proc Natl Acad Sci U S A*. **108**, 4194–4199 (2011).
10. J. M. Froula, M. Castellana-Cruz, N. M. Anabtawi, J. D. Camino, S. W. Chen, D. R. Thrasher, J. Freire, A. A. Yazdi, S. Fleming, C. M. Dobson, J. R. Kumita, N. Cremades, L. A. Volpicelli-Daley, Defining α-synuclein species responsible for Parkinson's disease phenotypes in mice. *J Biol Chem*. **294**, 10392–10406 (2019).
11. N. Bengoa-Vergniory, R. F. Roberts, R. Wade-Martins, J. Alegre-Abarrategui, Alpha-synuclein oligomers: a new hope. *Acta Neuropathol*. **134**, 819–838 (2017).
12. S. W. Chen, S. Drakulic, E. Deas, M. Ouberai, F. A. Aprile, R. Arranz, S. Ness, C. Roodveldt, T. Guilliams, E. J. De-Genst, D. Klenerman, N. W. Wood, T. P. J. Knowles, C. Alfonso, G. Rivas, A. Y. Abramov, J. M. Valpuesta, C. M. Dobson, N. Cremades, Structural characterization of toxic oligomers that are kinetically trapped during α-synuclein fibril formation. *Proc Natl Acad Sci U S A*. **112**, E1994-2003 (2015).
13. G. Fusco, S. W. Chen, P. T. F. Williamson, R. Cascella, M. Perni, J. A. Jarvis, C. Cecchi, M. Vendruscolo, F. Chiti, N. Cremades, L. Ying, C. M. Dobson, A. De Simone, Structural basis of membrane disruption and cellular toxicity by α-synuclein oligomers. *Science*. **358**, 1440–1443 (2017).
14. N. Cremades, S. W. Chen, C. M. Dobson, Structural Characteristics of α-Synuclein Oligomers. *Int Rev Cell Mol Biol*. **329**, 79–143 (2017).
15. J. Santos, P. Gracia, S. Navarro, S. Peña-Díaz, J. Pujols, N. Cremades, I. Pallarès, S.

bioRxiv preprint doi: https://doi.org/10.1101/2023.02.10.527650; this version posted February 10, 2023. The copyright holder for this preprint (which was not certified by peer review) is the author/funder. All rights reserved. No reuse allowed without permission.

Ventura, α-Helical peptidic scaffolds to target α-synuclein toxic species with nanomolar affinity. *Nat Commun*. **12**, 3752 (2021).

16. M. D. Tuttle, G. Comellas, A. J. Nieuwkoop, D. J. Covell, D. A. Berthold, K. D. Kloepper, J. M. Courtney, J. K. Kim, A. M. Barclay, A. Kendall, W. Wan, G. Stubbs, C. D. Schwieters, V. M. Y. Lee, J. M. George, C. M. Rienstra, Solid-state NMR structure of a pathogenic fibril of full-length human α-synuclein. *Nat Struct Mol Biol*. **23**, 409–415 (2016).

17. A. Farzadfard, J. N. Pedersen, G. Meisl, A. K. Somavarapu, P. Alam, L. Goksøyr, M. A. Nielsen, A. F. Sander, T. P. J. Knowles, J. S. Pedersen, D. E. Otzen, The C-terminal tail of α-synuclein protects against aggregate replication but is critical for oligomerization. *Commun Biol*. **5**, 123 (2022).

18. C. P. A. Doherty, S. M. Ulamec, R. Maya-Martinez, S. C. Good, J. Makepeace, G. N. Khan, P. van Oosten-Hawle, S. E. Radford, D. J. Brockwell, A short motif in the N-terminal region of α-synuclein is critical for both aggregation and function. *Nat Struct Mol Biol*. **27**, 249–259 (2020).

19. S. M. Ulamec, R. Maya-Martinez, E. J. Byrd, K. M. Dewison, Y. Xu, L. F. Willis, F. Sobott, G. R. Heath, P. van Oosten Hawle, V. L. Buchman, S. E. Radford, D. J. Brockwell, Single residue modulators of amyloid formation in the N-terminal P1-region of α-synuclein. *Nat Commun*. **13**, 4986 (2022).

20. P. Kumari, D. Ghosh, A. Vanas, Y. Fleischmann, T. Wiegand, G. Jeschke, R. Riek, C. Eichmann, Structural insights into α-synuclein monomer-fibril interactions. *Proc Natl Acad Sci U S A*. **118**, e2012171118 (2021).

21. C. K. Xu, M. Castellana-Cruz, S. W. Chen, Z. Du, G. Meisl, A. Levin, B. Mannini, L. S. Itzhaki, T. P. J. Knowles, C. M. Dobson, N. Cremades, J. R. Kumita, The Pathological G51D Mutation in Alpha-Synuclein Oligomers Confers Distinct Structural Attributes and Cellular Toxicity. *Molecules*. **27**, 1293 (2022).

22. B. M. Burmann, J. A. Gerez, I. Matečko-Burmann, S. Campioni, P. Kumari, D. Ghosh, A. Mazur, E. E. Aspholm, D. Šulskis, M. Wawrzyniuk, T. Bock, A. Schmidt, S. G. D. Rüdiger, R. Riek, S. Hiller, Regulation of α-synuclein by chaperones in mammalian cells. *Nature*. **577**, 127–132 (2020).

23. A. S. Wentink, N. B. Nillegoda, J. Feufel, G. Ubartaitė, C. P. Schneider, P. De Los Rios, J. Hennig, A. Barducci, B. Bukau, Molecular dissection of amyloid disaggregation by human HSP70. *Nature*. **587**, 483–488 (2020).

24. A. Franco, P. Gracia, A. Colom, J. D. Camino, J. Á. Fernández-Higuero, N. Orozco, A. Dulebo, L. Saiz, N. Cremades, J. M. G. Vilar, A. Prado, A. Muga, All-or-none amyloid disassembly via chaperone-triggered fibril unzipping favors clearance of α-synuclein toxic species. *Proc Natl Acad Sci U S A*. **118**, e2105548118 (2021).

bioRxiv preprint doi: https://doi.org/10.1101/2023.02.10.527650; this version posted February 10, 2023. The copyright holder for this preprint (which was not certified by peer review) is the author/funder. All rights reserved. No reuse allowed without permission.

Acknowledgements:

Authors thank the cryoEM CNB-CSIC facility (CRIOMECORR project ESFRI-2019-01-CSIC-16), the services of the CNB-CSIC Mass Spectrometry facility, the Biomolecular mass spectrometry facility (UL) funded by the BBSRC (BB/M012573/1), the Microscopy Services (UAB), the Laboratori de Luminiscència i Espectroscòpia de Biomolècules (UAB) and the Biophysical and Structural Chemistry Platform at IECB, CNRS UAR 3033, INSERM US001. We thank James Ault for technical support with HDX-MS experiments and David Brockwell for illuminating discussions on the P1 region of αS.

Funding:

Spanish Ministry of Economy and Competitiveness (MINECO) grant BIO2016-78310-R and BIO2017-91475-EXP (SV)

Spanish Ministry of Science and Innovation (MICINN) grant PID2019-105017RB-I00 (SV)

MICINN grant PID2019-105872 GB-I00 (JMV)

MICINN grant PID2019-111068GB-I00 (AM)

ICREA-Academia 2015 (SV)

MICINN doctoral grant FPU17/01157 (JS)

Early postdoc mobility project SNSF P2EZP2_184258 (AL)

Basque Government grant IT1201-19 (FM)

BBSRC BB/M011151/1 grant (EJB)

Sir Henry Dale Fellowship jointly funded by Wellcome and the Royal Society 220628/Z/20/Z (ANC)

Royal Society grant RGS\R2\222357 (ANC)

University Academic fellowship from the University of Leeds (ANC)

Royal Society Research Professorship RSRP/R1/211057 (SER)

Concluding remarks

Chapter 1:

- α-Helical amphipathic cationic peptides are conformational selective nanomolar binders of αS pathogenic species.
- PSMα3 binding to αS oligomers is not affected by a 100-fold excess of monomer. PSMα3 is therefore a promising molecule to implement in diagnosis platforms.
- α-Helical amphipathic cationic peptides inhibit αS aggregation by blocking oligomer to fibril conversion, being of therapeutic interest.
- PSMα3 inhibits oligomer-associated cellular damage.
- The binding properties of these α-helical peptides are encoded in their physicochemical features. This allows the computational identification of novel peptides with biological or therapeutic interest.
- LL-37 is a human endogenous peptide that coexists with αS in the brain and gastrointestinal tract and recapitulates the αS binding, inhibition and detoxifying properties of PSMα3.
- Targeting the physicochemical properties of αS oligomers and fibrils permits a conformation specific binding without detectable monomer interaction. These molecules hold potential for diagnosis and serve as a proof-of-principle for our initial hypothesis.

Chapter 2 and 3:

- Our organism has a repertoire of peptides and proteins with putative inhibitory activities that can play a role in controlling αS *in vivo*. This activity may have been evolutionary selected or just an accidental property derived from a more generic amyloid-targeting activity. Inducing the expression of these peptides could be a therapeutic strategy.
- The fuzzy coats of αS oligomers and fibrils have an important role in pathogenesis. Targeting these “invisible” regions holds the clue for a poorly explored therapeutic avenue.
- There is a repertoire of structurally diverse proteins that can control endogenous and exogenous amyloid formation in different organisms. This moonlighting inhibitors may be of therapeutic interest or be used to gain mechanistic insights into amyloid formation.
- There is an apparent overlap between antimicrobial, anti-biofilm and anti-amyloid activities

Chapter 4:

- αS oligomers are symmetric and well-organized particles. We identified a 6-fold symmetry and a 5-layer organization.
- The NAC domain is rigid in the oligomer, adopting a Greek-key like fold.
- The N-terminal domain of αS is partially collapsed and solvent-exposed in the oligomer. Two N-terminal regions, P1 and P2, play a major role in oligomer to fibril conversion.
- PSMα3 binding to P1 and P2 explains its inhibitory activity. PSMα3 illustrates that P1 and P2 are privileged targets for the design of oligomer binders.
- The G51D mutations affects oligomer to fibril transition and hinders oligomer disaggregation by the human Hsp70 disaggregation machinery. This provides a putative mechanism of pathogenesis for this familial variant associated with early onset parkinsonism.
- The G51D mutation illustrates that genetic mutations in P2 have the potential to affect the oligomer relation with other biological partners, insinuating a framework to understand why they cluster in this specific region.

Discussion

The research developed in this thesis dissertation presents new structural details on αS oligomers and explores a novel scenario for the rational design of oligomer-targeting ligands. This new data describes αS oligomers with unprecedented detail and illuminates some unanswered questions in the field. At the same time, this new information poses new enigmas and hypothesis.

In this section, I aim to discuss the present and future implications of our research while elaborating my personal view on diverse hypotheses and conjectures that could be developed from the presented conceptual framework.

1. Molecular basis of α-helical amphipathic peptides binding to α-synuclein oligomers

In the first chapter, we described and characterized a family of α-helical amphipathic peptides that bind αS oligomers with nanomolar affinity. We demonstrated that this binding is not sequence-specific but resides in two physicochemical properties, their amphipathic and cationic character. Accordingly, the peptide-oligomer interaction was discussed in terms of biophysical complementarity. Whereas these observations remain true, the subsequent characterization of αS oligomers in chapter 4 revealed that PSMα3 has a specific binding site in the P1-P2 region of αS. The relevance of this discovery is dual: (i) The distinct structural context of P1 and P2 in the monomer and the oligomer explains the conformational selectivity described for PSMα3 and peptides alike. (ii) Binding the region driving oligomer to fibril conversion also illuminates the mechanistic basis of the aggregation inhibition reported in chapter 1. This new structural understanding complements our previous efforts, enlightening the molecular basis of PSMα3 activities from both the peptide and the oligomer perspective. A clear mechanism of action also benefits the prospective application of this family of peptides for therapeutics and diagnosis.

Currently, few data on oligomer-specific binding molecules are available. It is then our hope that, beyond the direct applicability of these peptides, the here described binding principles as well as the description of P1-P2 as a promising binding site could have a future impact on the development of oligomer interacting molecules. Regarding this P1-P2 binding site, it is now our objective to assess if the α-helix of our peptides has a certain structural complementary with P1-P2 or if its contribution is limited to a scaffolding function.

2. Kinetically trapped type-B* oligomers as a model α-synuclein oligomers

In this thesis, we worked with kinetically trapped αS oligomers (type-B*) to obtain homogeneous preparations of oligomers that allowed us to address our intended scientific objectives. When we started this project, a critical question -raised by us and others- was related to the biological and mechanistic relevance of such kinetically trapped species. Type-B* oligomers are a gold-standard in the field, but it was not clear to which extent they can mimic αS oligomers formed in a typical aggregation reaction.

The results of our work shed light into this question and suggest that type-B* oligomers are reasonable equivalents of αS oligomers en route to the fibrils. We have demonstrated that (i) molecular binders designed towards type-B* oligomers also bind oligomers that have not been kinetically trapped and block their conversion to fibrils; (ii) PSMα3 binding sites (P1 and P2), identified in type-B* oligomers, account for such aggregation inhibition; (iii) The structural data obtained with type-B* is in agreement with the relevance of P1 and P2 in oligomer conversion to fibrils. Together our data indicates that type-B* oligomers are suitable -or at least “sufficient”- models to understand the structural biology of αS oligomers and develop molecular binders relevant for therapeutics and diagnosis.

3. Oligomer structure and transition to fibril

In this work, we found that the rigid core of the oligomer, assigned by ssNMR as residues 70 to 89 (NAC region), may adopt a Greek-key arrangement similar to that observed in the structure of αS fibrils. In the fibrils, the Greek-key folds are stacked on top of each other forming β-sheets that run perpendicular to the fibril axis and provide a scaffold for self-propagation. However, in the observed oligomer’s architecture, the Greek-keys are parallel to the oligomer axis, stablishing lateral interactions but not stacked into layers. Such arrangement reconciles previous kinetic and biophysical data; oligomers are nonfibrillar, unable to propagate by monomer addition and they lack the parallel β-sheet contribution characteristic of amyloid fibrils (Dear et al. 2020; Chen et al. 2015). Accordingly, the adoption of the Greek-key arrangement seems to be independent of fibrillation and the interlayer contacts of the amyloid structure. The proposed architecture also implies that the structural reorganization involving oligomer to fibril conversion requires a spatial reorientation of the Greek-keys.

It is also tempting to speculate that the presence of the Greek-key motive in αS fibrils is a reminiscence of its previous conformation in the oligomer, and thus an evidence of such pathway of amyloid formation. The *in vitro* amyloid fibril structures that show the highest divergence from the Greek-key arrangement include those aggregated in presence of lipids or formed by N-terminal truncations (Frieg et al. 2022; McGlinchey et al. 2021). Could be plausible to speculate that these polymorphs are the result of a different aggregation pathway that does not nucleate through the here studied oligomer? Regarding *in vivo* amyloid structures, MSA and JOS fibrils purified from patients brains share the Greek-key arrangement, whereas fibrils solved from PD, PDD and DLB do not (Schweighauser et al. 2020; Y. Yang, Shi, et al. 2022; Y. Yang, Garringer, et al. 2022). MSA and JOS have both earlier onset and are more aggressive than PD. Is it then possible that the fibril structure can help to trace back the aggregation pathway in disease? Are MSA and JOS fibrils formed through oligomer conversion whereas secondary nucleation or other mechanisms of primary nucleation dominate PD, PDD and DLB fibril formation? The answers to these questions could reshape our current understanding of the disease-relevance of αS oligomers and guide the development of disease-specific therapies.

Additionally, we demonstrated that this rigid Greek-key core does not suffice to drive oligomer to fibril conversion, even if it corresponds to the highly amyloidogenic core of mature amyloid fibrils. Such observation can be rationalized considering that the oligomer core is involved in the contacts that sustain the oligomer architecture, not being available to participate in the initial steps of fibril conversion. Thus, αS oligomers are metastable species that require core-flanking regions to escape from their local energetic minimum and advance towards the fibrillar state. It is the partially folded, but solvent-accessible, P1-P2 region the principal driver of this conversion. This segregation of the amyloid conversion activities at specific sequence stretches could have a profound impact on the design of therapeutic molecules. P1 and P2 have significant advantages as a target; they are the drivers of fibril conversion, populate distinct conformations in monomers, oligomers and fibrils, and can be targeted by complementary ligands as exemplified by PSMα3 binding.

4. G51D N-terminal polymorphism reshapes the disease landscape and impacts therapeutics

The connection between αS genetic mutations associated with fPD and protein aggregation has always been obscure. E46K, H50Q, and A53T aggregate faster than the WT, whereas A30P and

G51D have lower aggregation rates (Rutherford et al. 2014; J. Li, Uversky, and Fink 2001; Ono et al. 2011). These last two mutations also abrogate αS membrane binding, a proposed mechanism for aggregate toxicity (Stefanovic et al. 2015; Fusco et al. 2017). Indeed, the G51D mutation is one of the most aggressive genetic variants causing juvenile parkinsonism with an MSA-like phenotype (Kiely et al. 2013). Thus, aggregation propensity and membrane binding are insufficient to explain the link between these mutations and disease severity. Herein, we reported that G51D induces a conformational change in the N-terminal solvent-exposed regions of the oligomer that hinders oligomer disaggregation by the Hsp70-DNAJB1-Apg2 system. Unprocessed G51D oligomers may act as a source of pathogenicity exceeding the toxic potential of WT oligomers. In this framework, genetic mutations may not need to enhance aggregation or aggregate toxicity; becoming resistant or invisible to the quality control system may have an equally devastating effect.

This discovery could have a direct link to disease development. It is well-known that the gradual decline of the protein quality control system due to aging is at the root of idiopathic PD and similar late-onset neurodegenerative disorders. The undescribed effect of the G51D familial mutation bypasses the need of proteostasis impairment and thus explains the earlier onset associated with this mutation. If this hypothesis is true, it will stablish a direct link between oligomers' structural properties and disease onset. Importantly, this idea also suggests that, in health, our proteostasis network can efficiently deal with the oligomer thread.

Noteworthy, proteostasis recovery is an active line of research against amyloidosis (Friesen et al. 2017; Mesgarzadeh et al. 2022; V. Sorrentino et al. 2017). Whereas for idiopathic PD it could be an attractive avenue, our result suggests that it might be less effective in G51D-suffering patients. This new framework, together with the observed structural polymorphism, indicates that personalized medicine approaches would be essential to treat familial Parkinson's disease caused by individual αS variants.

5. Where do oligomers come from?

The symmetric and ordered architecture of αS oligomers leads to one final consideration. The spontaneous formation of such a symmetric, complex, and size-constrained structure in a non-natural and deleterious assembly is conceptually challenging, since the contacts leading to deleterious oligomerization are not expected to be under a positive selection during evolution.

Oligomers constitute a local thermodynamic minimum in the free-energy landscape of αS aggregation in which the hydrophobic NAC domain is blocked in a persistent and non-productive state (Nunilo Cremades et al. 2012; Dear et al. 2020; X. Yang et al. 2021; Lorenzen et al. 2014). Only after a structural conversion, amyloid fibrils are formed. In healthy individuals, αS oligomers are disaggregated and do not lead to disease development until late ages. Considering this, we dare to propose that the contacts that support oligomer formation are evolutionarily conserved (or at least not purged out) because they act as a kinetic trap that retains monomers in a non-seeding competent state, preventing fast amyloid formation and allowing chaperone disaggregation activity. In that sense, it is probable that under normal cellular conditions, low concentrations of spontaneously formed oligomers would be less pathogenic than seeding competent fibrils.

6. Future perspectives and challenges ahead

The identification of α-helical amphipathic peptides as nanomolar binders of αS toxic species in a non-sequence specific way suggest that these or similar bioactive peptides may play a physiological role in controlling synucleinopathies. They may also serve as a repository of potential therapeutic agents; either by exogeneous administration or via inducible endogenous expression. The discovery and characterization of some of these peptides is now fundamental to prove this hypothesis. Additionally, the *in vivo* analysis of LL-37 or similar peptides activities in animal models of PD is still a pending task in order to evaluate the potential of such peptides for therapeutic intervention. To pursue such objective, our laboratory has a funded research line.

Our research also converges with the hypothesis that diet and microbiome are associated with PD onset and progression. Several research endeavors tried to assess these connections (Keshavarzian et al. 2020; Sampson et al. 2016; Mischley, Lau, and Bennett 2017; Solch et al. 2022), and we hope that our research can help to delineate novel molecular factors to be monitored when addressing these challenging questions.

The nanomolar affinity and conformation selectivity of α-helical amphipathic immediately suggest their use for diagnostic purposes. We have developed a diagnosis platform that combines PSMα3 conformational specificity with anti-αS antibodies for sequence specificity. This device can detect picomolar amounts of oligomer in solution. We hope that this proof-of-principle, soon to be drafted into a manuscript, could inspire the development of conformation-specific diagnosis tools.

Regarding αS oligomers, the here developed research poses new questions related to the conformational transitions occurring along the aggregation reaction. Understanding how oligomers are assembled and identifying the specific contacts and regions involved is a promising area of research, not only for disease-related applications, but to understand the biology of αS and its interplay with evolution. Likewise, obtaining mechanistic and structural information on oligomer to fibril transitions could delineate a therapeutically addressable process to block amyloid progression. If it is possible to reduce oligomer conversion while stimulating its disaggregation, it will be the equivalent of restoring proteostasis and cellular health. We hope that in the near future the continuous advances of structural biology, combined with the development of molecular strategies to reduce oligomers' structural heterogenicity could allow accessing higher resolution information. Our group is already working in this direction.

In my opinion, one of the most impactful ideas derived from this thesis is the need of a detailed analysis of αS familial mutations. fPD presents a practical advantage for therapeutic intervention: its development can be predicted, and treatment can begin before neuronal dead and extensive degeneration occurs. If the pathology of specific familial mutations affects processes that can be clearly identified, there is hope that therapies that are ineffective in idiopathic PD can tackle or delay the molecular causes driving disease onset in familial syndromes.

References

Abedini, Andisheh, Fanling Meng, and Daniel P. Raleigh. 2007. “A Single-Point Mutation Converts the Highly Amyloidogenic Human Islet Amyloid Polypeptide into a Potent Fibrillization Inhibitor.” *Journal of the American Chemical Society* 129 (37): 11300–301. https://doi.org/10.1021/ja072157y.

Abedini, Andisheh, and Daniel P. Raleigh. 2006. “Destabilization of Human IAPP Amyloid Fibrils by Proline Mutations Outside of the Putative Amyloidogenic Domain: Is There a Critical Amyloidogenic Domain in Human IAPP?” *Journal of Molecular Biology* 355 (2): 274–81. https://doi.org/10.1016/j.jmb.2005.10.052.

Agerschou, Emil Dandanell, Patrick Flagmeier, Theodora Saridaki, Céline Galvagnion, Daniel Komnig, Laetitia Heid, Vibha Prasad, et al. 2019. “An Engineered Monomer Binding-Protein for α-Synuclein Efficiently Inhibits the Proliferation of Amyloid Fibrils.” *ELife* 8 (August): e46112. https://doi.org/10.7554/eLife.46112.

Aguzzi, Adriano, and Lawrence Rajendran. 2009. “The Transcellular Spread of Cytosolic Amyloids, Prions, and Prionoids.” *Neuron* 64 (6): 783–90. https://doi.org/10.1016/j.neuron.2009.12.016.

Anfinsen, C. B. 1973. “Principles That Govern the Folding of Protein Chains.” *Science (New York, N.Y.)* 181 (4096): 223–30. https://doi.org/10.1126/science.181.4096.223.

Angelova, Plamena R., Marthe H. R. Ludtmann, Mathew H. Horrocks, Alexander Negoda, Nunilo Cremades, David Klenerman, Christopher M. Dobson, et al. 2016. “Ca2+ Is a Key Factor in α-Synuclein-Induced Neurotoxicity.” *Journal of Cell Science* 129 (9): 1792–1801. https://doi.org/10.1242/jcs.180737.

Appel-Cresswell, Silke, Carles Vilarino-Guell, Mary Encarnacion, Holly Sherman, Irene Yu, Brinda Shah, David Weir, et al. 2013. “Alpha-Synuclein p.H50Q, a Novel Pathogenic Mutation for Parkinson’s Disease.” *Movement Disorders: Official Journal of the Movement Disorder Society* 28 (6): 811–13. https://doi.org/10.1002/mds.25421.

Arai, Y., M. Yamazaki, O. Mori, H. Muramatsu, G. Asano, and Y. Katayama. 2001. “Alpha-Synuclein-Positive Structures in Cases with Sporadic Alzheimer’s Disease: Morphology and Its Relationship to Tau Aggregation.” *Brain Research* 888 (2): 287–96. https://doi.org/10.1016/s0006-8993(00)03082-1.

Arosio, Paolo, Tuomas P. J. Knowles, and Sara Linse. 2015. “On the Lag Phase in Amyloid Fibril Formation.” *Physical Chemistry Chemical Physics: PCCP* 17 (12): 7606–18. https://doi.org/10.1039/c4cp05563b.

Balchin, David, Manajit Hayer-Hartl, and F. Ulrich Hartl. 2016. “In Vivo Aspects of Protein Folding and Quality Control.” *Science (New York, N.Y.)* 353 (6294): aac4354. https://doi.org/10.1126/science.aac4354.

Baldwin, Andrew J., Tuomas P. J. Knowles, Gian Gaetano Tartaglia, Anthony W. Fitzpatrick, Glyn L. Devlin, Sarah Lucy Shammas, Christopher A. Waudby, et al. 2011. “Metastability of Native Proteins and the Phenomenon of Amyloid Formation.” *Journal of the American Chemical Society* 133 (36): 14160–63. https://doi.org/10.1021/ja2017703.

Beerten, Jacinte, Wim Jonckheere, Stanislav Rudyak, Jie Xu, Hannah Wilkinson, Frederik De Smet, Joost Schymkowitz, and Frederic Rousseau. 2012. “Aggregation Gatekeepers Modulate Protein Homeostasis of Aggregating Sequences and Affect Bacterial Fitness.” *Protein Engineering, Design & Selection: PEDS* 25 (7): 357–66. https://doi.org/10.1093/protein/gzs031.

Beerten, Jacinte, Joost Schymkowitz, and Frederic Rousseau. 2012. “Aggregation Prone Regions and Gatekeeping Residues in Protein Sequences.” *Current Topics in Medicinal Chemistry* 12 (22):

2470–78. https://doi.org/10.2174/1568026611212220003.

Bertolini, Matilde, Kai Fenzl, Ilia Kats, Florian Wruck, Frank Tippmann, Jaro Schmitt, Josef Johannes Auburger, Sander Tans, Bernd Bukau, and Günter Kramer. 2021. "Interactions between Nascent Proteins Translated by Adjacent Ribosomes Drive Homomer Assembly." *Science (New York, N.Y.)* 371 (6524): 57–64. https://doi.org/10.1126/science.abc7151.

Bertoncini, Carlos W., Young-Sang Jung, Claudio O. Fernandez, Wolfgang Hoyer, Christian Griesinger, Thomas M. Jovin, and Markus Zweckstetter. 2005. "Release of Long-Range Tertiary Interactions Potentiates Aggregation of Natively Unstructured Alpha-Synuclein." *Proceedings of the National Academy of Sciences of the United States of America* 102 (5): 1430–35. https://doi.org/10.1073/pnas.0407146102.

Bloem, Bastiaan R., Michael S. Okun, and Christine Klein. 2021. "Parkinson's Disease." *Lancet (London, England)* 397 (10291): 2284–2303. https://doi.org/10.1016/S0140-6736(21)00218-X.

Bonetti, Daniela, Francesca Troilo, Maurizio Brunori, Sonia Longhi, and Stefano Gianni. 2018. "How Robust Is the Mechanism of Folding-Upon-Binding for an Intrinsically Disordered Protein?" *Biophysical Journal* 114 (8): 1889–94. https://doi.org/10.1016/j.bpj.2018.03.017.

Bousset, Luc, Laura Pieri, Gemma Ruiz-Arlandis, Julia Gath, Poul Henning Jensen, Birgit Habenstein, Karine Madiona, et al. 2013. "Structural and Functional Characterization of Two Alpha-Synuclein Strains." *Nature Communications* 4: 2575. https://doi.org/10.1038/ncomms3575.

Boyer, David R., Binsen Li, Chuanqi Sun, Weijia Fan, Michael R. Sawaya, Lin Jiang, and David S. Eisenberg. 2019. "Structures of Fibrils Formed by α-Synuclein Hereditary Disease Mutant H50Q Reveal New Polymorphs." *Nature Structural & Molecular Biology* 26 (11): 1044–52. https://doi.org/10.1038/s41594-019-0322-y.

Brundin, Patrik, Hanno Svoboda, Azad Bonni, and Gennaro Pagano. 2022. "This Is NOT the End for Immunotherapy in Parkinson's Disease - A Perspective from Early Drug Development Scientists." *Journal of Parkinson's Disease* 12 (8): 2293–96. https://doi.org/10.3233/JPD-229008.

Buell, Alexander K., Céline Galvagnion, Ricardo Gaspar, Emma Sparr, Michele Vendruscolo, Tuomas P. J. Knowles, Sara Linse, and Christopher M. Dobson. 2014. "Solution Conditions Determine the Relative Importance of Nucleation and Growth Processes in α-Synuclein Aggregation." *Proceedings of the National Academy of Sciences of the United States of America* 111 (21): 7671–76. https://doi.org/10.1073/pnas.1315346111.

Burmann, Björn M., Juan A. Gerez, Irena Matečko-Burmann, Silvia Campioni, Pratibha Kumari, Dhiman Ghosh, Adam Mazur, et al. 2020. "Regulation of α-Synuclein by Chaperones in Mammalian Cells." *Nature* 577 (7788): 127–32. https://doi.org/10.1038/s41586-019-1808-9.

Bussell, Robert, and David Eliezer. 2003. "A Structural and Functional Role for 11-Mer Repeats in Alpha-Synuclein and Other Exchangeable Lipid Binding Proteins." *Journal of Molecular Biology* 329 (4): 763–78. https://doi.org/10.1016/s0022-2836(03)00520-5.

Cascella, Roberta, Alessandra Bigi, Nunilo Cremades, and Cristina Cecchi. 2022. "Effects of Oligomer Toxicity, Fibril Toxicity and Fibril Spreading in Synucleinopathies." *Cellular and Molecular Life Sciences: CMLS* 79 (3): 174. https://doi.org/10.1007/s00018-022-04166-9.

Cascella, Roberta, Serene W. Chen, Alessandra Bigi, José D. Camino, Catherine K. Xu, Christopher M. Dobson, Fabrizio Chiti, Nunilo Cremades, and Cristina Cecchi. 2021. "The Release of Toxic Oligomers from α-Synuclein Fibrils Induces Dysfunction in Neuronal Cells." *Nature Communications* 12 (1): 1814. https://doi.org/10.1038/s41467-021-21937-3.

Castillo, Virginia, Fabrizio Chiti, and Salvador Ventura. 2013. "The N-Terminal Helix Controls the Transition between the Soluble and Amyloid States of an FF Domain." *PloS One* 8 (3): e58297.

https://doi.org/10.1371/journal.pone.0058297.

Castillo, Virginia, and Salvador Ventura. 2009. “Amyloidogenic Regions and Interaction Surfaces Overlap in Globular Proteins Related to Conformational Diseases.” *PLoS Computational Biology* 5 (8): e1000476. https://doi.org/10.1371/journal.pcbi.1000476.

Chatzi, Afroditi, Phanee Manganas, and Kostas Tokatlidis. 2016. “Oxidative Folding in the Mitochondrial Intermembrane Space: A Regulated Process Important for Cell Physiology and Disease.” *Biochimica Et Biophysica Acta* 1863 (6 Pt A): 1298–1306. https://doi.org/10.1016/j.bbamcr.2016.03.023.

Chen, Serene W., Srdja Drakulic, Emma Deas, Myriam Ouberai, Francesco A. Aprile, Rocío Arranz, Samuel Ness, et al. 2015. “Structural Characterization of Toxic Oligomers That Are Kinetically Trapped during α-Synuclein Fibril Formation.” *Proceedings of the National Academy of Sciences of the United States of America* 112 (16): E1994-2003. https://doi.org/10.1073/pnas.1421204112.

Chia, Sean, Johnny Habchi, Thomas C. T. Michaels, Samuel I. A. Cohen, Sara Linse, Christopher M. Dobson, Tuomas P. J. Knowles, and Michele Vendruscolo. 2018. “SAR by Kinetics for Drug Discovery in Protein Misfolding Diseases.” *Proceedings of the National Academy of Sciences of the United States of America* 115 (41): 10245–50. https://doi.org/10.1073/pnas.1807884115.

Chiti, Fabrizio, Martino Calamai, Niccolo Taddei, Massimo Stefani, Giampietro Ramponi, and Christopher M. Dobson. 2002. “Studies of the Aggregation of Mutant Proteins in Vitro Provide Insights into the Genetics of Amyloid Diseases.” *Proceedings of the National Academy of Sciences of the United States of America* 99 Suppl 4 (Suppl 4): 16419–26. https://doi.org/10.1073/pnas.212527999.

Chiti, Fabrizio, and Christopher M. Dobson. 2006. “Protein Misfolding, Functional Amyloid, and Human Disease.” *Annual Review of Biochemistry* 75: 333–66. https://doi.org/10.1146/annurev.biochem.75.101304.123901.

———. 2017. “Protein Misfolding, Amyloid Formation, and Human Disease: A Summary of Progress Over the Last Decade.” *Annual Review of Biochemistry* 86 (June): 27–68. https://doi.org/10.1146/annurev-biochem-061516-045115.

Choi, Minee L., Alexandre Chappard, Bhanu P. Singh, Catherine Maclachlan, Margarida Rodrigues, Evgeniya I. Fedotova, Alexey V. Berezhnov, et al. 2022. “Pathological Structural Conversion of α-Synuclein at the Mitochondria Induces Neuronal Toxicity.” *Nature Neuroscience* 25 (9): 1134–48. https://doi.org/10.1038/s41593-022-01140-3.

Ciudad, Sonia, Eduard Puig, Thomas Botzanowski, Moeen Meigooni, Andres S. Arango, Jimmy Do, Maxim Mayzel, et al. 2020. “Aβ(1-42) Tetramer and Octamer Structures Reveal Edge Conductivity Pores as a Mechanism for Membrane Damage.” *Nature Communications* 11 (1): 3014. https://doi.org/10.1038/s41467-020-16566-1.

Clarke, C. E. 2007. “Parkinson’s Disease.” *BMJ (Clinical Research Ed.)* 335 (7617): 441–45. https://doi.org/10.1136/bmj.39289.437454.AD.

Close, William, Matthias Neumann, Andreas Schmidt, Manuel Hora, Karthikeyan Annamalai, Matthias Schmidt, Bernd Reif, Volker Schmidt, Nikolaus Grigorieff, and Marcus Fändrich. 2018. “Physical Basis of Amyloid Fibril Polymorphism.” *Nature Communications* 9 (1): 699. https://doi.org/10.1038/s41467-018-03164-5.

Cohen, Samuel I. A., Sara Linse, Leila M. Luheshi, Erik Hellstrand, Duncan A. White, Luke Rajah, Daniel E. Otzen, Michele Vendruscolo, Christopher M. Dobson, and Tuomas P. J. Knowles. 2013. “Proliferation of Amyloid-Β42 Aggregates Occurs through a Secondary Nucleation Mechanism.”

Proceedings of the National Academy of Sciences of the United States of America 110 (24): 9758–63. https://doi.org/10.1073/pnas.1218402110.

Cox, Dezerae, Daniel R. Whiten, James W. P. Brown, Mathew H. Horrocks, Rebecca San Gil, Christopher M. Dobson, David Klenerman, Antoine M. van Oijen, and Heath Ecroyd. 2018. "The Small Heat Shock Protein Hsp27 Binds α-Synuclein Fibrils, Preventing Elongation and Cytotoxicity." *The Journal of Biological Chemistry* 293 (12): 4486–97. https://doi.org/10.1074/jbc.M117.813865.

Cremades, N., S. W. Chen, and C. M. Dobson. 2017. "Structural Characteristics of α-Synuclein Oligomers." *International Review of Cell and Molecular Biology* 329: 79–143. https://doi.org/10.1016/bs.ircmb.2016.08.010.

Cremades, Nunilo, Samuel I. A. Cohen, Emma Deas, Andrey Y. Abramov, Allen Y. Chen, Angel Orte, Massimo Sandal, et al. 2012. "Direct Observation of the Interconversion of Normal and Toxic Forms of α-Synuclein." *Cell* 149 (5): 1048–59. https://doi.org/10.1016/j.cell.2012.03.037.

De, Suman, Daniel R. Whiten, Francesco S. Ruggeri, Craig Hughes, Margarida Rodrigues, Dimitrios I. Sideris, Christopher G. Taylor, et al. 2019. "Soluble Aggregates Present in Cerebrospinal Fluid Change in Size and Mechanism of Toxicity during Alzheimer's Disease Progression." *Acta Neuropathologica Communications* 7 (1): 120. https://doi.org/10.1186/s40478-019-0777-4.

Dear, Alexander J., Thomas C. T. Michaels, Georg Meisl, David Klenerman, Si Wu, Sarah Perrett, Sara Linse, Christopher M. Dobson, and Tuomas P. J. Knowles. 2020. "Kinetic Diversity of Amyloid Oligomers." *Proceedings of the National Academy of Sciences of the United States of America* 117 (22): 12087–94. https://doi.org/10.1073/pnas.1922267117.

Deas, Emma, Nunilo Cremades, Plamena R. Angelova, Marthe H. R. Ludtmann, Zhi Yao, Serene Chen, Mathew H. Horrocks, et al. 2016. "Alpha-Synuclein Oligomers Interact with Metal Ions to Induce Oxidative Stress and Neuronal Death in Parkinson's Disease." *Antioxidants & Redox Signaling* 24 (7): 376–91. https://doi.org/10.1089/ars.2015.6343.

Dedmon, Matthew M., Kresten Lindorff-Larsen, John Christodoulou, Michele Vendruscolo, and Christopher M. Dobson. 2005. "Mapping Long-Range Interactions in Alpha-Synuclein Using Spin-Label NMR and Ensemble Molecular Dynamics Simulations." *Journal of the American Chemical Society* 127 (2): 476–77. https://doi.org/10.1021/ja044834j.

Dickson, Dennis W. 2012. "Parkinson's Disease and Parkinsonism: Neuropathology." *Cold Spring Harbor Perspectives in Medicine* 2 (8): a009258. https://doi.org/10.1101/cshperspect.a009258.

Dill, Ken A., and Justin L. MacCallum. 2012. "The Protein-Folding Problem, 50 Years On." *Science (New York, N.Y.)* 338 (6110): 1042–46. https://doi.org/10.1126/science.1219021.

Dishman, Acacia F., Robert C. Tyler, Jamie C. Fox, Andrew B. Kleist, Kenneth E. Prehoda, M. Madan Babu, Francis C. Peterson, and Brian F. Volkman. 2021. "Evolution of Fold Switching in a Metamorphic Protein." *Science (New York, N.Y.)* 371 (6524): 86–90. https://doi.org/10.1126/science.abd8700.

Dobson, Christopher M., Tuomas P. J. Knowles, and Michele Vendruscolo. 2020. "The Amyloid Phenomenon and Its Significance in Biology and Medicine." *Cold Spring Harbor Perspectives in Biology* 12 (2): a033878. https://doi.org/10.1101/cshperspect.a033878.

Doherty, Ciaran P. A., Sabine M. Ulamec, Roberto Maya-Martinez, Sarah C. Good, Jemma Makepeace, G. Nasir Khan, Patricija van Oosten-Hawle, Sheena E. Radford, and David J. Brockwell. 2020. "A Short Motif in the N-Terminal Region of α-Synuclein Is Critical for Both Aggregation and Function." *Nature Structural & Molecular Biology* 27 (3): 249–59. https://doi.org/10.1038/s41594-020-0384-x.

Durell, Stewart R., and Arieh Ben-Naim. 2017. “Hydrophobic-Hydrophilic Forces in Protein Folding.” *Biopolymers* 107 (8). https://doi.org/10.1002/bip.23020.

Dyson, H. J., and P. E. Wright. 1998. “Equilibrium NMR Studies of Unfolded and Partially Folded Proteins.” *Nature Structural Biology* 5 Suppl (July): 499–503. https://doi.org/10.1038/739.

Dyson, H. Jane, and Peter E. Wright. 2005. “Intrinsically Unstructured Proteins and Their Functions.” *Nature Reviews. Molecular Cell Biology* 6 (3): 197–208. https://doi.org/10.1038/nrm1589.

Eisenberg, David, and Mathias Jucker. 2012. “The Amyloid State of Proteins in Human Diseases.” *Cell* 148 (6): 1188–1203. https://doi.org/10.1016/j.cell.2012.02.022.

Eisenberg, David S., and Michael R. Sawaya. 2017. “Structural Studies of Amyloid Proteins at the Molecular Level.” *Annual Review of Biochemistry* 86 (June): 69–95. https://doi.org/10.1146/annurev-biochem-061516-045104.

Emin, Derya, Yu P. Zhang, Evgeniia Lobanova, Alyssa Miller, Xuecong Li, Zengjie Xia, Helen Dakin, et al. 2022. “Small Soluble α-Synuclein Aggregates Are the Toxic Species in Parkinson’s Disease.” *Nature Communications* 13 (1): 5512. https://doi.org/10.1038/s41467-022-33252-6.

Emmanouilidou, Evangelia, Katerina Melachroinou, Theodoros Roumeliotis, Spiros D. Garbis, Maria Ntzouni, Lukas H. Margaritis, Leonidas Stefanis, and Kostas Vekrellis. 2010. “Cell-Produced Alpha-Synuclein Is Secreted in a Calcium-Dependent Manner by Exosomes and Impacts Neuronal Survival.” *The Journal of Neuroscience: The Official Journal of the Society for Neuroscience* 30 (20): 6838–51. https://doi.org/10.1523/JNEUROSCI.5699-09.2010.

Englander, S. Walter, and Leland Mayne. 2014. “The Nature of Protein Folding Pathways.” *Proceedings of the National Academy of Sciences of the United States of America* 111 (45): 15873–80. https://doi.org/10.1073/pnas.1411798111.

———. 2017. “The Case for Defined Protein Folding Pathways.” *Proceedings of the National Academy of Sciences of the United States of America* 114 (31): 8253–58. https://doi.org/10.1073/pnas.1706196114.

Falcon, Benjamin, Wenjuan Zhang, Alexey G. Murzin, Garib Murshudov, Holly J. Garringer, Ruben Vidal, R. Anthony Crowther, Bernardino Ghetti, Sjors H. W. Scheres, and Michel Goedert. 2018. “Structures of Filaments from Pick’s Disease Reveal a Novel Tau Protein Fold.” *Nature* 561 (7721): 137–40. https://doi.org/10.1038/s41586-018-0454-y.

Falcon, Benjamin, Wenjuan Zhang, Manuel Schweighauser, Alexey G. Murzin, Ruben Vidal, Holly J. Garringer, Bernardino Ghetti, Sjors H. W. Scheres, and Michel Goedert. 2018. “Tau Filaments from Multiple Cases of Sporadic and Inherited Alzheimer’s Disease Adopt a Common Fold.” *Acta Neuropathologica* 136 (5): 699–708. https://doi.org/10.1007/s00401-018-1914-z.

Farzadfard, Azad, Jannik Nedergaard Pedersen, Georg Meisl, Arun Kumar Somavarapu, Parvez Alam, Louise Goksøyr, Morten Agertoug Nielsen, et al. 2022. “The C-Terminal Tail of α-Synuclein Protects against Aggregate Replication but Is Critical for Oligomerization.” *Communications Biology* 5 (1): 123. https://doi.org/10.1038/s42003-022-03059-8.

Flagmeier, Patrick, Suman De, Thomas C. T. Michaels, Xiaoting Yang, Alexander J. Dear, Cecilia Emanuelsson, Michele Vendruscolo, et al. 2020. “Direct Measurement of Lipid Membrane Disruption Connects Kinetics and Toxicity of Aβ42 Aggregation.” *Nature Structural & Molecular Biology* 27 (10): 886–91. https://doi.org/10.1038/s41594-020-0471-z.

Franco, Aitor, Jorge Cuéllar, José Ángel Fernández-Higuero, Igor de la Arada, Natalia Orozco, José M. Valpuesta, Adelina Prado, and Arturo Muga. 2021. “Truncation-Driven Lateral Association of α-Synuclein Hinders Amyloid Clearance by the Hsp70-Based Disaggregase.” *International Journal of Molecular Sciences* 22 (23): 12983. https://doi.org/10.3390/ijms222312983.

Franco, Aitor, Pablo Gracia, Adai Colom, José D. Camino, José Ángel Fernández-Higuero, Natalia Orozco, Alexander Dulebo, et al. 2021. “All-or-None Amyloid Disassembly via Chaperone-Triggered Fibril Unzipping Favors Clearance of α-Synuclein Toxic Species.” *Proceedings of the National Academy of Sciences of the United States of America* 118 (36): e2105548118. https://doi.org/10.1073/pnas.2105548118.

Frieg, Benedikt, Leif Antonschmidt, Christian Dienemann, James A. Geraets, Eszter E. Najbauer, Dirk Matthes, Bert L. de Groot, et al. 2022. “The 3D Structure of Lipidic Fibrils of α-Synuclein.” *Nature Communications* 13 (1): 6810. https://doi.org/10.1038/s41467-022-34552-7.

Friesen, Erik L., Mitch L. De Snoo, Luckshi Rajendran, Lorraine V. Kalia, and Suneil K. Kalia. 2017. “Chaperone-Based Therapies for Disease Modification in Parkinson’s Disease.” *Parkinson’s Disease* 2017: 5015307. https://doi.org/10.1155/2017/5015307.

Froula, Jessica M., Marta Castellana-Cruz, Nadia M. Anabtawi, José D. Camino, Serene W. Chen, Drake R. Thrasher, Jennifer Freire, et al. 2019. “Defining α-Synuclein Species Responsible for Parkinson’s Disease Phenotypes in Mice.” *The Journal of Biological Chemistry* 294 (27): 10392–406. https://doi.org/10.1074/jbc.RA119.007743.

Fusco, Giuliana, Serene W. Chen, Philip T. F. Williamson, Roberta Cascella, Michele Perni, James A. Jarvis, Cristina Cecchi, et al. 2017. “Structural Basis of Membrane Disruption and Cellular Toxicity by α-Synuclein Oligomers.” *Science (New York, N.Y.)* 358 (6369): 1440–43. https://doi.org/10.1126/science.aan6160.

Fusco, Giuliana, Tillmann Pape, Amberley D. Stephens, Pierre Mahou, Ana Rita Costa, Clemens F. Kaminski, Gabriele S. Kaminski Schierle, et al. 2016. “Structural Basis of Synaptic Vesicle Assembly Promoted by α-Synuclein.” *Nature Communications* 7 (September): 12563. https://doi.org/10.1038/ncomms12563.

Fusco, Giuliana, Maximo Sanz-Hernandez, and Alfonso De Simone. 2018. “Order and Disorder in the Physiological Membrane Binding of α-Synuclein.” *Current Opinion in Structural Biology* 48 (February): 49–57. https://doi.org/10.1016/j.sbi.2017.09.004.

Fuxreiter, Monika. 2018. “Fuzziness in Protein Interactions-A Historical Perspective.” *Journal of Molecular Biology* 430 (16): 2278–87. https://doi.org/10.1016/j.jmb.2018.02.015.

Gallardo, Rodrigo, Neil A. Ranson, and Sheena E. Radford. 2020. “Amyloid Structures: Much More than Just a Cross-β Fold.” *Current Opinion in Structural Biology* 60 (February): 7–16. https://doi.org/10.1016/j.sbi.2019.09.001.

Games, Dora, Elvira Valera, Brian Spencer, Edward Rockenstein, Michael Mante, Anthony Adame, Christina Patrick, et al. 2014. “Reducing C-Terminal-Truncated Alpha-Synuclein by Immunotherapy Attenuates Neurodegeneration and Propagation in Parkinson’s Disease-like Models.” *The Journal of Neuroscience: The Official Journal of the Society for Neuroscience* 34 (28): 9441–54. https://doi.org/10.1523/JNEUROSCI.5314-13.2014.

Ganesan, Ashok, Aleksandra Siekierska, Jacinte Beerten, Marijke Brams, Joost Van Durme, Greet De Baets, Rob Van der Kant, et al. 2016. “Structural Hot Spots for the Solubility of Globular Proteins.” *Nature Communications* 7 (February): 10816. https://doi.org/10.1038/ncomms10816.

Gazit, Ehud. 2002. “The ‘Correctly Folded’ State of Proteins: Is It a Metastable State?” *Angewandte Chemie (International Ed. in English)* 41 (2): 257–59. https://doi.org/10.1002/1521-3773(20020118)41:2<257::aid-anie257>3.0.co;2-m.

Giasson, B. I., I. V. Murray, J. Q. Trojanowski, and V. M. Lee. 2001. “A Hydrophobic Stretch of 12 Amino Acid Residues in the Middle of Alpha-Synuclein Is Essential for Filament Assembly.” *The*

Journal of Biological Chemistry 276 (4): 2380–86. https://doi.org/10.1074/jbc.M008919200.

Gil-Garcia, Marcos, Manuel Bañó-Polo, Nathalia Varejão, Michal Jamroz, Aleksander Kuriata, Marta Díaz-Caballero, Jara Lascorz, et al. 2018. "Combining Structural Aggregation Propensity and Stability Predictions To Redesign Protein Solubility." *Molecular Pharmaceutics* 15 (9): 3846–59. https://doi.org/10.1021/acs.molpharmaceut.8b00341.

Glabe, Charles G. 2008. "Structural Classification of Toxic Amyloid Oligomers." *The Journal of Biological Chemistry* 283 (44): 29639–43. https://doi.org/10.1074/jbc.R800016200.

Goedert, Michel, Maria Grazia Spillantini, Kelly Del Tredici, and Heiko Braak. 2013. "100 Years of Lewy Pathology." *Nature Reviews. Neurology* 9 (1): 13–24. https://doi.org/10.1038/nrneurol.2012.242.

Gracia, Pablo, José D. Camino, Laura Volpicelli-Daley, and Nunilo Cremades. 2020. "Multiplicity of α-Synuclein Aggregated Species and Their Possible Roles in Disease." *International Journal of Molecular Sciences* 21 (21): 8043. https://doi.org/10.3390/ijms21218043.

Grant, Barry J., Alemayehu A. Gorfe, and J. Andrew McCammon. 2010. "Large Conformational Changes in Proteins: Signaling and Other Functions." *Current Opinion in Structural Biology* 20 (2): 142–47. https://doi.org/10.1016/j.sbi.2009.12.004.

Grey, Marie, Sara Linse, Hanna Nilsson, Patrik Brundin, and Emma Sparr. 2011. "Membrane Interaction of α-Synuclein in Different Aggregation States." *Journal of Parkinson's Disease* 1 (4): 359–71. https://doi.org/10.3233/JPD-2011-11067.

Guerrero-Ferreira, Ricardo, Lubomir Kovacik, Dongchun Ni, and Henning Stahlberg. 2020. "New Insights on the Structure of Alpha-Synuclein Fibrils Using Cryo-Electron Microscopy." *Current Opinion in Neurobiology* 61 (April): 89–95. https://doi.org/10.1016/j.conb.2020.01.014.

Guerrero-Ferreira, Ricardo, Nicholas Mi Taylor, Ana-Andreea Arteni, Pratibha Kumari, Daniel Mona, Philippe Ringler, Markus Britschgi, et al. 2019. "Two New Polymorphic Structures of Human Full-Length Alpha-Synuclein Fibrils Solved by Cryo-Electron Microscopy." *ELife* 8 (December): e48907. https://doi.org/10.7554/eLife.48907.

Hamilton, R. L. 2000. "Lewy Bodies in Alzheimer's Disease: A Neuropathological Review of 145 Cases Using Alpha-Synuclein Immunohistochemistry." *Brain Pathology (Zurich, Switzerland)* 10 (3): 378–84. https://doi.org/10.1111/j.1750-3639.2000.tb00269.x.

Hmila, Issam, Nishant N. Vaikath, Nour K. Majbour, Daniel Erskine, Indulekha P. Sudhakaran, Vijay Gupta, Simona S. Ghanem, et al. 2022. "Novel Engineered Nanobodies Specific for N-Terminal Region of Alpha-Synuclein Recognize Lewy-Body Pathology and Inhibit in-Vitro Seeded Aggregation and Toxicity." *The FEBS Journal* 289 (15): 4657–73. https://doi.org/10.1111/febs.16376.

Houben, Bert, Emiel Michiels, Meine Ramakers, Katerina Konstantoulea, Nikolaos Louros, Joffré Verniers, Rob van der Kant, et al. 2020. "Autonomous Aggregation Suppression by Acidic Residues Explains Why Chaperones Favour Basic Residues." *The EMBO Journal* 39 (11): e102864. https://doi.org/10.15252/embj.2019102864.

Huttlin, Edward L., Raphael J. Bruckner, Joao A. Paulo, Joe R. Cannon, Lily Ting, Kurt Baltier, Greg Colby, et al. 2017. "Architecture of the Human Interactome Defines Protein Communities and Disease Networks." *Nature* 545 (7655): 505–9. https://doi.org/10.1038/nature22366.

Iłowska, Emilia, Jakub Barciszewski, Mariusz Jaskólski, Augustyn Moliński, Maciej Kozak, and Aneta Szymańska. 2022. "Identification of a Steric Zipper Motif in the Amyloidogenic Core of Human Cystatin C and Its Use for the Design of Self-Assembling Peptides." *International Journal of Molecular Sciences* 23 (10): 5800. https://doi.org/10.3390/ijms23105800.

Jahn, Thomas R., Martin J. Parker, Steve W. Homans, and Sheena E. Radford. 2006. “Amyloid Formation under Physiological Conditions Proceeds via a Native-like Folding Intermediate.” *Nature Structural & Molecular Biology* 13 (3): 195–201. https://doi.org/10.1038/nsmb1058.

Jahn, Thomas R., and Sheena E. Radford. 2008. “Folding versus Aggregation: Polypeptide Conformations on Competing Pathways.” *Archives of Biochemistry and Biophysics* 469 (1): 100–117. https://doi.org/10.1016/j.abb.2007.05.015.

Jarrett, J. T., and P. T. Lansbury. 1993. “Seeding ‘One-Dimensional Crystallization’ of Amyloid: A Pathogenic Mechanism in Alzheimer’s Disease and Scrapie?” *Cell* 73 (6): 1055–58. https://doi.org/10.1016/0092-8674(93)90635-4.

Kalia, Lorraine V., and Anthony E. Lang. 2015. “Parkinson’s Disease.” *Lancet (London, England)* 386 (9996): 896–912. https://doi.org/10.1016/S0140-6736(14)61393-3.

Kant, Rob van der, Nikolaos Louros, Joost Schymkowitz, and Frederic Rousseau. 2022. “Thermodynamic Analysis of Amyloid Fibril Structures Reveals a Common Framework for Stability in Amyloid Polymorphs.” *Structure (London, England: 1993)* 30 (8): 1178-1189.e3. https://doi.org/10.1016/j.str.2022.05.002.

Kayed, Rakez, Elizabeth Head, Jennifer L. Thompson, Theresa M. McIntire, Saskia C. Milton, Carl W. Cotman, and Charles G. Glabe. 2003. “Common Structure of Soluble Amyloid Oligomers Implies Common Mechanism of Pathogenesis.” *Science (New York, N.Y.)* 300 (5618): 486–89. https://doi.org/10.1126/science.1079469.

Ke, Pu Chun, Ruhong Zhou, Louise C. Serpell, Roland Riek, Tuomas P. J. Knowles, Hilal A. Lashuel, Ehud Gazit, et al. 2020. “Half a Century of Amyloids: Past, Present and Future.” *Chemical Society Reviews* 49 (15): 5473–5509. https://doi.org/10.1039/c9cs00199a.

Keshavarzian, Ali, Phillip Engen, Salvatore Bonvegna, and Roberto Cilia. 2020. “The Gut Microbiome in Parkinson’s Disease: A Culprit or a Bystander?” *Progress in Brain Research* 252: 357–450. https://doi.org/10.1016/bs.pbr.2020.01.004.

Kiely, Aoife P., Yasmine T. Asi, Eleanna Kara, Patricia Limousin, Helen Ling, Patrick Lewis, Christos Proukakis, et al. 2013. “α-Synucleinopathy Associated with G51D SNCA Mutation: A Link between Parkinson’s Disease and Multiple System Atrophy?” *Acta Neuropathologica* 125 (5): 753–69. https://doi.org/10.1007/s00401-013-1096-7.

Kjaergaard, Magnus, Alexander J. Dear, Franziska Kundel, Seema Qamar, Georg Meisl, Tuomas P. J. Knowles, and David Klenerman. 2018. “Oligomer Diversity during the Aggregation of the Repeat Region of Tau.” *ACS Chemical Neuroscience* 9 (12): 3060–71. https://doi.org/10.1021/acschemneuro.8b00250.

Knowles, Tuomas P., Anthony W. Fitzpatrick, Sarah Meehan, Helen R. Mott, Michele Vendruscolo, Christopher M. Dobson, and Mark E. Welland. 2007. “Role of Intermolecular Forces in Defining Material Properties of Protein Nanofibrils.” *Science (New York, N.Y.)* 318 (5858): 1900–1903. https://doi.org/10.1126/science.1150057.

Kolarova, Michala, Urmi Sengupta, Ales Bartos, Jan Ricny, and Rakez Kayed. 2017. “Tau Oligomers in Sera of Patients with Alzheimer’s Disease and Aged Controls.” *Journal of Alzheimer’s Disease: JAD* 58 (2): 471–78. https://doi.org/10.3233/JAD-170048.

Konno, Takuya, Owen A. Ross, Andreas Puschmann, Dennis W. Dickson, and Zbigniew K. Wszolek. 2016. “Autosomal Dominant Parkinson’s Disease Caused by SNCA Duplications.” *Parkinsonism & Related Disorders* 22 Suppl 1 (Suppl 1): S1-6. https://doi.org/10.1016/j.parkreldis.2015.09.007.

Kramer, Günter, Ayala Shiber, and Bernd Bukau. 2019. “Mechanisms of Cotranslational Maturation of Newly Synthesized Proteins." *Annual Review of Biochemistry* 88 (June): 337–64. https://doi.org/10.1146/annurev-biochem-013118-111717.

Krüger, R., W. Kuhn, T. Müller, D. Woitalla, M. Graeber, S. Kösel, H. Przuntek, J. T. Epplen, L. Schöls, and O. Riess. 1998. "Ala30Pro Mutation in the Gene Encoding Alpha-Synuclein in Parkinson's Disease." *Nature Genetics* 18 (2): 106–8. https://doi.org/10.1038/ng0298-106.

Kumar, Senthil T., Somanath Jagannath, Cindy Francois, Hugo Vanderstichele, Erik Stoops, and Hilal A. Lashuel. 2020. "How Specific Are the Conformation-Specific α-Synuclein Antibodies? Characterization and Validation of 16 α-Synuclein Conformation-Specific Antibodies Using Well-Characterized Preparations of α-Synuclein Monomers, Fibrils and Oligomers with Distinct Structures and Morphology." *Neurobiology of Disease* 146 (December): 105086. https://doi.org/10.1016/j.nbd.2020.105086.

Kumar, Senthil T., Anne-Laure Mahul-Mellier, Ramanath Narayana Hegde, Gwladys Rivière, Rani Moons, Alain Ibáñez de Opakua, Pedro Magalhães, et al. 2022. "A NAC Domain Mutation (E83Q) Unlocks the Pathogenicity of Human Alpha-Synuclein and Recapitulates Its Pathological Diversity." *Science Advances* 8 (17): eabn0044. https://doi.org/10.1126/sciadv.abn0044.

Kumari, Pratibha, Dhiman Ghosh, Agathe Vanas, Yanick Fleischmann, Thomas Wiegand, Gunnar Jeschke, Roland Riek, and Cédric Eichmann. 2021. "Structural Insights into α-Synuclein Monomer-Fibril Interactions." *Proceedings of the National Academy of Sciences of the United States of America* 118 (10): e2012171118. https://doi.org/10.1073/pnas.2012171118.

Kurochka, Andrii S., Dmytro A. Yushchenko, Petr Bouř, and Volodymyr V. Shvadchak. 2021. "Influence of Lipid Membranes on α-Synuclein Aggregation." *ACS Chemical Neuroscience* 12 (5): 825–30. https://doi.org/10.1021/acschemneuro.0c00819.

Laganowsky, Arthur, Cong Liu, Michael R. Sawaya, Julian P. Whitelegge, Jiyong Park, Minglei Zhao, Anna Pensalfini, et al. 2012. "Atomic View of a Toxic Amyloid Small Oligomer." *Science (New York, N.Y.)* 335 (6073): 1228–31. https://doi.org/10.1126/science.1213151.

Lang, Anthony E., Andrew D. Siderowf, Eric A. Macklin, Werner Poewe, David J. Brooks, Hubert H. Fernandez, Olivier Rascol, et al. 2022. "Trial of Cinpanemab in Early Parkinson's Disease." *The New England Journal of Medicine* 387 (5): 408–20. https://doi.org/10.1056/NEJMoa2203395.

Langenberg, Tobias, Rodrigo Gallardo, Rob van der Kant, Nikolaos Louros, Emiel Michiels, Ramon Duran-Romaña, Bert Houben, et al. 2020. "Thermodynamic and Evolutionary Coupling between the Native and Amyloid State of Globular Proteins." *Cell Reports* 31 (2): 107512. https://doi.org/10.1016/j.celrep.2020.03.076.

Lasagna-Reeves, Cristian A., Diana L. Castillo-Carranza, Urmi Sengupta, Audra L. Clos, George R. Jackson, and Rakez Kayed. 2011. "Tau Oligomers Impair Memory and Induce Synaptic and Mitochondrial Dysfunction in Wild-Type Mice." *Molecular Neurodegeneration* 6 (June): 39. https://doi.org/10.1186/1750-1326-6-39.

Lashuel, Hilal A., Dean Hartley, Benjamin M. Petre, Thomas Walz, and Peter T. Lansbury. 2002. "Neurodegenerative Disease: Amyloid Pores from Pathogenic Mutations." *Nature* 418 (6895): 291. https://doi.org/10.1038/418291a.

Lashuel, Hilal A., Benjamin M. Petre, Joseph Wall, Martha Simon, Richard J. Nowak, Thomas Walz, and Peter T. Lansbury. 2002. "Alpha-Synuclein, Especially the Parkinson's Disease-Associated Mutants, Forms Pore-like Annular and Tubular Protofibrils." *Journal of Molecular Biology* 322 (5): 1089–1102. https://doi.org/10.1016/s0022-2836(02)00735-0.

Lee, Ji-Eun, Jason C. Sang, Margarida Rodrigues, Alexander R. Carr, Mathew H. Horrocks, Suman De, Marie N. Bongiovanni, et al. 2018. "Mapping Surface Hydrophobicity of α-Synuclein Oligomers at the Nanoscale.” *Nano Letters* 18 (12): 7494–7501. https://doi.org/10.1021/acs.nanolett.8b02916.

Lee, Robin van der, Marija Buljan, Benjamin Lang, Robert J. Weatheritt, Gary W. Daughdrill, A. Keith Dunker, Monika Fuxreiter, et al. 2014. “Classification of Intrinsically Disordered Regions and Proteins.” *Chemical Reviews* 114 (13): 6589–6631. https://doi.org/10.1021/cr400525m.

Levinthal, Cyrus. 1968. “Are There Pathways for Protein Folding?” *Journal de Chimie Physique* 65: 44–45. https://doi.org/10.1051/jcp/1968650044.

———. 1969. “How to Fold Graciously.” *Mossbauer Spectroscopy in Biological Systems* 67: 22–24.

Li, Binsen, Peng Ge, Kevin A. Murray, Phorum Sheth, Meng Zhang, Gayatri Nair, Michael R. Sawaya, et al. 2018. “Cryo-EM of Full-Length α-Synuclein Reveals Fibril Polymorphs with a Common Structural Kernel.” *Nature Communications* 9 (1): 3609. https://doi.org/10.1038/s41467-018-05971-2.

Li, J., V. N. Uversky, and A. L. Fink. 2001. “Effect of Familial Parkinson’s Disease Point Mutations A30P and A53T on the Structural Properties, Aggregation, and Fibrillation of Human Alpha-Synuclein.” *Biochemistry* 40 (38): 11604–13. https://doi.org/10.1021/bi010616g.

Li, Yaowang, Chunyu Zhao, Feng Luo, Zhenying Liu, Xinrui Gui, Zhipu Luo, Xiang Zhang, Dan Li, Cong Liu, and Xueming Li. 2018. “Amyloid Fibril Structure of α-Synuclein Determined by Cryo-Electron Microscopy.” *Cell Research* 28 (9): 897–903. https://doi.org/10.1038/s41422-018-0075-x.

Linding, Rune, Joost Schymkowitz, Frederic Rousseau, Francesca Diella, and Luis Serrano. 2004. “A Comparative Study of the Relationship between Protein Structure and Beta-Aggregation in Globular and Intrinsically Disordered Proteins.” *Journal of Molecular Biology* 342 (1): 345–53. https://doi.org/10.1016/j.jmb.2004.06.088.

Linse, Sara, Tom Scheidt, Katja Bernfur, Michele Vendruscolo, Christopher M. Dobson, Samuel I. A. Cohen, Eimantas Sileikis, et al. 2020. “Kinetic Fingerprints Differentiate the Mechanisms of Action of Anti-Aβ Antibodies.” *Nature Structural & Molecular Biology* 27 (12): 1125–33. https://doi.org/10.1038/s41594-020-0505-6.

Liu, Hui, Christos Koros, Timo Strohäker, Claudia Schulte, Maria Bozi, Stefanos Varvaresos, Alain Ibáñez de Opakua, et al. 2021. “A Novel SNCA A30G Mutation Causes Familial Parkinson’s Disease.” *Movement Disorders: Official Journal of the Movement Disorder Society* 36 (7): 1624–33. https://doi.org/10.1002/mds.28534.

Lorenzen, Nikolai, Søren Bang Nielsen, Alexander K. Buell, Jørn Døvling Kaspersen, Paolo Arosio, Brian Stougaard Vad, Wojciech Paslawski, et al. 2014. “The Role of Stable α-Synuclein Oligomers in the Molecular Events Underlying Amyloid Formation.” *Journal of the American Chemical Society* 136 (10): 3859–68. https://doi.org/10.1021/ja411577t.

Lu, Jinxia, Shengnan Zhang, Xiaojuan Ma, Chunyu Jia, Zhenying Liu, Chengan Huang, Cong Liu, and Dan Li. 2020. “Structural Basis of the Interplay between α-Synuclein and Tau in Regulating Pathological Amyloid Aggregation.” *The Journal of Biological Chemistry* 295 (21): 7470–80. https://doi.org/10.1074/jbc.RA119.012284.

Luheshi, Leila M., Damian C. Crowther, and Christopher M. Dobson. 2008. “Protein Misfolding and Disease: From the Test Tube to the Organism.” *Current Opinion in Chemical Biology* 12 (1): 25–31. https://doi.org/10.1016/j.cbpa.2008.02.011.

Luk, Kelvin C., Victoria Kehm, Jenna Carroll, Bin Zhang, Patrick O’Brien, John Q. Trojanowski, and Virginia M.-Y. Lee. 2012. “Pathological α-Synuclein Transmission Initiates Parkinson-like Neurodegeneration in Nontransgenic Mice.” *Science (New York, N.Y.)* 338 (6109): 949–53. https://doi.org/10.1126/science.1227157.

Maraganore, Demetrius M., Mariza de Andrade, Alexis Elbaz, Matthew J. Farrer, John P. Ioannidis, Rejko Krüger, Walter A. Rocca, et al. 2006. "Collaborative Analysis of Alpha-Synuclein Gene Promoter Variability and Parkinson Disease." *JAMA* 296 (6): 661–70. https://doi.org/10.1001/jama.296.6.661.

Maroteaux, L., J. T. Campanelli, and R. H. Scheller. 1988. "Synuclein: A Neuron-Specific Protein Localized to the Nucleus and Presynaptic Nerve Terminal." *The Journal of Neuroscience: The Official Journal of the Society for Neuroscience* 8 (8): 2804–15. https://doi.org/10.1523/JNEUROSCI.08-08-02804.1988.

Masuda-Suzukake, Masami, Takashi Nonaka, Masato Hosokawa, Takayuki Oikawa, Tetsuaki Arai, Haruhiko Akiyama, David M. A. Mann, and Masato Hasegawa. 2013. "Prion-like Spreading of Pathological α-Synuclein in Brain." *Brain: A Journal of Neurology* 136 (Pt 4): 1128–38. https://doi.org/10.1093/brain/awt037.

McCann, Heather, Claire H. Stevens, Heidi Cartwright, and Glenda M. Halliday. 2014. "α-Synucleinopathy Phenotypes." *Parkinsonism & Related Disorders* 20 Suppl 1 (January): S62-67. https://doi.org/10.1016/S1353-8020(13)70017-8.

McClendon, Sebastian, Carla C. Rospigliosi, and David Eliezer. 2009. "Charge Neutralization and Collapse of the C-Terminal Tail of Alpha-Synuclein at Low PH." *Protein Science: A Publication of the Protein Society* 18 (7): 1531–40. https://doi.org/10.1002/pro.149.

McGlinchey, Ryan P., Xiaodan Ni, Jared A. Shadish, Jiansen Jiang, and Jennifer C. Lee. 2021. "The N Terminus of α-Synuclein Dictates Fibril Formation." *Proceedings of the National Academy of Sciences of the United States of America* 118 (35): e2023487118. https://doi.org/10.1073/pnas.2023487118.

Meisl, Georg, Julius B. Kirkegaard, Paolo Arosio, Thomas C. T. Michaels, Michele Vendruscolo, Christopher M. Dobson, Sara Linse, and Tuomas P. J. Knowles. 2016. "Molecular Mechanisms of Protein Aggregation from Global Fitting of Kinetic Models." *Nature Protocols* 11 (2): 252–72. https://doi.org/10.1038/nprot.2016.010.

Meisl, Georg, Tuomas P. J. Knowles, and David Klenerman. 2022. "Mechanistic Models of Protein Aggregation Across Length-Scales and Time-Scales: From the Test Tube to Neurodegenerative Disease." *Frontiers in Neuroscience* 16: 909861. https://doi.org/10.3389/fnins.2022.909861.

Meisl, Georg, Catherine K. Xu, Jonathan D. Taylor, Thomas C. T. Michaels, Aviad Levin, Daniel Otzen, David Klenerman, et al. 2022. "Uncovering the Universality of Self-Replication in Protein Aggregation and Its Link to Disease." *Science Advances* 8 (32): eabn6831. https://doi.org/10.1126/sciadv.abn6831.

Meisl, Georg, Xiaoting Yang, Erik Hellstrand, Birgitta Frohm, Julius B. Kirkegaard, Samuel I. A. Cohen, Christopher M. Dobson, Sara Linse, and Tuomas P. J. Knowles. 2014. "Differences in Nucleation Behavior Underlie the Contrasting Aggregation Kinetics of the Aβ40 and Aβ42 Peptides." *Proceedings of the National Academy of Sciences of the United States of America* 111 (26): 9384–89. https://doi.org/10.1073/pnas.1401564111.

Mendoza-Espinosa, Paola, Victor García-González, Abel Moreno, Rolando Castillo, and Jaime Mas-Oliva. 2009. "Disorder-to-Order Conformational Transitions in Protein Structure and Its Relationship to Disease." *Molecular and Cellular Biochemistry* 330 (1–2): 105–20. https://doi.org/10.1007/s11010-009-0105-6.

Mesgarzadeh, Jaleh S., Isabelle C. Romine, Ethan M. Smith-Cohen, Julia M. D. Grandjean, Jeffery W. Kelly, Joseph C. Genereux, and R. Luke Wiseman. 2022. "ATF6 Activation Reduces Amyloidogenic Transthyretin Secretion through Increased Interactions with Endoplasmic Reticulum Proteostasis Factors." *Cells* 11 (10): 1661. https://doi.org/10.3390/cells11101661.

Michaels, Thomas C. T., Andela Šarić, Samo Curk, Katja Bernfur, Paolo Arosio, Georg Meisl, Alexander J. Dear, et al. 2020. “Dynamics of Oligomer Populations Formed during the Aggregation of Alzheimer’s Aβ42 Peptide.” *Nature Chemistry* 12 (5): 445–51. https://doi.org/10.1038/s41557-020-0452-1.

Michaels, Thomas C. T., Anđela Šarić, Johnny Habchi, Sean Chia, Georg Meisl, Michele Vendruscolo, Christopher M. Dobson, and Tuomas P. J. Knowles. 2018. “Chemical Kinetics for Bridging Molecular Mechanisms and Macroscopic Measurements of Amyloid Fibril Formation.” *Annual Review of Physical Chemistry* 69 (April): 273–98. https://doi.org/10.1146/annurev-physchem-050317-021322.

Mirecka, Ewa A., Hamed Shaykhalishahi, Aziz Gauhar, Şerife Akgül, Justin Lecher, Dieter Willbold, Matthias Stoldt, and Wolfgang Hoyer. 2014. “Sequestration of a β-Hairpin for Control of α-Synuclein Aggregation.” *Angewandte Chemie (International Ed. in English)* 53 (16): 4227–30. https://doi.org/10.1002/anie.201309001.

Mischley, Laurie K., Richard C. Lau, and Rachel D. Bennett. 2017. “Role of Diet and Nutritional Supplements in Parkinson’s Disease Progression.” *Oxidative Medicine and Cellular Longevity* 2017: 6405278. https://doi.org/10.1155/2017/6405278.

Monsellier, Elodie, and Fabrizio Chiti. 2007. “Prevention of Amyloid-like Aggregation as a Driving Force of Protein Evolution.” *EMBO Reports* 8 (8): 737–42. https://doi.org/10.1038/sj.embor.7401034.

Morel, Bertrand, Lorena Varela, Ana I. Azuaga, and Francisco Conejero-Lara. 2010. “Environmental Conditions Affect the Kinetics of Nucleation of Amyloid Fibrils and Determine Their Morphology.” *Biophysical Journal* 99 (11): 3801–10. https://doi.org/10.1016/j.bpj.2010.10.039.

Morten, Michael J., Liina Sirvio, Huzefa Rupawala, Emma Mee Hayes, Aitor Franco, Carola Radulescu, Liming Ying, Samuel J. Barnes, Arturo Muga, and Ye Yu. 2022. “Quantitative Super-Resolution Imaging of Pathological Aggregates Reveals Distinct Toxicity Profiles in Different Synucleinopathies.” *Proceedings of the National Academy of Sciences of the United States of America* 119 (41): e2205591119. https://doi.org/10.1073/pnas.2205591119.

Mougenot, Anne-Laure, Simon Nicot, Anna Bencsik, Eric Morignat, Jérémy Verchère, Latefa Lakhdar, Stéphane Legastelois, and Thierry Baron. 2012. “Prion-like Acceleration of a Synucleinopathy in a Transgenic Mouse Model.” *Neurobiology of Aging* 33 (9): 2225–28. https://doi.org/10.1016/j.neurobiolaging.2011.06.022.

Münch, Christian, and Anne Bertolotti. 2010. “Exposure of Hydrophobic Surfaces Initiates Aggregation of Diverse ALS-Causing Superoxide Dismutase-1 Mutants.” *Journal of Molecular Biology* 399 (3): 512–25. https://doi.org/10.1016/j.jmb.2010.04.019.

Musteikytė, Greta, Akhila K. Jayaram, Catherine K. Xu, Michele Vendruscolo, Georg Krainer, and Tuomas P. J. Knowles. 2021. “Interactions of α-Synuclein Oligomers with Lipid Membranes.” *Biochimica Et Biophysica Acta. Biomembranes* 1863 (4): 183536. https://doi.org/10.1016/j.bbamem.2020.183536.

Nassar, Roy, Gregory L. Dignon, Rostam M. Razban, and Ken A. Dill. 2021. “The Protein Folding Problem: The Role of Theory.” *Journal of Molecular Biology* 433 (20): 167126. https://doi.org/10.1016/j.jmb.2021.167126.

Nerelius, C., A. Sandegren, H. Sargsyan, R. Raunak, H. Leijonmarck, U. Chatterjee, A. Fisahn, et al. 2009. “Alpha-Helix Targeting Reduces Amyloid-Beta Peptide Toxicity.” *Proceedings of the National Academy of Sciences of the United States of America* 106 (23): 9191–96. https://doi.org/10.1073/pnas.0810364106.

Neudecker, Philipp, Paul Robustelli, Andrea Cavalli, Patrick Walsh, Patrik Lundström, Arash Zarrine-Afsar, Simon Sharpe, Michele Vendruscolo, and Lewis E. Kay. 2012. "Structure of an Intermediate State in Protein Folding and Aggregation." *Science (New York, N.Y.)* 336 (6079): 362–66. https://doi.org/10.1126/science.1214203.

Nguyen, Phuong H., Ayyalusamy Ramamoorthy, Bikash R. Sahoo, Jie Zheng, Peter Faller, John E. Straub, Laura Dominguez, et al. 2021. "Amyloid Oligomers: A Joint Experimental/Computational Perspective on Alzheimer's Disease, Parkinson's Disease, Type II Diabetes, and Amyotrophic Lateral Sclerosis." *Chemical Reviews* 121 (4): 2545–2647. https://doi.org/10.1021/acs.chemrev.0c01122.

Nielsen, L., R. Khurana, A. Coats, S. Frokjaer, J. Brange, S. Vyas, V. N. Uversky, and A. L. Fink. 2001. "Effect of Environmental Factors on the Kinetics of Insulin Fibril Formation: Elucidation of the Molecular Mechanism." *Biochemistry* 40 (20): 6036–46. https://doi.org/10.1021/bi002555c.

Ono, Kenjiro, Tokuhei Ikeda, Jun-ichi Takasaki, and Masahito Yamada. 2011. "Familial Parkinson Disease Mutations Influence α-Synuclein Assembly." *Neurobiology of Disease* 43 (3): 715–24. https://doi.org/10.1016/j.nbd.2011.05.025.

Osterberg, Valerie R., Kateri J. Spinelli, Leah J. Weston, Kelvin C. Luk, Randall L. Woltjer, and Vivek K. Unni. 2015. "Progressive Aggregation of Alpha-Synuclein and Selective Degeneration of Lewy Inclusion-Bearing Neurons in a Mouse Model of Parkinsonism." *Cell Reports* 10 (8): 1252–60. https://doi.org/10.1016/j.celrep.2015.01.060.

Pagano, Gennaro, Kirsten I. Taylor, Judith Anzures-Cabrera, Maddalena Marchesi, Tanya Simuni, Kenneth Marek, Ronald B. Postuma, et al. 2022. "Trial of Prasinezumab in Early-Stage Parkinson's Disease." *The New England Journal of Medicine* 387 (5): 421–32. https://doi.org/10.1056/NEJMoa2202867.

Pallarès, Irantzu, Josep Vendrell, Francesc X. Avilés, and Salvador Ventura. 2004. "Amyloid Fibril Formation by a Partially Structured Intermediate State of Alpha-Chymotrypsin." *Journal of Molecular Biology* 342 (1): 321–31. https://doi.org/10.1016/j.jmb.2004.06.089.

Paravastu, Anant K., Richard D. Leapman, Wai-Ming Yau, and Robert Tycko. 2008. "Molecular Structural Basis for Polymorphism in Alzheimer's Beta-Amyloid Fibrils." *Proceedings of the National Academy of Sciences of the United States of America* 105 (47): 18349–54. https://doi.org/10.1073/pnas.0806270105.

Parrini, Claudia, Niccolò Taddei, Matteo Ramazzotti, Donatella Degl'Innocenti, Giampietro Ramponi, Christopher M. Dobson, and Fabrizio Chiti. 2005. "Glycine Residues Appear to Be Evolutionarily Conserved for Their Ability to Inhibit Aggregation." *Structure (London, England: 1993)* 13 (8): 1143–51. https://doi.org/10.1016/j.str.2005.04.022.

Pasanen, Petra, Liisa Myllykangas, Maija Siitonen, Anna Raunio, Seppo Kaakkola, Jukka Lyytinen, Pentti J. Tienari, Minna Pöyhönen, and Anders Paetau. 2014. "Novel α-Synuclein Mutation A53E Associated with Atypical Multiple System Atrophy and Parkinson's Disease-Type Pathology." *Neurobiology of Aging* 35 (9): 2180.e1-5. https://doi.org/10.1016/j.neurobiolaging.2014.03.024.

Pastore, Annalisa, and Piero Andrea Temussi. 2022. "Crowding Revisited: Open Questions and Future Perspectives." *Trends in Biochemical Sciences* 47 (12): 1048–58. https://doi.org/10.1016/j.tibs.2022.05.007.

Peelaerts, W., L. Bousset, A. Van der Perren, A. Moskalyuk, R. Pulizzi, M. Giugliano, C. Van den Haute, R. Melki, and V. Baekelandt. 2015. "α-Synuclein Strains Cause Distinct Synucleinopathies after Local and Systemic Administration." *Nature* 522 (7556): 340–44. https://doi.org/10.1038/nature14547.

Perni, Michele, Patrick Flagmeier, Ryan Limbocker, Roberta Cascella, Francesco A. Aprile, Céline Galvagnion, Gabriella T. Heller, et al. 2018. “Multistep Inhibition of α-Synuclein Aggregation and Toxicity in Vitro and in Vivo by Trodusquemine.” *ACS Chemical Biology* 13 (8): 2308–19. https://doi.org/10.1021/acschembio.8b00466.

Pieri, Laura, Karine Madiona, Luc Bousset, and Ronald Melki. 2012. “Fibrillar α-Synuclein and Huntingtin Exon 1 Assemblies Are Toxic to the Cells.” *Biophysical Journal* 102 (12): 2894–2905. https://doi.org/10.1016/j.bpj.2012.04.050.

Polymeropoulos, M. H., C. Lavedan, E. Leroy, S. E. Ide, A. Dehejia, A. Dutra, B. Pike, et al. 1997. “Mutation in the Alpha-Synuclein Gene Identified in Families with Parkinson’s Disease.” *Science (New York, N.Y.)* 276 (5321): 2045–47. https://doi.org/10.1126/science.276.5321.2045.

Pountney, Dean L., Rachel Lowe, Marian Quilty, James C. Vickers, Nicolas H. Voelcker, and Wei Ping Gai. 2004. “Annular Alpha-Synuclein Species from Purified Multiple System Atrophy Inclusions.” *Journal of Neurochemistry* 90 (2): 502–12. https://doi.org/10.1111/j.1471-4159.2004.02533.x.

Quist, Arjan, Ivo Doudevski, Hai Lin, Rushana Azimova, Douglas Ng, Blas Frangione, Bruce Kagan, Jorge Ghiso, and Ratnesh Lal. 2005. “Amyloid Ion Channels: A Common Structural Link for Protein-Misfolding Disease.” *Proceedings of the National Academy of Sciences of the United States of America* 102 (30): 10427–32. https://doi.org/10.1073/pnas.0502066102.

Radivojac, Predrag, Lilia M. Iakoucheva, Christopher J. Oldfield, Zoran Obradovic, Vladimir N. Uversky, and A. Keith Dunker. 2007. “Intrinsic Disorder and Functional Proteomics.” *Biophysical Journal* 92 (5): 1439–56. https://doi.org/10.1529/biophysj.106.094045.

Reinle, Kevin, Axel Mogk, and Bernd Bukau. 2022. “The Diverse Functions of Small Heat Shock Proteins in the Proteostasis Network.” *Journal of Molecular Biology* 434 (1): 167157. https://doi.org/10.1016/j.jmb.2021.167157.

Reumers, Joke, Sebastian Maurer-Stroh, Joost Schymkowitz, and Fréderic Rousseau. 2009. “Protein Sequences Encode Safeguards against Aggregation.” *Human Mutation* 30 (3): 431–37. https://doi.org/10.1002/humu.20905.

Riek, Roland, and David S. Eisenberg. 2016. “The Activities of Amyloids from a Structural Perspective.” *Nature* 539 (7628): 227–35. https://doi.org/10.1038/nature20416.

Robustelli, Paul, Stefano Piana, and David E. Shaw. 2020. “Mechanism of Coupled Folding-upon-Binding of an Intrinsically Disordered Protein.” *Journal of the American Chemical Society* 142 (25): 11092–101. https://doi.org/10.1021/jacs.0c03217.

Roterman, Irena, Mateusz Banach, and Leszek Konieczny. 2017. “Propagation of Fibrillar Structural Forms in Proteins Stopped by Naturally Occurring Short Polypeptide Chain Fragments.” *Pharmaceuticals (Basel, Switzerland)* 10 (4): 89. https://doi.org/10.3390/ph10040089.

Rousseau, Frederic, Luis Serrano, and Joost W. H. Schymkowitz. 2006. “How Evolutionary Pressure against Protein Aggregation Shaped Chaperone Specificity.” *Journal of Molecular Biology* 355 (5): 1037–47. https://doi.org/10.1016/j.jmb.2005.11.035.

Rutherford, Nicola J., Brenda D. Moore, Todd E. Golde, and Benoit I. Giasson. 2014. “Divergent Effects of the H50Q and G51D SNCA Mutations on the Aggregation of α-Synuclein.” *Journal of Neurochemistry* 131 (6): 859–67. https://doi.org/10.1111/jnc.12806.

Sampson, Timothy R., Justine W. Debelius, Taren Thron, Stefan Janssen, Gauri G. Shastri, Zehra Esra Ilhan, Collin Challis, et al. 2016. “Gut Microbiota Regulate Motor Deficits and Neuroinflammation in a Model of Parkinson’s Disease.” *Cell* 167 (6): 1469-1480.e12. https://doi.org/10.1016/j.cell.2016.11.018.

Sanderson, John B., Suman De, Haiyang Jiang, Matteo Rovere, Ming Jin, Ludovica Zaccagnini, Aurelia Hays Watson, et al. 2020. “Analysis of α-Synuclein Species Enriched from Cerebral Cortex of Humans with Sporadic Dementia with Lewy Bodies.” *Brain Communications* 2 (1): fcaa010. https://doi.org/10.1093/braincomms/fcaa010.

Santos, Jaime, Valentín Iglesias, Carlos Pintado, Juan Santos-Suárez, and Salvador Ventura. 2020. “DispHred: A Server to Predict PH-Dependent Order-Disorder Transitions in Intrinsically Disordered Proteins.” *International Journal of Molecular Sciences* 21 (16): 5814. https://doi.org/10.3390/ijms21165814.

Santos, Jaime, Valentín Iglesias, and Salvador Ventura. 2020. “Computational Prediction and Redesign of Aberrant Protein Oligomerization.” *Progress in Molecular Biology and Translational Science* 169: 43–83. https://doi.org/10.1016/bs.pmbts.2019.11.002.

Santos, Jaime, Irantzu Pallarès, Valentín Iglesias, and Salvador Ventura. 2021. “Cryptic Amyloidogenic Regions in Intrinsically Disordered Proteins: Function and Disease Association.” *Computational and Structural Biotechnology Journal* 19: 4192–4206. https://doi.org/10.1016/j.csbj.2021.07.019.

Santos, Jaime, Jordi Pujols, Irantzu Pallarès, Valentín Iglesias, and Salvador Ventura. 2020. “Computational Prediction of Protein Aggregation: Advances in Proteomics, Conformation-Specific Algorithms and Biotechnological Applications.” *Computational and Structural Biotechnology Journal* 18: 1403–13. https://doi.org/10.1016/j.csbj.2020.05.026.

Schafer, N. P., B. L. Kim, W. Zheng, and P. G. Wolynes. 2014. “Learning To Fold Proteins Using Energy Landscape Theory.” *Israel Journal of Chemistry* 54 (8–9): 1311–37. https://doi.org/10.1002/ijch.201300145.

Schwartz, Russell, and Jonathan King. 2006. “Frequencies of Hydrophobic and Hydrophilic Runs and Alternations in Proteins of Known Structure.” *Protein Science: A Publication of the Protein Society* 15 (1): 102–12. https://doi.org/10.1110/ps.051741806.

Schweighauser, Manuel, Yang Shi, Airi Tarutani, Fuyuki Kametani, Alexey G. Murzin, Bernardino Ghetti, Tomoyasu Matsubara, et al. 2020. “Structures of α-Synuclein Filaments from Multiple System Atrophy.” *Nature* 585 (7825): 464–69. https://doi.org/10.1038/s41586-020-2317-6.

Sherman, M. Y., and A. L. Goldberg. 2001. “Cellular Defenses against Unfolded Proteins: A Cell Biologist Thinks about Neurodegenerative Diseases.” *Neuron* 29 (1): 15–32. https://doi.org/10.1016/s0896-6273(01)00177-5.

Shi, Yang, Wenjuan Zhang, Yang Yang, Alexey G. Murzin, Benjamin Falcon, Abhay Kotecha, Mike van Beers, et al. 2021. “Structure-Based Classification of Tauopathies.” *Nature* 598 (7880): 359–63. https://doi.org/10.1038/s41586-021-03911-7.

Solch, Rebecca J., Julia O. Aigbogun, Andrew G. Voyiadjis, Grant M. Talkington, Revonda M. Darensbourg, Samantha O’Connell, Keith M. Pickett, Sarah R. Perez, and Demetrius M. Maraganore. 2022. “Mediterranean Diet Adherence, Gut Microbiota, and Alzheimer’s or Parkinson’s Disease Risk: A Systematic Review.” *Journal of the Neurological Sciences* 434 (March): 120166. https://doi.org/10.1016/j.jns.2022.120166.

Sorrentino, Vincenzo, Mario Romani, Laurent Mouchiroud, John S. Beck, Hongbo Zhang, Davide D’Amico, Norman Moullan, et al. 2017. “Enhancing Mitochondrial Proteostasis Reduces Amyloid-β Proteotoxicity.” *Nature* 552 (7684): 187–93. https://doi.org/10.1038/nature25143.

Sorrentino, Zachary A., and Benoit I. Giasson. 2020. “The Emerging Role of α-Synuclein Truncation in Aggregation and Disease.” *The Journal of Biological Chemistry* 295 (30): 10224–44. https://doi.org/10.1074/jbc.REV120.011743.

Sorrentino, Zachary A., Niran Vijayaraghavan, Kimberly-Marie Gorion, Cara J. Riffe, Kevin H. Strang, Jason Caldwell, and Benoit I. Giasson. 2018. “Physiological C-Terminal Truncation of α-Synuclein Potentiates the Prion-like Formation of Pathological Inclusions.” *The Journal of Biological Chemistry* 293 (49): 18914–32. https://doi.org/10.1074/jbc.RA118.005603.

Spillantini, M. G., R. A. Crowther, R. Jakes, M. Hasegawa, and M. Goedert. 1998. “Alpha-Synuclein in Filamentous Inclusions of Lewy Bodies from Parkinson’s Disease and Dementia with Lewy Bodies.” *Proceedings of the National Academy of Sciences of the United States of America* 95 (11): 6469–73. https://doi.org/10.1073/pnas.95.11.6469.

Spillantini, M. G., and M. Goedert. 2000. “The Alpha-Synucleinopathies: Parkinson’s Disease, Dementia with Lewy Bodies, and Multiple System Atrophy.” *Annals of the New York Academy of Sciences* 920: 16–27. https://doi.org/10.1111/j.1749-6632.2000.tb06900.x.

Spillantini, M. G., M. L. Schmidt, V. M. Lee, J. Q. Trojanowski, R. Jakes, and M. Goedert. 1997. “Alpha-Synuclein in Lewy Bodies.” *Nature* 388 (6645): 839–40. https://doi.org/10.1038/42166.

Stefanovic, Anja N. D., Saskia Lindhoud, Slav A. Semerdzhiev, Mireille M. A. E. Claessens, and Vinod Subramaniam. 2015. “Oligomers of Parkinson’s Disease-Related α-Synuclein Mutants Have Similar Structures but Distinctive Membrane Permeabilization Properties.” *Biochemistry* 54 (20): 3142–50. https://doi.org/10.1021/bi501369k.

Strodel, Birgit. 2021. “Energy Landscapes of Protein Aggregation and Conformation Switching in Intrinsically Disordered Proteins.” *Journal of Molecular Biology* 433 (20): 167182. https://doi.org/10.1016/j.jmb.2021.167182.

Sun, Yunpeng, Shouqiao Hou, Kun Zhao, Houfang Long, Zhenying Liu, Jing Gao, Yaoyang Zhang, Xiao-Dong Su, Dan Li, and Cong Liu. 2020. “Cryo-EM Structure of Full-Length α-Synuclein Amyloid Fibril with Parkinson’s Disease Familial A53T Mutation.” *Cell Research* 30 (4): 360–62. https://doi.org/10.1038/s41422-020-0299-4.

Sun, Yunpeng, Houfang Long, Wencheng Xia, Kun Wang, Xia Zhang, Bo Sun, Qin Cao, et al. 2021. “The Hereditary Mutation G51D Unlocks a Distinct Fibril Strain Transmissible to Wild-Type α-Synuclein.” *Nature Communications* 12 (1): 6252. https://doi.org/10.1038/s41467-021-26433-2.

Sunde, M., and C. Blake. 1997. “The Structure of Amyloid Fibrils by Electron Microscopy and X-Ray Diffraction.” *Advances in Protein Chemistry* 50: 123–59. https://doi.org/10.1016/s0065-3233(08)60320-4.

Sveinbjornsdottir, Sigurlaug. 2016. “The Clinical Symptoms of Parkinson’s Disease.” *Journal of Neurochemistry* 139 Suppl 1 (October): 318–24. https://doi.org/10.1111/jnc.13691.

Theillet, Francois-Xavier, Andres Binolfi, Beata Bekei, Andrea Martorana, Honor May Rose, Marchel Stuiver, Silvia Verzini, et al. 2016. “Structural Disorder of Monomeric α-Synuclein Persists in Mammalian Cells.” *Nature* 530 (7588): 45–50. https://doi.org/10.1038/nature16531.

Thibaudeau, Tiffany A., Raymond T. Anderson, and David M. Smith. 2018. “A Common Mechanism of Proteasome Impairment by Neurodegenerative Disease-Associated Oligomers.” *Nature Communications* 9 (1): 1097. https://doi.org/10.1038/s41467-018-03509-0.

Tokuriki, Nobuhiko, and Dan S. Tawfik. 2009. “Protein Dynamism and Evolvability.” *Science (New York, N.Y.)* 324 (5924): 203–7. https://doi.org/10.1126/science.1169375.

Tompa, Peter, and Monika Fuxreiter. 2008. “Fuzzy Complexes: Polymorphism and Structural Disorder in Protein-Protein Interactions.” *Trends in Biochemical Sciences* 33 (1): 2–8. https://doi.org/10.1016/j.tibs.2007.10.003.

Tompa, Peter, Csilla Szász, and László Buday. 2005. "Structural Disorder Throws New Light on Moonlighting." *Trends in Biochemical Sciences* 30 (9): 484–89. https://doi.org/10.1016/j.tibs.2005.07.008.

Törnquist, Mattias, Thomas C. T. Michaels, Kalyani Sanagavarapu, Xiaoting Yang, Georg Meisl, Samuel I. A. Cohen, Tuomas P. J. Knowles, and Sara Linse. 2018. "Secondary Nucleation in Amyloid Formation." *Chemical Communications (Cambridge, England)* 54 (63): 8667–84. https://doi.org/10.1039/c8cc02204f.

Trexler, Adam J., and Elizabeth Rhoades. 2009. "Alpha-Synuclein Binds Large Unilamellar Vesicles as an Extended Helix." *Biochemistry* 48 (11): 2304–6. https://doi.org/10.1021/bi900114z.

Tuttle, Marcus D., Gemma Comellas, Andrew J. Nieuwkoop, Dustin J. Covell, Deborah A. Berthold, Kathryn D. Kloepper, Joseph M. Courtney, et al. 2016. "Solid-State NMR Structure of a Pathogenic Fibril of Full-Length Human α-Synuclein." *Nature Structural & Molecular Biology* 23 (5): 409–15. https://doi.org/10.1038/nsmb.3194.

Uéda, K., H. Fukushima, E. Masliah, Y. Xia, A. Iwai, M. Yoshimoto, D. A. Otero, J. Kondo, Y. Ihara, and T. Saitoh. 1993. "Molecular Cloning of CDNA Encoding an Unrecognized Component of Amyloid in Alzheimer Disease." *Proceedings of the National Academy of Sciences of the United States of America* 90 (23): 11282–86. https://doi.org/10.1073/pnas.90.23.11282.

Ulamec, Sabine M., David J. Brockwell, and Sheena E. Radford. 2020. "Looking Beyond the Core: The Role of Flanking Regions in the Aggregation of Amyloidogenic Peptides and Proteins." *Frontiers in Neuroscience* 14: 611285. https://doi.org/10.3389/fnins.2020.611285.

Ulamec, Sabine M., Roberto Maya-Martinez, Emily J. Byrd, Katherine M. Dewison, Yong Xu, Leon F. Willis, Frank Sobott, et al. 2022. "Single Residue Modulators of Amyloid Formation in the N-Terminal P1-Region of α-Synuclein." *Nature Communications* 13 (1): 4986. https://doi.org/10.1038/s41467-022-32687-1.

Ulmer, Tobias S., Ad Bax, Nelson B. Cole, and Robert L. Nussbaum. 2005. "Structure and Dynamics of Micelle-Bound Human α-Synuclein." *Journal of Biological Chemistry* 280 (10): 9595–9603. https://doi.org/10.1074/jbc.M411805200.

Uversky, V. N., J. R. Gillespie, and A. L. Fink. 2000. "Why Are 'Natively Unfolded' Proteins Unstructured under Physiologic Conditions?" *Proteins* 41 (3): 415–27. https://doi.org/10.1002/1097-0134(20001115)41:3<415::aid-prot130>3.0.co;2-7.

Vaikath, Nishant N., Issam Hmila, Vijay Gupta, Daniel Erskine, Martin Ingelsson, and Omar M. A. El-Agnaf. 2019. "Antibodies against Alpha-Synuclein: Tools and Therapies." *Journal of Neurochemistry* 150 (5): 612–25. https://doi.org/10.1111/jnc.14713.

Van Roey, Kim, Bora Uyar, Robert J. Weatheritt, Holger Dinkel, Markus Seiler, Aidan Budd, Toby J. Gibson, and Norman E. Davey. 2014. "Short Linear Motifs: Ubiquitous and Functionally Diverse Protein Interaction Modules Directing Cell Regulation." *Chemical Reviews* 114 (13): 6733–78. https://doi.org/10.1021/cr400585q.

Ventura, Salvador. 2005. "Sequence Determinants of Protein Aggregation: Tools to Increase Protein Solubility." *Microbial Cell Factories* 4 (1): 11. https://doi.org/10.1186/1475-2859-4-11.

Ventura, Salvador, Jesús Zurdo, Saravanakumar Narayanan, Matilde Parreño, Ramón Mangues, Bernd Reif, Fabrizio Chiti, et al. 2004. "Short Amino Acid Stretches Can Mediate Amyloid Formation in Globular Proteins: The Src Homology 3 (SH3) Case." *Proceedings of the National Academy of Sciences of the United States of America* 101 (19): 7258–63. https://doi.org/10.1073/pnas.0308249101.

Vilar, Marçal, Hui-Ting Chou, Thorsten Lührs, Samir K. Maji, Dominique Riek-Loher, Rene Verel, Gerard Manning, Henning Stahlberg, and Roland Riek. 2008. “The Fold of Alpha-Synuclein Fibrils.” *Proceedings of the National Academy of Sciences of the United States of America* 105 (25): 8637–42. https://doi.org/10.1073/pnas.0712179105.

Watson, Matthew D., and Jennifer C. Lee. 2019. “N-Terminal Acetylation Affects α-Synuclein Fibril Polymorphism.” *Biochemistry* 58 (35): 3630–33. https://doi.org/10.1021/acs.biochem.9b00629.

Waudby, Christopher A., Christopher M. Dobson, and John Christodoulou. 2019. “Nature and Regulation of Protein Folding on the Ribosome.” *Trends in Biochemical Sciences* 44 (11): 914–26. https://doi.org/10.1016/j.tibs.2019.06.008.

Waudby, Christopher A., Tuomas P. J. Knowles, Glyn L. Devlin, Jeremy N. Skepper, Heath Ecroyd, John A. Carver, Mark E. Welland, John Christodoulou, Christopher M. Dobson, and Sarah Meehan. 2010. “The Interaction of AlphaB-Crystallin with Mature Alpha-Synuclein Amyloid Fibrils Inhibits Their Elongation.” *Biophysical Journal* 98 (5): 843–51. https://doi.org/10.1016/j.bpj.2009.10.056.

Weihofen, Andreas, YuTing Liu, Joseph W. Arndt, Christian Huy, Chao Quan, Benjamin A. Smith, Jean-Luc Baeriswyl, et al. 2019. “Development of an Aggregate-Selective, Human-Derived α-Synuclein Antibody BIIB054 That Ameliorates Disease Phenotypes in Parkinson’s Disease Models.” *Neurobiology of Disease* 124 (April): 276–88. https://doi.org/10.1016/j.nbd.2018.10.016.

Wentink, Anne S., Nadinath B. Nillegoda, Jennifer Feufel, Gabrielė Ubartaitė, Carolyn P. Schneider, Paolo De Los Rios, Janosch Hennig, Alessandro Barducci, and Bernd Bukau. 2020. “Molecular Dissection of Amyloid Disaggregation by Human HSP70.” *Nature* 587 (7834): 483–88. https://doi.org/10.1038/s41586-020-2904-6.

Wright, Peter E., and H. Jane Dyson. 2009. “Linking Folding and Binding.” *Current Opinion in Structural Biology* 19 (1): 31–38. https://doi.org/10.1016/j.sbi.2008.12.003.

Xu, Catherine K., Marta Castellana-Cruz, Serene W. Chen, Zhen Du, Georg Meisl, Aviad Levin, Benedetta Mannini, et al. 2022. “The Pathological G51D Mutation in Alpha-Synuclein Oligomers Confers Distinct Structural Attributes and Cellular Toxicity.” *Molecules (Basel, Switzerland)* 27 (4): 1293. https://doi.org/10.3390/molecules27041293.

Yang, Xue, Baifan Wang, Cody L. Hoop, Jonathan K. Williams, and Jean Baum. 2021. “NMR Unveils an N-Terminal Interaction Interface on Acetylated-α-Synuclein Monomers for Recruitment to Fibrils.” *Proceedings of the National Academy of Sciences of the United States of America* 118 (18): e2017452118. https://doi.org/10.1073/pnas.2017452118.

Yang, Yang, Holly J. Garringer, Yang Shi, Sofia Lövestam, Xianjun Zhang, Abhay Kotecha, Mehtap Bacioglu, et al. 2022. “New *SNCA* Mutation and Structures of α-Synuclein Filaments from Juvenile-Onset Synucleinopathy.” Preprint. Neuroscience. https://doi.org/10.1101/2022.11.23.517690.

Yang, Yang, Yang Shi, Manuel Schweighauser, Xianjun Zhang, Abhay Kotecha, Alexey G. Murzin, Holly J. Garringer, et al. 2022. “Structures of α-Synuclein Filaments from Human Brains with Lewy Pathology.” *Nature* 610 (7933): 791–95. https://doi.org/10.1038/s41586-022-05319-3.

Yoshino, Hiroyo, Makito Hirano, A. Jon Stoessl, Yoko Imamichi, Aya Ikeda, Yuanzhe Li, Manabu Funayama, et al. 2017. “Homozygous Alpha-Synuclein p.A53V in Familial Parkinson’s Disease.” *Neurobiology of Aging* 57 (September): 248.e7-248.e12. https://doi.org/10.1016/j.neurobiolaging.2017.05.022.

Zarranz, Juan J., Javier Alegre, Juan C. Gómez-Esteban, Elena Lezcano, Raquel Ros, Israel Ampuero, Lídice Vidal, et al. 2004. “The New Mutation, E46K, of Alpha-Synuclein Causes Parkinson and Lewy Body Dementia.” *Annals of Neurology* 55 (2): 164–73. https://doi.org/10.1002/ana.10795.

Zhang, Shengnan, Yu-Qing Liu, Chunyu Jia, Yeh-Jun Lim, Guoqin Feng, Enquan Xu, Houfang Long, et al. 2021. “Mechanistic Basis for Receptor-Mediated Pathological α-Synuclein Fibril Cell-to-Cell Transmission in Parkinson’s Disease.” *Proceedings of the National Academy of Sciences of the United States of America* 118 (26): e2011196118. https://doi.org/10.1073/pnas.2011196118.

Zhao, Kun, Yaowang Li, Zhenying Liu, Houfang Long, Chunyu Zhao, Feng Luo, Yunpeng Sun, et al. 2020. “Parkinson’s Disease Associated Mutation E46K of α-Synuclein Triggers the Formation of a Distinct Fibril Structure.” *Nature Communications* 11 (1): 2643. https://doi.org/10.1038/s41467-020-16386-3.

Appendix 1 – Supplementary information of chapter 1

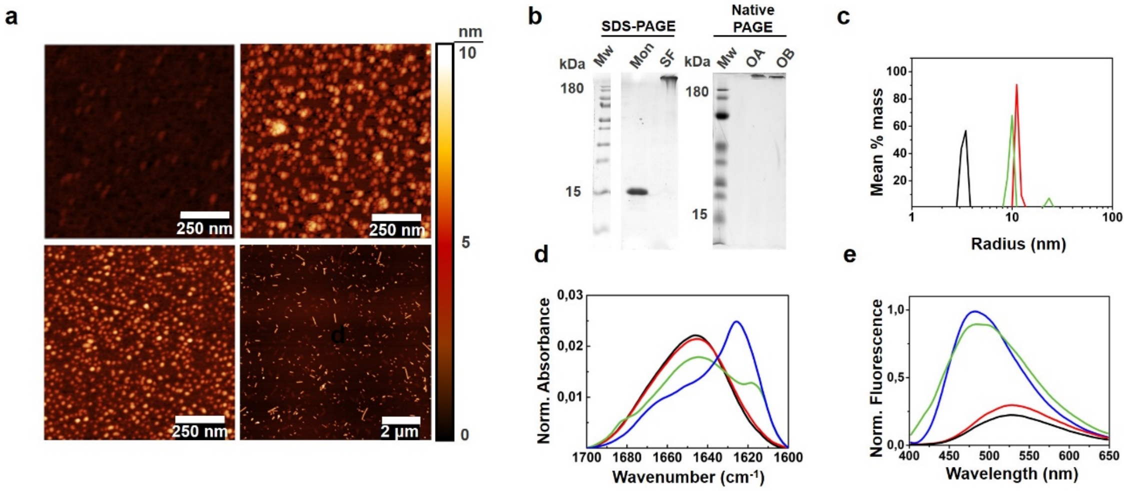

Supplementary Figure 1. Characterization of αS species. The size, morphology, purity, structure and hydrophobicity of the αS species used in this study were analyzed in order to provide a molecular basis for further result interpretation. a) AFM analysis of monomeric αS (top left), type A* (top right) and type B* (bottom left) oligomers and sonicated fibrils (bottom right) are shown. Statistical size distribution analysis yielded a 5.1 ± 0.4 nm height and 28 ± 6 nm diameter for type A* oligomers, 4.4 ± 0.9 nm height and 32 ± 5 nm diameter for type B* oligomers, and a 6.3 ± 0.3 nm height, 95 ± 14 nm width and 300 ± 140 nm length for sonicated fibrils. Scale bar and height color code are shown. Results are consistent between two independent replicates. These data are in good agreement with the diffusive behavior of the αS species as mentioned in the article and also in agreement with previously published data[1]. b) Electrophoretic behavior and purity of the αS species in denaturing (left) or native PAGE (right). No fragments or other contamination are visible in the sample. Importantly, no monomeric αS (referred to as Mon in the figure) is visible in the oligomeric (in both type A* and type B* oligomers, referred to as OA and OB, respectively, in the figure) or fibrillar protein preparations (referred to as SF in the figure). Aggregated species are larger than 180 kDa and thus do not enter the wells, in agreement with previously published data[1]. Results are consistent between two independent replicates. c) DLS analysis of αS species. A fairly homogeneous size distribution is visible for monomeric αS (black) as well as type A* (red) and type B* (green) oligomers. The fibrillar αS samples showed a very large polydispersity index preventing their analysis by this technique. Size distributions are given in % mass. d) Normalized infrared (IR) spectra of monomeric αS (black), type A* oligomers (red), type B* oligomers (green) and fibrils (blue). A clearly disordered conformation can be seen for the monomer and type A* oligomers while a substantial β-sheet structure is observed in the type B* oligomers, if less than in the fibrils, as expected and reported previously[1, 2]. In particular, deconvolution analysis yielded a β-sheet content of 0 % for monomer and type A* oligomers, 35 % for type B* and 56.4 % for fibrils, also in good agreement with previously published data[1, 2]. e) ANS binding analysis of αS species. The normalized fluorescent spectra of the different samples show a higher hydrophobicity, seen as an enhanced fluorescence emission and a spectral blue-shift of type B* oligomers (green) and fibrils (blue) compared with monomeric (black) αS and type A* oligomers (red), which show a similarly low intensity and are not blue-shifted. This is in good agreement with previously published data[1, 2]. Unprocessed scans of the blots in the are presented in the Source Data file.

a

Residue	Wt	1	2	3	4	5	6	7	8	9	10	11	12	13	14	15	16	17	18	19	20	21	22
α-helical predicted content	2.6	3.2	1.8	1.8	1.9	1.1	0.9	0.4	0.6	0.4	0.4	0.7	0.7	0.6	0.6	0.5	0.8	1.4	2.0	2.9	2.3	2.5	2.9

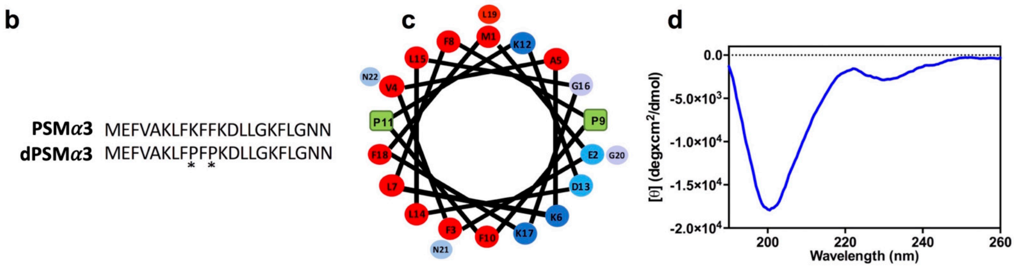

Supplementary Figure 2. Design of a non-amphipathic PSMα3 variant (dPSMα3). (**a**) Computational proline scanning. Predicted α-helical propensity according to the AGADIR score; higher values indicate higher predicted α-helical propensity. (**b**) Sequence alignment of PSMα3 and dPSMα3. (**c**) Helical wheel projection of dPSMα3 sequences showing the theorical location of the introduced prolines (green) (red, hydrophobic residues; blue pallet, hydrophilic residues depending on their character). (**d**) Far-UV circular dichroism spectrum of dPSMα3.

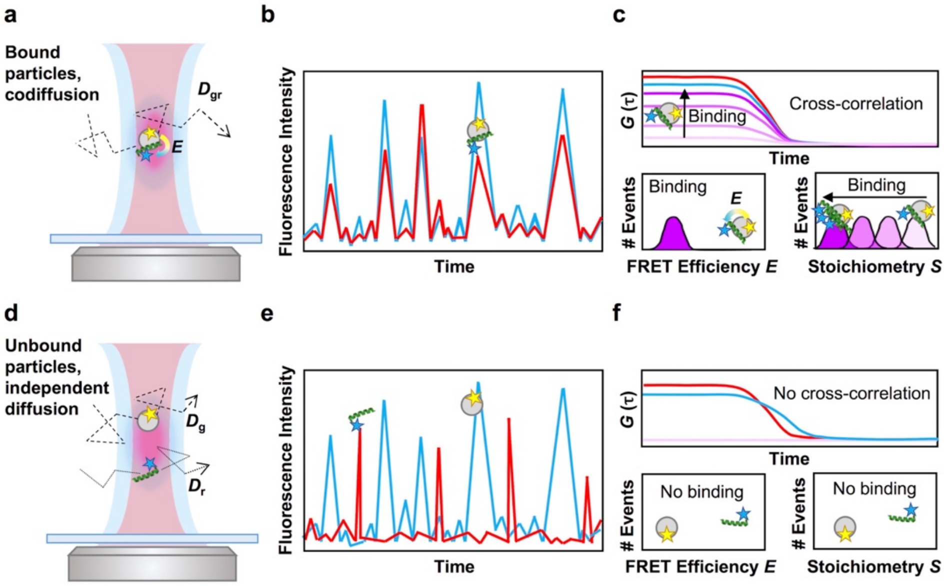
a
Bound particles, codiffusion
D_{gr}
E
b
Fluorescence Intensity
Time
c
G (τ)
Binding
Cross-correlation
Time
# Events
Binding
E
FRET Efficiency E
# Events
Binding
Stoichiometry S
d
Unbound particles, independent diffusion
D_g
D_r
e
Fluorescence Intensity
Time
f
G (τ)
No cross-correlation
Time
# Events
No binding
FRET Efficiency E
# Events
No binding
Stoichiometry S

Supplementary Figure 3. Schematic figure showing the dual-color time-resolved fluorescence spectroscopy approach to characterize the binding of the peptides to the different αS species. The upper panels (**a-c**) illustrate a scenario where binding occurs whereas the lower panels (**d-f**) serve as an example of a non-binding scenario. (**a**) Two interacting molecules labeled with a green and a red dye (depicted as a yellow or blue star, respectively) freely co-diffuse through the dual-laser confocal volume. The co-diffusion of the molecules is indicated as D_{gr} while FRET between the dyes in the complex is indicated as *E.* (**b**) Illustration of a fluorescence time-trace of the co-diffusing molecules where intensity bursts of the green and red detection channels (blue and red traces, respectively) coincide in time. (**c**) the upper panel illustrates a positive cross-correlation scenario (purple lines) where the cross-correlation amplitude (*G*) is directly proportional to the degree of binding. The bottom left panel depicts a FRET efficiency (*E*) distribution from interacting molecules while the bottom right panel shows the green dye-to-red dye (donor-to-acceptor) fluorescence stoichiometry of those interacting particles and shows how the stoichiometry decreases with an increasing binding degree. (**d-f**) illustrate the same parameters in the case where no interaction is observed.

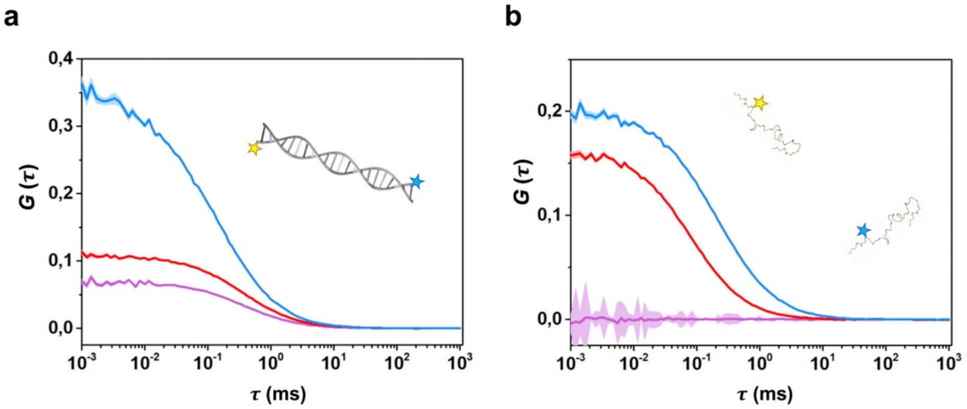

Supplementary Figure 4. Fluorescence cross-correlation spectroscopy positive and negative control. Auto-correlation curves of AF488 (blue) and Atto647N (red) and cross-correlation curves (purple) of samples containing (**a**) 10 nM of doubly-labelled dsDNA molecule or (**b**) 15 nM of non-interacting AF488-αS and Atto647N-αS (15 nM each). The amplitude (*G*) error is shown as faint colored area for the corresponding correlation curves.

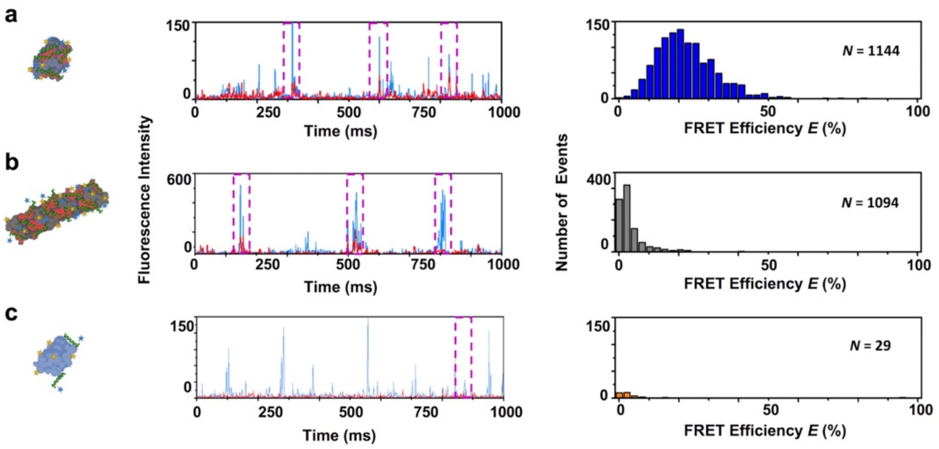

Supplementary Figure 5. αS-PSMα3 binding analyzed by Fluorescent single-particle spectroscopy. Representative intensity time traces (left panels) and intensity-calculated FRET efficiency histograms (right panels) for samples containing (**a**) ~1 nM αS type B* oligomers and ~5 nM PSMα3, (**b**) ~5 nM αS fibrils and ~5 nM PSMα3 and (**c**) 1 nM αS type A* oligomers and ~5 nM PSMα3 (concentrations expressed as protein/peptide mass concentrations; particle concentrations in the range of pM). In the intensity traces, events displaying both donor and acceptor intensities above αS monomer threshold (see materials and methods) are shown in purple dashed boxes. These events were then used to calculate the intensity-based FRET efficiency *E* histograms. The total number of FRET events, *N*, used to calculate each histogram is shown in each panel. These results show, directly from the intensity raw data, the high avidity of both PSMα3 for either type B* oligomers or fibrils (**a-b**) and the low ability to bind non-toxic aggregated species like the type A* oligomers (**c**). Acquisition times were the same for all data shown.

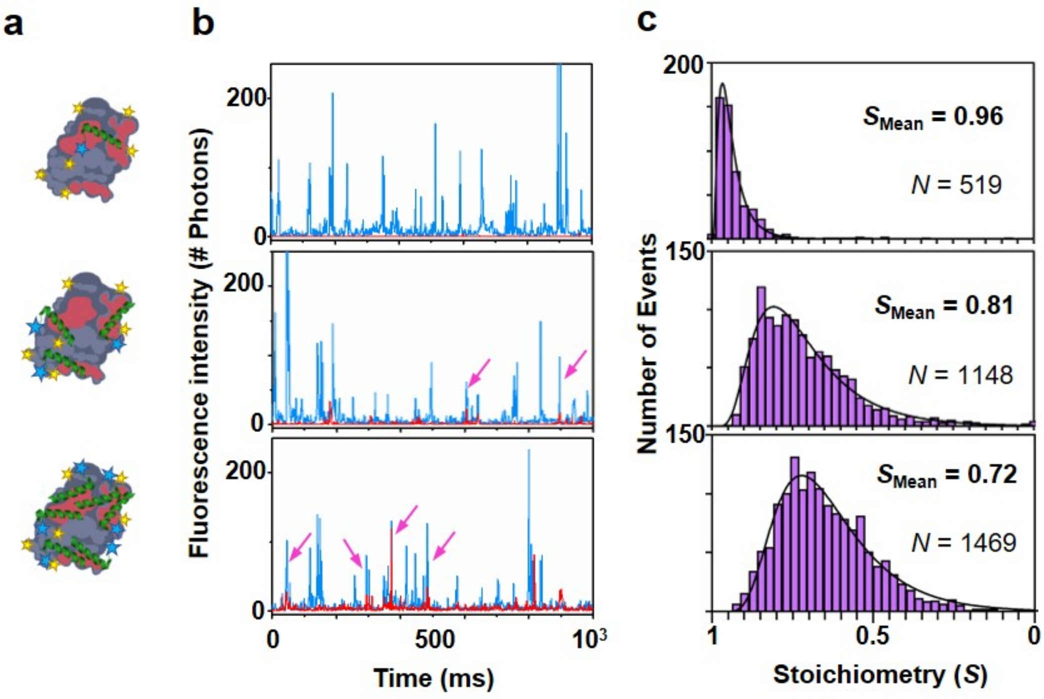

Supplementary Figure 6. Single-particle fluorescence stoichiometry analysis. Data is provided to illustrate the experimental approach leading to a burst-wise fluorescence stoichiometry analysis which complements the dcFCCS analysis to obtain the binding curves shown in this work. **a)** Schematic representations of type B* oligomers bound to increasing (top to bottom) concentrations of PSM*α*3. **b)** Intensity-based raw data corresponding to 1-second time frames (intensity time traces) of binding experiments with ~1 nM type B* oligomers (blue) and ~0.1 nM (top), ~2 nM (middle) and ~10 nM (bottom) PSM*α*3 (red). Note that the concentrations are given as protein/peptide mass concentrations and that particle concentrations are significantly lower, always under single-particle regime (for example in the case of type B* oligomers, 1 nM of mass concentration corresponds to ~30 pM oligomer particle concentration). Two-color coincident events that were intensity threshold-selected for stoichiometry analysis are shown with pink arrows in the figure panels. **c)** Fluorescence stoichiometry distributions from the experiments shown in **b)**. Increasing PSM*α*3 concentrations yield lower stoichiometry values as more peptide molecules can be bound to one oligomer. The log normal-fitted mean stoichiometry value (S_{Mean}) is shown. The total number of events (*N*), which increases with increasing PSM*α*3 concentrations, is also shown. Acquisition times were the same for all data shown.

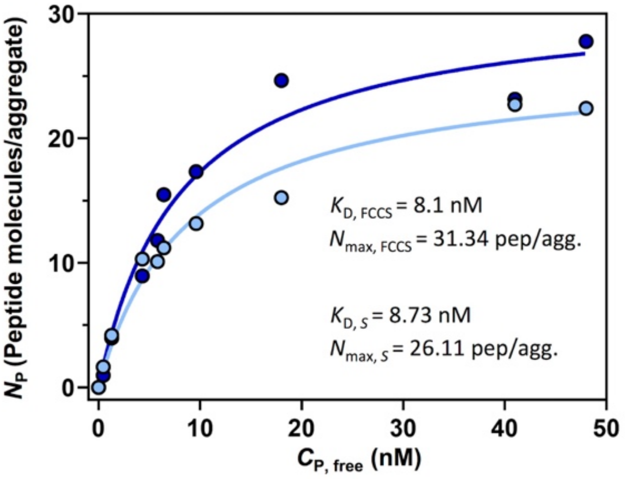

Supplementary Figure 7. Comparison of the titration binding curves of αS type B* oligomers with PSMα3 peptide obtained by dcFCCS or dual-color single-particle fluorescence spectroscopy analysis. The number of peptide molecules bound to one oligomer (N_P) at increasing peptide concentrations was calculated independently by dcFCCS (dark blue circles) or fluorescence stoichiometry analysis in dual-color single-particle fluorescence experiments (light blue circles), yielding very similar titration binding curves that resulted in very similar binding parameters when analyzed using a model of n identical and independent binding sites per αS aggregated species (solid lines). The fitted parameters K_D and N_{max} are also shown for each analytical approach. These results show how two different analytical methods, one which correlates fluorescence fluctuations over whole time traces and another one which analyzes single fluorescent bursts, can be applied to obtain very similar binding parameters, thus validating our strategy.

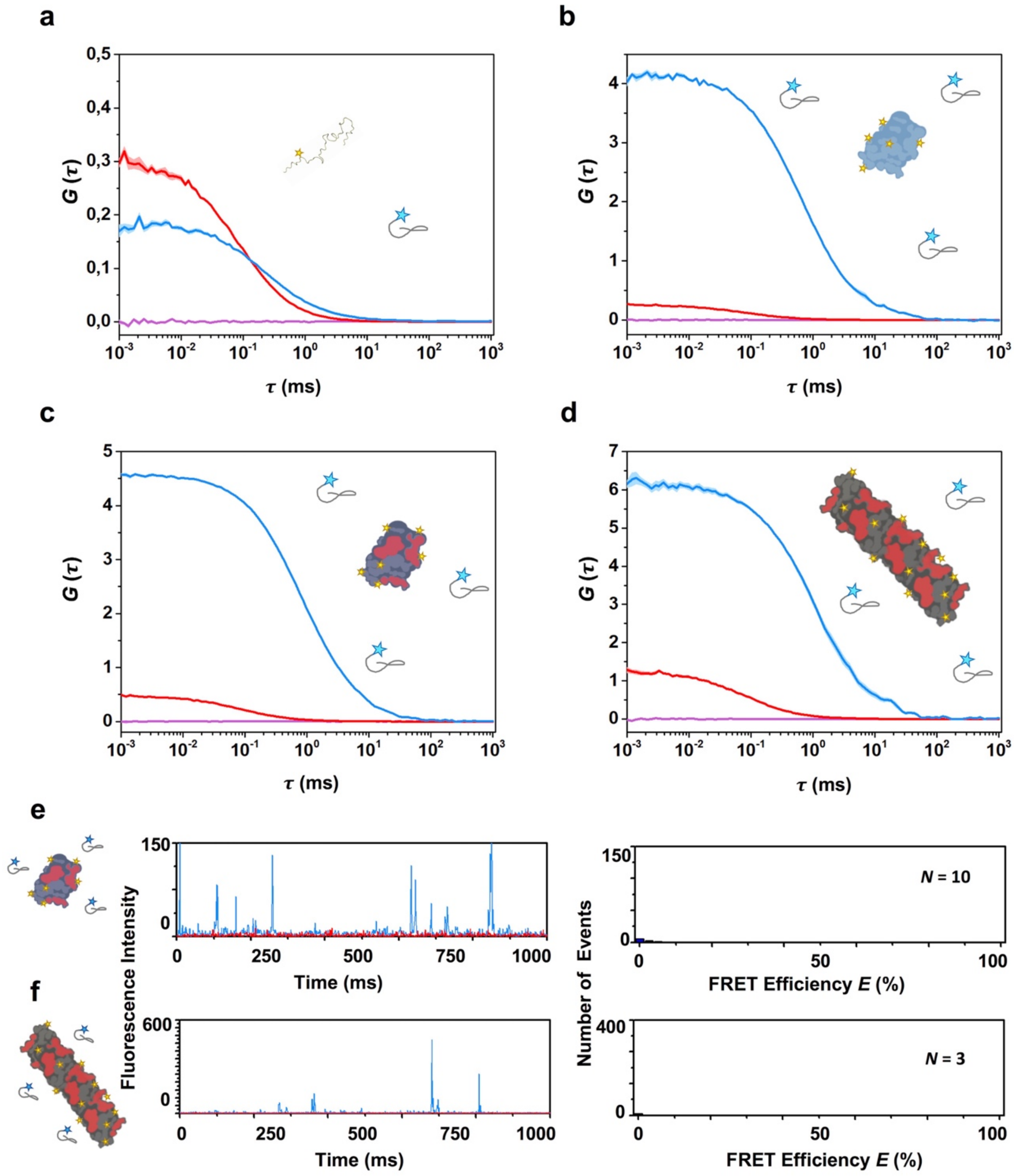

Supplementary Figure 8. Interaction of dPSMα3 with the different αS species. (**a-d**) Auto-correlation curves for αS and dPSMα3 and cross-correlation curves for interacting molecules are shown in blue, red and purple lines, respectively. The amplitude (*G*) error is shown in faint blue, red and purple, respectively. ~15 nM αS monomer (**a**), ~1 nM type A* (**b**), type B* (**c**) oligomers and sonicated fibrils (**d**) were allowed to interact with ~15 nM dPSMα3. No cross-correlation is observed in any case. (**e-f**) αS-dPSMα3 binding analyzed by dual-color single-particle fluorescent spectroscopy. Representative intensity time traces (left panels) and intensity-calculated FRET efficiency histograms (right panels) for samples containing (**e**) ~1 nM αS type B* oligomers and

~5 nM dPSMα3, (**f**) ~5 nM αS fibrils and ~5 nM dPSMα3. FRET single-particle fluorescence data directly show the inability of dPSMα3 to interact with either type B* oligomers or fibrils (**e, f**), as just few, if any, events were observed in comparison to the experiments with the PSMα3 peptide. Acquisition times were the same for all data shown.

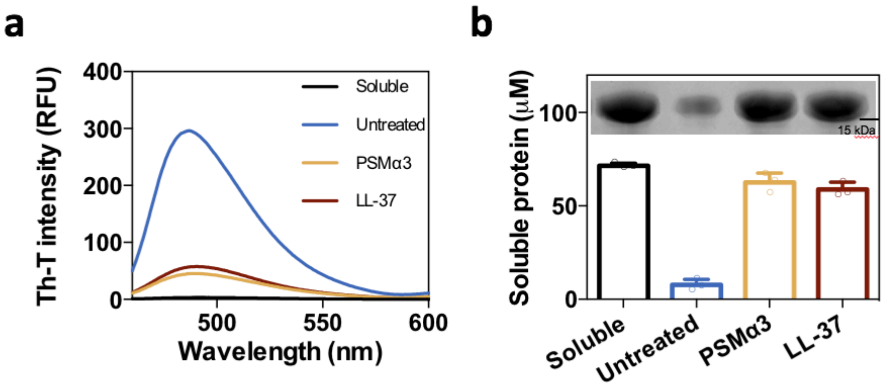

Supplementary Figure 9. Orthogonal validation of PSMα3 and LL-37 anti-aggregational activity. (**a**) Thioflavin-T fluorescence spectra in the presence of monomeric *α*S (Soluble) and end-point *α*S aggregation reactions (70μM) performed in the absence (Untreated) and in the presence of 35 μM of PSMα3 or LL-37. Spectra were recorded from 460 to 600 nm with an excitation wavelength of 445 nm. (**b**) Characterization of the amount of soluble *α*S in end-point aggregation reaction samples after sedimentation. The same samples were analyzed by SDS-PAGE (top panel) and quantification was performed by measuring the absorbance at 280 nm (ε = 5960 M^{-1} cm^{-1}). Protein quantities were measured in triplicate. Data were expressed as mean ± S.D (n = 3 independent experiments). Red lines indicate the position of the 15 and 20 kDa bands of the protein ladder. Unprocessed scans of the blots in the are presented in the Source Data file.

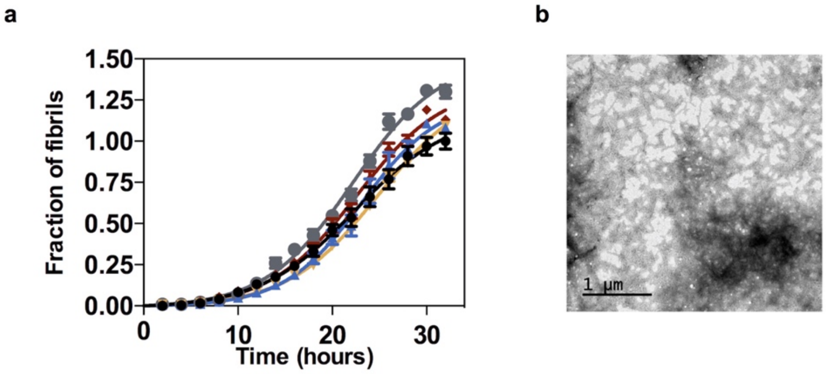

Supplementary Figure 10. Effect of dPSMα3 on *in vitro* αS amyloid fibrillation. (**a**) Aggregation kinetics of 70 µM αS and titration of the inhibitory activity of dPSMα3 at different concentrations: 35 µM (green), 14 µM (orange), 7 µM (blue), 3.5 µM (gray) and in the absence of dPSMα3 (black). Data were expressed as mean ± s.e.m (n = 9 independent experiments). (**b**) TEM micrograph of the end point of the aggregation kinetics in the presence of 70 µM of dPSMα3.

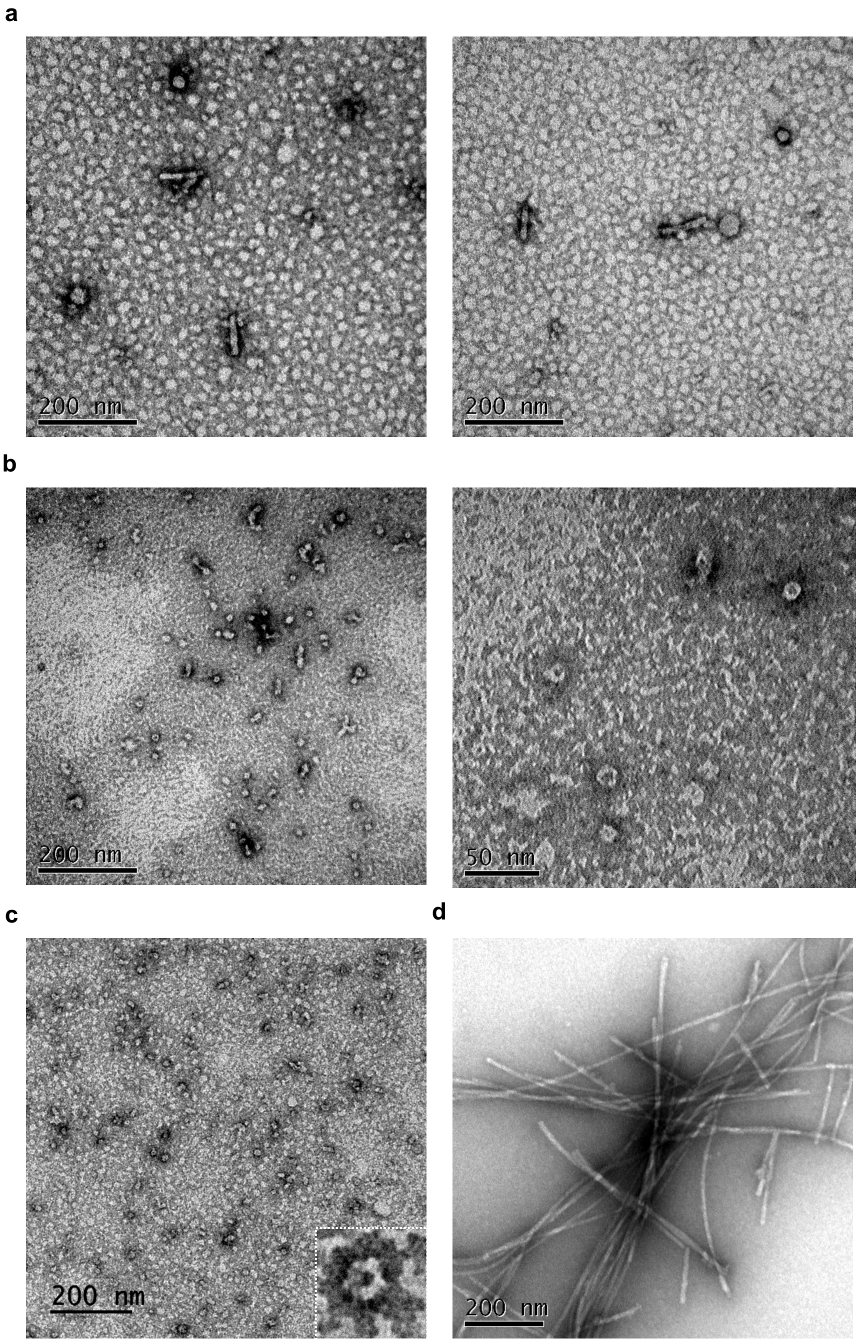

Supplementary Figure 11. Representative TEM micrographs of αS low molecular weight aggregates. Low molecular weight aggregates of αS aggregated for 12 hours in the absence (**a**) and the presence (**b**) of PSMα3. (**c**) Type B* oligomer preparation. Inset shows a type B* oligomer at high magnification. (**d**) End point αS amyloid fibrils. Results are consistent between two independent replicates.

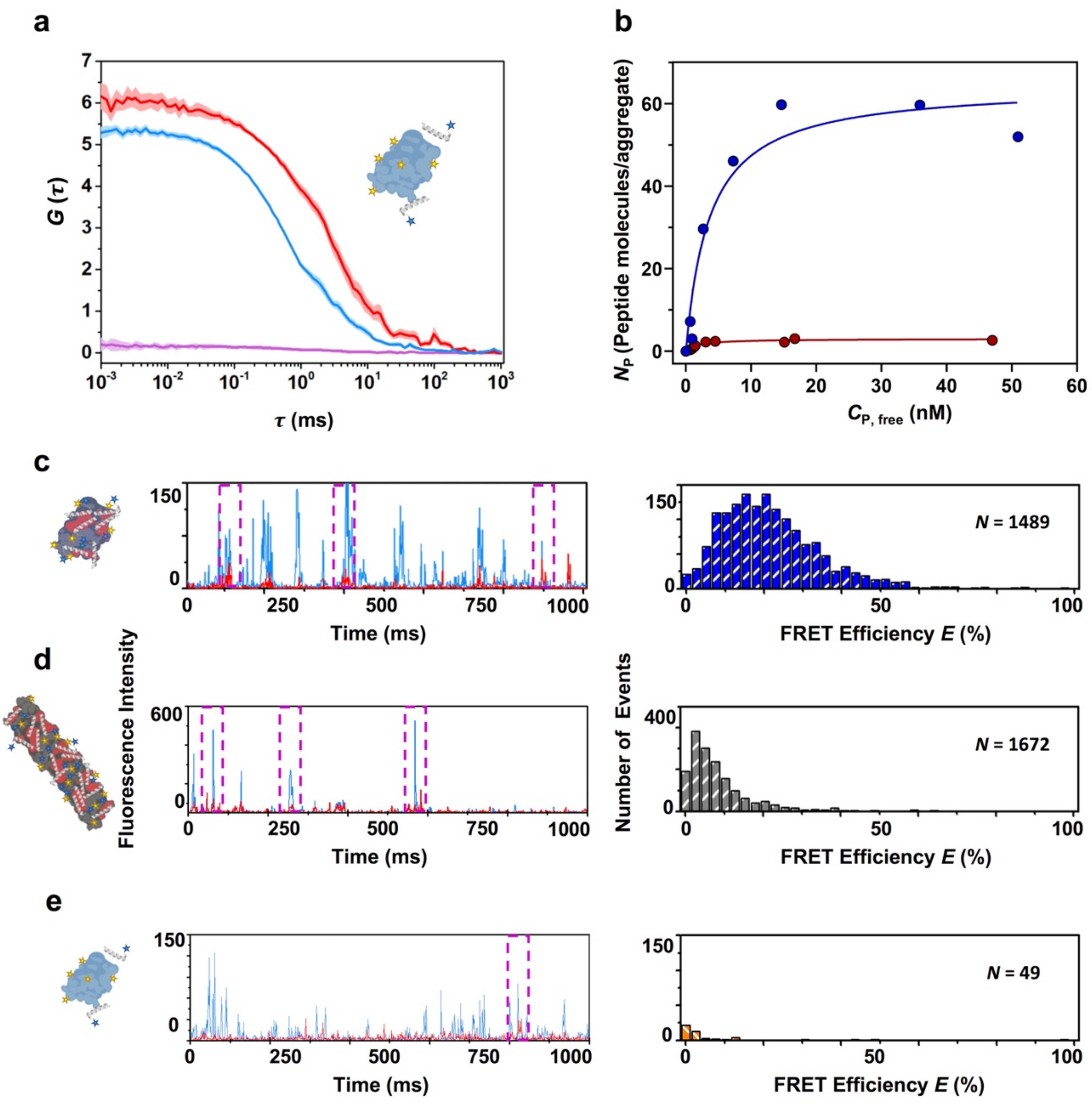

Supplementary Figure 12. Interaction of LL-37 with αS aggregates by FCCS and fluorescent single-particle spectroscopy. (**a**) Auto-correlation curves for αS (blue) and LL-37 (red) and cross-correlation curve for the interacting molecules (purple) in samples containing ~1 nM type A* oligomers and ~5 nM LL-37 peptide. The amplitude (G) error is shown as faint colored area for the corresponding correlation curves. (**b**) Titration binding curves for the interaction of LL-37 with type A* oligomers (red circles) or type B* oligomers (blue circles) obtained by dcFCCS, showing their corresponding analysis assuming a model of n independent binding sites per αS aggregated species (solid lines). (**c-e**) αS-LL-37 binding analyzed by Fluorescent single-particle spectroscopy. Representative intensity time traces (left panels) and intensity-calculated FRET efficiency histograms (right panels) for samples containing (**c**) ~1 nM αS type B* oligomers and ~5 nM LL-37, (**d**) ~5 nM αS fibrils and ~5 nM LL-37 and (**e**) ~1 nM αS type A* oligomers and ~5 nM LL-37. Acquisition times were the same for all data shown.

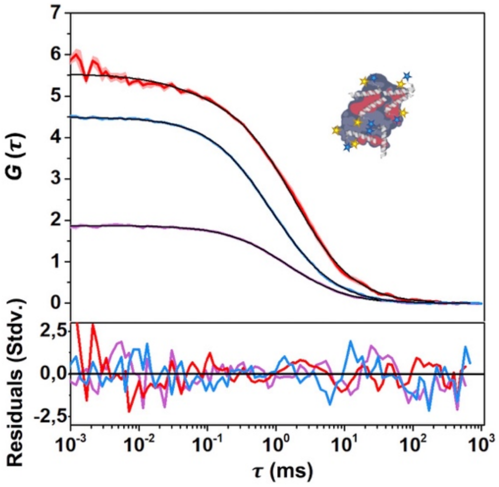

Supplementary Figure 13. Fitting of fluorescence correlation and cross-correlation data. Representative auto-correlation and cross-correlation curves of a sample of 1 nM type B* oligomers and 5 nM LL-37 peptide are shown in blue, red and purple lines, respectively. The amplitude (*G*) error is shown as faint colored area for the corresponding correlation curves. Best fits to 1-diffusion component (cross-correlation) or 2-diffusion component (auto-correlations) simple diffusion models are shown as black lines. The residual analysis of the best fits is also shown as standard deviation in colored lines for each correlation curve fit.

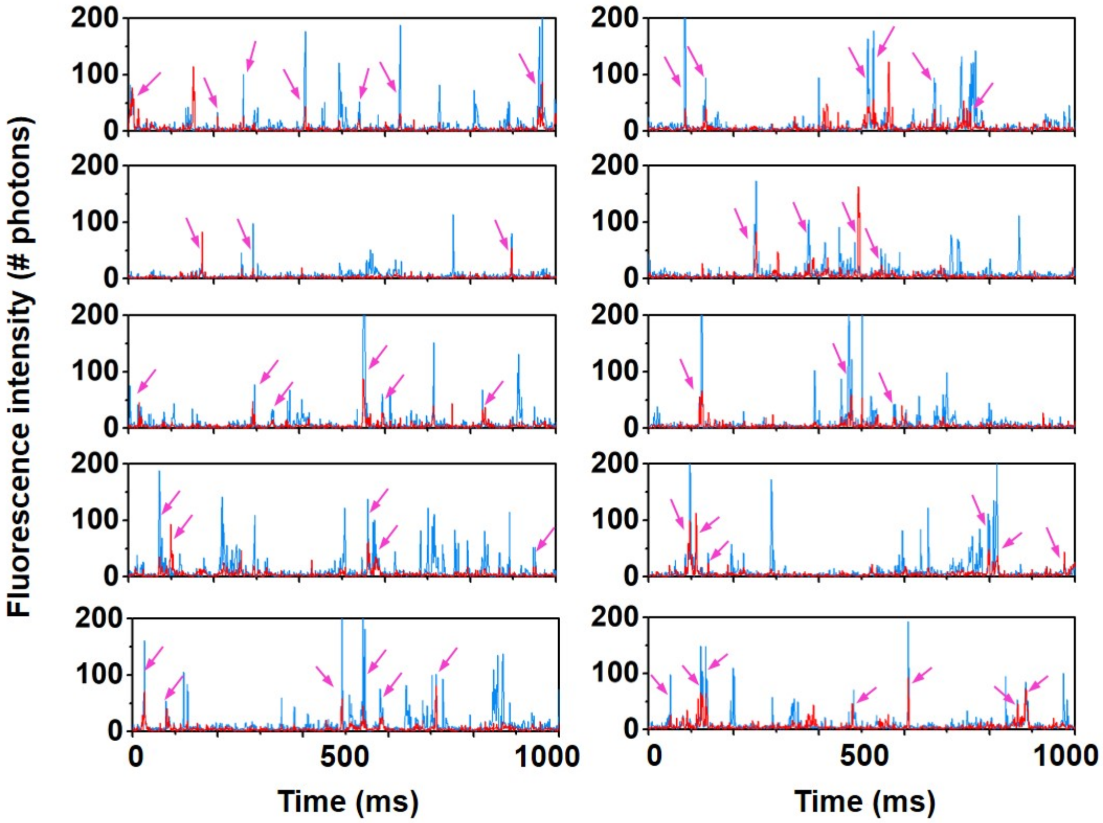

Supplementary Figure 14. Single-particle conditions in time-resolved fluorescence spectroscopy experiments. 10 representative 1-second intensity time traces (raw data) from a binding experiment with ~1 nM type B* oligomers (blue) and ~10 nM PSMα3 (red) are shown (note that concentrations are given as protein/peptide mass concentrations and that particle concentrations are significantly lower). Two-color coincident events that were intensity threshold-selected for fluorescence stoichiometry analysis are shown with pink arrows. The aggregate/complex-event frequency allows for optimal single-event selection and further burst-wise FRET and stoichiometry analysis, in full agreement with the aggregate mean volume occupancy (<*N*> far below 1) as explained elsewhere in the article.

Supplementary Table 1. Computational analysis of redesigned variants.

Name	Mutacion	Sequence	Activity	H*	μ_{H}**	AGADIR	Net charge	Change in FoldX stability (kcal/mol)
PSMα3	-	MEFVAKLFKFFKDLLGKFLGNN	+++	0.54	0.56	2.65	2	-
dPSMα3	K9P_F11P	MEFVAKLFPFPKDLLGKFLGNN	-	0.57	0.44	0.40	1	3.67
All_Leu	Hydrophobic face to Leu	LELLAKLLKLLKDLLGKLLGNN	+++	0.57	0.58	66.14	2	-1.46
All_Leu19	Hydrophobic face to Leu without 3 C-ter residues	LELLAKLLKLLKDLLGKLL	+++	0.72	0.70	65.17	2	-1.46
Scaffold_19	Hydrophobic face to Leu without 3 C-ter residues A5E_G16K	LELLEKLLKLLKDLLKKLL	+++	0.62	0.77	77.68	2	-1.03
Anionic scaffold	Scaffold19 K6E_K12E	LELLEELLKLLEDLLKKLL	-	0.65	0.75	78.26	-2	0.65

* H indicates the mean hydrophobicity of the peptides.
** μ_{H} indicates the helical hydrophobic moment of the peptides.

Supplementary Table 2. Identified human peptide candidates. The screening of the human peptides database (EROP-Moscow) for cationic peptides with more than 10 residues, an AGADIR value > 2 and a helical hydrophobic moment (μ_H) > 0.2.

Peptide sequence	AGADIR	μ_H	Cysteines
>E02311ǀANTIMICROBIAL PEPTIDE CATHELICIDIN LL37ǀHUMAN (HOMO SAPIENS), COMMOM CHIMPANZEE (PAN TROGLODYTES) LLGDFFRKSKEKIGKEFKRIVQRIKDFLRNLVPRTES	5.10	0.521	No
>E02310ǀANTIMICROBIAL PEPTIDE CATHELICIDIN FALL 39ǀHUMAN (HOMO SAPIENS), COMMOM CHIMPANZEE (PAN TROGLODYTES) FALLGDFFRKSKEKIGKEFKRIVQRIKDFLRNLVPRTES	4.92	0.529	No
>E19967ǀSALUSIN BETAǀHUMAN (HOMO SAPIENS) AIFIFIRWLLKLGHHGRAPP	2.14	0.306	No
>E06260ǀANAPHYLATOXIN C3A PEPTIDE LGE27ǀHUMAN (HOMO SAPIENS) LGEACKKVFLDCCNYITKLRRQHARAS	5.63	0.493	Yes
>E06257ǀANAPHYLATOXIN C3A PEPTIDE SLG25ǀHUMAN (HOMO SAPIENS) SLGEACKKVFLDCCNYITELRRQHA	4.72	0.48	Yes
>E01232ǀMELANIN CONCENTRATING HORMONEǀRAT (RATTUS NORVEGICUS), HUMAN (HOMO SAPIENS), MOUSE (MUS MUSCULUS) DFDMLRCMLGRVYRPCWQV	3.82	0.406	Yes
>E06261ǀANAPHYLATOXIN C3A PEPTIDE CNY21ǀHUMAN (HOMO SAPIENS) CNYITELRRQHARASHLGLAR	4.17	0.241	Yes
>E05394ǀBETA DEFENSIN 4ǀHUMAN (HOMO SAPIENS) EFELDRICGYGTARCRKKCRSQEYRIGRCPNTYACCLRKWDESLLNRTKP	3.09	0.32	Yes
>E04240ǀBETA DEFENSIN 6, HBD6ǀHUMAN (HOMO SAPIENS) FFDEKCNKLKGTCKNNCGKNEELIALCQKSLKCCRTIQPCGSIID	3.23	0.231	Yes

References

1. Chen SW, *et al.* Structural characterization of toxic oligomers that are kinetically trapped during alpha-synuclein fibril formation. *Proc Natl Acad Sci U S A* **112**, E1994-2003 (2015).

2. Fusco G, *et al.* Structural basis of membrane disruption and cellular toxicity by alpha-synuclein oligomers. *Science* **358**, 1440-1443 (2017).

Appendix 2 – Supplementary information of chapter 2

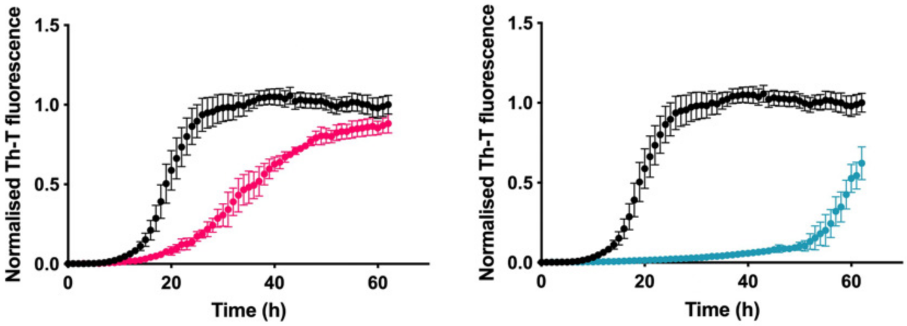

Experimental validation of two computationally identified human endogenous peptides with inhibitory capacity. Aggregation kinetics of 50 μM αS in absence (black) and presence of the human two computationally identified neuropeptides (left panel; pink) and (right panel; blue). Intensity of Th-T fluorescence is plotted as a function of time. Measurements were performed in a 96-well plate at 100 RPMs, in PBS and in presence of Teflon polyballs (1/8'' diameter).

Appendix 3 – Supplementary information of chapter 4

Materials and Methods:

αS expression and purification

αS expression was performed using a pT7-7 plasmid encoding the αS gene in *Escherichia coli* BL21 (DE3) cells. Cells were grown in LB medium supplemented with 100 µg/mL ampicillin or in isotope-enriched M9 minimal media supplemented with ^{13}C-glucose and ^{15}N-ammonium chloride to obtain uniformly ^{13}C^{15}N labelled samples. Protein expression was induced at an optical density of 0.6-0.8 (600 nm) with 1 mM isopropyl β-D-thiogalactopyranoside (IPTG) for 4 h. Cells were harvested by centrifugation and washed up by resuspension and centrifugation in PBS pH 7.4. The cell pellets were resuspended in 10 mL per culture liter in lysis buffer (50 mM Tris pH 8, 150 mM NaCl, 1 µg/mL pepstatin, 20 µg/mL aprotinin, 1 mM benzamidine, 1 mM PMSF, 1 mM EDTA, and 0.25 mg/mL lysozyme), lysed by sonication and centrifuged at 20,000 *g* for 30 min. The supernatant was boiled during 10 min at 95 °C and centrifuged again at 20,000 *g* for 30 min. The soluble fraction was treated with 136 µL/mL of 10% w/v streptomycin sulfate and incubated for 15 minutes. Upon centrifugation, soluble extracts were fractionated by adding 1:1 of saturated ammonium sulfate. The insoluble fraction was resuspended in 10 mL Tris 20 mM pH 8 per culture liter and dialyzed against Tris 20 mM pH 8. The dialyzed protein was filtered with a 0.22 µm filter and loaded onto an anion exchange column HiTrap Q HP (GE Healthcare, Chicago, USA). Tris 20 mM pH 8 and Tris 20 mM pH 8, NaCl 0.5 M were used as buffer A and buffer B. Fractions containing αS were further purified using size exclusion chromatography (Hiload 26/60 Superdex 75 preparation grade, GE Healthcare, Chicago, USA). Purified monomeric αS was dialyzed against 5 L ammonium acetate 50 mM in two steps; 4 h and overnight. Finally, protein purity was addressed using 15% SDS-PAGE. The purest fractions were lyophilized and stored at −80 °C. For the experiments, αS lyophilized aliquots were resuspended to a final concentration of 210 µM using PBS pH 7.4. αS concentration was determined by measuring the absorbance at 280 nm and using the extinction coefficient 5960 M^{-1} cm^{-1}. For mutants lacking tyrosine 39, we used 4470 M^{-1} cm^{-1} as the extinction coefficient. All αS variants were purified under the same conditions.

Preparation of kinetically trapped αS oligomers and formation of the oligomer-PSMα3 complex

For the preparation of oligomeric samples, after the size exclusion step, purified αS was dialyzed against 5 L Milli-Q water and lyophilized for 48 h in aliquots of 6 mg. Aliquots were resuspended to a final concentration of 800 µM in PBS pH 7.4, filtered through 0.22 µm PVDF filters and incubated at 37 °C under quiescent conditions for 20–24 h. The incubated reaction was then ultracentrifuged at 288,000 *g* in a SW55Ti Beckman rotor, to remove fibrillar species formed during the incubation. The excess of monomeric protein was removed by four consecutive cycles of cleaning using 100 kDa centrifuge filters (Merck, Darmstadt, Germany). Oligomer concentration was measured using molar extinction coefficients determined using amino acid analysis (WT: 7000 M^{-1} cm^{-1}; G51D: 12000 M^{-1} cm^{-1}) in agreement with previous reports (*1*).

Oligomer-PSMα3 complex was prepared by incubating purified oligomer with a 3-fold molar excess of PSMα3 for 30 minutes. As previously reported, PSMα3 binds to αS oligomers with nanomolar affinity (K_D = 6.67 nM) and with a 1:1 PSMα3: αS monomer ratio (*2*). PSMα3 excess is removed by two consecutive cycles of cleaning with PBS pH 7.4 using 100 kDa centrifuge filters (Merck, Darmstadt, Germany).

Solid-state NMR spectroscopy

1.5 mg of ^{13}C, ^{15}N labeled oligomer solution (PBS pH 7.4) was pipetted (approximately 50 µL) in a 4 mm Bruker rotor. All spectra were acquired in a 14.1 T Bruker magnet using a 4 mm Bruker HCN probe at 11 kHz MAS, 269 K probe temperature, resulting in sample temperature ~278 K. All 1D spectra were acquired with 64 scans with recycle delay of 3 sec. All cross-polarization based experiments were performed with a contact time of 600 us. The 2D 1H-13C INEPT spectra were acquired with 64 scans, 140 increments in indirect dimension, recycle delay of 2.2 sec, t1=7.7 ms, t2=18.4 ms resulting in a total acquisition time of 5.5 h. Both dimensions were apodized with Bruker QSine SSB=4 functions. The CP 2D 50 ms PDSD spectra was acquired with 512 scans, 300 increments in indirect dimension, recycle delay of 3 sec, t1=7.6 ms, t2=18.4 ms (with 90 kHz ^{1}H SPINAL-64 decoupling) resulting in total acquisition time of 128 h. Both dimensions were apodized with Bruker QSine SSB=3 functions. The spectra were processed and analyzed using TopSpin3.61 and CcpNmr version 2.4.1 programs.

Negative staining electron microscopy

For negative staining electron microscopy analysis, samples were diluted to a concentration of 0.2-0.05 mg/mL in PBS and placed onto glow-discharged carbon-coated copper grids to adsorb for 1 min. The excess of sample was carefully blotted using ashless filter paper. Grids were negatively stained with 2% (w/v) uranyl acetate for 1 min and excess of uranyl acetate was absorbed using ashless filter paper. A TEM JEOL JEM1400 microscope was used operating at an accelerating voltage of 120 kV equipped with a CCD GATAN 794 MSC 600HP camera. Representative images of each grid were selected. For particle analysis and 2D classification, images were acquired using a JEOL JEM 1010 electron microscope operated at 100 kV and equipped with a CCD camera (4 K × 4 K TemCam-F416, TVIPS). Images were recorded at a 50,000 × nominal magnification with a sampling rate of 2.4 Å/px. These images were processed following the Scipion3 processing workflow (*3*). Images were CTF-corrected using CTFFIND4 (*4*). Particles were automatically selected using Xmipp3 (*5*) and 2D-classified using Relion2 (*6*) and CryoSPARC (*7*).

CryoEM data adquisition

Aliquots of 4 µL of αS oligomers and αS oligomers-PSMα3 complexes were vitrified using a Vitrobot Mark IV (FEI) and were incubated onto Quantifoil R 2/2 300 mesh grids with an additional ultrathin continuous carbon layer, blotted for 2 s at 22 °C and 95% humidity and plunged into liquid ethane. The cryoEM grids were checked and data from the best one was acquired in a 200 kV FEI Talos Arctica equipped with a Falcon III direct electron detector at the Centro Nacional de Biotecnología (CNB) cryoEM facility. A total of 967 movies for αS oligomers and 852 movies for αS oligomers-PSMα3 complexes were acquired at a nominal magnification of 73,000x (corresponding to a pixel size of 1.37 A/pix), with a defocus range of 1.4 to 3.2 µm. Exposure was set to 0.9322 e-/Å/sec and 30 frames were collected in total, with an overall dose of 28 e-/Å for αS oligomers and 1.06 e-/Å/sec and a total dose of 32 e-/Å for αS oligomers-PSMα3 complexes.

Image processing and three-dimensional reconstruction

Image processing of αS oligomers and αS oligomers-PSMα3 complexes was performed following a similar workflow. All programs used for image processing to obtain the different 3D maps are implemented in the Scipion software platform. First, the movies were aligned using MotionCor2 (*8*) and the outputs were subjected to CTF determination using Gctf (*9*). Particles were automatically picked with Xmipp3 –auto-picking software. The 193,427 (αS oligomers) and 187,446 (αS oligomers-PSMα3 complex) extracted particles were subjected to several 2D classifications using Relion 2.0 and Cryosparc to exclude bad particles and ice contamination. Some of the best 2D classes were used as a template to generate an initial model using both Cryosparc and RANSAC (*10*). In both cases, models were low-pass filtered to 50 Å and used for a 3D classification of 85,628 (αS oligomers) and 76,730 (αS oligomers-PSMα3 complex) particles contained in the best 2D classes performed without symmetry imposition. The particles of the best classes were used for a further 3D auto-refine using Relion 2.0 and yielded cylindrical oligomeric structures at 18.5 Å (αS oligomers) and 19 Å (αS oligomers-PSMα3 complex) resolution (**Table S3**). Subsequent imposition of C6 symmetry generated slightly higher resolution structures of the oligomeric assemblies at 16 Å and 16.7 Å resolution, respectively (**Table S3**).

Disulfide engineering

Disulfide bond engineering was performed using the 2N0A structure as a template due to its fitting into the oligomer density. The disulfide design was performed using disulfide by design 2.0 (*11*), which proposed residues 71 and 92 as the only available alternative under the default conditions (Chi3 angle: +97/-87 with Tolerance,30.00; Ca-Cb-S angle: 114.60 with Tolerance,10.00). The purified protein was fully oxidized without the need for further treatment (**Fig. S5B**)

High-Performance Liquid Chromatography

Monomeric oxidized V71C-T92C αS (0.5 mg/mL) was reduced in 0.1 M Tris-HCl (pH 8.4) containing 50 mM DTT for 2 h at RT. Additional control samples of oxidized V71C-T92C αS in the absence of DTT and WT αS were incubated under identical conditions. All samples were quenched with aqueous trifluoroacetic acid (TFA) solution to a final concentration of 1%. Acid-quenched proteins were analyzed by Reversed-phase high-performance liquid chromatography (RP-HPLC) using a linear 5-60% gradient of acetonitrile with 0.1% TFA over 90 min in a 4.6-mm C4 column (Phenomenex) at a flow rate of 0.75 ml/min.

Small-angle x-ray scattering data acquisition

SAXS measurements were performed on an in-house instrument at Aarhus University. The instrument is a modified NanoSTAR from Bruker AXS with a homebuilt scatterless pinhole in front of the sample and an Excillum liquid metal jet source (*12*). αS oligomers at a concentration of 4.6, 2.0, and 1.3 mg/mL were measured in the same flow-through capillary. Scattering from the buffer was measured and subtracted as background and the data were converted to absolute intensity scale using the scattering from a pure water sample as standard (*13*). The azimuthally averaged intensity $I(q)$ was calculated from the two-dimensional data as a function of the modulus of the scattering vector q. The data were displayed in Guinier plots of $\ln(I(q))$ vs q^2 and Kratky plots of $q^2\ I(q)$ vs q to check for, respectively, aggregation and flexibility. The former also gives the radius of gyration R_g and the forward scattering $I(0)$. An Indirect Fourier Transformation (IFT) of the data (*14*) was used for obtaining the pair distance distribution function, $p(r)$, which is a histogram of distances between pairs of points within the structure.

Modelling of Small-angle x-ray scattering data

A model based on super-ellipsoid of revolution was constructed (*15*). It consists of a super-ellipsoid core with a cylindrical hole along the symmetry axis of super-ellipsoid surrounded by a shell with a different (lower) density and constant width. Both the outer surface and the core-shell interface were graded by including Gaussian factors as done by Maric et al. (*15*). This publication also contains the equations required for calculating the present model scattering. The shape parameter of the super-ellipsoid was fixed at t = 4 for both core and shell. The scattering from the internal structure of the shell with the random coils were included as described in (*16*) using an extra term with the form factor of the shell subtracted from the random coil scattering. The latter was described by the scattering from Gaussian chains multiplied by a cross-section Guinier term $\exp(-R_c^2 q^2/4)$, where R_c is the cross-section radius (*17*). The intensity of the models is expressed on absolute scale using a excess scattering density of 2.00×10^{-10} cm/g for the protein. The monomer was set to 14.5 kDa for αS.

The model depends on the following parameters. The core radius R, the axis ratio ε, the grading width of the core-shell interface σ_{in}, the radius of the hole in the core R_{hole}, the width of the shell W_{shell}, the grading width of the outer surface of the shell σ_{shell}, where the restraint $W_{shell} = 2\ \sigma_{shell}$ was used. Additional parameters are relative density of the shell ρ_{shell}, the radius of the random coils chains R_c and the aggregation number N_{agg}. The fraction of protein in core f_{core} and shell ($1 - f_{core}$) can be calculated from the other fit parameters. The mass of a protein chain in the shell was used for calculating the radius of gyration R_g for the random coil chains scattering using an expression for unfolded polypeptide chains (*18*).

In a log-log plot, the data sets (**Fig. S13A**) are nearly identical for the different concentrations except for scale factors. The data display a crossover towards constant intensity as q goes to zero. At higher q, it is followed by a power-law behaviour with an exponent of approximately –4. At even higher q, there is a shoulder with a subsequent power law with a lower exponent, in agreement with the presence of some polymer-like scattering due to the presence of some random coils in the structure.

Guinier plots of the data a $\ln(I(q))$ vs q^2 at the highest concentrations (**Fig. S13B**) show a linear behaviour. The radius of gyration is $R_g = 76.1 \pm 0.3$ Å and the forward scattering $I(0) = 1.31 \pm 0.01$ cm^{-1}. An Indirect Fourier Transformation (IFT) of the data[3, 4] gave the functions and the fits displayed in (**Fig. S13C**) for a maximum distance of 265 Å. The IFT gave as values $R_g = 80.5 \pm 0.2$ Å and $I(0) = 1.384 \pm 0.003$ cm^{-1}, deviating slightly from the values determined by the Guinier plot and fit. Kratky plots of $q^2\ I(q)$ vs q (**Fig. S13D**) have a maximum at low q in agreement with a compact globular-like structure and levels off at large *q* in agreement with additional presence of random coil scattering.

To display the resulting structures, a program was written that generates dummy atoms with a density that follows that determined by the modelling (*15*). The resulting dummy atoms and coordinates are saved in PDB format. The density of the dummy atoms represents the ensemble average, so the chain structures are not present in the dummy atom representations.

Crosslinking experiments and mass spectrometry analysis (XL-MS)

30 µg of αS oligomers and αS oligomers-PSMα3 complexes were subjected to chemical crosslinking by incubation with 15 mM DMTMM in PBS pH 7.4 for 30 min at RT. The reactions were quenched for 15 min at RT by adding 50 mM Tris-HCl pH 7.0. DMTMM-crosslinked samples were incubated in Laemmli sample buffer (0.02% [w/v] bromophenol blue, 2% [w/v] SDS, 10% [v/v] glycerol, 60 mM Tris-HCl pH 6.8) for 5 min at 96 °C and loaded onto a 12% polyacrylamide gel. The gel was stained, and the visible bands were excised and subjected to automated reduction, alkylation with iodoacetamide and trypsin digestion in a Proteineer DP robot (Bruker Daltonics). The resulting peptide mixture was speed-vac dried and re-dissolved in 0.1% (v/v) formic acid. Liquid chromatography–mass spectrometry (LC-MS/MS) analysis was carried out using a nano-LC Ultra HPLC (Eksigent, Framingham, MA) coupled online to a 5600 triple TOF mass spectrometer (AB Sciex, Framingham, MA) through a nanospray III ion source (AB Sciex) equipped with a fused silica PicoTip emitter (10 µm x 12 cm; New Objective, Woburn, MA). Peptides were fractionated at a flow rate of 0.250 mL/min at 50 °C under gradient elution conditions. The ion source was operated in positive ionization mode at 150 °C with a potential difference of 2300 V.

For peptide identification, raw MS data was searched against a custom-made database containing the amino-acid sequence of human αS or PSMα3. The MS/MS ion search was performed with MeroX 2.0 (*19*). Search parameters were set as follows: DMTMM as crosslinker and trypsin as enzyme, allowing 3 missed cleavages for Arg and Lys. Carbamidomethylation (Cys) and oxidation (Met) were set as fixed and variable modifications, respectively. Analysis was performed with MS and MS/MS tolerances of 10 and 20 ppm, respectively. Peptide identifications were filtered at an FDR < 5% and an XlinkX score > 30 and all the MS2 spectra of the resulting peptides were manually revised.

Hydrogen-deuterium exchange-mass spectrometry (HDX-MS)

HDX-MS experiments were performed using an automated HDX liquid handling robot (LEAP Technologies, Ft Lauderdale, FL, USA) coupled to an Acquity M-Class LC and HDX manager (Waters, UK). Samples contained 50 µM of αS monomer or oligomer in PBS buffer, pH 7.4. The robot was used to transfer 95 µL of deuterated buffer (PBS, pD 7.4, 0.01% w/v DDM) to 5 µL of protein-containing solution and the mixture was incubated at 4°C for 0, 0.5, 1 or 5 min. Three replicate measurements were performed for each time point and for each protein condition. 75 µL of quench buffer (PBS buffer, 4 M guanidine HCl, 0.05% w/v DDM, pH 2.1) was added to 75 µL of the labelling reaction to quench the deuterium labelling reaction. 50 µL of the quenched sample was injected into an Enzymate immobilised pepsin column (Waters, UK). A VanGuard Pre-column [Acquity UPLC BEH C18 (1.7 µm, 2.1 mm x 5 mm, Waters, UK)] was used to trap the peptides produced for 3 min. A C18 column (75 µm, 2.1 mm x mm, Waters, UK) separated peptides using a gradient of 0-40% (v/v) acetonitrile (0.1% v/v formic acid) in H_2O (0.3% v/v formic acid) over 7 min at 40 µL min^{-1}. Separated peptides from the LC column were infused into a Synapt G2Si mass spectrometer (Waters, UK) operated in $HDMS^E$ mode. Peptides were separated by ion mobility prior to CID fragmentation in the transfer cell for peptide identification. Deuterium uptake was quantified at the peptide level.

Data analysis was performed using PLGS (v3.0.2) and DynamX (v3.0.0) (Waters, UK). Search parameters in PLGS were: peptide and fragment tolerances: automatic, minimum fragment ion matches: 1, digest reagent: non-specific, false discovery rate: 4. Restrictions for peptides in DynamX were: minimum intensity: 1000, minimum products per amino acid: 0.3, maximum sequence length: 25, maximum error = 5 ppm, file threshold: 3. Peptides with significant increase/decrease in deuterium uptake were identified using a cut off of 0.5 Da. Woods plots were generated using Deuteros (*20*).

Assembly kinetics into amyloid

αS amyloid aggregation was monitored in non-binding 96 well plates (Corning, Corning, NY, USA). Each 100 µL reaction contained 100 µM αS and 20 µM thioflavin-T (Th-T) in PBS pH 7.4. Aggregation kinetics were recorded using a Spark plate reader (Tecan, Switzerland) at 37 °C and 600 rpm with a time interval of 15 minutes (Ex. 445 nm, Em: 495 nm).

Isolation of low molecular weight aggregates generated during αS in vitro aggregation

αS aggregation was performed as described in the previous section. For *wild-type*, ∆N11, ∆P1, ∆P2, ∆∆ and Y39A endpoint samples were recovered for the plate, whereas for S42A and G51D variants, we recovered the samples at the time point of maximal inhibition (28 hours). To isolate the oligomeric fraction, we adapted the centrifugation-based protocol developed by Kumar and coworkers (*21*). αS preparations (400 µL) were subjected to ultracentrifugation at 100,000 g for 60 min at 20 °C in a SW55Ti Beckman rotor to remove larger fibrillar species. The soluble fraction was then filtrated through 100 kDa centrifuge filters (Merck, Darmstadt, Germany) to fractionate low molecular weight aggregates and monomeric αS. The filtrated sample contains monomeric αS, whereas oligomers are retained in the upper section of the filter in a volume of 30-50 µL. The monomer excess was then washed by diluting the sample in PBS pH 7.4 to 500 µL and the procedure repeated twice. The oligomeric fraction is then recovered by carefully pipetting (ca. 30-50 µL) and was subsequently analyzed by transmission electron microscopy as previously described above. This procedure allows a morphological characterization of low molecular weight aggregates generated in the aggregation reaction by concentrating these low populated species and removing the large excess of monomer that would preclude their visualization by EM in an unprocessed sample.

Far circular dichroism analysis

Far-UV CD spectra of the oligomer preparations were recorded on a Jasco J-815 CD spectrometer (Halifax, Canada) at 25 °C. Oligomer concentration was adjusted to 5 µM in PBS pH 7.4. CD signal was measured from 260 nm to 190 nm at 1 nm bandwidth, 1 sec of response time and a scan speed of 200 nm/min on a 0.1 cm quartz cell. Ten to twenty accumulations were recorded and averaged for each measurement.

Dynamic light scattering

Oligomer size was determined by dynamic light scattering using a Zetasizer Nano ZS (Malvern Instruments Limited, UK) at 25 °C at a fixed angle of 90 °. Three different measures of twenty runs were recorded for each sample.

Chaperone disaggregation

Hsc70, DNAJB1 and Apg2 chaperones were produced as previously reported (*22*). αS oligomers (3 µM) were mixed with 10 µM Hsc70, 5 µM DNAJB1 and 1 µM Apg2 in the presence of an ATP-regeneration system (8 mM phosphoenol pyruvate and 20 ng/µL pyruvate kinase). After incubating the samples in 40 mM Hepes-KOH pH 7.6, 50 mM KCl, 5 mM MgCl2, and 2 mM DTT at 30 °C, disaggregation was started by ATP (2 mM) addition. At the desired incubation times, samples were analyzed by Native-PAGE (4-16% Bis-Tris, Invitrogen) and immunoblotting using anti-αS (Invitrogen PA5-85343, 1:2000 dilution) or anti-Hsc70 (Abcam ab51052; 1:5000) antibodies. As a control, a known concentration of monomeric αS was run under the same experimental conditions.

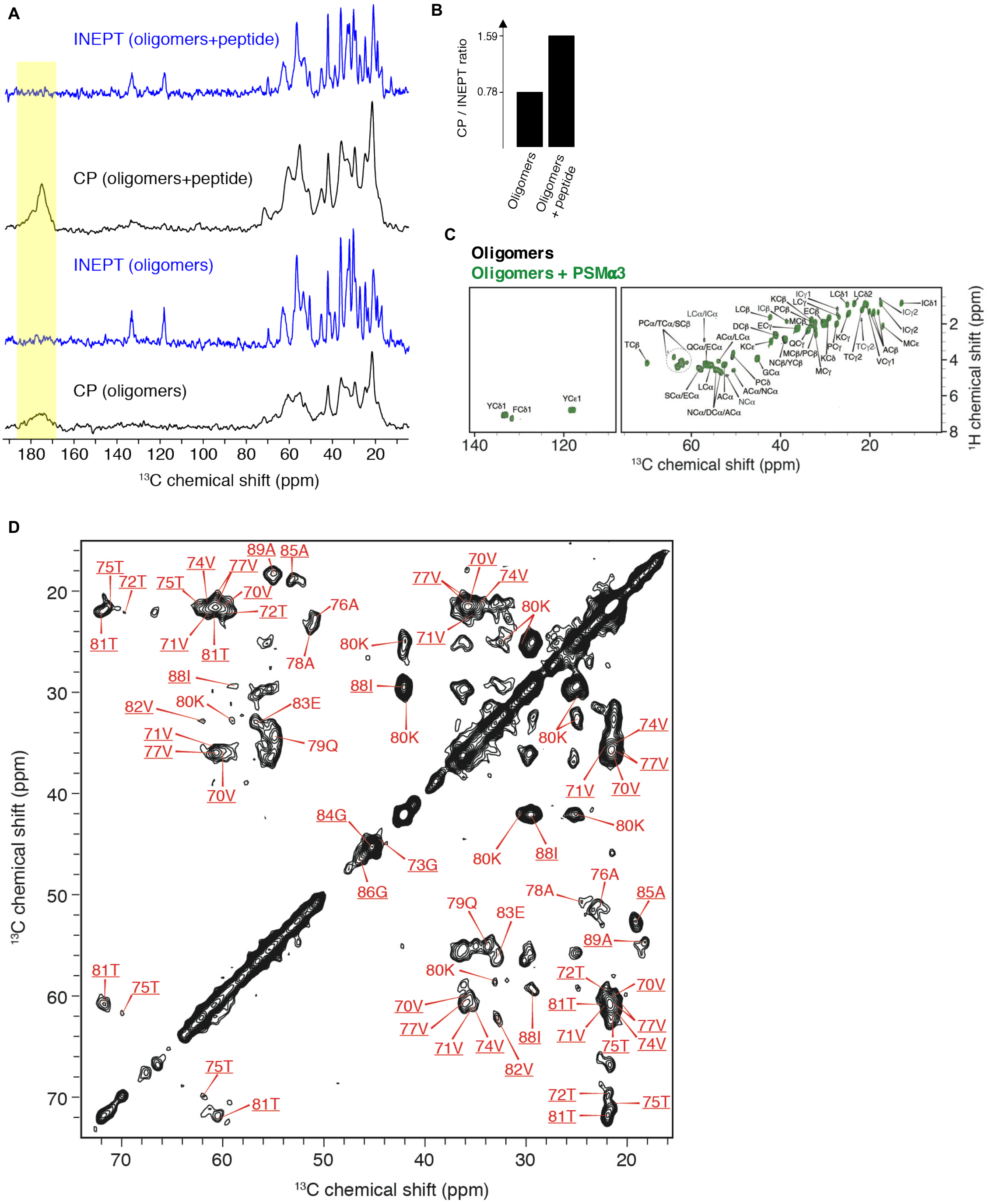

Figure S1. **MAS solid-state NMR analysis of ^{13}C-labelled αS oligomers and oligomers in complex with PSMα3.** (**A**) 1D ^{13}C spectra of oligomers and oligomers + PSMα3 peptide, detected using cross-polarization (CP) and INEPT as an initial ^{1}H to ^{13}C polarization transfer. The carbonyl spectral region is highlighted in pale yellow. (**B**) Ratio of CP/INEPT peak intensities integrated for the spectral region 0-75 ppm. (**C**) 2D ^{1}H-^{13}C INEPT spectra of oligomers (black) and oligomers + PSMα3 peptide (green). (**D**) 2D ^{13}C-^{13}C PDSD correlation spectrum (mixing time of 50 ms) of oligomers. Residues were assigned based on a previous study of αS fibrils (PDB: 2N0A) (*23*). Residues underlined have a chemical shift difference between oligomers and fibrils as $\Delta C\alpha < 1$ppm and $\Delta C\beta < 2$ppm. Residues not underlined as $1 < \Delta C\alpha < 2$ppm and $\Delta C\beta < 2$ppm. Spectra correspond to 1.5 mg of ^{13}C, ^{15}N labeled oligomer solution in PBS pH 7.4 in the absence and presence of PSMα3. Oligomer-PSMα3 complex was prepared as described in the materials and methods section.

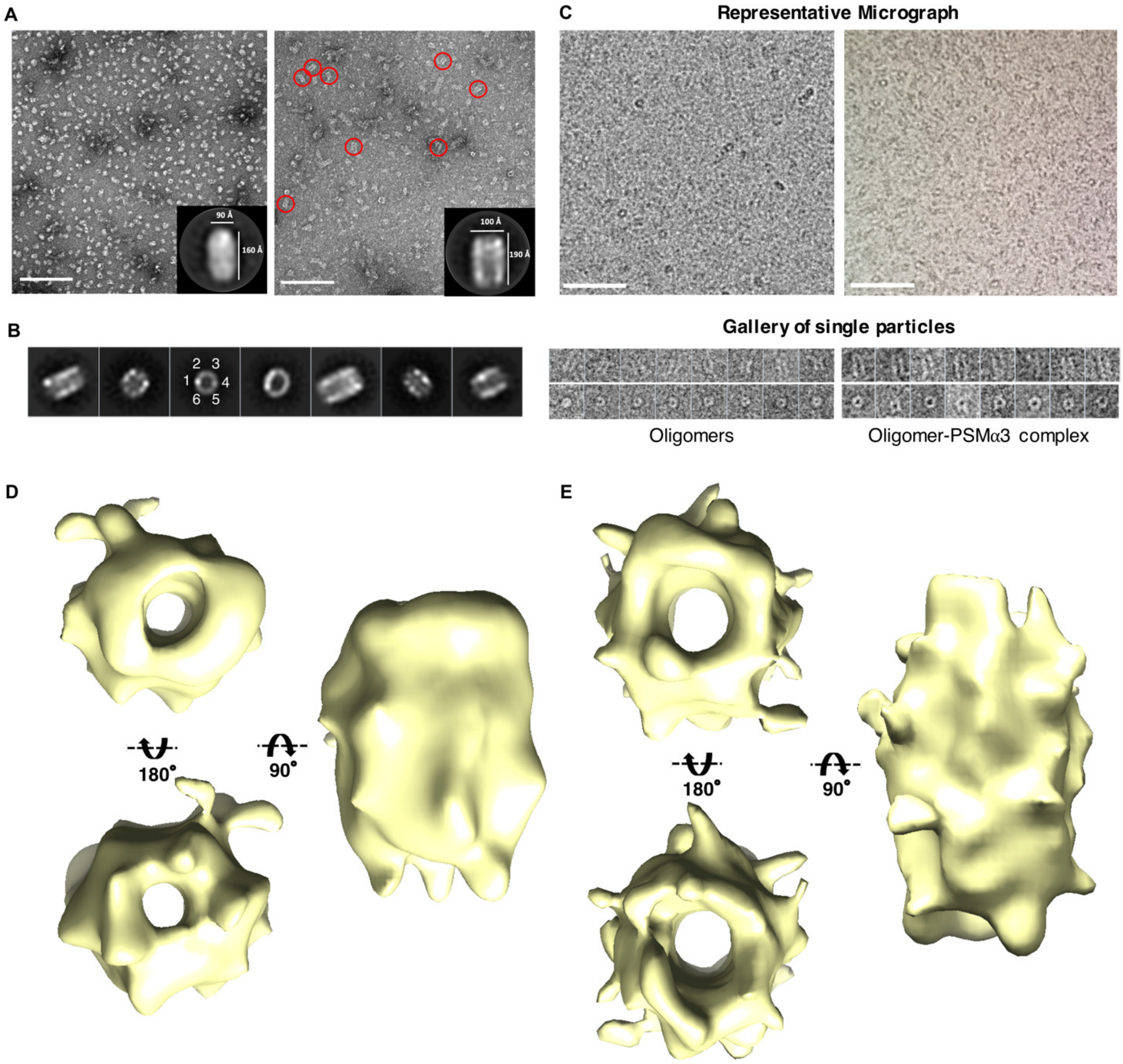
A
90 Å
160 Å
100 Å
190 Å
B
2 3
1 4
6 5
C
Representative Micrograph
Gallery of single particles
Oligomers
Oligomer-PSMα3 complex
D
180°
90°
E
180°
90°

Figure S2. **Electron microscopy characterization of αS oligomers in the absence and presence of PSMα3.** (**A**) Representative EM micrographs from negatively-stained free αS oligomers (left) and oligomer-PSMα3 complexes (right). Insets show a representative 2D class to illustrate PSMα3 induced rigidification. Scale bar: 100 nm. (**B**) Representative 2D classification of particles collected in panel **A**. (**C**) Representative micrographs and gallery of single particles obtained from the cryoEM analysis of αS oligomers in the absence or presence of PSMα3. Scale bar: 100 nm. (**D**) 3D reconstruction of αS oligomers in the absence of PSMα3 (18.5 Å resolution). No symmetry applied (c1). (**E**) 3D reconstruction of αS oligomers in complex with PSMα3 (19 Å resolution). No symmetry applied (c1).

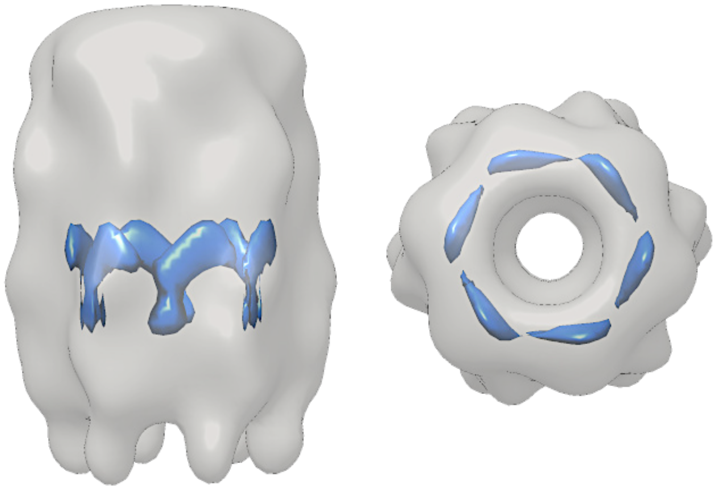

Figure S3. **Visualization of αS oligomer cryo-EM density at high visualization thresholds.** The denser region of the cryoEM map (σ = 3.4) is shown in blue inside the complete oligomer structure (σ = 1) in gray.

Class I

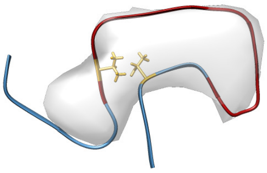

2N0A

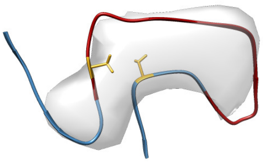

6LRQ (A53T)

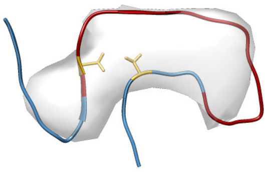

7E0F (G51D)

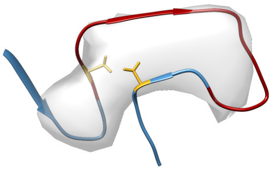

6L4S (E46K)

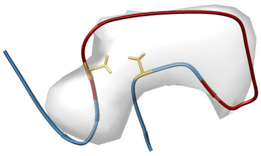

6PEO (H50Q)

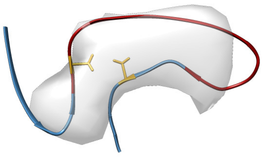

6XYO:B (MSA type I filament)

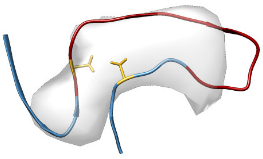

6XYP:B (MSA type II-1 filament)

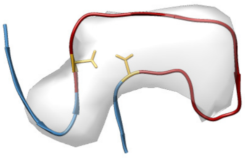

6XYQ:B (MSA type II-2 filament)

Class II

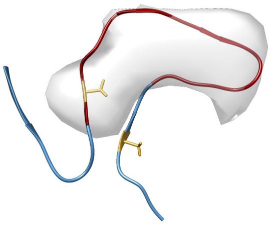

6CU7

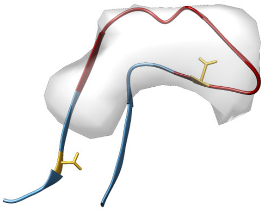

6SSX

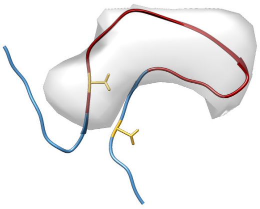

60SJ

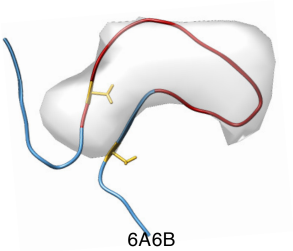

6A6B

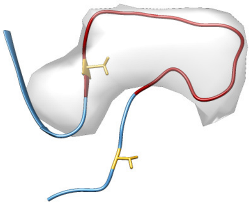

6OSM (1-103)

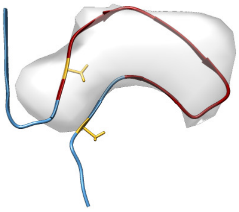

6OSL (1-122)

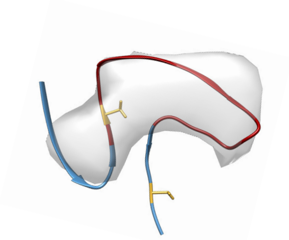

6XYO:A (MSA type I filament)

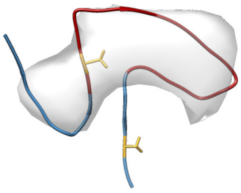

6XYP:A (MSA type II-1 filament)

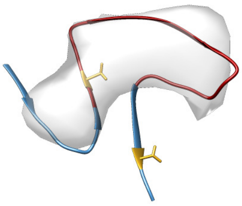

6XYQ:A (MSA type II-2 filament)

Class III

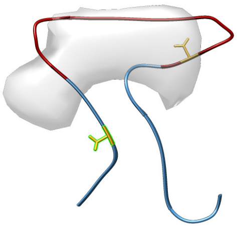

6UFR (E46K)

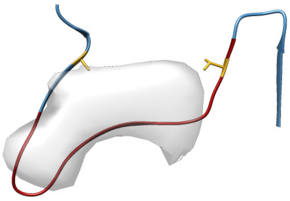

7LC9:A

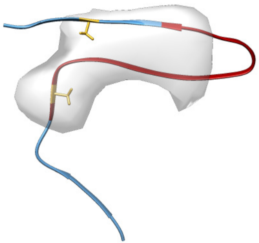

7LC9:B

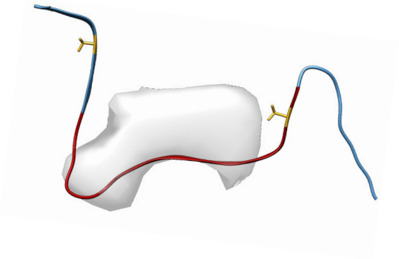

6L1T (Tyr39phos)

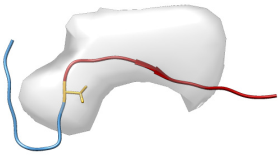

6CU8

Figure S4. **Overlay of the denser cryo-EM density (σ = 3.4) with the NAC domain of resolved αS fibrils.** Residues assigned as the rigid core of αS oligomers are shown in red (70-89). Valine 71 and threonine 92 in yellow. PDB code is noted below each structure with a short indication of the fibril origin in brackets. The analyzed structures were classified into three classes for easy visual inspection. Class I: Structures that fit the density in which residues Val 71 and Thr 92 are oriented for cysteine crosslinking and at a distance < 10 Å between their Cα. Class II: Structures that fit the density but residues Val 71 and Thr 92 are not oriented for cysteine crosslinking or at a distance > 10 Å between their Cα. Class III: structures that do not overlay with the cryoEM density.

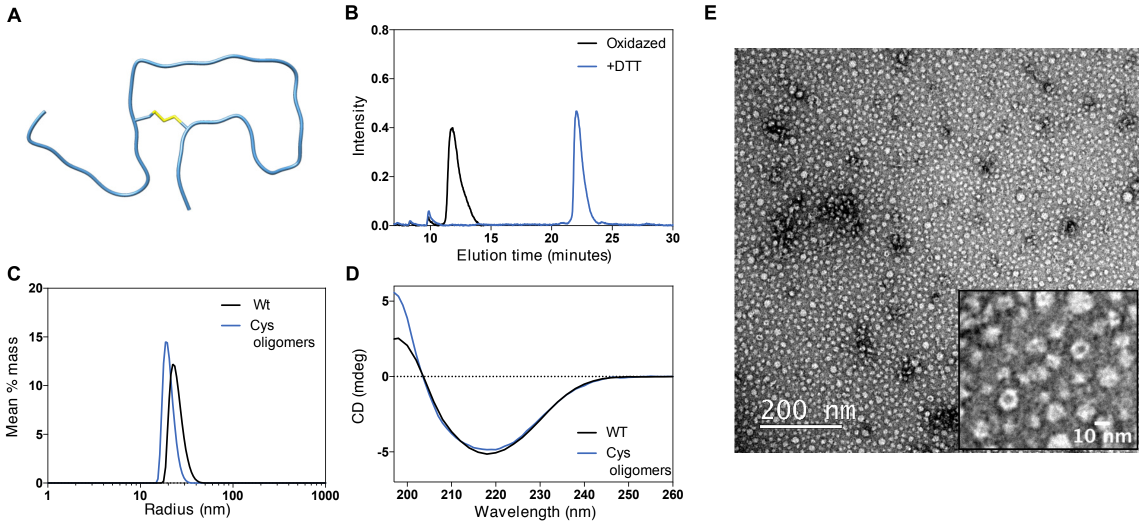

Figure S5. **Analysis of the V71C-T92C variant and its ability to assemble into oligomers.** (**A**) Predicted model of the 2N0A αS fibril (*23*) with a disulfide between residues 71 and 92 formed. (**B**) Reverse phase HPLC chromatograms of freshly purified untreated (black) and DTT-treated monomeric V71C-T92C αS (blue). V71C-T92C αS monomers are then natively oxidized. (**C**) Dynamic light scattering of WT and V71C-T92C kinetically trapped oligomers. (**D**) Circular dichroism spectra of WT and V71C-T92C oligomers. (**E**) Representative negatively-stained EM micrograph of V71C-T92C oligomers.

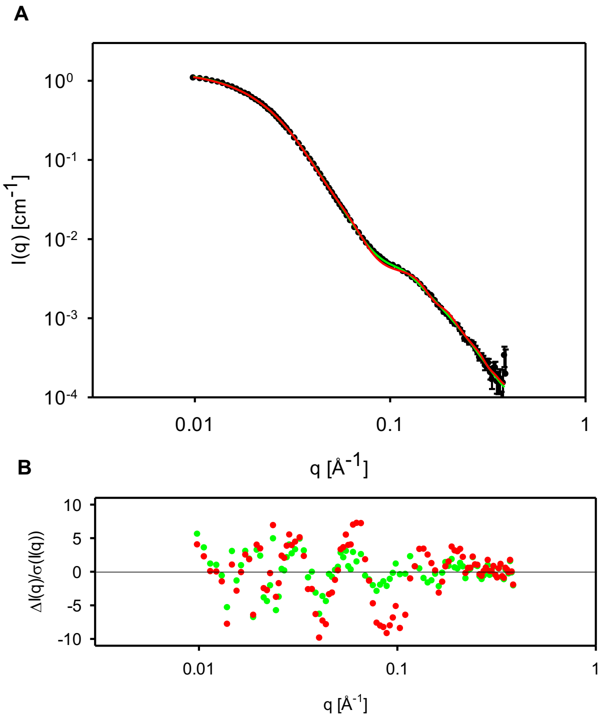

Figure S6. **SAXS analysis of oligomer organization**. (**A**) SAXS data in log-log plot with fits. The data for the αS oligomers are shown as black points. The fit for a model with one random coil chain per monomer is shown as the green curve and the fit for a model with two random coil chains per monomer is shown as a red curve. The two models have reduced chi-square of, respectively, $\chi^2 = 5.9$ and $\chi^2 = 17.3$, demonstrating a better fit with only one chain per monomer. (**B**) Residual of the difference between model and experimental intensities divided by the standard error on the data from counting statistics, colored as in (a).

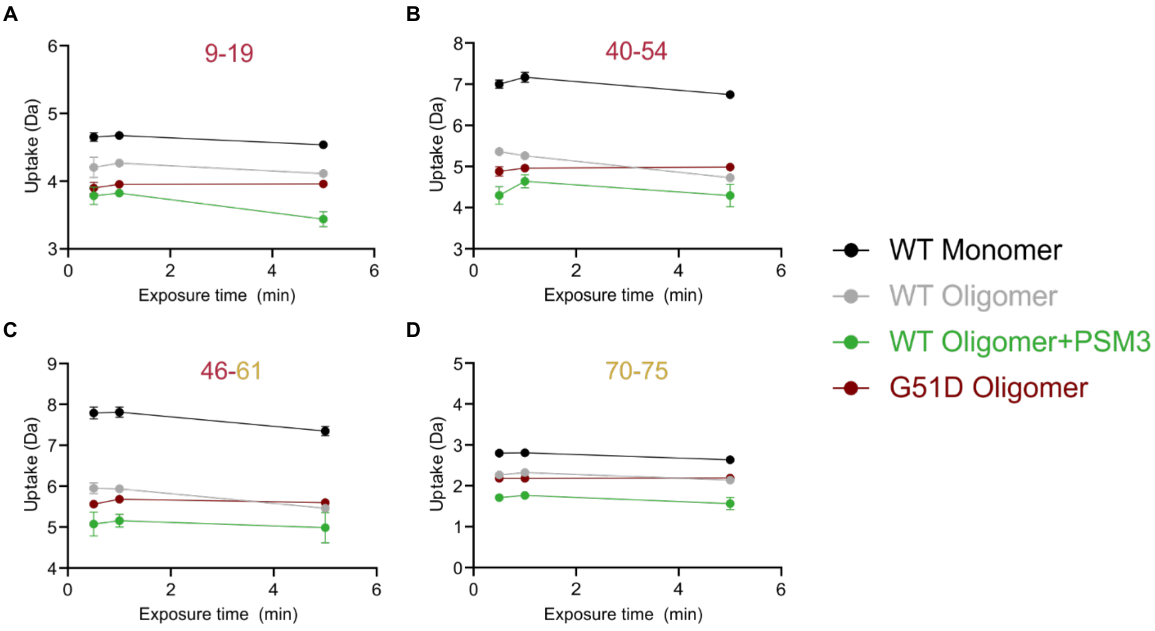

Figure S7. The N-terminal and NAC regions display significant protection from deuterium uptake in oligomeric states by HDX-MS. Example deuterium uptake plots for residues (**A**) 9-19 (**B**) 40-45 (**C**) 46-61 and (**D**) 70-75 across thirty second, one minute and five minute exposure timepoints. Protection from deuterium incorporation occurs across the N-terminal region and in the NAC region in the WT oligomeric states compared to monomer. Binding of PSMα3 increases the degree of protection observed. The degree of protection observed in the G51D oligomer is comparable to WT oligomers (in the absence of PSMα3).

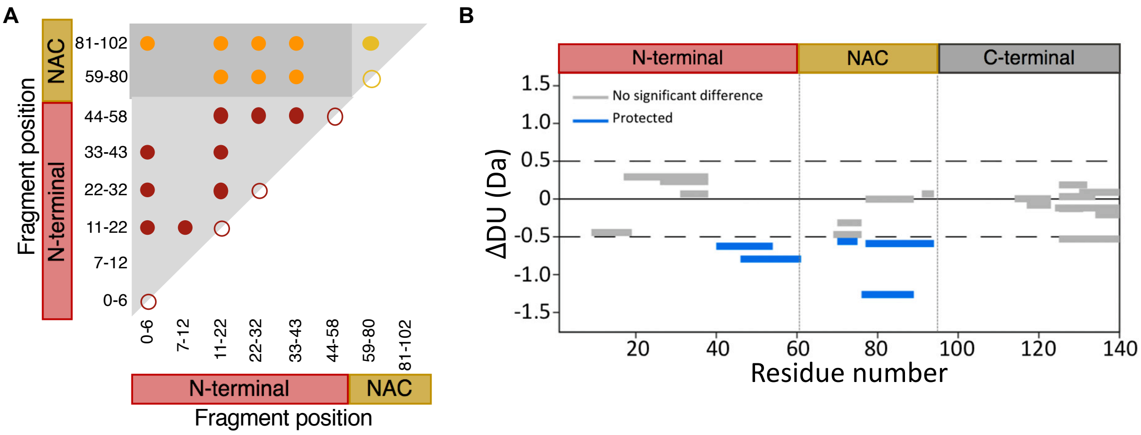

Figure S8. **Mapping structural contacts in oligomer structure by XL-MS and HDX-MS**. (**A**) Illustration of the N-terminal domain (red), NAC domain (gold) and N-terminal to NAC (orange) contacts identified by crosslinking αS oligomers with DMTMM. Open circles represent crosslinks between identical fragments (necessarily intermolecular). (**B**) Wood's plots showing the difference in deuterium uptake (ΔDU) when comparing αS oligomers in complex with PSMα3 and free αS oligomers by HDX-MS at the sixty second exposure time point. Oligomers that contain PSMα3 are protected from exchange in the P1 and P2 regions (consistent with XL-MS data that these regions bind PSMα3, **Fig. 2B**) and NAC regions suggesting additional structural changes in PSMα3 containing oligomers, whilst other regions in the N-terminal domain and the C-terminal domains show no significant difference in deuterium uptake.

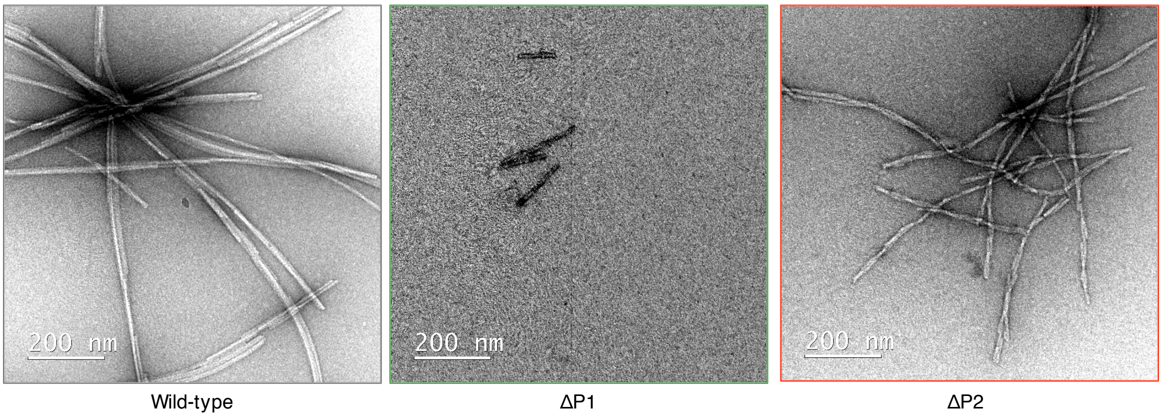
200 nm
200 nm
200 nm
Wild-type
ΔP1
ΔP2

Figure S9. **Representative nsEM micrographs of WT, ΔP1 and ΔP2 variants at the end point of the aggregation reaction.** For ΔP1 and ΔP2 variants most of the grid area was devoid of fibrils. We show representative images of those observed.

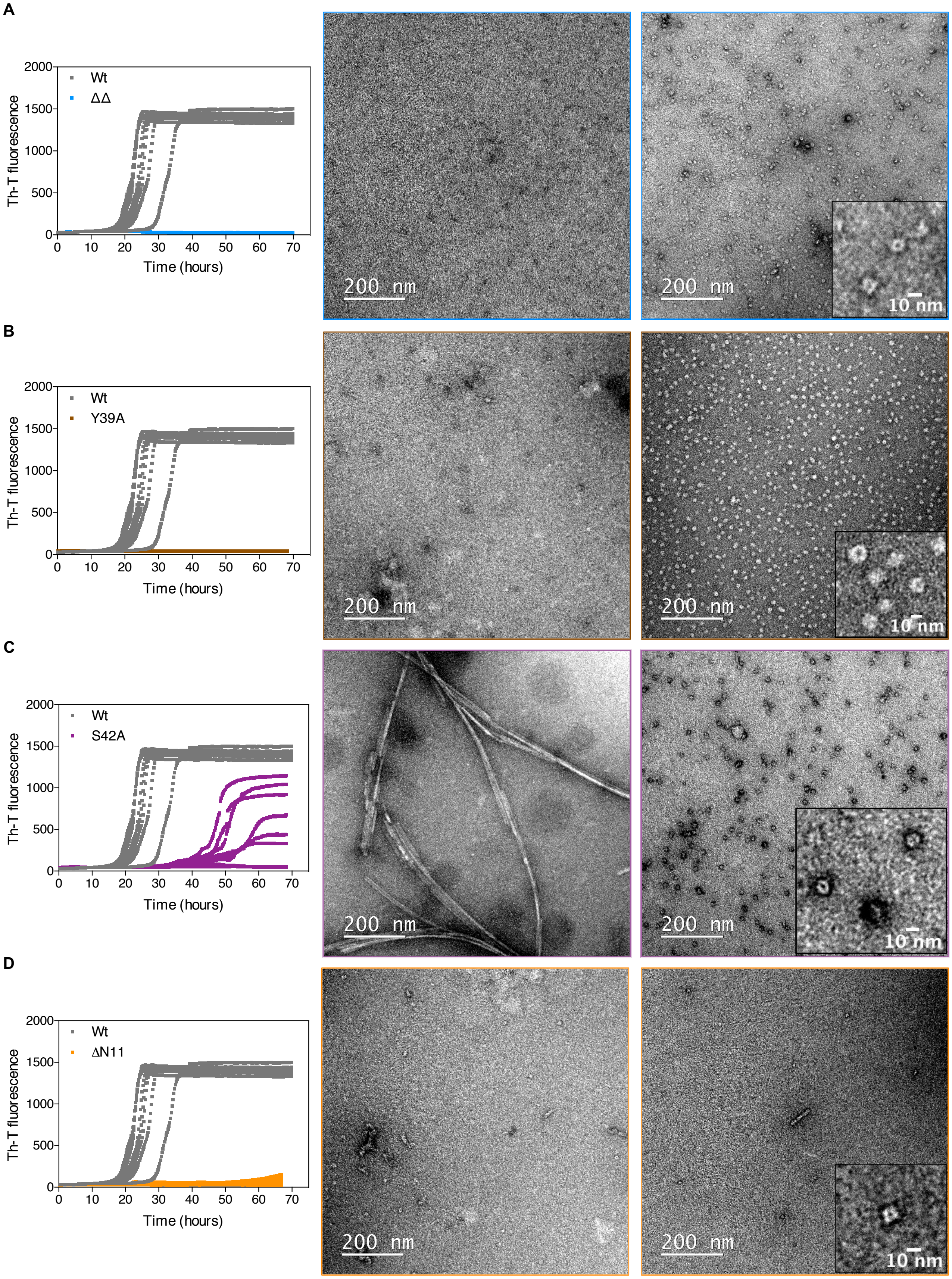
A
2000
1500
1000
500
0
Th-T fluorescence
0 10 20 30 40 50 60 70
Time (hours)
Wt
ΔΔ
200 nm
200 nm
10 nm
B
2000
1500
1000
500
0
Th-T fluorescence
0 10 20 30 40 50 60 70
Time (hours)
Wt
Y39A
200 nm
200 nm
10 nm
C
2000
1500
1000
500
0
Th-T fluorescence
0 10 20 30 40 50 60 70
Time (hours)
Wt
S42A
200 nm
200 nm
10 nm
D
2000
1500
1000
500
0
Th-T fluorescence
0 10 20 30 40 50 60 70
Time (hours)
Wt
ΔN11
200 nm
200 nm
10 nm

Figure S10. **Analysis of amyloid and oligomer formation of ΔΔ, Y39A, S42A and ΔN11 αS variants.** (**A-C**) Left: Kinetics of amyloid formation monitored by Th-T fluorescence. Center: Representative nsEM micrographs at the endpoint of the aggregation reaction. Right: Representative nsEM micrographs of the oligomeric fraction isolated at the endpoint (ΔΔ, Y39A and ΔN11) or after 28 hours of assembly (S42A).

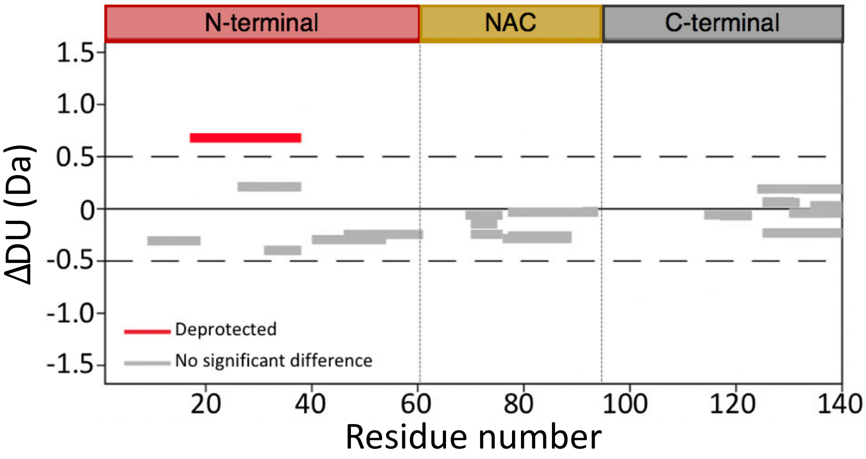

Figure S11. **G51D oligomers show polymorphism compared to WT oligomers by HDX-MS.** Woods plot showing the relative solvent exposure/hydrogen bonding of G51D αS oligomers compared with WT αS oligomers by HDX-MS at the sixty second timepoint of exposure to deuterium. Deprotection from deuterium uptake occurs in the N-terminal region, shown as peptides colored in red.

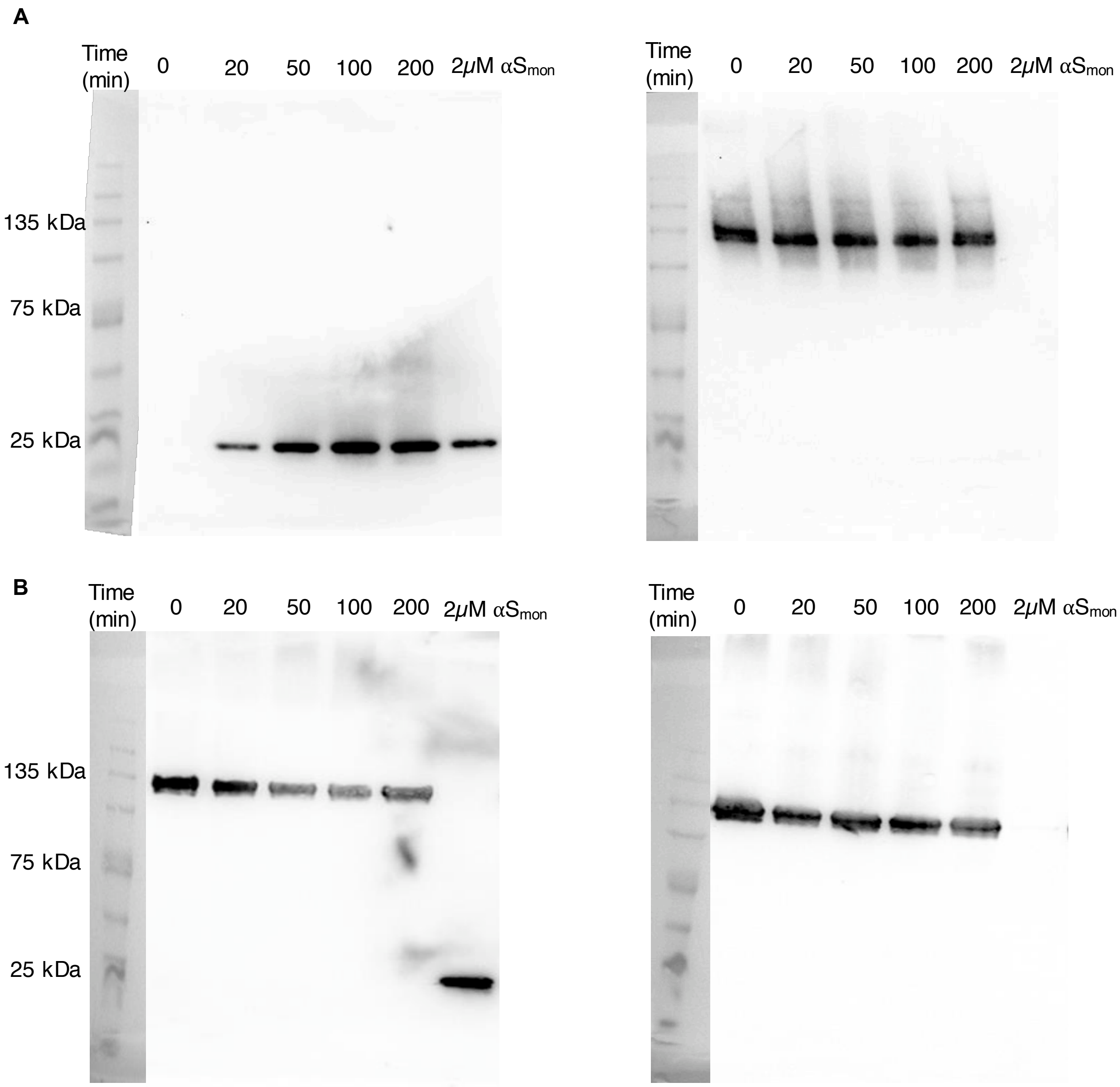
A
Time (min)
0
20
50
100
200
2μM αSmon
135 kDa
75 kDa
25 kDa
B
Time (min)
0
20
50
100
200
2μM αSmon
135 kDa
75 kDa
25 kDa

Figure S12. G51D oligomers are resistant to the human disaggregase chaperone system. Native-PAGE and immunoblotting with anti-αS (left panels) and anti-Hsc70 (right panels) of disaggregation reactions at different incubation times. 3 µM of (**A**) WT oligomers or (**B**) G51D oligomers were incubated with 10 µM Hsc70, 5 µM DnaJB1, and 1 µM Apg2 at 30 °C in the presence of ATP and an ATP-regeneration system. 2 µM of monomeric αS in the absence of chaperones were used as controls. Molecular weight markers are shown in lane 1.

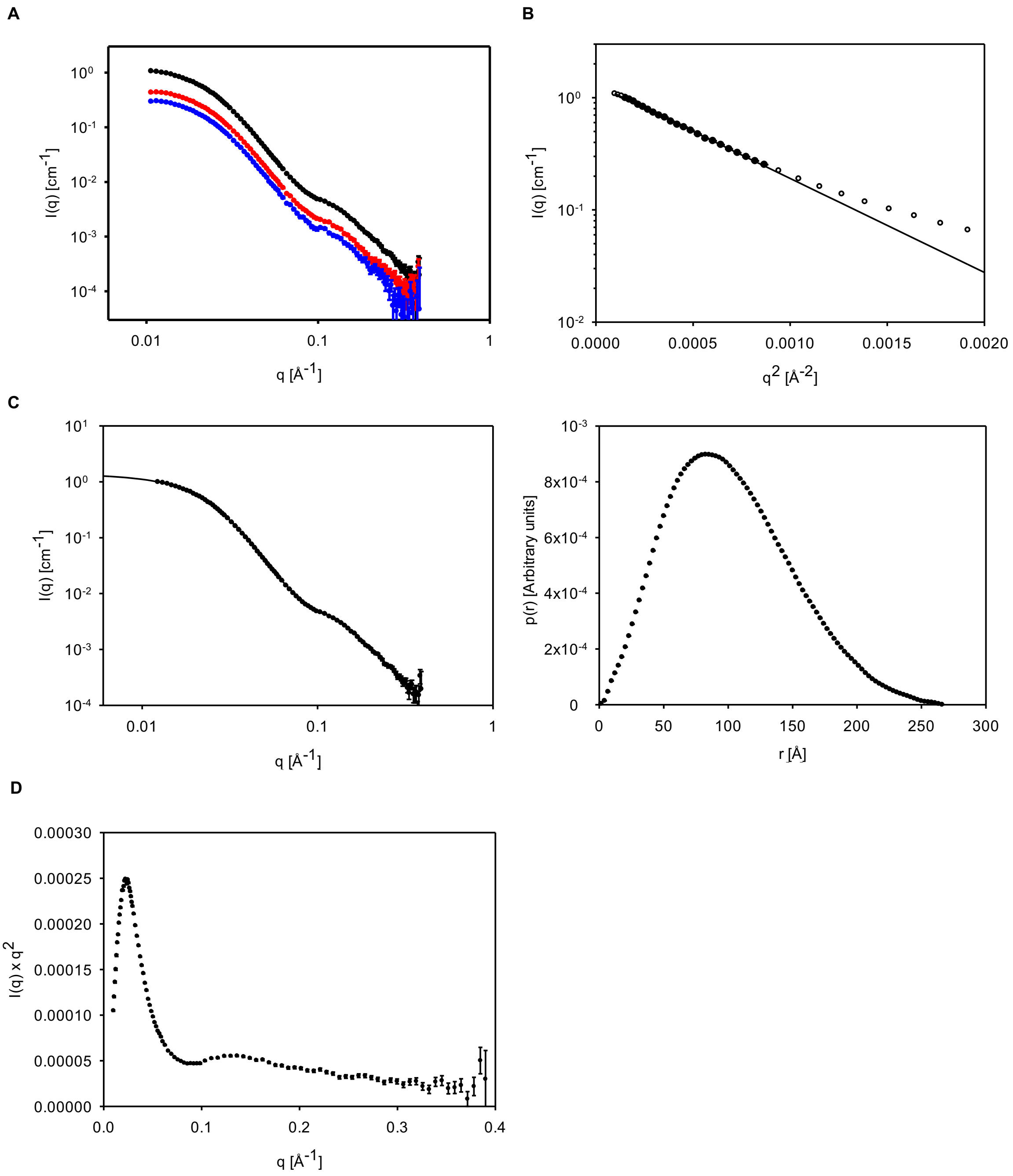

Figure S13. SAXS measurements and data analysis. (**A**) Concentration series for αS oligomer. From top to button: 4.6, 2.0, 1.3 mg/mL. (**B**) Guinier plots of the data for the high concentration samples of αS. Only the data points filled with black have been used for the fit (straight line). (**C**) Left: IFT fits to the data (lines) for the high concentration samples of αS (points). Right: Pair distance distribution functions for αS. (**D**) Kratky plots of the data for the high concentration samples of αS.

Table S1. ^{13}C chemical shift differences between αS fibrils (BMRB entry 25518) (*23*) and oligomers.

Residue	ΔCα (ppm)	ΔCβ (ppm)
70V	<0.1	<0.1
71V	<0.1	<0.1
72T	<0.1	<0.1
73G	-0.3	
74V	<0.1	<0.1
75T	<0.1	0.3
76A	-1.2	-0.9
77V	<0.1	<0.1
78A	-1.3	0.9
79Q	-2.4	-0.7
80K	1.2	-0.3
81T	<0.1	0.5
82V	-0.5	1.2
83E	-2.2	-0.4
84G	<0.1	
85A	0.5	-0.7
86G	<0.1	
87S	not detected	not detected
88I	0.7	-1.7
89A	<0.1	0.5

Table S2. Parameter values obtained from the SAXS analysis. The parameters are described in the methods section.

Parameter	**αS oligomers**
N_{agg}	31.5 ± 0.1
R [Å]	42.7 ± 1.7
e	1.58 ± 0.05
s_{core} [Å]	9.6 ± 1.8
W_{shell} [Å]calculated	52.2
R_{hole} [Å]	5.7 ± 1.7
s_{shell} [Å]	26.6 ± 0.4
r_{shell}	0.114 ± 0.008
f_{core} calculated	0.519
R_c [Å]	7.9 ± 0.5
R_{g} [Å] calculated	15.9

Table S3. CryoEM data acquisition and processing

Data collection & processing	**αS oligomers**	**αS oligomers-PSMα3**
Microscope	FEI Talos Arctica	FEI Talos Arctica
Voltage (KV)	200	200
Camera	Falcon 3	Falcon 3
Total dose ($e^-/Å^2$)	28	32
Frames	30	30
Dose per frame ($e^-/Å^2$)	0.932	1.06
Defocus range	-1.4 to -3.2	-1.4 to -3.2
Pixel size (Å)	1.37	1.37
Initial number of particles	193,427	187,446
Final number of particles	38,069	26,658
FSC threshold	0.143	0.143
Symmetry	C1/C6	C1/C6
Map resolution (Å)	18.5/16	19/16.7

References:

1. C. K. Xu, M. Castellana-Cruz, S. W. Chen, Z. Du, G. Meisl, A. Levin, B. Mannini, L. S. Itzhaki, T. P. J. Knowles, C. M. Dobson, N. Cremades, J. R. Kumita, The Pathological G51D Mutation in Alpha-Synuclein Oligomers Confers Distinct Structural Attributes and Cellular Toxicity. *Molecules*. **27**, 1293 (2022).
2. J. Santos, P. Gracia, S. Navarro, S. Peña-Díaz, J. Pujols, N. Cremades, I. Pallarès, S. Ventura, α-Helical peptidic scaffolds to target α-synuclein toxic species with nanomolar affinity. *Nat Commun*. **12**, 3752 (2021).
3. J. M. de la Rosa-Trevín, A. Quintana, L. Del Cano, A. Zaldívar, I. Foche, J. Gutiérrez, J. Gómez-Blanco, J. Burguet-Castell, J. Cuenca-Alba, V. Abrishami, J. Vargas, J. Otón, G. Sharov, J. L. Vilas, J. Navas, P. Conesa, M. Kazemi, R. Marabini, C. O. S. Sorzano, J. M. Carazo, Scipion: A software framework toward integration, reproducibility and validation in 3D electron microscopy. *J Struct Biol*. **195**, 93–99 (2016).
4. A. Rohou, N. Grigorieff, CTFFIND4: Fast and accurate defocus estimation from electron micrographs. *J Struct Biol*. **192**, 216–221 (2015).
5. V. Abrishami, A. Zaldívar-Peraza, J. M. de la Rosa-Trevín, J. Vargas, J. Otón, R. Marabini, Y. Shkolnisky, J. M. Carazo, C. O. S. Sorzano, A pattern matching approach to the automatic selection of particles from low-contrast electron micrographs. *Bioinformatics*. **29**, 2460–2468 (2013).
6. S. H. W. Scheres, RELION: implementation of a Bayesian approach to cryo-EM structure determination. *J Struct Biol*. **180**, 519–530 (2012).
7. A. Punjani, J. L. Rubinstein, D. J. Fleet, M. A. Brubaker, cryoSPARC: algorithms for rapid unsupervised cryo-EM structure determination. *Nat Methods*. **14**, 290–296 (2017).
8. S. Q. Zheng, E. Palovcak, J.-P. Armache, K. A. Verba, Y. Cheng, D. A. Agard, MotionCor2: anisotropic correction of beam-induced motion for improved cryo-electron microscopy. *Nat Methods*. **14**, 331–332 (2017).
9. K. Zhang, Gctf: Real-time CTF determination and correction. *J Struct Biol*. **193**, 1–12 (2016).
10. J. Vargas, A.-L. Álvarez-Cabrera, R. Marabini, J. M. Carazo, C. O. S. Sorzano, Efficient initial volume determination from electron microscopy images of single particles. *Bioinformatics*. **30**, 2891–2898 (2014).
11. D. B. Craig, A. A. Dombkowski, Disulfide by Design 2.0: a web-based tool for disulfide engineering in proteins. *BMC Bioinformatics*. **14**, 346 (2013).
12. J. Lyngsø, J. S. Pedersen, A high-flux automated laboratory small-angle X-ray scattering instrument optimized for solution scattering. *J Appl Crystallogr*. **54**, 295–305 (2021).
13. J. S. Pedersen, A flux- and background-optimized version of the NanoSTAR small-angle X-ray scattering camera for solution scattering. *J Appl Crystallogr*. **37**, 369–380 (2004).
14. J. S. Pedersen, S. Hansen, R. Bauer, The aggregation behavior of zinc-free insulin studied by small-angle neutron scattering. *Eur Biophys J*. **22**, 379–389 (1994).
15. S. Maric, T. K. Lind, J. Lyngsø, M. Cárdenas, J. S. Pedersen, Modeling Small-Angle X-ray Scattering Data for Low-Density Lipoproteins: Insights into the Fatty Core Packing and Phase Transition. *ACS Nano*. **11**, 1080–1090 (2017).
16. J. S. Pedersen, C. Svaneborg, Scattering from block copolymer micelles. *Current Opinion in Colloid & Interface Science*. **7**, 158–166 (2002).
17. P. Debye, Molecular-weight Determination by Light Scattering. *J. Phys. Chem.* **51**, 18–32 (1947).
18. J. E. Kohn, I. S. Millett, J. Jacob, B. Zagrovic, T. M. Dillon, N. Cingel, R. S. Dothager, S. Seifert, P. Thiyagarajan, T. R. Sosnick, M. Z. Hasan, V. S. Pande, I. Ruczinski, S. Doniach, K. W. Plaxco, Random-coil behavior and the dimensions of chemically unfolded proteins. *Proc Natl Acad Sci U S A*. **101**, 12491–12496 (2004).

19. M. Götze, J. Pettelkau, R. Fritzsche, C. H. Ihling, M. Schäfer, A. Sinz, Automated assignment of MS/MS cleavable cross-links in protein 3D-structure analysis. *J Am Soc Mass Spectrom*. **26**, 83–97 (2015).

20. A. M. Lau, J. Claesen, K. Hansen, A. Politis, Deuteros 2.0: peptide-level significance testing of data from hydrogen deuterium exchange mass spectrometry. *Bioinformatics*. **37**, 270–272 (2021).

21. S. T. Kumar, S. Donzelli, A. Chiki, M. M. K. Syed, H. A. Lashuel, A simple, versatile and robust centrifugation-based filtration protocol for the isolation and quantification of α-synuclein monomers, oligomers and fibrils: Towards improving experimental reproducibility in α-synuclein research. *J Neurochem*. **153**, 103–119 (2020).

22. Y. Cabrera, L. Dublang, J. A. Fernández-Higuero, D. Albesa-Jové, M. Lucas, A. R. Viguera, M. E. Guerin, J. M. G. Vilar, A. Muga, F. Moro, Regulation of Human Hsc70 ATPase and Chaperone Activities by Apg2: Role of the Acidic Subdomain. *J Mol Biol*. **431**, 444–461 (2019).

23. M. D. Tuttle, G. Comellas, A. J. Nieuwkoop, D. J. Covell, D. A. Berthold, K. D. Kloepper, J. M. Courtney, J. K. Kim, A. M. Barclay, A. Kendall, W. Wan, G. Stubbs, C. D. Schwieters, V. M. Y. Lee, J. M. George, C. M. Rienstra, Solid-state NMR structure of a pathogenic fibril of full-length human α-synuclein. *Nat Struct Mol Biol*. **23**, 409–415 (2016).